

HEPATITIS C VIRUS NONSTRUCTURAL PROTEIN 5A:
HOST CELL PROTEIN-PROTEIN INTERACTIONS
AND
CHARACTERIZATION OF PHOSPHORYLATED RESIDUES

by

Taeyo Dawn Mary Chestley

A thesis submitted to the Faculty of Graduate Studies

of

The University of Manitoba

In partial fulfillment of the requirements of the degree of

Doctor of Philosophy

Department of Medical Microbiology and Infectious Diseases

University of Manitoba

Winnipeg, Manitoba

Copyright © 2017 by Taeyo Dawn Mary Chestley

Abstract

Hepatitis C virus (HCV) is a hepatotropic pathogen present in approximately 2.8% of the population with 3-4 million new infections every year. Up to 85% of infections progress to a chronic disease associated with development of steatosis, cirrhosis and hepatocellular carcinoma. Viral protein, Nonstructural 5A (NS5A), has eluded a defined role in the HCV life cycle despite being essential to viral propagation and host cell modulation. NS5A is a phosphoprotein appearing as two molecular weight proteoforms by SDS-PAGE referred to as the basally phosphorylated and hyperphosphorylated forms. Different NS5A phospho-proteoforms may direct its function acting as a molecular switch between replication and assembly. Two aspects of NS5A biology were addressed: 1) NS5A host cell protein-protein interactions and 2) defining phosphorylation sites on NS5A. To identify NS5A-host protein-protein interactions, a novel tandem affinity purification (TAP) technique was implemented. A HBH (histidine-biotin-histidine) tag was affixed to NS5A-2a (JFH1) and cells were generated stably expressing this construct. Tagged proteins were purified using native-state (nTAP) and cross-linked, denaturing (xdTAP) using immobilized metal chelate and streptavidin resins. Purified samples were subjected to tandem-mass spectrometry and database searching to generate an NS5A interacting protein list. Co-immunoprecipitation and colocalization confirmed host cell Cell Cycle and Apoptosis Regulator protein 2 (CCAR2) as an NS5A interacting protein. Phosphorylation analysis used NS5A isolated as a tagged protein, part of a subgenomic (SG) replicon, or a tagged protein within a SG replicon. Subsequent tandem mass spectrometry allowed for identification of 28 phosphorylation sites, 20 of which were

novel. Phosphoablant and phosphomimetic mutation of the phosphoacceptor sites were used to evaluate the impact of phosphorylating these residues to the JFH1 virus. While majority of these mutations had no impact, T204D, T210A/D, S225D, S229A/D, S232A/D, S235A/D, S238A/D, T334A/D, and T363A/D mutants were reduced in their replicative capacity. NS5A phospho-proteoform ratios were evaluated with S151D, S225A and S232A mutants primarily basally phosphorylated while T213D, T210A/D were mainly hyperphosphorylated. Mutants T210D, S229A, S229D, and S235A failed to produce virus. A novel observation was made that NS5A is principally hyperphosphorylated at early time-points post RNA electroporation but past 72 hours the basally phosphorylated form predominates.

Dedication

For Andrew, Seylene, Dad and Mom.
I love you all forever and always.

Acknowledgments

First and foremost I would like to thank my supervisor Dr. Michael Carpenter. Mike, I am eternally grateful for all of your guidance and support both professionally and personally. Your encouragement of me was inexhaustible, constantly pushing me to reach my fullest potential. You were so generous with your time, knowledge and always had an open door to discuss anything. I always knew I could count on your support when it came to any aspect of my PhD, from providing constructive criticism to spending entire days completing 24 consecutive electroporations! You always inspired me to think critically and dig deeper to gain a full understanding of each topic and helped mould me into a better scientist. Furthermore, you were continuously compassionate and empathetic, especially when I needed your support the most. Thank you Mike, I could not have a better-suited supervisor and I will forever be grateful for your guidance.

I would like to thank my committee members Dr. Blake Ball and Dr. Brian Mark. Thank you both for your support, guidance and constructive critiques. I am so grateful that you both granted your valuable time and efforts in support of my PhD.

I would like to thank my external examiner, Dr. John Pezacki. Thank you for agreeing to provide your time as an examiner for both your constructive critiques as well as for travelling to Winnipeg to attend my defence.

A thank you to my hepatitis lab mates past and present. I am grateful not only to the assistance that you provided in the lab but the moral support and encouragement. A special thank you to Xiaojie Hu and Jessie Varga. Xiaojie, your kindness and support were perpetual and I really appreciate support. Jessie, thank you for your friendship and support and for always reminding me where I needed to be.

My sincerest thanks go out to the Department of Medical microbiology for their support. Thank you to Dr. Keith Fowke for always being approachable, encouraging and supportive. A very special thanks to Angela Nelson for her constant patience in answering questions, keeping me up-to-date and for always being so kind.

To Dr. Garrett Westmacott, Stewart McCorristor and Dr. Patrick Choy of the Proteomics Core at the National Microbiology Laboratory thank you all for your assistance and support. Thank you for providing me with the mass spectrometry data that provided the foundation of this project.

Thank you to the DNA Core at the National Microbiology lab for all of the hard work they put into the sequencing of my constructs and the producing all of my primers.

Thank you to Dr. Anna Majer for helping me produce the confocal microscopy images.

Above all, I wholeheartedly thank my family because without their support and encouragement I could have never taken on or completed this degree. To my incredible husband Andrew, I love you. I have always been inspired by your strength, drive and

determination. You never wavered in your support of my ambitions and continuously provided constant encouragement. You always told me I could do this and helped me to be stronger, smarter and braver than I ever thought was possible. Andrew, I always know I can count on your love and support in every aspect of my life. Thank you for always being there for me. Seylene, you and I have been best friends our entire lives. Your empathy and love have always gotten me through tough times. You are fiercely loyal and I know I can always count on your support and encouragement. Baby sisters are supposed to look up to their big sisters, but I look up to you. To my Dad, Douglas Chestley, thank you for being the best Dad a girl could ever have. You have done so much for me over the years and taught me so many things. Dad, you are a confident and proud man and always gave me the courage to be confident in myself. Your girls are always your first priority and even now I know that I can always count on you to drop everything to help me out. Thank you to my Mom, Darlene Chestley, for being my rock. Everything I am today is because of you and your sacrifices. You are a wonderful person who makes everyone feel special and loved. You gave all of yourself to your girls by providing unconditional love. You gave your time unselfishly and guided me throughout my entire life. You are my Mom, best friend and hero and there are not enough words to properly thank you for everything.

To my dogs, Boston, Crumbs and Tigger, thank you for always being there with unconditional love and a tail wag for me.

Abbreviations/Glossary

AB Buffer - Ammonium Bicarbonate buffer
ACN – Acetonitrile
ADAP - Adhesion and degranulation promoting adaptor protein
Akt – Protein kinase B
AKT1- RAC-alpha serine/threonine-protein kinase
Apo - Apolipoprotein
ATXN1 - Ataxin-1
BCA – Bicinchoninic acid
BH - Bcl-2 homology domain
Bin1 (Amphysin II) – Myc box-dependent-interacting protein 1
BSA – Bovine serum albumin
CBP - Calmodulin binding peptide
CCAR2 - Cell Cycle and Apoptosis Regulator 2
CD81 - Cluster of differentiation 81
CDK1 – Cyclin-dependent kinase 1
CDK12 - Cyclin-dependent kinase 12
CID – Collision-induced dissociation
CKIalpha – Casein Kinase I alpha
CKIdelta- Casein Kinase I delta
CKII – Casein Kinase II
CLDN1 - Claudin-1
Co-IP- Co-immunoprecipitation
DAA - Direct-acting antiviral
DAPI - 4',6-diamidino-2-phenylindole
DMEM - Dulbecco's modified Eagle's medium
DMSO - dimethyl sulfoxide
DSG - Disuccinimidyl glutarate
DSS - Disuccinimidyl suberate
dTAP – Denatured tandem affinity purification
DTT - 1,4-Dithiothreitol
EDTA - Ethylenediaminetetraacetic acid
EGF-Epidermal growth factor
EGFR - Epidermal growth factor receptor
eIF2 - Eukaryotic initiation factor 2
eIF3 - Eukaryotic initiation factor 3
eIF4F – Eukaryotic initiation factor 4 F
EMCV - Encephalomyocarditis virus
EphA2 - Ephrin type-A receptor 2
ER – Endoplasmic reticulum
ESG - Ethylene glycol bis(succinimidyl succinate)
ESI - Electrospray ionization
FADD - Fas-associated protein with death domain

FBS - Fetal bovine serum
FKBP8/38- FK506 binding protein 8/38
FPLC – Fast protein liquid chromatography
GFP – Green fluorescent protein
HA tag – Human influenza hemagglutinin amino acids 98-106 tag
HBH tag - Biotinylation recognition signal flanked by two hexahistidine sequences
HCC - Hepatocellular carcinoma
HCD – High-energy collisional dissociation
HCV - Hepatitis C virus
hp70S6K – Human phospho-p70 S6 kinase
hpe – Hours post electroporation
hpi – Hours post infection
hpt –Hours post transfection
HRP – Horseradish peroxidase
Hsp – Heat shock protein
HSPG - Heparin sulfate proteoglycans
hVAP-A – H-vesicle-associated membrane protein-associated protein A
IAA – Iodoacetamide
IF – Immunofluorescence
IFN – Interferon
ILF3 – Interleukin enhancer-binding factor 3
IPO5 – Importin 5
IRES – Internal ribosome entry site
IRF3 - Interferon regulatory transcription factor 3
ISDR - Interferon Sensitivity Determining Region
JFH1- Japanese fulminant hepatitis virus 1
JNK – c-Jun N-terminal kinases
KLD - Kinase-Ligation DpnI
LATS2 - Serine/threonine-protein kinase LATS2
LCS – Low-complexity sequence
LDLR - Low-density lipoprotein receptor
m/z – Mass to charge ratio
M2H - Mammalian two-hybrid system
MALDI - Matrix assisted laser desorption ionization
MEK1 - Dual specificity mitogen-activated protein kinase kinase 1
MKK6 - Dual specificity mitogen-activated protein kinase kinase 6
mTOR – Mechanistic target of rapamycin
NF-KB – Nuclear factor kappa-light-chain enhancer of activated B cells
NKRF - NF-Kappa-B-repressing factor
NLS - Nuclear localization signal
NMR – Nuclear magnetic resonance
NP-40 - Igepal CA-630
NPC1L1 - Niemann-Pick C1-Like 1
NS - Nonstructural
nTAP – Native state tandem affinity purification
NUP - Nuclear pore complex protein

OCLN – Occludin
OGDH - Oxoglutarate dehydrogenase
ORF - Open reading frame
PAGE – Polyacrylamide gel electrophoresis
PARP - Poly ADP ribosome polymerase
PBS – Phosphate-buffered saline
PBST - Phosphate-buffered saline, 0.1% Tween
PCR - Polymerase Chain Reaction
PFA – Paraformaldehyde
Phosphoablatant – mutation of a phosphorylated serine/threonine residue to alanine that does not function as a phosphoacceptor site
Phosphomimetic – mutation of a phosphorylated serine/threonine residue to an aspartic acid that functions of mimic the negative charge associated with the addition of a phosphate
PI3K - Phosphoinositide 3-kinase
PKA- α - cAMP-dependent protein kinase catalytic subunit alpha
PKR – Protein kinase R
Plk1 – Serine/threonine-protein kinase PLK1
PPI – Protein-protein interaction
protA- Immunoglobulin-interacting domain of Protein A
PVDF LF – Polyvinylidene fluoride low fluorescence membrane
RBM17 - RNA-binding motif protein 17
REAP - Rapid, Efficient, And Practical cell fractionation method
RIG-I - Retinoic acid-inducible gene I
RIPA - Radioimmunoprecipitation assay buffer
SCA - Six spinocerebellar ataxia types
SCX – Strong cation exchange
SDS – Sodium dodecyl sulfate
SG - Subgenomic
SH3 - Src homology 3 domain
SOD1 - Superoxide dismutase
SR-B1 - Scavenger receptor class B type I
SVR – Sustained virological response
TAP - Tandem Affinity Purification
TBE - Tris-borate/EDTA
TBST – Tris-buffered saline, 0.1% Tween
TEMED – Tetramethylethylenediamine
TFA - Trifluoroacetic acid
TfR1 - Transferrin receptor 1
TIPE2 – Tumour necrosis factor alpha-induced protein 8-like 2
TNFR1 - Tumour necrosis factor receptor type 1
TNF α - Tumour necrosis factor alpha
TOM – Translocase of the outer membrane
TRADD - Tumour necrosis factor receptor type 1-associated DEATH domain protein
TRAF2 - TNF receptor-associated factor 2
UBP - Urea Buffer with Phosphate

UEB - Urea exchange buffer

UTR- Untranslated region

VSV-G – Vesicular stomatitis virus glycoprotein

wt - Wild type

xdTAP - Cross-linked denaturing tandem affinity purification

Y2H - yeast two hybrid

ZAP70 - Tyrosine-protein kinase ZAP-70

Table of Contents

Abstract	I
Dedication	III
Acknowledgments	IV
Abbreviations/Glossary	VI
Table of Contents	X
List of Figures	XVII
List of Tables	XXI
Chapter 1: Introduction	1
1.1 Hepatitis C Virus	1
1.1.1 Burden	1
1.1.2 HCV Virology.....	8
1.1.3 HCV Life Cycle.....	13
1.1.4 HCV Cell Culture Models	17
1.1.5 HCV Animal Models.....	20
1.2 Non-Structural 5A Protein	21
1.2.1 NS5A Structure and Function	21
1.3 NS5A Interactions within the host cell	25
1.3.1. NS5A and apoptosis	25
1.3.2 TRAF2 and TRADD	26
1.3.3 Bax.....	29
1.3.4 p53	30

1.3.5 PI3K	31
1.3.6 Bin1 (Amphiphysin II)	32
1.3.7 FKBP8/FKBP38	34
1.3.8 Other Proteins	36
1.3.9 Reproducibility of NS5A-host cell PPIs	36
1.4 Studying protein-protein interactions	38
1.4.1 Protein identification using mass spectrometry and database searching	42
1.5 Phosphorylation as a differential controller of PPIs	45
1.5.1 NS5A phosphorylation.....	46
1.5.2 Kinases involved in NS5A phosphorylation.....	48
1.5.3 NS5A phosphoacceptor sites.....	48
1.5.4 Regulatory role of phosphorylation in the HCV life cycle	53
1.6 Study Rationale and Hypothesis	54
Chapter 2: Materials and Methods.....	57
2.1 General Laboratory Techniques	57
2.1.1 Cell Culture	57
2.1.2 iProof Polymerase Chain Reaction (PCR)	58
2.1.3. General Cloning Strategy	58
2.1.4 Effectene Cell Culture Transfection.....	60
2.1.5. Xtreme Gene Cell Culture Transfection.....	60
2.1.6 SDS-PAGE and Western Blots	61
2.1.7 Indirect Immunofluorescence	64
2.1.7.1 JFH1-HT Infection for Indirect Immunofluorescence	66
2.1.8 REAP Method of Nuclear/Cytoplasmic Cellular Fractionation	66
2.2 Generation of HBH-NS5A and HBH-GFP Stable Cell Lines.....	67

2.2.1 Creating HBH-tagged NS5A-2a and GFP.....	67
2.2.2 Retrovirus Production	68
2.2.3 Generation of stable cell lines	68
2.3 Non-Denaturing Tandem Affinity Purification (nTAP).....	69
2.3.1 Non-denaturing TAP Harvest of HBH tagged NS5A and GFP-tagged protein.....	69
2.3.2 Non-denaturing Metal Chelate Purification of HBH tagged NS5A and GFP using the FPLC	70
2.3.3 Non-denaturing Metal Chelate Purification of HBH tagged NS5A and GFP using batch methods with cobalt magnetic beads.....	71
2.3.4 Biotin/Streptavidin Purification of HBH tagged NS5A and GFP.....	71
2.4 Denaturing (dTAP) and Cross-Linked/Denaturing (xdTAP) Tandem Affinity Purification	72
2.4.1 Denaturing TAP (dTAP) and cross-linked denaturing (xdTAP) Harvest of HBH tagged NS5A and GFP-tagged total protein.....	72
2.4.2 dTAP/xdTAP Metal Chelate Chromatography and Streptavidin capture for the purification of HBH tagged proteins	74
2.5 Digestion and Purification of Peptides for Mass Spectrometry Analysis.....	75
2.5.1 Reduction/Alkylation/Trypsin Digestion of Peptides from Streptavidin Capture	75
2.5.2 Strong Cation Exchange (SCX) Purification of Peptides.....	76
2.6 Mass Spectrometry Analysis of TAP Purified Protein Complexes	76
2.6.1 Mass Spectrometry.....	76
2.6.2 Mass Spectrometry Data Analysis.....	78
2.7 Confirmation of nTAP and xdTAP NS5A-2a Protein-Protein Interaction Candidates.....	78

2.7.1 TAP Confirmation Expression Plasmids.....	78
2.7.2 Confirmation of TAP Interaction Candidates by Co-Immunoprecipitation	79
2.8 Generation of SG JFH1 and SG JFH1-NS5A-HBH replicon Huh7.5 cell lines.....	80
2.9 Purification of HBH-NS5A-2a from stable cell lines and HBH-tagged NS5A from SG JFH1 in Huh7.5 cells for phosphorylation site identification using dTAP	82
2.10 Purification of JFH1 NS5A protein from SG JFH1 Huh7.5 cell line by continuous elution gel electrophoresis.....	82
2.11 Identification of phosphorylation sites in NS5A-2a using Mass Spectrometry.....	84
2.12 NS5A phosphoacceptor site mutagenesis	87
2.13 RNA Isolation and Quantitative real-time reverse transcriptase PCR	88
2.14 Western Blot Analysis of NS5A from Electroporated Huh7.5 Cells.....	90
2.15 TCID₅₀/ml Analysis of HCV Viral Titer.....	90
Chapter 3: Identification of host cell interacting proteins of hepatitis C virus nonstructural 5A protein by a novel tandem affinity purification, mass spectrometry based approach	92
3.1 Introduction and Rationale	92
3.2 Results	93
3.2.1 Creation GP2 293 cells stably expressing HBH-tagged NS5A.....	93
3.2.2 Optimization of the TAP protocol.....	98
3.2.3 Identification of NS5A-2a interacting proteins by nTAP and mass spectrometry	109
3.2.4 Identification of NS5A-2a interacting proteins by xdTAP and mass spectrometry	118
3.2.5 Confirmation of TAP candidate interactions with NS5A using Co-IP.....	128
3.2.6 Evaluation of NS5A-2a/CCAR2 cell colocalization	137

3.2.7 Quantification of CCAR2 in NS5A-2a expressing cells	147
3.3 Summary.....	150
Chapter 4: Mapping and characterization of phosphorylation sites on hepatitis	
C virus nonstructural 5A protein	151
4.1 Introduction and Rationale	151
4.2 Results	151
4.2.1 Expression of JFH1 NS5A to identify phosphoacceptor sites by mass spectrometry	151
4.2.2 Phosphoblatant and mimetic mutations of phosphoacceptor sites in pJFH1	161
4.2.3 Analysis of JFH1 RNA replication efficiency of phosphoblatant (alanine) and phosphomimetic (aspartate) mutation of positively identified NS5A phosphoacceptor sites.....	162
4.2.4 Impact of NS5A phosphoacceptor site mutations on the abundance and ratio of basally and hyperphosphorylated NS5A protein.....	166
4.2.5 Determining the effects of phosphoablatant (alanine) and phosphomimetic (aspartate) mutations of positively identified phosphoacceptor sites on JFH1 infectious virus production.....	172
4.2.6 NS5A from electroporated JFH1 is predominately hyperphosphorylated until 48 hpe.....	175
4.2.7 Reduction of p58 in SG JFH1 overtime.....	178
4.3 Summary.....	180
Chapter 5: Discussion.....	182

5.1 Identification of host cell – hepatitis C virus NS5A protein-protein interactions (PPIs) by tandem affinity purification and mass spectrometry/database searching	182
5.1.1 Generation of stable cell lines expressing HBH-tagged NS5A-2a.....	182
5.1.2 TAP optimization	184
5.1.3 Mass spectrometry identification of nTAP HBH-NS5A-2a-host PPI	187
5.1.4 Mass spectrometry identification of xdTAP HBH-NS5A-2a-host PPI.....	190
5.1.5 Reproducibility of NS5A-host cell PPIs	193
5.1.6 Confirmation of nTAP and xdTAP NS5A interacting candidates.....	196
5.2 Mapping and characterization of phosphorylation sites on hepatitis C virus NS5A protein	206
5.2.1 Phosphorylation requirements for NS5A from different genotypes	208
5.2.2 Conservation of phosphoacceptor sites identified in NS5A JFH1	209
5.2.3 Phospho-proteoform effects on HCV life cycle	210
5.2.4 NS5A phosphomutant effects on HCV RNA replication	211
5.2.5 NS5A phosphomutant effects on NS5A phosphoform protein abundance.....	214
5.2.6 NS5A phosphomutant effects on infectious JFH1 titers.....	217
5.2.7 NS5A phospho-proteoform abundance impact on the HCV lifecycle.....	218
5.2.8 NS5A/PI4KIII α Interaction	219
5.2.9 NS5A tyrosine phosphorylation.....	221
5.2.10 NS5A protein production from non-replicative phosphomutants versus GND	223
5.2.11 NS5A phosphorylation at early-time points post electroporation	223
5.2.12 Reduction of p58 levels in long-term passage of established SG JFH1 Huh7.5 replicon cells	225
5.2.13 Issues involving phosphorylation studies.....	226

5.3 Conclusions.....	228
5.4 Future Directions	230
Chapter 6: References	234
Chapter 7: Appendix 1.....	288
Chapter 8: Appendix 2: NS5A Phosphorylation Site Evidence	309

List of Figures

Figure 1. 1. Schematic representation of the HCV virion.....	10
Figure 1. 2. HCV genome.	13
Figure 1. 3. HCV life cycle.	16
Figure 1. 4. Structure of the HCV subgenomic replicon	17
Figure 1. 5. Organization of the HCV NS5A protein..	24
Figure 1. 6. NS5A interaction with the TNF α /TNFR-1 signaling cascade.....	29
Figure 1. 7. Protein identification by mass spectrometry.	44
Figure 3. 1. Cloning of the HCV NS5A-2a ORF into the pQCXIN-HBH vector..	94
Figure 3. 2. Production of GP2 293 stable cell lines expressing HBH tagged proteins..	95
Figure 3. 3. Evaluation of HBH-tagged HCV proteins expressed in GP2 293 cells.	97
Figure 3. 4. Identification of host proteins interacting with HBH-tagged NS5A-2a using the HBH native state (n) TAP protocol.....	98
Figure 3. 5. Chromatogram of NS5A-2a-HBH protein purified with cobalt purification using an FPLC.....	99
Figure 3. 6. Evaluation of different buffers for extraction and purification by native state TAP (nTAP).....	103
Figure 3. 7. Comparison of FPLC cobalt column and batch cobalt bead purifications of NS5A-HBH-2a tagged protein.....	105
Figure 3. 8. Comparison of 100ul and 25ul of streptavidin magnetic beads in the purification of NS5A-HBH-2a protein.	107
Figure 3. 9. Fully optimized nTAP protocol.....	108

Figure 3. 10. nTAP purified HBH-NS5A-2a and HBH-GFP for the identification of interacting proteins.....	110
Figure 3. 11. Coverage of NS5A and GFP by mass spectrometry.....	112
Figure 3. 12. Validation of a previously identified NS5A interacting protein, p53, by nTAP (cobalt-streptavidin)	113
Figure 3. 13. Specific interaction of NKRF with HBH-NS5A-2a throughout nTAP purification.....	118
Figure 3. 14. Chemical cross-linking and purification of samples expressing HBH-NS5A-2a..	121
Figure 3. 15. Non-specific capture of NS5A interacting TAP candidate proteins by FLAG antibody affinity resin co-precipitation	130
Figure 3. 16. Co-immunoprecipitation of FLAG-NS5A-2a with myc-tagged candidate proteins.....	133
Figure 3. 17. Validation of myc co-immunoprecipitation using FLAG-NS5a-2a and FLAG-GFP as prey proteins.	134
Figure 3. 18. Evaluation of CCAR2 interaction with NS5A-2a domains.....	136
Figure 3. 19. Colocalization of FLAG-NS5A-2a and CCAR2 in co-transfected cells..	138
Figure 3. 20. Colocalization of FLAG-NS5A-2a and CCAR2 in transfected 293TN and Huh7.5 cells viewed with a laser scanning confocal microscope.....	144
Figure 3. 21. Co-localization of NS5A-2a and CCAR2 in HBH-NS5A-2a GP2 293 cells, SG JFH1/Huh7.5 and JFH1-HT/Huh7.5 cells.	146
Figure 3. 22. Expression of NS5A-2a does not affect CCAR2 overall protein levels...	149

Figure 4. 1. Continuous gel electrophoretic separation of total protein from wt SG JFH1 replicon Huh7.5 cells.	154
Figure 4. 2. Expression of NS5A-HBH-2a from SG JFH1-NS5A-HBH replicon Huh7.5 cells	156
Figure 4. 3. Mass spectrometry spectrum of a peptide identifying phospho-T164 from NS5A peptide produced from dTAP purified HBH-NS5A-2a.	158
Figure 4. 4. Positively identified phosphoacceptor sites and residues identified on phosphopeptides from NS5A JFH1.	160
Figure 4. 5. Effects of NS5A-2a phosphomutants on the JFH1 HCV protein synthesis, RNA replication, and virus production.	162
Figure 4. 6. Effects of mutating sequences of phosphoacceptor sites in HCV JFH1 NS5A-2a protein identified through mass spectrometry on RNA genome replication..	165
Figure 4. 7. Evaluation of NS5A antibody NS5A-Ab02 for quantitative detection of NS5A-2a by Western blot.....	167
Figure 4. 8. Effects of cell confluency on NS5A-2a p58/p56 phospho-proteoform signal ratio in SG wt JFH1 Huh7.5 replicon cells	168
Figure 4. 9. Impact of the phosphoblatant and phosphomimetic mutations of NS5A-2a on the abundance of the p58 and p56 phospho-proteoforms.	171
Figure 4. 10. NS5A phosphoacceptor site mutation effects on HCV JFH1 released infectious virus.....	174
Figure 4. 11. Analysis of NS5A phospho-proteoforms early time-points post electroporation of JFH1 RNA.	177

Figure 4. 12. NS5A-2a p58/p56 ratio in SG JFH1 replicons after extended passage in cell culture.	179
Figure 4. 13. Introduction of wt SG JFH1 and JFH1 into SG JFH1-NS5A-HBH Huh7.5 cells.	180
Figure A 1. Conservation of NS5A phosphoacceptor sites	308

List of Tables

Table 1.1. FDA approved treatments for HCV infection.....	7
Table 3. 1. HBH-NS5A-2a interacting candidates revealed by nTAP Mass spectrometry/database searching	114
Table 3. 2. Mass spectrometry identified proteins from the xdTAP purification at different PFA concentrations to crosslink HBH-NS5A-2a protein interactions.....	122
Table 3. 3. Proteins identified by mass spectrometry/database searching from xdTAP purification of HBH-NS5a-2a expressing cells using different chemical cross-linker prior to capture.....	126
Table 4. 1. NS5A phosphorylation sites identified from each source where NS5A was expressed.....	152
Table A 1. Cloning primer nucleotide sequences.	288
Table A 2. Primary antibodies.....	291
Table A 3. FLAG and myc-tagged expression vector cloning.....	293
Table A 4. NS5A phosphoacceptor site mutagenesis primers.	297

Chapter 1: Introduction

1.1 Hepatitis C Virus

1.1.1 Burden

1.1.1.1 HCV Global Impact

Hepatitis C virus (HCV) is a hepatotropic pathogen present in approximately 2.8% of the world's population, newly infecting 3-4 million individuals every year (1). In approximately 80% of those afflicted, acute infection progresses to chronic disease which can result in the development of hepatic steatosis, fibrosis, cirrhosis and hepatocellular carcinoma (HCC) (2). Globally, approximately 27% of liver cirrhosis, 25% of HCC and 366,000 deaths annually are attributed to HCV infection (3). End-stage liver cirrhosis due to HCV infection is now the leading indicator for liver transplantation in developed countries (4). Data from the USA has determined that HCV related mortality rates increased more than 50% from 1999-2007, and that 50% of HCC cases were due to viral infections. These continually rising HCC incidence rates have led HCC related fatalities to become the fastest growing cancer-related deaths (5,6). HCV and is now responsible for more fatalities in the USA than human immunodeficiency virus (HIV) (7).

HCV morbidity and mortality forecast modeling based on 2005 incident rates predicted a dire future. If infections were left undiagnosed and untreated, by 2060 HCV would be responsible for cirrhosis in 1.76 million people, resulting in 400,000 cases of HCC and one million deaths (8). The incidence of HCV is concentrated in the baby boomer

population, born between 1945-1964. The spread was primarily due to the lack of adequate blood screening methodologies prior to 1992. The CDC has recommended screening the entire US baby boomer population due to the often asymptomatic nature of the infection (9). In contrast, a Canadian-based task force recommended identifying those at increased risk of HCV in order to implement screening (10). This decision has been met with disappointment from many prominent Canadian scientists citing the fact that risk-based approaches have failed previously, that harms to the patient were overemphasized and that the potential for patient isolation were alleviated by the development of new direct-acting antivirals (DAA) and their price reductions (10).

HCV is a bloodborne pathogen and transmission is primarily through injection drug use although unsafe healthcare practices, vertical transmission, and sexual contact also contribute (11). Currently, no HCV vaccine exists and, until recently therapy was limited to a combination of pegylated- α -interferon (IFN) and ribavirin with varying efficacy (12). Despite the dire statistics surrounding HCV, dramatic success with recently approved DAAs have achieved a sustained virological response (SVR) (absence of HCV genome detection 12 or 24 weeks post treatment) in the majority of patients enrolled in clinical trials thus “curing” individuals of the infection. Although extremely efficacious, high drug and administration costs coupled with the potential for drug resistance indicate that continued HCV studies and the development of novel treatment modalities will remain in high demand.

1.1.1.2 HCV Pathogenesis

Humans, chimpanzees and possibly tree shrews are the only organisms susceptible to HCV infection with hepatocytes serving as the primary cellular target (13). Other cell types support viral replication, albeit at extraordinarily low levels. HCV replication has been observed in non-hepatocytes of infected patients and cell culture models including: cholangiocarcinoma cells (bile duct epithelial cells) (14), endothelial cells of the blood-brain barrier (15), cerebral spinal fluid (16), epithelial intestinal cells (17), B cells (18–20) and T cells (21–24).

HCV infection has been able to spread relatively easily as the acute phase of infection is often asymptomatic leaving afflicted individuals undiagnosed. If symptoms are present, they are often nebulous and may include malaise, nausea, fatigue, anorexia, and jaundice (25). There are very rare occurrences where acute HCV infection can result in fulminant hepatitis, a prodigious liver necrosis leading to impairment of liver functions and encephalitis but these cases are exceptional (26). In 15-20% of acute cases, there is spontaneous clearance of the virus within one week to three years after the original infection and this clearance is believed to be the result of a vigorous T cell assault (27,28). For those individuals that are unable to clear HCV during the acute phase, the infection becomes persistent and progresses to a chronic disease in 80-85% of those afflicted (2). Liver disease progression is gradual and protracted in chronic HCV infection and can take 20 years for damage to become apparent (29).

Failure of the host immune response to eliminate persistent HCV infection results in chronic liver inflammation that activates regenerative mechanisms leading to fibrosis and eventually liver cirrhosis (30). The estimated incidence of cirrhosis in HCV patients was found to be 20%, 20 years following infection and 41% at 30 years post infection (31). HCC is a major risk factor for individuals with HCV-induced cirrhotic livers with an annual rate increase per year of up to 4% (5). HCV is considered to be carcinogenic both by direct expression of the viral proteins and indirectly through chronic inflammation, oxidative stress and increasing hepatocyte proliferation (32). There is a discrepancy in the risk of developing HCC based on infecting HCV genotype with genotype 1b infections representing a higher risk factor (33). Steatosis, (accumulation of fatty acids/lipids in the liver) is a frequent complication observed in HCV infections, with a higher prevalence observed in genotype 3 infections (34). A single point mutation in the HCV Core protein, Y164F, *in vitro* resulted in a significant increase in cellular lipid droplet accumulation when compared to wild-type (wt) virus (35).

In spite of HCV's propensity for hepatocyte infection, several extrahepatic complications have been associated with HCV infection and include insulin resistance, type 2 diabetes (36–38), non-Hodgkin lymphoma (39,40), mixed cryoglobulinemia (41), renal disease (42) and cognitive dysfunction (43). However, it has not been elucidated whether the extrahepatic manifestations of HCV infection are the result of direct virus infection of the tissue or is occurring indirectly via the host immune response and impaired liver functions.

1.1.1.3 HCV Treatment

One of the largest hurdles in treating HCV infection is the identification and diagnosis of infected individuals. It is estimated that 44% of infected individuals unknowingly harbour the virus and are chronic carriers (44). Currently, there is no protective or neutralizing vaccine or prophylactic measure capable of preventing HCV infection, and thus treatment is applied post-exposure. Historically, HCV therapy was limited to a combination of pegylated- α -interferon (IFN α) and the non-specific ribonucleoside analog, ribavirin, with varying efficacy: 40% response for genotype 1 and 80% for genotype 2 or 3 infections (12). Treatment was typically accompanied by severe side effects and was further complicated by the presence of liver damage.

The HCV epidemic and the expectant rise in HCV morbidity and mortality rates spurred efforts to develop antiviral medications. 2011 heralded a new age of HCV treatment when two HCV DAAs, Boceprevir and Telaprevir were approved for clinical use in combination with IFN α and ribavirin (45,46). Unfortunately, DAA-resistant strains quickly emerged due to the rapid and large production of virus daily coupled with the high mutation rate associated with the viral polymerase (47). As therapeutic targets, three HCV nonstructural (NS) proteins; NS3 (protease), NS5A, and NS5B (polymerase) have been successfully pursued by targetting the enzyme's active site (48), binding the protein directly (49) or halting genome replication (50), respectively. These compounds include: Asunaprevir, Boceprevir, Telaprevir, Paritaprevir, Grazoprevir, Simeprevir, Vaniprevir, and Voxilaprevir (NS3) (51), Daclatasvir, Ledipasvir, Ombitasvir, Elbasvir, and Velpatasvir (NS5A) (49) and Sofosbuvir and Dasabuvir (NS5B) (50) (Table 1.1).

Successful anti-HCV compounds need to achieve an SVR, exclude the need for IFN treatment, and can be functional even in a damaged liver (52). However, HCV can develop resistance to DAAs due to the error-prone nature of the NS5B polymerase in combination with selection of resistant quasispecies variants (53,54). The genetic barrier to resistance of the first generation of NS3 and NS5A DAAs and non-nucleoside inhibitors of NS5B proved to be quite low in *in vitro* based systems with several resistance mutations observed (55). Due to the high likelihood of developing genetic resistance, the most successful treatment regimens use a combination of DAAs targeting more than one viral protein. Epclusa which incorporates an NS5A inhibitor, and a nucleoside analog reported a SVR in 99% of liver non-complicated patients (56). Remarkably the treatment was broadly effective in a genotype independent manner (56). This was a significant achievement as many of the previous and current treatments were more successful with specific genotypes (Table 1.1). One of the greatest hurdles to DAA treatment is affordability. Simeprevir, Sofosbuvir, and Ledipasvir/Sofosbuvir treatments range in price from \$80,000 to \$94,500 for a 12-week course (57,58). As new drugs come to market, price competition will help in alleviating some of the associated costs.

Table 1.1. FDA approved treatments for HCV infection. Information adapted and compiled from review article: Li and De Clercq, 2017 (56).

Treatment	FDA Approval Date and Genotypes Approved	Average SVR12 from clinical trials without cirrhosis(56)
Victrelis® IFN α /RBV + Boceprevir	May 2011 Genotype: 1	Discontinued
Incivek® IFN α /RBV + Telaprevir	May 2011 Genotype: 1	Discontinued
Sovaldi® RBV + Sofosbuvir or IFN α /RBV + Sofosbuvir	December 2013 Genotypes: 1, 2, 3, 4	G1: 87.6% G2: 95.6% G3: 91.3% G4: 92.3% G5: 100% G6: 100%
Olysio® Simeprevir + Sofosbuvir or IFN α /RBV + Simeprevir	November 2013 Genotypes: 1, 4 Genotype: 1	G1: 93.8% or 65.9% G4: 97.9% or 66.6%
Harvoni® Ledipasvir + Sofosbuvir	October 2014 Genotypes: 1, 4, 5, 6	G1: 96.1% G4: 91.6% G5: 96.8% G6: 95.6%
Viekira Pak™ Ombitasvir + Paritaprevir + Ritonavir + Dasabuvir	December 2014 Genotype: 1	G1: 96.9%
Technivie™ Ombitasvir + Paritaprevir + Ritonavir or +RBV	July 2015 Genotype: 4	G1: 95% G4: 90.9% or 100%
Daklinza™ + Sovaldi® Daclatasvir + Sofosbuvir	July 2015 Genotypes: 1, 3	G1: 99% G3: 96.3%
Zepatier™ Grazoprevir + Elbasvir	January 2016 Genotypes: 1, 4	G1: 95.5% G4: 94.1%
Epclusa® Sofosbuvir + Velpatasvir	June 2016 Genotypes: 1,2,3,4,5,6	G1: 98.7% G2: 99.5% G3: 96.8% G4: 98.9% G5: 96.5% G6: 100% G7: 100% ** one patient

1.1.2 HCV Virology

1.1.2.1 HCV Diversity

HCV was postulated to be a novel virus in 1975, responsible for inducing transfusion-induced hepatitis in patients negative for hepatitis-A and B antigens (59). In 1989 the virus was isolated, sequenced, and was formally identified as the agent responsible for non-A, non-B hepatitis (60). HCV was classified into the *Hepacivirus* genus of the *Flaviviridae* virus family (61). Seven genotypes and 67 subtypes have been recognized with genotypes differing by 31-33% and subtypes differing by 12-20% at the nucleotide level (61,62). Worldwide, the genotypic distribution of HCV varies. Genotype 1 is the most prevalent and along with genotypes 2 and 3, are found globally. Genotypes 4, 5, 6 and 7 are found less broadly with discrete areas in Africa, the Middle East, and Southeast Asia (63). HCV circulates in afflicted individuals as a heterogeneous population of closely related quasispecies, the result of error-prone generation of nascent genomes combined with selection of these sequences for both viral function and immune evasion (53). The HCV polymerase, NS5B, contributes to this diversity, as it lacks proof-reading ability and is particularly error-prone with the propensity to produce uracil to cytosine substitutions. The error rate is estimated to be 3.5×10^{-5} per replication cycle (54). Infection of new individuals creates an HCV quasispecies genetic bottleneck whereas only virions that have successfully avoided antibody-mediated neutralization and display an efficient entry phenotype are selected for new infection (64).

The origin of HCV remains unknown, as a zoonotic source has never been conclusively determined. Recently, two hepaciviruses were identified as HCV homologs in both dogs

and horses with up to 50% nucleotide consensus, but no evidence of zoonotic transmission, even among highly susceptible veterinarians, has been documented (65,66).

1.1.2.2 HCV Virion

HCV exists as a lipovirion. The virion is composed of viral RNA encapsulated by the Core protein and is cloaked with a host-derived lipid envelope spiked with the two HCV glycoproteins, E1 and E2, which exist as a heterodimer. HCV virions appear as pleomorphic particles with an asymmetrical internal structure and a smooth surface when viewed by electron microscopy (67). The lipovirion is the result of tight association of the core virion with serum derived lipoproteins whose function is to transport lipids in serum (68). Two models have been proposed for the structure of this particle: first, inclusion suggests a particle where the lipids and accompanying proteins are incorporated into the virion (69) and second, a model where the association is peripheral and is facilitated by apolipoproteins (70). An inverse correlation between buoyancy and HCV infectivity exists. Low-density virus isolated from human plasma, chimpanzee or hepatoma cell culture have a higher infectivity, and therefore the most highly infectious HCV particles are associated with very low density and low-density lipoproteins (71–73). However, the associated apolipoproteins differ between virions isolated from patients or cell culture. Serum-derived virus contains apoA1, apoB48, apoB100, apoC1 and apoE whereas cell culture derived HCV include apoE, apoC1, variable apoB (74), with apoE being essential for infectivity (75). A schematic representation of the HCV virion and two lipoprotein association models is presented in Fig.1.1.

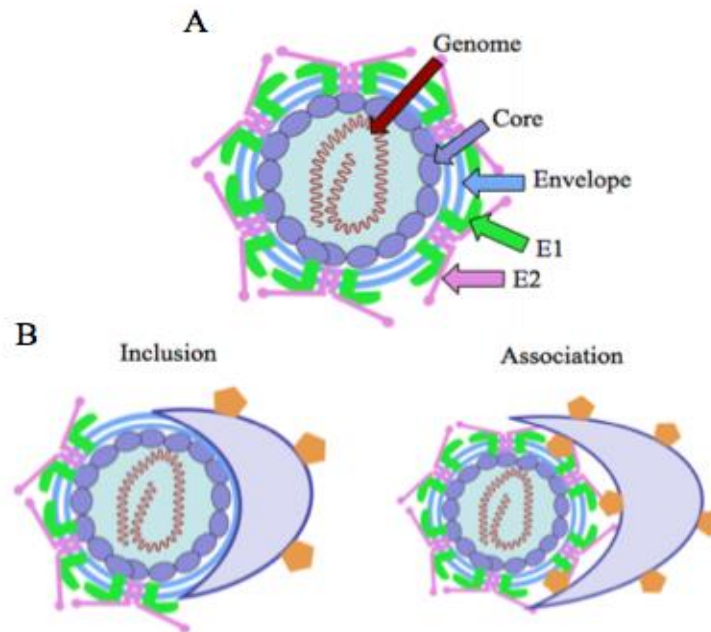


Figure 1.1. Schematic representation of the HCV virion. **(A)** The positive strand RNA genome (red) is contained within the viral capsid by the Core protein (purple). A lipid envelope (blue) is derived from host membranes, which is studded with the E1 (green) and E2 (pink) glycoproteins. **(B)** HCV lipovirion association models. There currently are two hypothesized as to how the HCV virion associates with host lipoproteins. The inclusion model (**left**) proposes that lipoproteins incorporate directly into the virion (69). The association model (**right**) suggests that lipoproteins are peripherally attached to the virion. Image modified from Lindenbach et al., 2013 and Vieyres, 2014 (74,76).

1.1.2.3 HCV Genome

The HCV genome consists of a 9.6 kb single-stranded positive sense RNA encoding for a single open reading frame (ORF) of ~3000 amino acids flanked by 5' and 3' untranslated regions (UTRs) (Fig.1.2) (77). The positive sense RNA genome provides a replication template for negative polarity RNA strands intermediates required for genome amplification. The 5' and 3' termini of the RNA genome are highly ordered containing complex secondary structures that are involved in regulating the HCV life cycle. The 5' UTR contains an internal ribosome entry site (IRES), a structural motif that initiates cap-

independent translation. Whereas canonical eukaryotic translation recruits ribosomes and proteins required for host protein translation via the 5' terminal cap on mRNA, (78,79) the HCV IRES itself directly recruits the 40S subunit of the ribosome followed by eIF3 and the eIF2-GTP-tRNA complexes (80).

The 3' UTR possesses a polypyrimidine/polyuridine tract that terminates in three stem loops described as the 3'X box regions, with genome replication believed to be initiated at this site (81). The 3'UTR has also been shown to stimulate IRES-mediated translation of the viral polyprotein (82). A stretch of RNA within the NS5B coding region (5BSL3.2) binds to a region within the 3'UTR to form a "kissing loop" structure required for RNA replication (83,84). The 3'UTR-5BSL3.2 interaction may circularize the genome and enhance replication by allowing the replication complexes to remain continuously in contact with the genomic template (84). A functional link between the two distant viral termini has been suggested whereby elements in the 5' UTR IRES bind the 5BSL3.2 cruciform structure in NS5B to mediate circularization of the HCV genome and modulate HCV protein translation (85) (Fig. 1.2).

The HCV polyprotein is cleaved co- and post-translationally by both host and viral proteases to liberate ten mature HCV proteins. Three structural proteins include Core, E1, and E2. The Core protein is an RNA-binding protein that envelopes the HCV genome creating the viral capsid that is post-translationally cleaved at the C-terminus into a 21 kDa mature protein (86). A ribosomal frameshift in the Core protein reading frame results in the production of a 17 kDa F protein (87). E1 and E2 are 30 kDa and 64

kDa highly glycosylated proteins anchored within the HCV envelope as a disulfide-linked covalent heterodimer that engages host cellular receptors facilitating viral entry (88). p7 is a small hydrophobic protein that hexamerizes to form a viroporin ion channel. While dispensable for RNA replication, p7 is critical for HCV assembly and release (89,90). NS2 is a 23 kDa cysteine protease that cleaves the junction between NS2 and NS3. It has intrinsic protease activity only requiring residues 1-2 from NS3, but its activity is significantly enhanced in the presence of residues 81-213 of NS3 (91). The 70 kDa NS3 protein contains both a serine protease domain at the N-terminus and an NTPase/helicase domain at the C-terminus. Along with its cofactor, NS4A, NS3 is responsible for the liberation of the HCV nonstructural proteins (92,93). The cofactor, NS4A, is 8 kDa and, in addition to enhancing the protease activity of NS3, also contains a transmembrane alpha helix that tethers the NS3/4A complex to membranes (94). NS4B is a 27 kDa integral membrane protein with an undefined function in the viral life cycle but has been reported to have NTPase activity (95). NS4B also triggers host membrane alterations leading to the formation of localized vesicles termed the “membranous web” that presumably provides a platform for HCV replication (96). NS5A is a phosphoprotein of undefined function that exists, by SDS-PAGE analysis, in both a basal (56 kDa) and a hyperphosphorylated (58 kDa) form and is essential for viral replication and assembly (97–99). The RNA-dependent-RNA polymerase, NS5B, is a 68 kDa protein containing characteristic fingers, palm and thumb subdomains and a typical GDD polymerase active site that is responsible for HCV genome replication (100) (Fig.1.2).

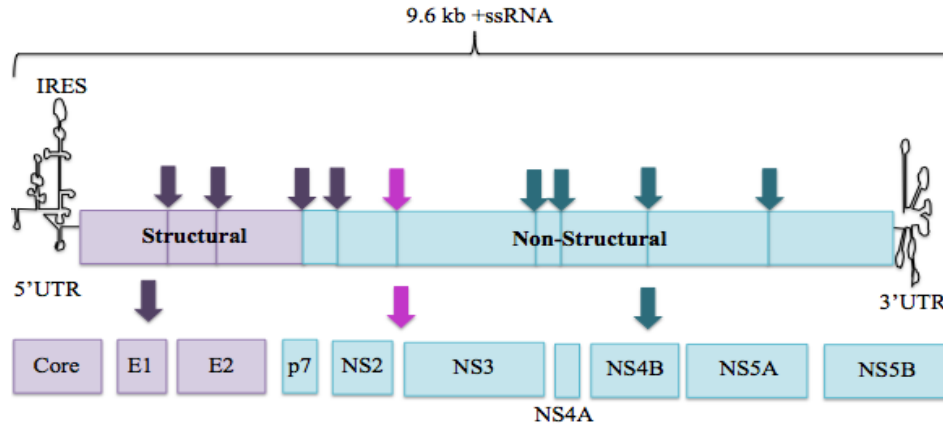


Figure 1. 2. HCV genome. HCV has a 9.6 kb single-stranded positive-sense RNA genome. Translation of the viral polyprotein is driven by the IRES located in the 5'UTR. The polyprotein is cleaved co- and post-translationally by host proteases (purple arrows), the viral NS2 autoprotease (pink arrow) and the viral NS3/4A protease (teal arrows) to release ten mature viral proteins. Cores, E1, and E2 are structural proteins that compromise the capsid and envelope glycoproteins, respectively (purple). The nonstructural proteins, p7, NS2, NS3, NS4A, NS4B, NS5A, and NS5B, are required at different steps of viral replication and assembly (blue). Adapted from Bartenschlager et al., 2013 (101)

1.1.3 HCV Life Cycle

HCV entry into host cells is mediated by a series of interactions between the virion and cellular receptors. Initial attachment of HCV to a cell surface is mediated by a low-affinity interaction with heparin sulfate proteoglycans (HSPG) via positively charged residues within E2 and the negative residues within glycosaminoglycans and through virion-incorporated apoE interacting with the Low-density lipoprotein receptor (LDLR) (102–105). The cellular receptor, Scavenger receptor class B type I (SR-B1) is involved in the attachment process by interacting with the HCV-associated lipoproteins and by utilizing its lipid transfer activities to both expose and bind the E2 glycoprotein (106–108). With E2 now unsheathed, the glycoprotein can bind the receptor cluster of differentiation 81 (CD81) (109,110).

Several other HCV entry factors have been identified and include: occludin (OCLN) (111,112), transferrin receptor 1 (TfR1) (113), Niemann-Pick C1-Like 1 (NPC1L1) (114), epidermal growth factor receptor (EGFR) and ephrin type-A receptor 2 (EphA2) (115). Binding of E2 to CD81 and antagonism of Ras and Rho signaling through EGFR promotes the lateral movement of attached virions to cellular tight junctions where CD81 contacts the tight junction protein, Claudin-1 (CLDN1) (115–117). This interaction promotes the internalization of HCV through receptor-mediated endocytosis into clathrin-coated, Rab5 containing early endosomes (117,118). The HCV envelope fuses with the endosomal membrane upon acidification of the endosome that is potentially mediated by a change in conformation in putative class II fusion peptide within E1, and releases the HCV genome into the cytoplasm (119,120) (Fig.1.3). HCV may also spread to naïve cells through direct cell-to-cell transmission relying on the same entry factors (CD81, CLDN1, OCLN, SR-BI, and LDLr) to facilitate entry (121,122) (Fig.1.3).

With the positive-polarity RNA genome released from the virion, translation and proteolytic processing results in the generation of 10 proteins, which become membrane associated either by transmembrane integration or through protein-lipid bilayer association. The HCV proteins, principally NS4B, induce vesicular alterations in the membranes of the endoplasmic reticulum (ER), termed the membranous web, where the HCV NS proteins and RNA accumulate to produce the HCV replication complex (96,123). The NS5B polymerase produces negative strand genome to serve as replication templates for positive-sense RNA genome that are packaged into nascent virions,

translated, or utilized for replication. The control over which template is used for each function or how the switch from replication/translation to packaging occurs is ill defined.

The viral assembly process is completed as the newly produced virions bud through the ER. The Core protein, located on the surface of cellular lipid droplets, in complex with NS5A, is recruited to nascent viral particles egressing from the ER. NS2 works as a mediator to bring together a complex of E1-E2, p7, and NS3/4A and in turn, the p7-NS2-NS3-4a complex recruits Core from the lipid droplets to the sites of virion assembly (124–127). RNA is delivered to the Core protein present on lipid droplets and initiates formation of the nucleocapsid (124,128). E1/E2 are trafficked to the ER, possibly by interaction with NS2, and form a heterodimer complex that passes through the Golgi to obtain their glycan modifications and impregnates the viral envelope (88,127,129). The p7 protein is believed to function as an ion channel to neutralize the acidic pH of the host secretory compartment as HCV utilizes the host secretory pathway to exocytose the nascent virions (130). Through exocytosis HCV acquires its lipid envelope and associated lipoproteins becoming lipidated in a post-ER compartment and by the same process as VLDL synthesis (131) (Fig.1.3).

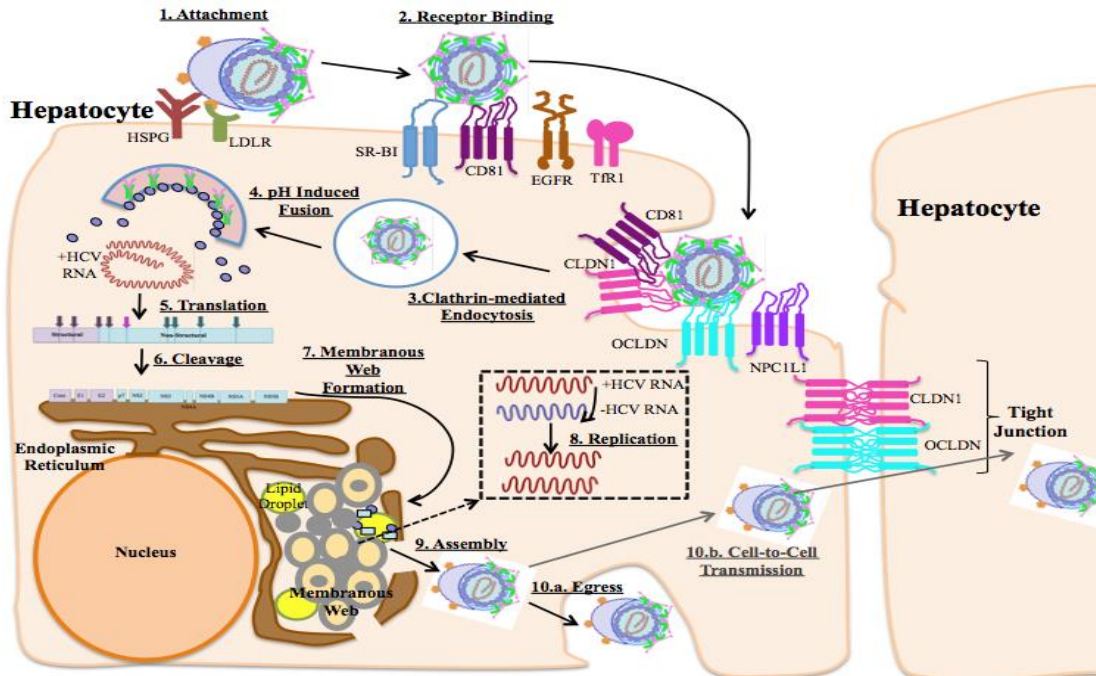


Figure 1. 3. HCV life cycle. (1) HCV hepatocyte entry is mediated by the initial attachment of the lipoviroparticle binding HSPG, LDLR, and SR-B1. (2) HCV glycoproteins E1/E2 interact with several cellular receptors CD81, TFR1, NPC1L1, EGFR and EphA2. (3) Binding of E2 to CD81 promotes lateral movement of CD81 and attached virions move to cellular tight junctions where CD81 and CLDN1 initiate the internalization of HCV through receptor-mediated endocytosis into clathrin-coated, Rab5-containing early endosomes. (4) Fusion between the HCV envelope and the endosomal membrane is triggered by acidification releasing the positive sense RNA genome into the cytosol and allowing (5) direct translation of the HCV polyprotein driven by the IRES. (6) Ten viral proteins, three structural (Core, E1, E2) and seven non-structural (p7, NS2, NS3, NS4A, NS4B, NS5A, NS5B) are produced by host and cellular proteases and associate with host ER membranes. (7) NS4B induces the formation of the membranous web by altering host ER membranes. (8) The HCV replication complex is formed within the membranous web where the NS5B viral polymerase copies the positive strand genome into negative strand genome. These negative strand RNAs serve as templates for generating positive sense genomic RNA which is subsequently packaged into nascent virions, translated or used for further genome amplification. Nascent virions are assembled while budding through the ER where interaction between NS2-p7 NS3/4a recruits Core/NS5A on the surface of lipid droplets to the replication complexes. (9) RNA is loaded onto the Core protein located on lipid droplets to form the nucleocapsid. E1/E2 are recruited to the newly acquired viral envelope. HCV utilizes the host secretory pathway to exocytose the virions and the p7 ion channel buffers the process maintaining a neutral pH. (10.a.) Nascent HCV particles become lipidated and obtain their low buoyancy using the VLDL intra- and extra-cellular maturation and secretion pathways. (10.b.) Alternatively, HCV may spread to naïve cells through direct cell-to-cell transmission. Figure adapted from Lindenbach et al., 2013 and Bartenschlager et al., 2013 (74,101).

1.1.4 HCV Cell Culture Models

Historically, HCV infection has been difficult to study because of an inability to propagate the virus in cell culture. Considerable efforts were made to overcome these deficits by developing systems modeling HCV infection. The first breakthrough in a cell culture system was the development of an HCV Con1b subgenomic (SG) replicon. The SG replicon is a bicistronic construct which contains an HCV IRES that translates neomycin phosphotransferase (neomycin/G418 drug resistance) followed by an encephalomyocarditis virus (EMCV) IRES which drives expression of HCV structural genes (NS3-NS5B) (132) (Fig. 1.4). Upon transfection of SG replicon RNA into a human hepatoma cell line (Huh-7), the RNA is translated and initiates autonomous replication of viral RNA. Cells with productive SG RNA replication can be selected for with the drug G418 whereas cells not supporting RNA replication quickly lose the input RNA and the ability to produce the necessary drug resistance protein (132).

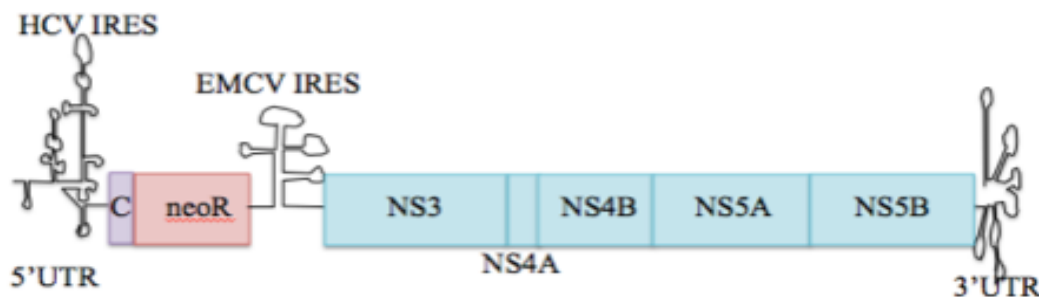


Figure 1. 4. Structure of the HCV subgenomic replicon. The HCV subgenomic replicon is a bicistronic positive sense RNA molecule. The IRES present at the 5' end allows for the direct translation of a neomycin resistance cassette allowing for drug selection of cells containing the subgenomic replicon. The EMCV IRES is responsible for driving translation of the HCV nonstructural proteins. Once introduced into a susceptible cell line (Huh-7, Huh7.5 or Huh7.5.1) the SG replicon perpetually replicates HCV NS RNA without any production of infectious virus thereby specifically modeling HCV replication. Adapted from Woerz, et al., 2009 (133). In addition, full-length replicons have the same general structure except that the EMCV IRES drives the entire HCV coding region Core-NS5B.

Serial passage of SG replicons in cell culture, accompanied with continuous selection, typically causes the accumulation of mutations in the NS proteins resulting in SG replicons with enhanced replicative capacity. Single replication enhancing mutations were identified in the Con1b replicons in the central region of NS5A, NS4B and NS5B as well as synergistic mutations in the N-terminus of NS3 and NS5A-NS5B (134–139). The most potent Con1b mutant harbored an S2204I mutation in NS5A that increases replication by 10,000 fold also causing a significant reduction in the hyperphosphorylated form of NS5A known as p58 (134,140,141). Replication enhancing mutations appear to be specific to the cell culture model as these mutations are unable to produce viable infectious HCV when injected into chimpanzee models. Where the mutated viruses do propagate in the animal model, it is due to reversion to a wild-type sequence (142,143).

Huh-7 cells that are permissive for SG replicons (132) and were originally isolated from an epithelial cell colony from hepatoma tissue surgically removed from a Japanese male with well differentiated HCC (144). However, over time Huh-7 cells have diverged from the original line resulting in disparate phenotypes that differ in their ability to support productive HCV replication (145). This may have led to a number of the discrepancies seen in the literature regarding basic HCV cell culture analysis.

An attempt to improve upon the Huh-7 cells came about with the development of Huh7.5 cells. These cells were derived from Huh-7 cells that were supporting a HCV Con1b SG replicon. The cells were cured of replicon by treatment with IFN and the resulting cells when re-transfected with SG replicons were found to be more capable of supporting HCV

replication (146). This clearly showed that, in addition to the viral sequence, the host environment is also crucial for productive viral replication. The increased susceptibility of Huh7.5 cells is possibly due to an impediment in the host innate immune system resulting from a T155I mutation in the double-stranded RNA helicase enzyme, retinoic acid-inducible gene I (RIG-I) that leads to ineffectual interferon regulatory transcription factor 3 (IRF3) signaling (147). Huh7.5.1 cells were a subsequent cell line developed by curing Huh7.5 cells of a SG Con1b replicon with IFN further increasing susceptibility to HCV replication. It is also believed that this increase in HCV replication support is due to additional deficiencies in the innate immune response (148).

While SG replicons became the standard for HCV studies, a model that allowed analysis of the complete virus replication cycle, from infection to virus production was lacking. A monumental stride was made with the discovery of the HCV strain JFH1, the first HCV isolate capable of producing infectious virus in cell culture without adaptive mutations (Fig.1.4). The JFH1 strain (Japanese fulminant hepatitis 1), was isolated from a 32-year old Japanese male with fulminant hepatitis and when sequenced and phylogenetically analyzed, clustered with HCV genotype 2a sequences (149). A SG replicon was constructed utilizing the JFH1 sequence and was found to be the first replicon that replicated with reasonable efficiency in the absence of cell culture mutations (150). The most salient feature of JFH1 was that wt viral RNA when introduced into cell culture produced infectious progeny capable of generating infection in chimpanzees (73,148,151). Attempts to characterize the uniqueness of JFH1 have been inconclusive implicating elements across almost the entire HCV ORF with some studies highlighting

sequences within NS3, NS5A, NS5B and Core (100,152–155). JFH1 produces moderate titers typically $<10^3$ ffu/ml in cell culture leading several groups to serial passage JFH1 replicons and virus to generate cell-culture replication enhancing mutations (155–159). Two intra-strain chimeric HCV viruses generated from splicing the N-terminal to NS2 region of strain J6 (another genotype 2a virus) with the NS3 to C-terminus region of JFH1 (J6/JFH1) or utilizing a splice site within NS2 (Jc1) replicate, spread and produce more viral particles than JFH1 alone (73,160,161).

A further improvement has been made in cell culture models when Huh7.5 cells were transduced with a cDNA library and identified SEC14L2 as a factor promoting replication of HCV from patient samples (162). Stable expression of SEC14L2 in Huh7.5 cells supported 1a, 1b and J6 replicons as well as 1a, 1b and 3a viruses from patient sera although replication levels are still weak overall (162).

1.1.5 HCV Animal Models

In 1997, RNA transcribed from cDNA clones of HCV genotype 1a strain H77 was used to infect chimpanzees and thus established the first, albeit very inconvenient, animal model (163). Since using chimpanzees for HCV research is difficult, expensive and highly restricted the development of additional small animal models has been a high priority research endeavor. Xenograft transplantation of human hepatocytes into immunodeficient mice expressing a plasminogen activator transgene were developed as the first murine model to sustain HCV infection (164). However, experimentation with these mice is susceptible to human donor variability, low scalability and high cost. There

has been some success in creating humanized mice containing human CD81 and OCLN genes that allowed HCV entry (165). Further refinement by the addition of an immune suppressant allows recapitulation over the entire HCV life cycle (166). Unfortunately, this model is still expensive and is not widely available. Tree shrews (*Tupaia belangeri chinensis*) have recently emerged as a potential small animal model for HCV infection as 14 of 30 animals were successfully infected with J6/JFH1 virus (167). While many molecular tools would need to be developed for use in tree shrews, there is potential to develop these animals for laboratory use.

1.2 Non-Structural 5A Protein

NS5A is a viral phosphoprotein that is vital for the HCV life cycle as it is essential for replication, virion production and for modulating the host cell to create an environment favorable for the HCV life cycle. NS5A is also the target for a number of DAAs. Despite the integral requirement of NS5A to HCV propagation and its targeted role in drug therapy, its mechanism of function in each every case has remained ill defined.

1.2.1 NS5A Structure and Function

NS5A is composed of three discrete domains separated by low-complexity sequences (LCSI and LCSII) and is located within the cell cytoplasm anchored to membranes via an N-terminal amphipathic helix (168–171) (Fig.1.5.A). Crystal structures of domain 1 have revealed that NS5A contains a zinc-coordination motif, a putative RNA-binding groove, and that functional NS5A exists as a dimer in open, closed or multiple conformations (172–174) (Fig.1.5.B). Domain 1 is required for RNA replication and facilitates NS5A's

interaction with Core and LDs, a key provision for viral assembly (128). The crystal structure of domain I revealed that the dimer creates a pocket that can facilitate RNA binding and that a single zinc atom is coordinated by cysteine residues (C39, C57, C59, C80) within the N-terminus (172) (Fig.1.5.B, left). Domains 2 and 3 are intrinsically disordered which may provide a flexible region conducive to phosphorylation and multiple protein interactions (175–177). Domain 2 is essential for viral replication but is dispensable for virion production (178,179). Domain 3 is crucial for HCV assembly (98,180). Domains 2/3 have both demonstrated some plasticity as deletions have not impaired RNA replication, and viable infectious virus has been cultivated containing large insertions in D3 (134,141,181–183). Based on these observations it has been suggested that numerous NS5A dimers may anchor themselves to membranes via the amphipathic helix creating a long basic cleft suitable for coordinating the movement of HCV RNA during viral RNA replication and packaging (184). In support of this, previous studies have confirmed the RNA binding capacity of NS5A (185).

HCV produces only ten proteins and given a comparison with other viruses who produce many more; it suggests multiple roles for each protein. Moreover, a previous study determined that less than 5% of the HCV NS proteins participated in active HCV replication (186). This begs the question: what other function(s) does NS5A have?

By SDS-PAGE analysis, NS5A appears as two forms with molecular weights of 56, and 58 kDa. In JFH1 there is an 18 amino acid insertion near the C-terminus of NS5A that increases its size on SDS-PAGE to 63 and 65 kDa. For historical reasons, the JFH1

phospho-proteoforms are still referred to as “p56” and “p58”, representing the basally phosphorylated and hyperphosphorylated states (187). Phosphorylation of NS5A is believed to occur post-cleavage primarily on serine but also on a small number of threonine residues (188). The function(s) of NS5A phosphorylation remains unknown, but hypotheses have suggested roles in subcellular localization, virus RNA replication and packaging, and effects on cellular physiology (189).

NS5A is localized to the cytoplasm associated with membranes of the ER and Golgi at the perinucleus, the mitochondrial inner membrane and matrix and also on LDs via interaction with the Core protein (128,171,190–192). Interestingly, NS5A contains a stretch of proline and valine residues at its C-terminus (positions 354-362, Con1b accession numbering) that is characteristic of a nuclear localization signal (NLS) and in fact, has functional activity when this sequence is added to various proteins (193) (Fig.1.5.A). N-terminal truncated versions of the NS5A protein have been shown to transit to the nucleus and activate transcription (193,194). It is likely that the amphipathic sequence in the N-terminus prohibits nuclear transit by tethering the protein to the membrane. As full-length NS5A is not observed in the nucleus of cultured cells, the biological relevance of these observations are not clear (128,171,190,191). The NS5A NLS region supports interaction with nuclear pore complex proteins (NUPs) resulting in the relocation of the NUPs and their associated cargo to the membranous web likely to aid in the establishment of the virus replication complex (195,196).

NS5A amino acids 237-276 in genotype 1b NS5A have been termed the Interferon Sensitivity Determining Region (ISDR). Early studies provided evidence that ISDR

substitutions lead to favorable outcomes in genotype 1b infected patients treated with IFN α therapy although other studies have not been able to confirm these observations (197–200) (Fig.1.5). NS5A also contains Class I and Class II polyproline motifs present within LCS I and II, respectively which are capable of interacting with host proteins containing a Src homology 3 (SH3) domain (201–204) (Fig.1.5). There are also three Bcl-2 homology domains (BH3, BH1, and BH2) that belong to the Bcl-2 family of proteins involved in cellular apoptosis regulation (205) (Fig.1.5).

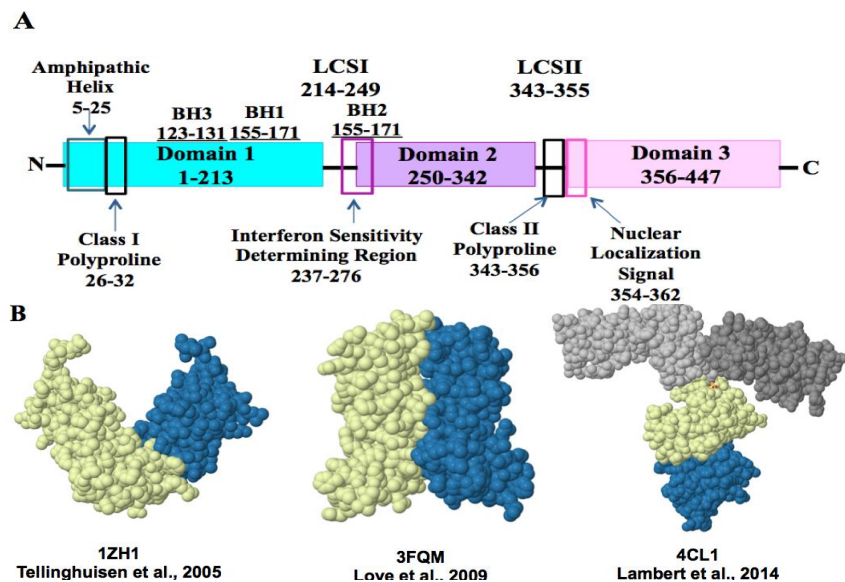


Figure 1. 5. Organization of the HCV NS5A protein. (A) The NS5A protein is composed of three domains (D) separated by two low-complexity sequences, LCS I and LCS II. D1 contains an amphipathic helix that directs NS5A membrane association (168–170). NS5A contains two characteristic polyproline motifs, a Class I and Class II motif known to interact with host protein SH3 domains (201–204). Three Bcl-2 homology domains exist within the NS5A sequences (BH1, BH2, BH3) (205) as well as a nuclear localization signal (193). A controversial interferon sensitivity determining region (ISDR) is present within LCS I and D2 where specific amino acid sequences are believed to affect the virus’ response to IFN (197–200). All numbering is from the NS5A 1b genotype. NS5A from JFH1 has an 18 amino acid insertion within D3. Figure adapted from references (206,207). (B) Crystal structures of NS5A domain 1. NS5A domain 1 1ZH1 (172), 3FQM (173) and 4CL1 (174) were obtained from the Protein Data Bank (208,209) and visualized using JSmol viewer in the symmetry display mode. Different conformations of NS5A dimers/multimers were obtained using X-ray crystallography and the NS5A-D1 dimer from genotype 1b is in an open conformation (172) (left) while NS5A-D1 dimer from genotype 1a is closed (173) (middle) and two NS5A-1a -D1 dimeric forms (174).

1.3 NS5A Interactions within the host cell

NS5A has been deemed the “promiscuous protein” as it has the ability to bind a prodigious array of host proteins, with more than 130 interactions now reported (207,210). Since the exact function of NS5A remains elusive, and the majority of the proteins are not involved directly in viral replication (186), a major role of NS5A may be to modulate the host environment through protein-protein interactions (PPIs) thereby making it conducive to HCV propagation. While this many interactions may seem improbable, it is worth considering that many of these PPIs may be the result of identifying proteins within complexes and are not due to direct interaction with singular proteins. Furthermore, many interactions may not occur concurrently and may be influenced by temporal and spatial constraints as well as by the different isoforms (genotype specific) and proteoforms of NS5A. Many model systems and environments have been employed in identifying NS5A PPIs and evaluating their biological consequences. The following section summarizes a subset of identified NS5A host protein interactions and their influence on the host cell and the HCV life cycle.

1.3.1. NS5A and apoptosis

Apoptosis is a mechanism utilizing programmed cell death to eliminate extraneous and inimical host cells. Halting cellular apoptosis is one method employed by some viruses to persist and continue their propagation. Numerous studies have demonstrated the anti-apoptotic properties of NS5A through its association with host cellular proteins.

However, the biological association with apoptosis is somewhat controversial as HCV proteins overall have been suggested to have both pro- and anti-apoptotic effects (211).

Huh7.5 cell infection with J6/JFH1 virus induces apoptosis (212), and HCV infected patient histology analysis suggested an increase in hepatocyte apoptosis although there was no correlation with viral load (213). Increased apoptosis in hepatocytes can induce fibrosis by constitutively activating regenerative mechanisms while suppressing apoptosis extends cell survival and allows for the accumulation of mutations (214). NS5A expression has been found to be protective against cellular apoptosis by obstructing several host cellular pathways mediated through protein interactions as described below.

1.3.2 TRAF2 and TRADD

Tumour necrosis factor alpha (TNF α) is a pleiotropic cytokine that initiates various cellular signaling cascades resulting in differentiation, proliferation, and extrinsic apoptosis activation. TNF α , a ligand binding the TNFR1 receptor, results in receptor trimerization and recruitment of Tumour necrosis factor receptor type 1-associated DEATH domain protein (TRADD). TRADD can initiate both apoptotic and cell proliferative pathways through additional PPIs. TRADD binds to Fas-associated protein with death domain (FADD) which then recruits procaspase-8 leading to the cleavage and activation of effector caspase-3 protease that in turn cleaves targets such as Poly ADP ribosome polymerase (PARP) and results in DNA fragmentation and apoptosis (215). TRADD is also capable of recruiting TNF receptor-associated factor 2 (TRAF2) to activate the NF-KB, JNK and p38 signaling pathways ultimately leading to cellular proliferation and apoptosis (215) (Fig.1.6).

NS5A has been implicated in the circumvention of TNF α signaling, resulting in increased cellular survival. Initial observations were made that HepG2 cells stably expressing NS5A-1a were resistant to TNF α induced apoptosis by both a lack of Annexin V staining and PARP cleavage (216). This refractory effect was substantiated in Huh-7 cells stably expressing NS5A-1b as increased survival and a lack of apoptotic products were observed compared to control cells during TNF α exposure (217). Mechanistically, NS5A may influence the TRADD-FADD interaction upstream of caspase-8 activation as overexpression of NS5A-1b failed to stop cell death when FADD or caspase-8 was overexpressed (217). However, TNF α activation of TNFR-1 also recruits TRADD and TRAF-2 and leads to NF-KB activation and increased cellular proliferation (218). As such, NF-KB reporter activation was tested and NS5A expression did not reduce TNF α 's ability to induce NF-KB activation. Therefore, NS5A expression resulted in protection from TNF α induced apoptosis but did not affect TNF α 's ability to promote cellular proliferation through NF-KB.

In contrast to the previous report, TNF α stimulated, actinomycin D-treated HEK293 cells when transfected with NS5A-1b, did not activate an NF-KB reporter gene, while control cells showed full reporter stimulation (219). NS5A-1b was shown to interfere with TRADD-TRAF2 interaction as determined by *in vitro* binding assays and co-immunoprecipitation (Co-IP) experiments. Overexpressing FLAG-TRAF2 and NS5A in Cos-7 cells indicated that TRAF2 and NS5A interacted resulting in TRAF2's inability to activate the NF-KB reporter (219). TRAF2 also activates the JNK pathway, and a follow-up study determined that the NS5A-TRAF2 interaction in HEK293 cells

synergistically potentiates TNF α stimulation of the JNK pathway by increasing phosphorylation of c-Jun (downstream effector of the JNK pathway) (220). Co-IP experiments in HEK293 cells revealed that while NS5A did not directly interfere with the TRADD/TRAF2 interaction, NS5A did affect the TRADD/FADD interaction (220). However, when HEK293 cells were induced with TNF α and actinomycin D to induce apoptosis, it was determined that transfected NS5A-1b was not protective as determined by PARP cleavage and cell viability assays (220). There are many possible reasons for the discrepancy between the two studies, but the most obvious explanation is the different cell lines were utilized and there was most likely a discrepancy in NS5A abundance given expression differences between stable integration and plasmid transfection.

The protective effects of NS5A on TNF α induced apoptosis were also evaluated *in vivo* with transgenic mice expressing NS5A-1a under the control of the liver-specific apoE promoter. Cells expressing NS5A-1a exhibited less histological apoptotic effects than matched controls (221). Evidence for a TRADD/NS5A-1a interaction was determined by performing *in vitro* pull-down of purified proteins and cellular Co-IPs in doubly transfected HEK293 cells coupled with colocalization experiments. NS5A also interfered with the TRADD/FADD complex as FADD failed to retrieve TRADD in the presence of NS5A (221). These studies reveal that NS5A is able to modify the TNF α induced signaling cascade through two key effectors, TRAF2 and TRADD (219–221).

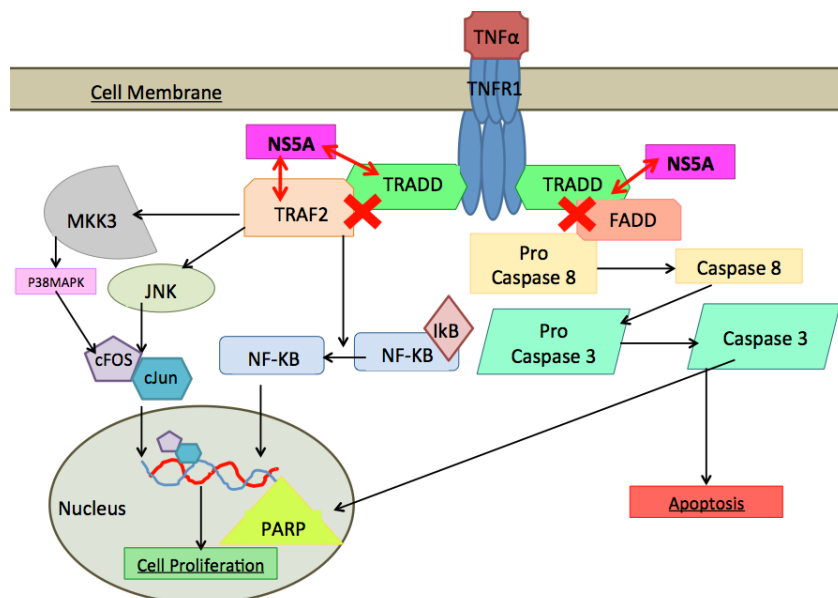


Figure 1. 6. NS5A interaction with the TNF α /TNFR-1 signaling cascade. TNF α binding to TNFR-1 activates cellular apoptotic, proliferation and survival pathways. The activated TNFR1 receptor recruits the TRADD protein. TRADD has the ability to initiate both apoptotic and cell proliferative pathways through additional PPIs. On the apoptosis, side TRADD binds to FADD recruiting procaspase-8 leading to the cleavage and activation of effector caspase-3 protease that in turn cleaves targets such as Poly ADP ribosome polymerase (PARP) and results in DNA fragmentation and apoptosis. On the proliferation side TRADD recruits TRAF2 and leads to activation of the NF-KB and JNK and p38 activation of transcription effectors cFos and cJun ultimately leading to cellular proliferation. Interactions between NS5A and TRADD and NS5A and TRAF2 (red double headed arrows) have been demonstrated (219–221) that interfere with their ability to bind effector proteins (red X) and influences the downstream signalling cascade. Figure modified from references (215,218).

1.3.3 Bax

Bcl-2 proteins are organized into a family based on the presence of conserved Bcl-2 homology domains that regulate intrinsic apoptosis (222). Sequence analysis of NS5A-1b revealed the presence of three Bcl-2 domains, BH1, BH2 and BH2, suggesting NS5A may be a Bcl-2 homologue and thus an effector of intrinsic apoptosis (205). Huh-7 and Hep3B cells stably expressing NS5A-1b were challenged with an intrinsic apoptotic inducer, sodium phenylbutyrate, and both cell lines were resistant to apoptosis as indicated by a DNA fragmentation assay (205). Bax is a proapoptotic protein containing

Bcl-2 homology domains, BH1, BH2 and BH3, that upon mitochondrial insertion induces the release of cytochrome C resulting in apoptosis (222). Sodium phenylbutyrate treatment results in the relocation of Bax from the cytoplasm to the nucleus and then finally to the nuclear membrane. In FLAG-NS5A transfected cells treated with Sodium phenylbutyrate, Bax failed to reach the nuclear membrane thus inhibiting apoptosis. It was also demonstrated that NS5A colocalized with Bax in the nucleus. An NS5A/Bax interaction was confirmed by Co-IP experiments in Hep3B cells, and deletion analysis revealed the interaction was dependent of NS5A's Bcl-2 domains (205). Interestingly, these studies were unable to replicate the NS5A/Bax interaction in transfected Cos-7 cells (205). NS5A has since been reported as a Bcl-2 homologue and a Bax interactor based on this landmark paper. However, while NS5A N-terminal deletions do enter the nucleus (193,194) the biological relevancy of Sodium phenylbutyrate treated Hep3B cells must be carefully considered as NS5A has not been observed in the nucleus in any standard cell culture model or in patient samples (128,171,190,191).

1.3.4 p53

p53 is a multifaceted tumor suppressor protein involved in several cellular processes including metabolism, inhibition of cell proliferation and cell death. Regulation of p53 functions are mediated through its subcellular localization, stability, and conformation. As a transcriptional activator, activated p53 relocalizes from the cytoplasm to the nucleus eliciting responsive gene expression (223). The NS5A-1a/p53 interaction was determined by *in vitro* pull-downs, mammalian two-hybrid assays (M2H) and Co-IP of NS5A-1a and p53 transfected HepG2 cells (224). In these cells, NS5A transfection

repressed p53 transactivation of a luciferase reporter construct containing p53 binding sites (224). The inability of p53 to induce transcription was due to sequestration of p53 to the perinuclear membrane by NS5A (224). Co-IP confirmed a p53/NS5A-1b interaction in Cos-7 and Hep3B cells overexpressing both constructs. Similarly, p53 transcriptional transactivation was inhibitory, and subcellular sequestration was observed in NS5A expressing cells (225). Sequestering of p53 was also deemed responsible for a lower percentage of Hep3B cell undergoing apoptosis in the presence of NS5A (225). The NS5A-p53 interaction, which suppresses apoptosis, appears to be consistent with NS5A from sub-genotypes 1a and 1b.

1.3.5 PI3K

Phosphoinositide 3-kinases (PI3Ks) are a group of kinases that catalyze the phosphorylation of the inositol ring of phosphatidylinositol lipids. These in turn act as secondary messengers, modulating downstream proteins to activate cellular processes such as cell growth, proliferation, immunity, metabolism, and apoptosis. Akt kinase is recruited to membranes by binding to these phospholipids where it has a direct effect on glucose metabolism, protein translation, and deactivation of pro-apoptotic signals (226). Co-IPs in epidermal growth factor (EGF) treated NS5A-1b Tet-Off HeLa cells and in Huh-7 SG replicon cells determined that the NS5A N-terminus interacts with the p85 catalytic subunit of PI3K (227). Phospho-specific antibodies revealed increased phosphorylation of the PI3K subunit p85, Akt, and Akt's downstream effector, Bad. EGF-treated cells expressing NS5A-1b or point mutations in the N-terminus of NS5A

were incapable of binding p85 in Tet-off HeLa cells indicated that the interaction with PI3K was essential for apoptotic suppression (227).

A second study demonstrated an interaction between NS5A-1b and 2a with PI3K subunit p85 in transfected Cos-7 cells and SG replicon Huh-7 cells (228). This interaction was shown to enhance the phosphotransferase activity of PI3K 10-fold when PI3K was isolated from SG replicon cells compared to control cells. Phospho-specific antibodies revealed that in addition, NS5A expression increased Akt and Bad phosphorylation (228). SG replicon Huh-7 cells were also found to be resistant to apoptosis stimulated by serum starvation and etoposide treatment over Huh-7 cells without replicons although the precise involvement of NS5A was not elucidated (228).

1.3.6 Bin1 (Amphiphysin II)

Altered expression of Bin1 is associated with several malignancies due to its involvement in clathrin-mediated endocytosis, membrane recycling, membrane remodeling, actin polymerization, transformation, stress signaling, cell cycle regulation and apoptosis (229). Bin1 contains an SH3 domain capable of binding polyproline motifs, such as those present in NS5A. Bin1 was identified as an NS5A interacting partner by GST-NS5A-1b capture of ³³P labeled Huh-7 cell lysate followed by identification of spots on a 2-dimensional gel by mass spectrometry (230). The Bin1/NS5A-1b interaction was confirmed by Co-IP in SG replicon cells with the interaction mapped to the SH3 domain in Bin1. However, the interaction was deemed non-essential to HCV replication when the

Bin1 SH3 domain was added to SG replicon cells as a competitive inhibitor of the interaction (230).

A subsequent investigation involving deletion mutants revealed that both the Bin1 SH3 domain and the Class II polyproline LCSII motif in NS5A were crucial in facilitating the protein interaction. Additionally, an NS5A mutant with alanines substituted for prolines was unable to inhibit apoptosis induced by ectopically overexpressing Bin1 in Bin1-lacking HepG2 cells while wt NS5A prevented apoptotic cell death (203). These same mutations were introduced into an HCV-1b infectious clone, but when inoculated into a chimpanzee, no productive infection was observed. This is not necessarily a conclusive test to state that the NS5A/Bin1 interaction is essential for infectious virus production in chimps but rather that the NS5A polyproline motif likely plays a role in either protein stability or, these regions have other roles related to virus production (203).

The Bin1/NS5A interaction has also been implicated in the reduction of NS5A hyperphosphorylation. NS5A isolated from double transfected NS5A-3XFLAG and HA-Bin1 293T cells produced less hyperphosphorylated NS5A (p58) in an *in vitro* kinase assay compared to when NS5A-3XFLAG was transfected alone (231). D2-D3 from NS5A are disordered protein regions, and when the Bin1 SH3 domain was complexed with NS5A-1b D2-D3, NMR spectroscopy revealed a conformational change in NS5A that increased flexibility and accessibility of NS5A D3 thus demonstrating that this protein interaction induces a conformational change in NS5A (177).

1.3.7 FKBP8/FKBP38

NS5A has been shown to interact with FK506 binding proteins 8/38. There is confusion in the literature regarding FKBP8 and FKBP38, and although numerous articles use the names synonymously, they are in fact unique isoforms. FKBP8 and FKBP38 both have identical sequences in the FK506-binding domain, the three sets of tetratricopeptide repeats, calmodulin binding site, and a transmembrane domain. The exception is that FKBP8 contains an extra 58 residues at its N-terminus and produces a 50 kDa versus 38 kDa protein (232). Both of these proteins are immunophilins with cis-trans peptidyl propyl enzymatic activity that bind to Bcl-2 domains (233).

A yeast-2-hybrid (Y2H) screen of human brain and liver libraries revealed FKBP38 as an NS5A-1b binding partner, but it was unclear whether this article was referring to FKBP38 or FKBP8. Co-IP experiments confirmed that NS5A was able to precipitate both isoforms (232). An FKBP8/38 antibody, reactive to both isoforms, was developed to assess endogenous expression levels of both isoforms in 293T, Huh-7, HepG2 and FLC-4 cells. FKBP8 was the dominant isoform, and thus subsequent tests focused on FKBP8 (232). Co-IPs were used to determine a genotype independent interaction as transfected NS5A-1a, 1b and 2a all successfully precipitated overexpressed FKBP8 in 293T cells. NS5A directly interacted with the tetratricopeptide repeat domain on FKBP8, and a ternary complex was formed between NS5A, FKBP8, and Hsp90 utilizing FKBP8 as the docking site (232). RNA interference studies of FKBP8 in Huh-7 cells revealed that HCV replication required FKBP8 both in the SG replicon and in the JFH1 infection models (232).

A follow-up study utilized alanine scanning substitutions in NS5A to determine that FKBP8 interaction required a single valine, V121, in NS5A and that this substitution reduced the replicative capacity of the SG replicon in Huh-7 cells (234). NS5A-1b cloned from an IFN resistant patient was employed in a Y2H screen and revealed an interaction with FKBP38 that was confirmed by Co-IP with HA-FKBP38 and Myc-His-NS5A-1b doubly transfected Cos-7 cells. Co-IP of endogenous FKBP38 with NS5A was also demonstrated in SG replicon Huh-7 cells (235). Interestingly, deletion mapping revealed that the interaction was facilitated by NS5A amino acids 148-236, containing the Bcl-2 domain and not V121. This contradiction might be due to the different FKBP8/38 isoforms which were not evaluated at the time (234,235).

Stably expressed NS5A in Huh7 cells depleted of Bcl-2 were resistant to staurosporine and cycloheximide-induced apoptosis when measured by PARP cleavage. This phenotype was reversed by FKBP38 siRNA suggesting that NS5A may be able to inhibit apoptosis through its interaction with FKBP38 (235). Under serum-starved conditions, NS5A was able to out-compete FKBP38 binding to mTOR kinase. FKBP38 binding inactivates mTOR which in turn fails to phosphorylate its downstream targets to initiate apoptosis (236). Interestingly there appears to be further regulation of the NS5A/FKBP8/38/Hsp90 complex formation as the calcium-regulated S100 proteins (S100A1, S100A2, S100A6, S100B and S100P) can bind the tetratricopeptide repeat domain of FKBP8/38 and displace both NS5A and Hsp90 in a calcium-dependent manner (237). Overexpression of the S100 proteins and treatment with a calcium ionophore caused displacement of NS5A from FKBP8/38, which impacted the protein levels of SG

replicons in Huh-7 cells(237). These studies identified the dependence of HCV on the NS5A/FKBP8/38 interaction for both virus propagation and suppressing apoptosis.

1.3.8 Other Proteins

Besides apoptosis regulation, NS5A has been implicated in additional interactions to create an environment conducive to HCV propagation. eIF4F, a protein crucial for initiation of protein translation, has been reported to interact with NS5A (238,239). This interaction causes an NS5A association with the polysome, increase in eIF4E phosphorylation, eIF4F complex assembly, mTOR pathway activation and eIF4E-40S assembly (238,239). NS5A has also been implicated in facilitating IFN resistance, and the NS5A-1b-PKR interaction may contribute to this phenotype. However, this interaction may be either genotype or strain specific as studies using NS5A-2a and 3a failed to interact with PKR (240–243). NS5A has also been shown to disrupt cellular metabolism, and interaction with Hexokinase resulted in increased glucose metabolism via the glycolysis pathway (244). TIPE2 is a protein involved in the regulation of inflammation and neoplasia and its interaction with NS5A led to its degradation and an increase in genome instability (245).

1.3.9 Reproducibility of NS5A-host cell PPIs

It is evident even from this limited listing that NS5A has an extensive interactome. While NS5A interaction studies have revealed many host protein interactions, the interactome must be looked at critically. In general, there tends to be little overlap generated between PPI studies, especially when comparing high-throughput PPI studies. A Y2H study

investigating the HCV protein-host protein interactions from each of the ten HCV proteins produced a list of 278 HCV protein-host PPIs, but only 10 PPIs had been previously described in the literature resulting in a 3.6% overlap (246). This study identified 97 NS5A/host protein interactions with 38 previously published NS5A/host PPIs leading to 39% overlap (246).

A Y2H screen used to identify interactions between HCV JFH1 proteins and host cellular factors provided another example of the little overlap seen with large studies. This resulted in 112 identified PPIs but only 18 of these were previously reported resulting in a 16% overlap (247). The same study investigated whether HCV-host PPIs identified using one HCV genotype were seen in studies with a different genotype (1b, 1a, and 2a) (247). 326 HCV protein-host protein PPIs were evaluated that included 160 PPIs from genotype 1b HCV proteins, 81 from genotype 1a and 85 from genotype 2a. Not one PPI overlapped when all three genotypes were compared and only 19 PPIs from genotypes 1a to 1b, four from 1a to 2a and 14 between 1b and 2a were found (247).

A more recent study into the HCV-host protein interactomes used immunoprecipitation to purify HCV Core, NS2, NS3/4A, NS4B, NS5A and NS5B and compared the mass spectrometry/database searched identified host interacting candidate proteins of the six HCV proteins (98 total), to a curated list of previously identified HCV interacting partners, (543 PPIs total) (248). Here, 74 Core, NS2, NS3/4A, NS4B, NS5A and NS5B interactions with host proteins from the author's study and the literature were identified

resulting in a 24.5% overlap (248). In the case of NS5A, 17 PPIs were identified of which eight were previously reported (248).

This lack of overlap is not surprising as large-scale interactome studies often have weak overlaps. Reports have indicated a 0.03% overlap in yeast PPIs and a 0.1% overlap in human PPI large scale studies (249,250). Much of the discrepancy between studies can be attributed to differences in model systems and experimental procedure, but reproducibility is still an issue; as such protein interactions really should be evaluated by a number of different methods in several model systems where possible.

1.4 Studying protein-protein interactions

Determining a protein's interactome provides important insight into a protein's function and global effect and over the years several methods have been developed for performing such studies. One of the most common methods is Co-IP in which a specific antibody directed to a protein or an incorporated tag is incubated with a cellular lysate to capture the "bait" protein and any other interacting proteins in complex with the bait. While a gold standard in many respects, there are some disadvantages: 1) availability of antibodies/capture resins that have high specificity and avidity for the protein of interest or the affinity tag, 2) potential competition of the antibody and interacting partners for a common epitope on the bait protein, and 3) the fact that the lysis procedure destroys any spatial constraints, an issue shared by most PPI studies using cell lysates (251).

The yeast-two hybrid (Y2H) system has also been used to define PPIs. The system employs two plasmids; the first encodes a yeast promoter DNA binding domain fused in-frame to a protein of interest (bait) while the second plasmid typically contains a yeast RNA transactivation domain fused to a library of cDNA fragments (prey). When the two plasmids are introduced into yeast cells, if the bait and prey proteins interact, it bridges the DNA binding domain and the transactivation domain allowing transcription of a reporter gene. Reporter genes enable the selection of positive interactions. Although this system is relatively simple to manipulate and detects typically binary interactions *in vivo*, it too, has disadvantages including, 1) in most variants of the Y2H, interactions must occur in the nucleus for transactivation to occur, (an issue for proteins such as HCV-NS5A that is absent from the nucleus), and 2) the potential for improper protein folding or lack of post-translational modifications due to expression in a heterologous system. Although the Y2H has been a workhorse for PPI identification, it has a relatively high false positive rate (252). To improve on some of these potential drawbacks, the mammalian two-hybrid system (M2H) is performed similarly to the Y2H but in a native environment for protein expression, which is not reliant on nuclear transactivation. However, M2H still relies on the complementation of two protein fragments to reconstitute a functional enzyme and thus is susceptible to steric hindrance, conformational changes and artificial co-expression that negates spatial, temporal and abundance constraints (253).

Co-purification using conventional chromatography or batch affinity methods involves subjecting lysates to matrices, which separate proteins (and complexes) based on

chemical properties of the bait protein. More commonly, a bait sequence is tagged with an affinity epitope sequence then expressed prior to lysis. One criticism of this method is that weak or transient interactions can be difficult to capture especially if stringent wash conditions are employed (254). Tandem affinity purification (TAP) is a variant method in which bait proteins are tagged with two unrelated purification epitopes and are subjected to two purification steps. Affinity tags such as the CBP-protA tag (a calmodulin binding peptide and the immunoglobulin-interacting domain of Protein A) and variations including FLAG and myc epitopes have been used and due to the two rounds of purification substantially reduce non-specific background. However, while the process has the benefit of using lysates from natural sources, it is still limited when dealing with weak or transient interactions and of course allows cellular compartmental mixing during to purification (255).

Recently, a new set of TAP tags has been developed. Originally devised to study ubiquitination in yeast, it employs a bait protein with two affinity tags: a biotinylation recognition signal (which is biotinylated when expressed *in vivo*) flanked by two hexahistidine sequences (HBH tag) (256). His-tag purification is based on the high affinity of the imidazole side chain of histidine for metal ions that are bound to an immobilized chelating agent such as nickel or cobalt (257). This first step in purification, immobilized metal chelate affinity chromatography or HIS-purification, removes many contaminants as well as any predominant host biotinylated cellular proteins (258). The second purification step involves a 75 amino acid sequence, found in both prokaryotes and eukaryotes, that is recognized by an endogenous host biotinylase which attaches a

biotin moiety to a specific lysine within recognition sequence (259). After the amino acid sequence has been biotinylated, it can be captured using streptavidin. Streptavidin has a very high affinity for biotin ($K_d=10^{-15}\text{M}$) (260).

One unique aspect of this TAP tag combination is that both metal chelate and biotin-purification can withstand denaturing conditions. When combined with protein chemical cross-linking, it opens up the possibility to purify elements of a protein complex with weak/transient interactions to extremely high purity (261). Chemical cross-linking involves incubating cells or lysates with small molecules containing reactive side chains that form covalent bonds with specific amino acid side chains. Different cross-linkers have different length spacer arms, for example: paraformaldehyde (PFA, spacer arm 2 Å), disuccinimidyl glutarate (DSG, spacer arm 7.7 Å), disuccinimidyl suberate (DSS, spacer arm 11.4 Å), and ethylene glycol bis(succinimidyl succinate) (EGS, spacer arm 16.1 Å) (262). The length of the spacer is an important consideration given that the cross-link is typically specific to one amino acid such as lysine. In the absence of juxtaposed lysine residues within reach of the cross-linkers' spacer arm reactive sites, no cross-linking occurs. Following cross-linking, samples can be purified under denaturing conditions through the two affinity tags, and interacting proteins will remain bound to the bait protein due to the covalent linkage. Mass spectrometry and database searching can then be used to identify interacting proteins. It is important to remember that the cross-linking needs to be performed on a limited scale. If all the lysine sites were cross-linked, it would severely impair subsequent purification (one large holo-protein complex would be created) or analysis (trypsin, which digests at lysine and arginine would be impaired).

As NS5A is partially hydrophobic, it can be a more challenging protein to purify (169,171). Native state purification therefore requires more stringent methods including detergent addition to isolate NS5A and its potential membrane-associated partners from the cellular matrix. In principle, applying cross-linking prior to cell lysis would cement these weaker interactions and limits cellular compartment mixing potentially leading to more biologically relevant identification of PPIs.

1.4.1 Protein identification using mass spectrometry and database searching

The use of mass spectrometry and database searching for the identification of protein interaction partners of affinity-purified targets now allows mapping of a protein's global interactome. Purified "bait" protein in association with its interacting partners are digested with a specific protease (commonly trypsin, AspN or GluC), desalted, and concentrated prior to analysis (263) (Fig.1.7). This technique is referred to as a "bottom up" approach as peptides are used for the identification of a protein in contrast to the "top-down" approach where intact proteins are injected. Mass spectrometers measure the mass to charge (m/z) ratio of ions in the gas phase. In order to generate these charged species, mass spectrometry employs two major soft ionization techniques: matrix assisted laser desorption ionization (MALDI) and electrospray ionization (ESI). With MALDI, samples are mixed with a matrix solution and plated on a metal surface. Pulsed laser ionization energy is adsorbed by the matrix transferring protons to analytes, which are transferred into the mass spectrometer analysis chamber. In ESI, analytes are mixed with an acidified volatile liquid then injected through a narrow orifice with high voltage applied. A Taylor cone is produced, and desolvation of the sample leads to protonated

analytes entering the mass spectrometer. Irrespective of ionization technique, charged analytes are assessed by several mechanisms, the one relevant to this work being a hybrid device containing a linear ion trap and an Orbitrap mass analyzer.

To reduce sample complexity, peptide mixtures are fractionated prior to injection into the mass spectrometer. Reverse phase matrices remain the most appropriate choice as they use volatile acetonitrile for peptide elution rather than salt (264) (Fig.1.7). As peptides enter the mass spectrometer their m/z is measured in the Orbitrap mass analyzer at high resolution (full width at half height maximum = 65000). Based on initial interrogation of the sample, parent ions are then selected, one at a time, typically by abundance and charge to be further fragmented in a collision cell. Energy coupled with inert gases leads to random fragmentation along the peptide backbone to produce b (contains the N-terminus) and y (contains the C-terminus) ions of the peptide. The daughter ions are reanalyzed in either the ion trap or in the Orbitrap (265) (Fig.1.7). The entire process is referred to as tandem mass spectrometry. Coupling the initially determined mass with the spacing between fragment ion masses provides information on the sequence present in the peptide (266). Several search engines are available to evaluate the data and provide statistically meaningful interpretation. Higher confidence in protein identification results from the identification of more than one peptide and even more so if the peptides are unique to a particular protein isoform.

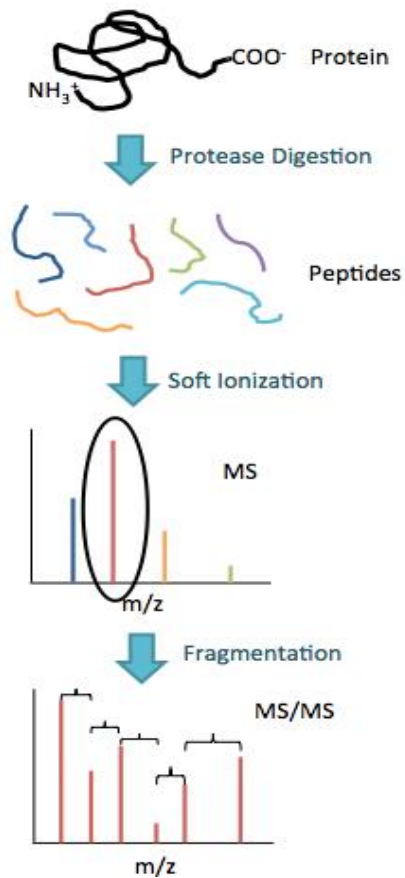


Figure 1. 7. Protein identification by mass spectrometry. A protein (black) is digested with a protease (trypsin, AspN, GluC) to generate peptides (colored) that are subjected to soft ionization. In electrospray ionization (ESI) systems, a high voltage source and volatile buffers are used to transform the peptide into gas-phase ions before injection into the mass spectrometer. In the mass analyzer, the atomic weights of the peptides are determined and presented as data depicting the ion intensity of individual peptides versus their mass/charge (m/z) ratio. Mass spectrometry will detect not every peptide present in a protein as illustrated by the absence of the light blue, teal and purple peptides in the third box image. To obtain amino acid sequence information for an individual peptide, the most abundant peptide at any given time (indicated by the red peak in box 3, circled) is selected for fragmentation by colliding the peptide with an inert gas (CID) or using higher Rf voltage (HCD) to introduce random breaks in the polypeptide backbone. The resulting peptide fragments from tandem mass spectrometry produce b and y ions (CID) or predominantly y ions (HCD). The molecular weights of these ions can be used to determine the sequence of the peptides. Software algorithms are utilized to determine the most appropriate amino acid sequence while database searching compares these interpretations to give the identity of a peptide.

1.4.1.1. NS5A PPIs identified by mass spectrometry and database searching

Using affinity purification coupled to mass spectrometry identification has been used in various incarnations to study HCV-host PPIs. FLAG-tagged HCV NS5A protein was immunoprecipitated from 293 cells expressing NS5A and the proteins were resolved on a 2D gel, compared to a FLAG-NS5B 293 cell line and a unique spot to the NS5A 2D gel was identified as Hsp27 (267). HeLa cells expressing NS5A-1b-FLAG were used to isolate NS5A and bands that were unique (compared to an empty vector control) were analyzed by mass spectrometry revealing Bin1 as an interacting partner (231). A TAP procedure utilizing protA, TEV protease cleavage site, and CBP tag fused to NS5A and NS5B used mass spectrometry to identify Hsp72 as an interacting protein (268). Another series of experiments used an internal FLAG-Streptactin tag within the C-terminus of NS5A in a Jc1 infection of Huh7.5.1 cells, to isolate NS5A by streptactin. Combined with Stable Isotope Labelling with Amino Acids in Cell Culture to distinguish real interactions from background proteins revealed Rab18 as an NS5A interacting partner (269).

1.5 Phosphorylation as a differential controller of PPIs

Besides PPI studies, mass spectrometry has made important contributions to studies of protein composition, especially with respect to post-translational modification like phosphorylation. Protein phosphorylation is a dynamic, reversible process whereby a protein kinase catalyzes the transfer of a phosphate moiety from an ATP molecule to a serine, threonine or tyrosine residue on a eukaryotic protein (270). Phosphorylation of a protein is a crucial post-translational modification that regulates numerous of cellular processes including: signal transduction, immunity, inflammation, cell cycle progression,

morphogenesis, metabolism, differentiation, cellular trafficking and apoptosis (271).

Phosphorylation is believed to effect one-third of all proteins in the proteome (272).

Phosphorylation affects a protein's overall structure often leading to a conformational change that often serves to activate/deactivate regulatory proteins and promote/interfere with protein interactions.

A classic example of phosphorylation impacting protein interaction is with the apoptotic regulatory protein Bad. Unphosphorylated Bad binds to the Bcl-XL protein and promotes apoptosis, but when Bad is phosphorylated on serines 112 and 136, it instead binds the 14-3-3 protein becoming cytoplasmically sequestered which results in cell survival (273). The polyglutamine expansion of the Ataxin-1 (ATXN1) protein in the brain leads to the development of a neurodegenerative disorder known as six spinocerebellar ataxia types (SCA). The polyglutamine expanded form of ATXN1 preferentially binds the RNA-binding motif protein 17 (RBM17) but only when S776 of ATXN1 is phosphorylated resulting in an ATXN1/RBM17 complex that associated with increased SCA pathogenicity (274). The Adhesion and degranulation promoting adaptor protein (ADAP) in T cells becomes phosphorylated on tyrosine residues following T-cell receptor stimulation. The phosphorylation of Y571 leads to ADAP's interaction with ZAP70 kinase, a complex required for proper T-cell migration and thus phosphorylation acts to regulate the migratory signaling pathways in T cells (275).

1.5.1 NS5A phosphorylation

HCV NS5A is differentially phosphorylated and two major forms are apparent when resolved by SDS-PAGE; referred to as the basally (56 kDa) and hyperphosphorylated (58

kDa) phospho-proteoforms (97). Basal phosphorylation of NS5A occurs after mature NS5A is liberated from the polyprotein and following additional phosphorylation generates hyperphosphorylated NS5A (188,276,277). Requirements for the production of the p58 vary according to genotype. NS5A-1b may require the expression of other HCV proteins including: NS4A (97), NS2 (278) or NS3-NS5A (276,279,280). NS5A from HCV genotypes 1a and 2a can produce both phospho-proteoforms independent of the other HCV proteins (281). The role that NS5A phosphorylation plays in the HCV life cycle is extremely controversial. It has been speculated that phosphorylation plays a role in switch the virus life cycle from genome replication to RNA packaging (141,282,283).

NS5A interactions with host proteins can affect the phosphorylation status of NS5A and has been proposed as a regulatory mechanism during the HCV life cycle. NS5A-1b (but not 1a) interacts with hVAP-A only when basally phosphorylated, and hyperphosphorylation disrupts this interaction resulting in decreased genome replication (140). A similar observation was made with the NS5A-1b-PI4KIII α interaction whereby hyperphosphorylation disrupts the interaction resulting in impeded replication of the Con1b replicon (284). An interaction between NS5A-2a and vinexin β was established, and the expression of vinexin β was positively correlated with both hyperphosphorylation and replication in a CKI- α dependent manner (285). An interaction between NS5A and Bin1 has also been found to reduce NS5A phosphorylation (231).

1.5.2 Kinases involved in NS5A phosphorylation

Several cellular kinases appear to have involvement in phosphorylating serine and threonine residues within NS5A. These kinases have been identified using either direct *in vitro* kinase assays or by kinase inhibition studies utilizing RNA interference or inhibitory drugs and include: CKII (180,286–288), CKI- α (282,289–291), CKI- δ (287,292), Plk1(293), PKA- α (294), LATS2 (295), MEK1, MKK6, AKT1 and hp70S6K (287). The importance of CKI- α , CKII, PIK1, and CaMKII expression were studied in the context of the HCV life cycle and expression of these kinases positively correlated with levels of NS5A hyperphosphorylation, genome replication and infectious viral titer (289,290,292,293,296). Using a phospho-specific NS5A S235 antibody, it was discovered that inhibitors to CKI- α , PIK1, or CaMKII specifically reduced phosphorylation at S235 suggesting kinase redundancy in the kinases that operate at this site (296).

1.5.3 NS5A phosphoacceptor sites

1.5.3.1 Identification of phosphorylated residues in NS5A by mass spectrometry

Identification of phosphorylated residues by mass spectrometry generally proceeds as described in section 1.4.1 where proteins are digested into peptides, and tandem mass spectrometry coupled with database searching identifies the amino acid signatures of a parental ion. The search is run with a variable modification (phosphorylation) to identify phosphates on S/T/Y residues. While including a variable modification has the detriment of increasing the search space, the phosphate moiety itself introduces additional issues,

which complicates identification of these modifications. First, phosphates are labile features, and during tandem mass spectrometry fragmentation energy destined for backbone fragmentation is instead used to strip the phosphate from the polypeptide thus providing less abundant daughter fragments necessary for determining the peptide sequence. Second, phosphorylated peptides tend to be more hydrophilic than non-phosphorylated species and can be more easily lost during capture or certain resin types. Third, phosphorylated peptides often appear less frequently than their unphosphorylated cognates and less abundant species are typically detected less often thereby necessitating enrichment prior to analysis. Fourth, when a phosphopeptide is detected, fine-mapping the modified residue can be complicated when a peptide contains multiple S, T, and Y residues and unless tandem mass spectrometry fragmentation has occurred between these sites, it cannot be determined exactly which amino acid was the acceptor site (297). Fifth, since phosphorylation adds negative charge to a peptide, it can lead to loss of detection of a peptide by mass spectrometry analysis. Following trypsin digestion (and in an acidic environment), most peptides have at least a +2 charge (one positive charge for the N-terminus NH_3 group, and a second from the lysine/arginine side chain). In ESI, the mass spectrometer is typically programmed to exclude +1 charged ions, which are often chemical contaminants. However, if phosphorylation decreases the net peptide charge below +2, that peptide will not be considered for subsequent fragmentation. (298).

Although some of these issues are difficult to resolve, a number of improvements can be made. Using purified or partially-purified samples to increase the likelihood of picking a relevant peptide and specifically enriching for phosphorylated peptides using enrichment

techniques such as titanium dioxide deal with the sub stoichiometric amounts of phosphorylated compared to unphosphorylated peptides.

1.5.3.2 Identification of phosphoacceptor sites on NS5A

With some evidence suggesting differential phosphorylation of NS5A may act as a molecular switch during HCV life cycle, there is a need to identify the sites affected within NS5A. Several attempts have been made. A mutagenesis study was performed on serines clustered in the NS5A LCS region, with deletion analysis revealing that this region was critical for hyperphosphorylation (188). Although phosphorylation residues was not confirmed biochemically, serine to alanine mutagenesis of S225, S229, and S232 in the NS5A region of a SG 1b replicon reduced p58 protein levels (188). The serine residues within the LCS region are highly conserved among most HCV isolates suggesting evolutionary importance (141). Several studies have since been performed employing serine to alanine substitution in the LCS and revealed that S229A, S232A and S235A mutations in the con1b replicon and S225A, S229A, S232A, and S235A mutations in the JFH1 replicon not only produced less hyperphosphorylated NS5A but decrease viral replication (141,299).

A study involving deletion of NS5A domain 3 in the HCV J6/JFH1 virus revealed resulted in decreased p58 expression and impaired HCV production but had no effect on replication. S457 at the extreme C-terminus of NS5A was shown to be a pivotal residue in as an alanine substitution mutation reduced p58 formation and infectivity. Both

phenotypes were rescued by a negatively charged aspartic acid serving as a phosphomimetic substitution (180).

The first NS5A phosphorylation site identified biochemically was S349 using Edman degradation on GST-NS5A-1a expressed in BHK21 cells (300). Mass spectrometry has largely supplanted this technique and S222 was the first phosphorylation site in NS5A to be mapped using mass spectrometry in the context of baculovirus expressed NS5A-1b (301). However, it is unclear if a more appropriate cellular environment or the presence of other HCV proteins may have had a different effect on NS5A phosphorylation.

Immunoprecipitation of NS5A from a Con1b replicon coupled with mass spectrometry analysis identified S249 as a major phosphorylated species (302). This marks the first time that an NS5A phosphorylation site was identified in a cellular context with active HCV replication (302). Subsequently, LeMay et al. 2013, used mass spectrometry to identify S222 as an NS5A phosphoacceptor site in the context of the SG JFH1 replicon (303). A phosphoablative alanine mutation of S222 had no effect on JFH1 replication or infectious titer, but the phosphomimetic aspartic acid mutation slightly reduced replicative capacity (303). Masaki et al. 2014, also identified NS5A phosphopeptides, again encompassing the serines of the LSCI region, but were unable to fine-map which residues were involved (289). Mutational analysis of serine residues in JFH1 revealed severe replication deficiencies associated with S229A and S235A (289).

Ross-Thriepland and Harris, 2014, isolated One-Strep tagged NS5A from Huh-7 cells harboring the SG JFH1 replicon and were able to assign S146, S222, S225, and T348 as

phosphorylated residues (304). Phosphopeptides containing S228, S229, S230, and S232 were also identified but could not be unequivocally assigned to a particular residue (304). Abrogating the phosphoacceptor sites in JFH1 with S225A, S229A, and S232A mutations reduced replication competence whereas mimicking the phosphate charge with S225D and S232D “rescued” the viruses to wt levels (304). Eyre et al. 2016, used a similar methodology and isolated FLAG-tagged NS5A in the context of the full-length JC1 infectious viral infection of Huh7.5 cells (305). Using mass spectrometry analysis to and fine-mapping, previously identified phosphoacceptor sites S222 and T348 were confirmed (303,304) and S235 was newly identified for the first time from an infectious virus (305). Alanine mutagenesis of S235 revealed that phosphorylation of this residue was essential for HCV genome replication and appears to involve the PI4KIII α protein (305). It was further ascertained that S235 phosphorylation redistributes NS5A within the cell and thus likely plays a role in HCV replication compartment formation (305). Amino acids S222, S235, and S238 were NS5A phosphoacceptor sites identified by mass spectrometry from a full-length J6/JFH1 HCV infection of Huh7.5.1 cells (306). Mutational analysis in J6/JFH1 revealed that ablating S235 phosphorylation suppressed viral replication and produced a dominant phenotype in double and triple mutations containing S235A/S222A/S238A suggesting that S235 phosphorylation is a dominant requirement for J6/JFH1 HCV viral replication (306). Furthermore, S235 phosphorylation was revealed to be a major component of p58 by an NS5A-phospho-S235 antibody (306). NS5A phospho-specific S222, S235, and S238 antibodies were used to demonstrate that there were higher levels of phosphorylated S235 and S238 and

lower levels of S222 present in p58 (307). These studies also demonstrated that phosphorylation of S238 likely required S235 to be phosphorylated first (307).

Several studies have attempted to directly evaluate the ability of cellular kinases to phosphorylate NS5A *in vitro*. T360 from NS5A-1b was revealed as a PKA kinase acceptor site, and Con1b replicons bearing T360A/E mutations resulted in replicons with reduced replication (175). Mutation of the equivalent residue in Jc1 HCV, T356A, was unable to replicate or produce infectious virus while T356E behaved as wt (175). LATS2 phosphorylated NS5A-1b identified S71 as a phosphorylated site and S71A severely reduced the replication of the Con1b replicon (295). NMR spectroscopy was used to follow an *in vitro* kinase reaction where a NS5A D2/3 mutant served as a CK2 substrate revealing S401, S408, S429, S434 and T435 as likely phosphoacceptor sites (177).

1.5.4 Regulatory role of phosphorylation in the HCV life cycle

Phosphorylation of NS5A is believed to act as a regulatory mechanism for the HCV viral life cycle. Studies using 1b SG replicon systems have shown that a reduction in p58 levels enhances viral replication, often by many orders of magnitude (141,282).

However, complete elimination of p58 in this context eradicates replication indicating that a small amount of p58 is still required (141,283). Interestingly, in studies utilizing JFH1, the opposite conclusion was formed whereby increased p58 levels correlated with increased genome replication (299) and decreased p58 expression resulted in higher infectious viral titers (308). Recently it was discovered that Daclatasvir, a DAA compound that inhibits HCV replication through an interaction with NS5A, severely

reduced NS5A hyperphosphorylation while having little effect on basal phosphorylation (292). It has also been suggested that a critical ratio between the two NS5A phospho-proteoforms may be required to achieve optimal HCV replication (282).

1.6 Study Rationale and Hypothesis

End-stage liver cirrhosis due to HCV infection is now the leading indicator for liver transplantation in developed countries (4) and HCV related morbidity and mortality rates are expected to rise as previously asymptomatic baby boomers are diagnosed with infections (9). Currently, there is no protective vaccine and although recently developed DAAs are now boasting SVR rates of >95% (56) the emergence of virus escape mutants with resistance are a possibility due to the high mutation rate of HCV. Moreover, the long-term effects of having HCV infection even after cure are only now being assessed. A better understanding of this virus and how it affects the host cell can only improve the ability to eradicate it. As a major regulator in the virus life cycle as well as a critical antiviral target, it is interesting that the basic function of the NS5A viral protein remains so incomplete, particularly considering how little of the protein seems to be involved directly in virus replication functions. It seems likely that the “extra” NS5A protein in the cell is interacting with host cellular proteins to facilitate viral propagation. To provide further insight into the biology of the NS5A protein in the context of the host cell:

- 1. I hypothesize that since NS5A deregulates cellular functions, it is likely that these perturbations are due to virus protein-host protein interactions. Using Tandem Affinity Purification method coupled to mass spectrometry and**

database analysis, previously undiscovered NS5A-host protein-protein interactions ultimately responsible for these phenotypes will be identified.

Phosphorylation of NS5A is believed to play a role in regulating virus replication and packaging. NS5A phosphorylation may also represent an anti-HCV target; Daclatasvir, an extremely potent anti-HCV compound, affects NS5A hyperphosphorylation while having no effect on basal phosphorylation (292) raising the possibility that the two phospho-proteoforms of NS5A may play distinct replication roles. Different phosphorylation states may ultimately also affect NS5A's ability to interact with host proteins, and these interactions may be required for successful completion of the viral life cycle (303–306). Incorporation of phosphorylation analysis from multiple protein expression systems may provide further insight into the role that this post-translational modification plays in the HCV replication cycle. To study NS5A phosphorylation:

- 2. I hypothesize that using by using several different expression systems for NS5A coupled with purification and mass spectrometry/database searching novel NS5A phosphoacceptor sites will be identified. Mutational analysis of the identified phosphoacceptor sites will allow characterization of their impact on the HCV life cycle.**

The following objectives have been used to address these hypotheses:

- 1. Create stable cell lines ubiquitously expressing affinity tagged HBH-NS5A-2a from the JFH1 strain and confirm protein expression**

- 2.** Isolate proteins in complex with HBH-NS5A-2a from 293 cells using Tandem Affinity Purification (TAP) in both native state (nTAP) and by using chemical cross-linkers to fix interactions prior to purification (xdTAP)

- 3.** Use mass spectrometry to identify NS5A interacting proteins from nTAP and cross-linked denaturing tandem affinity purification (xdTAP).

- 4.** Validate NS5A interacting candidates using Co-IP and colocalization.

- 5.** Isolate NS5A from HBH-NS5A-2a 293 cells using nTAP and dTAP and NS5A and SG JFH1-NS5A-HBH from subgenomic replicon Huh7.5 cells using nTAP, dTAP, and continuous-elution electrophoresis to identify phosphoacceptor sites by mass spectrometry.

- 6.** Mutate identified NS5A phosphoacceptor sites to phosphoablatant alanine and phosphomimetic aspartic acid residues to characterize the effects on HCV JFH1 replication, NS5A phospho-proteoform ratios, and infectious titers.

Chapter 2: Materials and Methods

2.1 General Laboratory Techniques

2.1.1 Cell Culture

The cell lines utilized throughout these studies were the GP2-293 (Clontech, cat# 613505), 293TN (SBI, cat# LV900A-1), and Huh7.5 (a kind gift from Dr. Charles Rice, Rockefeller University, NY). GP2-293 and 293TN cells are derivatives of the prototypic HEK293 human embryonic kidney cell line with the addition that GP2-293 cells are were stably transduced to express the retroviral *gag* and *pol* genes and 293TN carries the SV40 large T antigen. Human hepatoma Huh7.5 cells were generated by curing human hepatoma Huh-7 cells containing the subgenomic HCV Con1b replicon through prolonged treated with IFN- α (146). These cells more efficiently support HCV replicon and virus replication. All cells were cultured in Dulbecco's modified Eagle's medium (DMEM, Gibco, cat# 11995-065) supplemented with 10% fetal bovine serum (FBS) (Gibco, cat# 10082-147), 1X penicillin-streptomycin-glutamine (Gibco, cat#15070-063) and 1X MEM non-essential amino acids (Gibco, cat# 11140076) (complete DMEM) in a humidified 37°C incubator with 5% CO₂. Cells were passaged when monolayers reached 70-80% confluency by removing media, washing once with phosphate-buffered saline (PBS) and dissociating cells from flasks/plates with TrypLE Express (Gibco, cat# 12605-010), returning 5-10% for stock maintenance. Huh7.5 cells containing HCV replicons were maintained with the addition of 0.4 mg/ml Geneticin® (G418) (Gibco, cat# 10131035) in complete DMEM.

2.1.2 iProof Polymerase Chain Reaction (PCR)

All PCR amplifications were performed with the iProof High-Fidelity DNA polymerase kit (BioRad, cat #172-5300) in a 50 μ l reaction volume (1X iProof HF Buffer, 10mM dNTP, 5 μ M of each primer, 1ng template DNA, 0.5 μ l iProof DNA polymerase and sterile dH₂O). Nucleotide sequences of the primers are in Appendix Table A1. Thermocycling was completed in an Eppendorf Mastercycler ep Gradient S thermocycler with the recommended iProof High-Fidelity DNA polymerase kit program consisting of an initial denaturation of 30 seconds at 98°C, 35 cycles each of a denaturation at 98°C for ten seconds, annealing at two degrees below the melting temperature of the primers for 30 seconds, extension of one minute per kilobase of the amplification target at 72°C and a final ten minute extension at 72°C. PCR products were purified using the QIAquick PCR Purification Kit (Qiagen, cat# 28106) using the manufacturer's protocol.

2.1.3. General Cloning Strategy

Gene expression and mutant-viral constructs utilized a general cloning strategy. Inserts were generated by PCR (section 2.1.2), and vector plasmids were isolated using the QIAprep Spin Miniprep Kit (Qiagen, cat# 27104) according to the manufacturer's recommendations. 500ng of insert DNA and vector DNA were digested with 10-20 units of restriction enzyme(s) (NEB) in a 30 μ l final reaction volume according to the protocol recommended by the NEB double digest finder (309). Total digested insert or vector DNA were mixed with a 6X DNA load dye solution (30% glycerol, 0.00025% bromophenol blue) separated on a 0.7% agarose gel (Tris-borate/EDTA (TBE) containing 0.0001% ethidium bromide) at 110V for 60 minutes. DNA bands were extracted and

purified using the QIAEXII Agarose Gel Extraction Kit (Qiagen, cat# 20021) following the manufacturer's instructions. To approximate the volume of digested product required for a 3:1 ratio of insert to vector DNA in each ligation, 5µl of gel extracted vector and insert DNA were evaluated by gel electrophoresed and DNA concentrations were approximated. DNA was added to a 20ul volume ligation consisting of 10 units of T₄ DNA ligase (New England Biolabs cat# M0202L), 1 X T₄ DNA ligase buffer and dH₂O. Ligations were incubated for either one hour at room temperature or overnight at 16°C. Constructs were transformed into chemically competent *E.coli* TOP10 cells (Invitrogen, cat# 4040-10) by adding 2ul of the ligation mixture to 50ul of thawed bacterial cells for 30 minutes on ice and subsequently heat shocking the mixture for 30 seconds in a 42°C water bath. Bacterial cells were returned to ice and 250ul of nutrient rich SOC media (Invitrogen, cat#15544-034) was added to cells for a one-hour recovery period shaking at 150 rpm in a 37°C incubator. Transformed bacteria were plated on selective LB plates containing 100µg/ml ampicillin or 50ug/ml kanamycin and incubated overnight at 37°C.

Colonies were screened by extracting plasmid DNA using the QIAprep Spin Miniprep Kit (Qiagen, cat# 27104) followed by restriction digest with restriction enzymes flanking the insert DNA followed by gel electrophoresis. Constructs positive for the insert were verified by Sanger sequencing at the Genomics Core (National Microbiology Laboratory, Winnipeg). Sequencing data was evaluated using the modules Seqman and Editseq in the Lasergene 7 DNASTar software. (DNASTAR Lasergene, DNASTAR Inc, Madison, WI). After confirmation of the correct nucleotide sequence, plasmids were prepared using

either the Endofree Plasmid Maxiprep kit (Qiagen, cat# 12362) or the Plasmid Plus Midi kit (Qiagen, cat# 12943).

2.1.4 Effectene Cell Culture Transfection

Transfection of plasmid DNA into adherent cells for transient gene expression was performed using Effectene transfection reagent (Qiagen, cat#301425). Adherent cells were seeded to produce 70% monolayers the following day. The transfection mixture for a 35mm plate consisted of 100ul of EC buffer, 1ug DNA, 8ul of enhancer and 10ul of Effectene. For a 10cm plate, the mixture was 300ul of EC buffer, 4ug of total DNA, 32ul of enhancer and 50ul of Effectene. EC buffer, DNA, and enhancer were combined, vortexed for 10 seconds, and incubated at room temperature for five minutes. Effectene was added and the mixture was vortexed for 10 seconds followed by a 10-minute incubation at room temperature. During the second incubation, media from plated cells was removed, and cells were washed with PBS before adding fresh complete DMEM (3ml for a 35mm plate, 9ml for a 10cm plate). DMEM (0.9 ml for a 35 mm plate, 2.7 ml for a 10 cm plate) was added to the transfection complex, which was then added drop-wise to the cells. Cells were incubated for 48 hours in a humidified 37°C incubator at 5% CO₂ prior to harvest.

2.1.5. Xtreme Gene Cell Culture Transfection

X-tremeGENE HP Transfection reagent (Sigma, cat# 6366244001) was alternatively used for transient transfections. Cells were seeded 24 hours prior to produce 70% monolayers. X-tremeGENE HP DNA Transfection reagent was equilibrated to room

temperature for 15 minutes then mixed by vortexing. For cells in a 35mm dish, 2ug of DNA was mixed with 200ul of serum and antibiotic-free DMEM, and 6ul of X-tremeGENE HP DNA Transfection reagent. For a 10cm plate, 10ug of DNA was mixed with 1ml serum and antibiotic-free DMEM, and 30ul of X-tremeGENE HP DNA Transfection reagent. Transfection complexes were incubated for 15 minutes during which time recipient cells had their media removed, were washed with PBS and had fresh complete DMEM returned. The transfection mixture was added to the cells in a drop-wise manner and incubated for 48 hours prior to harvest.

2.1.6 SDS-PAGE and Western Blots

2.1.6.1 Protein Quantification

Total protein quantification of cellular lysates was determined using the Pierce™ BCA Protein Assay Kit (Pierce, cat# 23227) with modifications described by the Janes Lab, University of Virginia (310). A six-point standard curve consisting of bovine serum albumin standard diluted to 4, 2, 1, 0.5, 0.25 and 0 mg/ml was constructed by adding 7.5ul of each diluent with 2.5ul of the protein lysis buffer to a 96-well plate. 7.5ul of the protein lysate of unknown concentration was added, in duplicate, to a well along with 2.5ul of water and 200ul of the BCA solution (50 parts solution A to 1 part solution B) and incubated at 37°C for 15 minutes. The absorbance of each sample was determined by excitation at A₅₆₃ in a SpectraMax Plus spectrophotometer, and the average concentration of the unknown samples was determined by comparison to the absorbencies of the standard curve.

2.1.6.2 SDS-PAGE

Total protein samples were extracted in Igepal CA-630 (Sigma, cat# I8896) (referred to as NP-40 from here on), Triton-X 100 (Sigma, cat# X100) or Radioimmunoprecipitation assay buffer (RIPA buffer) (Sigma, cat# R0278) (150mM NaCl, 1.0% NP40, 0.5% sodium deoxycholate, 0.1% SDS, 50mM Tris, pH 8.0) were mixed 5:1 with 6X Load Buffer (125mM Tris-HCl pH 6.8, 2% SDS, 20% glycerol, 0.2% bromophenol blue, 2% β -mercaptoethanol). Proteins extracted with a 2% SDS (in PBS) lysis solution were mixed 5:1 with the aforementioned 6X load buffer containing no SDS. Protein mixtures were boiled for five minutes at 99°C in a thermocycler and resolved on precast SDS-PAGE gels (NuPAGE Novex 4-12% Bis-Tris gels (ThermoFisher), ExpressPlus™ PAGE gel (Genscript) or NuPAGE Novex 7% Tris-Acetate protein gels (ThermoFisher)) alongside MagicMark™ XP Western Protein Standard (ThermoFisher, cat# LC5602). Electrophoresis was performed in either a Hoeffer minigel apparatus or an XCell SureLock® MiniVCell in 1X MOPS buffer (ThermoFisher, cat# NP001) or 1X Tris-Acetate buffer (NML Media) at 130-160V until the desired separation was achieved.

2.1.6.3 Silver Staining

Silver staining of SDS-PAGE gels utilized the PlusOneSilver Stain kit (GE Healthcare, cat# 17-1150-01). SDS-PAGE gels were rocked gently in fixing solution (10% acetic acid/ 40% methanol) overnight. The following day, SDS-PAGE gels were incubated in fresh fixing solution for 15 minutes followed by a 30-minute incubation in 100ml sensitizing solution (30% methanol/ 5% sodium thiosulfate 17g sodium acetate) and then washed three times, for five minutes each in H₂O. Gels were then stained with 2.5%

silver nitrate stain for 20 minutes and again washed twice for one minute before the addition of 100ml of developing solution (6.25g sodium carbonate, 100ul 37% formaldehyde). Development proceeded for four to six minutes until the desired staining intensity and was halted by adding stop solution (3.65g of EDTA in 250ml) for 10 minutes with gentle rocking. Silver stained SDS-Page gels were washed with H₂O three times, five minutes before being scanned.

2.1.6.4 Chemiluminescent Western Blotting

Proteins were transferred from SDS-PAGE gels to nitrocellulose membrane (Invitrogen, cat# IB3010-02) using the iBlot semi-dry transfer system (Invitrogen) program 1 for 7 minutes. Membranes were blocked for a minimum of one hour in 5% skim milk powder (SMP, Carnation) in 1X TBS (50mM Tris, pH 7.4, 150 NaCl) with 0.1% Tween 20 (TBST) followed by the addition of primary antibodies diluted in 5% SMP in TBST as per concentrations listed in Appendix Table A2 and incubated overnight with rotation at 4°C. The following day, membranes were washed three times, 10 minutes with TBST and secondary antibody incubations were performed with an HRP conjugated goat anti-mouse (KPL, cat# KP-01-15-16) antibody or an HRP conjugated goat anti-rabbit (Epitomics, cat# #053-1) at a 1: 20,000 dilution in 5% skim milk powder in TBST for 1 hour at room temperature. Membranes were washed three times with TBST for 10 minutes and then exposed to the chemiluminescent HRP substrate Immobilon detection reagent (Millipore, cat# WBKLS0500) for one minute. HRP amplified signals were

detected on Amersham hyperfilm ECL film (GE cat# 28906839) for 30-60 seconds before development in a film processor (SRX-201A, Konica Minolta, Tokyo, Japan).

2.1.6.5 LI-COR Near Infrared Western Blotting

Proteins were transferred from SDS-PAGE gels to PVDF LF membrane (Bio-Rad, cat# 1620264) via the Trans-Blot Turbo Transfer system (Bio-Rad). Membranes were blocked for a minimum of one hour in 50% Odyssey blocking Buffer TBS (LI-COR cat# 927-50100) in PBS. Primary antibodies (diluted as per Appendix Table A2) were added in 50% Li-Cor Odyssey Buffer in PBS, including 0.1% Tween 20 (PBST) solution and incubated overnight with rotation at 4°C. Membranes were washed three times, five minutes with PBST prior to incubation for one hour with 700nm fluorescently labelled anti-rabbit secondary antibody (Li-Cor) and/or 800nm fluorescently labelled anti-mouse both at a 1:20,000 concentration in 50% Li-Cor Odyssey Buffer in PBS, 0.1% Tween 20, 0.01% SDS. Finally, membranes were washed four times; five minutes each, twice with PBST and twice with PBS before drying. Dried membranes were imaged with the LI-COR Odyssey Infrared Imaging System scanner (LiCor Biosciences, Mandel Scientific, cat# LIC-9201-00). Protein bands were quantified using Image Studio Lite software version 3.1 (LI-COR) using the profile tab to define boxes around protein bands and calculating the signal background using background subtraction method (set to median, one pixel, all sides).

2.1.7 Indirect Immunofluorescence

3x10⁵ GP2 293 cells stably expressing N or C-terminally HBH NS5A-2a, HBH-GFP, Huh7.5 or SG JFH1 replicons in Huh7.5 cells were plated into a 35mm dish containing

three 13mm Thermanoc Plastic Coverslips (Invitrogen, cat# 174950). For fixation, cells were washed twice with 1ml of PBS per well before adding 1ml of 2% PFA in PBS for 10 minutes at room temperature. Cells were then washed three times with 1ml of PBS before permeabilizing with 1ml of 0.25% Triton X-100 in PBS for five minutes prior to being washed three times with 1ml of PBS. Coverslips were removed from the 6-well dish and placed in a humidified chamber where 50ul of IF Blocking Buffer (2% BSA/2% FBS in TBST) was added for an hour. Coverslips were then washed three times with PBS after which primary antibody was added (Appendix Table A2) in IF blocking buffer was added and incubated at 4°C overnight. The following day, coverslips were washed three times with PBS, before the addition of the Goat anti-Rabbit IgG (H+L) Dylight 488 conjugated secondary antibody (ThermoFisher, cat# 35502) and/or Donkey anti-Mouse IgG (H+L) Cross-Adsorbed DyLight 594 secondary antibody (ThermoFisher, cat# dSA5-10168) diluted 1:1000 in IF blocking buffer for a total of one hour. Cells were washed three times with PBS before counterstaining with 50ul of a 30uM DAPI solution (ThermoScientific, cat# 62247) in PBS for a total of five minutes. The coverslips were washed a final four times in PBS and mounted using ProLong Gold Antifade Mountant (Molecular Probes, cat# P10144) onto a SUPERFROST glass microscope slide (SYBRON, cat# 4951) and sealed with a clear nail polish. Slides were viewed under the 488 and 593 fluorescent detection channels using an Axiovert 200M fluorescence microscope (Zeiss) with the 32X objective. Alternatively, high-resolution images were obtained using the LSM 700 laser scanning confocal microscope (Zeiss). Cells were plated onto Nunc Lab-Tek 8-chamber slides (ThermoFisher, cat# 154453PK), processed as above and covered with a 13mm glass cover slide (ThermoFisher, cat#12-544-18).

Images were obtained using the 20X and 40X objectives with laser power set at 2.0, and the master gain was adjusted between 700-900 units while the digital gain did not exceed 1.9. Images were analyzed using the Zen Lite software package (Zen 2.3 Lite).

2.1.7.1 JFH1-HT Infection for Indirect Immunofluorescence

1×10^3 Huh7.5 cells were plated into a single well of Nunc Lab-Tek 8-chamber slides (ThermoFisher, cat# 154453PK). The next day 100ul of JFH1-HT virus was added to a chamber, incubated for four hours after which, 200ul of complete DMEM was added. Cells were fixed 48 hpi. JFH1-HT (J. Boutilier and M. Carpenter, unpublished) was a serially passaged JFH1 virus (151) containing six cell culture adapted mutations (L9V and M56L in p7, T180P and I290M in NS3 and D278N and C465S in NS5A).

2.1.8 REAP Method of Nuclear/Cytoplasmic Cellular Fractionation

Fractionation of whole cell lysate into nuclear and cytoplasmic fractions was by the Rapid, Efficient, And Practical (REAP) method as described by Suzuki et al., 2010 (311). 2.5×10^5 293TN, HBH-NS5A-2a and HBH-GFP GP2 293 cells were plated into a 35mm dish and incubated overnight producing a 60-80% monolayer the following day. Cells were harvested by removing media, washing twice with 1ml of cold PBS, and adding another milliliter of PBS into which the adherent cells were scraped. Harvested cells were centrifuged for 10 seconds at 10,000xg, the supernatant was discarded, and the cell pellet suspended by trituration in 900ul of cold REAP Buffer (0.1% NP40 in PBS). From the resuspended cells, 300ul was removed as the “whole cell lysate.” The remaining cell suspension was spun for 10 seconds, and 300ul of the resulting supernatant was removed

as the “cytosolic fraction” after which the remaining supernatant was discarded. The pellet was washed in 1ml of REAP Buffer and resuspended in 180ul of 2% SDS in PBS, becoming the “nuclear fraction.” Both the “whole cell lysate” and the “nuclear fraction” were sonicated at level two, thrice for five seconds to homogenize the nucleic acids using a microson ultrasonic cell disruptor with micro tip attachment (Mandel, HS-Q500-110). The REAP fractionated samples were evaluated by SDS-PAGE and Li-COR Western blotting (2.1.6.2 and 2.1.6.5).

2.2 Generation of HBH-NS5A and HBH-GFP Stable Cell Lines

2.2.1 Creating HBH-tagged NS5A-2a and GFP

To perform Tandem Affinity Purifications (TAP) “bait” proteins were tagged with an HBH tag (255,256). The N-terminally and C-terminally tagged HBH-NS5A-2a expression vectors were created by PCR amplification of the NS5A-2a ORF from the pJFH1 plasmid (a kind gift from Dr. Takaji Wakita (151) (Accession # AB047640) using primers 650F/651R and 652Fr/653Rr, respectively). Control GFP expression vectors HBH tagged at both N and C-termini were produced by PCR amplification using primers 616F/617R and 618F/619R, respectively, on template pEGFP-N1 (Clontech, cat# 6085-1). Nucleotide sequences of the aforementioned primers are listed in Appendix Table A1. PCR amplification was performed using the iProof PCR methodology described in section 2.1.2. The NS5A-2a amplicons to be N- and C-terminally tagged were digested with BsiWI/EcoRI and NotI/BSiWI respectively. GFP amplicons to be N- and C-terminally tagged were digested with BamHI/EcoRI and NotI/AgeI, respectively. All amplicons were inserted into a respectively digested modified pQCXIN retrovirus vector

(Clontech, cat# 631514) modified to contain the HBH tag sequence either upstream or downstream of the multiple cloning site (MCS) and an IRES-neo cassette (K. Hsu, K. Lee and M Carpenter, unpublished).

2.2.2 Retrovirus Production

GP2 293 cells were seeded at 3×10^6 cells per 10cm dish and incubated overnight to produce a 70% monolayer the following day. Cells were co-transfected with 2ug of HBH tagged protein expression vector and 2ug of pVSVG-G (Vesicular stomatitis virus glycoprotein) (Clontech, cat# 631530) vector using the Effectene transfection methodology outlined in section 2.1.4 (Qiagen, cat#301425). After 48 hours, supernatants containing mature retroviruses were passed through a 0.2 um SFCA filter (VWR, cat# 28199-401). The retroviral-containing solution was mixed with PEGIt (Systems Biosciences, cat# LV810A-1), followed by an overnight incubation at 4°C, centrifuged the following morning, 4°C for three hours at 20,000xg, and the supernatant was discarded. Retroviral pellets were resuspended in 1ml DMEM and stored at -80°C.

2.2.3 Generation of stable cell lines

GP2 293 cells were seeded at 4.4×10^5 cells in a 35mm dish to produce a 50% monolayer the following day. The next morning, media was removed, cells were washed once with 1ml PBS, and 500µl of retrovirus in a solution containing 5µg/ml polybrene (Sigma-Aldrich, cat# 107689) was added. The infection was left for six hours, after which, fresh media was added to bring the total volume in the well to 3ml. Drug selection utilizing the neomycin resistance cassette within the pQCXIN vector was started 24 hours after

infection using G418 at a final concentration of 650 μ g/ml. Cells were passaged for ten days under selection, splitting the cells at 80% confluency. Expression from the constructs was confirmed by SDS-PAGE and Chemiluminescent Western blotting techniques described in 2.1.6.2 and 2.1.6.4, respectively utilizing the RGS_{H4} antibody that detects the HBH tag. Positive expression of N- and –C-terminally tagged GFP proteins were confirmed by viewing the fluorescence of GFP with a 488-excitation channel on the Axiovert 200M fluorescence microscope (Zeiss). Cytoplasmic expression of the HBH-NS5A-2a and NS5A-HBH-2a proteins was confirmed using Indirect Immunofluorescence as described in section 2.1.7.

2.3 Non-Denaturing Tandem Affinity Purification (nTAP)

2.3.1 Non-denaturing TAP Harvest of HBH tagged NS5A and GFP-tagged protein

11.4 x 10⁶ GP2 293 cells expressing various constructs were plated onto a single 15cm plate resulting in a 70-80% monolayer the next day. Cells were scrapped into their media, transferred to a 50 ml conical tube and pelleted by centrifugation for at 800xg for 15 minutes at 4°C. Cell pellets were washed twice with 10ml ice cold PBS then lysed in 10ml of nTAP lysis buffer (50mM NaPO₄ pH 8.0, 150mM NaCl, 0.5% NP40 and Protease and Phosphatase Inhibitors (Roche, cat# cOmplete, EDTA-free 11873580001 and PhosSTOP 4906845001) for 30 minutes on ice. Nucleic acids were removed by adding 300 units of Benzonase (Millipore cat# 70746-4) and MgCl₂ to a 2mM final concentration followed by incubating at room temperature for 30 minutes. Cell extracts were stored at -80°C for up to two weeks and on the day of use were thawed

and aliquoted into 1ml fractions for clarification by centrifugation for one hour at 16,000xg, 4°C. The soluble supernatant was used for nTAP purification.

2.3.2 Non-denaturing Metal Chelate Purification of HBH tagged NS5A and GFP using the FPLC

An Akta FPLC (GE Healthcare) A and B lines, the P960 pump and a 1ml HisPur Cobalt Chromatography column (Pierce, cat# 90093) were primed with Buffer A (50mM NaPO₄ pH 8.0, 150mM NaCl, 0.1% NP40) and Pump B with Buffer B (50mM NaPO₄ pH 8.0, 150mM NaCl, 0.1% NP40, 500mM imidazole). Lysates were diluted 1:10 in TAP Buffer A and loaded onto a cobalt column using the P960 high load pump at a flow rate of 0.5ml/minute. The column was washed with 10ml of Buffer A. HBH tagged proteins were eluted using a stepwise gradient with imidazole at concentrations of 10mM, 150mM, and 500mM over 200 minutes while 1ml fractions were collected and stored at 4°C. Fractionated samples containing the HBH tagged protein were confirmed using dot blot procedure in combination with chemiluminescent western blotting with an anti-RGSH₄ antibody as described in section 2.1.6.4. nTAP purifications were evaluated using the Silver Staining methodology described in section 2.1.6.3.

2.3.2.1 Dot blot identification of FPLC fractions containing HBH tagged proteins

18-50ul of 1ml fractions were mixed with 5ul 6X SDS load buffer and boiled for 20 minutes at 99°C. A square of nitrocellulose was moistened with TBS before securing it to the dot blot apparatus. The samples were transferred to the membrane using vacuum suction. Wells of the membrane were washed twice with TBST, and the membrane was

removed and processed as a traditional chemiluminescent western blot as described in section 2.1.6.4 after the transfer step.

2.3.3 Non-denaturing Metal Chelate Purification of HBH tagged NS5A and GFP using batch methods with cobalt magnetic beads

100ul of packed cobalt-based His-Tag Isolation and Pull-down Dynabeads (ThermoFisher, cat# 10103D) was added to the soluble lysate from a single 15 cm plate of cells. All soluble total proteins were quantified (2.1.6.1) and equilibrated to the lowest concentration and loaded equivalently onto 100ul cobalt beads. Cobalt beads were washed twice with 850ul of H₂O and twice with 850ul of Buffer A; each wash was 30 seconds end-over-end rotation in buffer A followed by 150 seconds on the magnetic rack. Precleared protein lysates described in section 2.3.1 were added to the cleaned cobalt beads, and binding was allowed to proceed for a total of 20 minutes with end-over-end rotation at 4°C. Bound protein complexes were washed four times with 850ul of Buffer A and transferred to a fresh 1.5ml Eppendorf tube preceding elution. The elution was a two-step process whereas the first elution consisted of the addition of 850ul of Buffer B and a 20-minute end-over-end incubation at 4°C, removal of the supernatant a second elution comprised of 100ul of Buffer B and a five-minute incubation at room temperature. Eluates were pooled and added directly to cleaned streptavidin beads (Section 2.3.4).

2.3.4 Biotin/Streptavidin Purification of HBH tagged NS5A and GFP

Cobalt purified protein complexes derived from the nTAP FPLC based cobalt column purification (2.3.2) were pooled in a 15ml conical tube, and a total of 25ul packed

Streptavidin T1 MyOne BSA coated Dynabeads (ThermoFisher, cat# 6560) were added (200ul of bead slurry resulted in 100ul of packed streptavidin beads after washing). HBH tagged protein complexes isolated by the cobalt bead batch method (2.3.3) were added directly to 25ul packed Streptavidin T1 MyOne BSA coated Dynabeads (ThermoFisher, cat# 6560). Streptavidin T1 MyOne BSA coated Dynabeads were conditioned by washing four times, twice with H₂O and twice with the TAP Lysis Buffer with washes consisting of a 150 second end-over-end rotation followed by magnetic capture for 150 seconds. Streptavidin beads were added to the FPLC or batch cobalt eluates for 20 minutes at room temperature with end over end rocking. Following capture, binding supernatant was removed, and the beads were washed four times, twice with the TAP Lysis Buffer and twice with the TAP Lysis Buffer without NP40 detergent. Following the final wash, all liquid was carefully removed, and the streptavidin beads were frozen at -80°C.

2.4 Denaturing (dTAP) and Cross-Linked/Denaturing (xdTAP) Tandem Affinity Purification

2.4.1 Denaturing TAP (dTAP) and cross-linked denaturing (xdTAP) Harvest of HBH tagged NS5A and GFP-tagged total protein

11.4 x 10⁶ GP2 293 stable cell lines were plated onto five 15cm plates to yield a 70-80% monolayer the following day. Cells were harvested using a rubber policeman to scrape them down in their media, transferred to a 50 ml conical tube and pelleted at 800xg for 10 minutes in a JS 7.5 swinging bucket rotor, 4°C. Harvested cells were washed twice with 50ml ice-cold PBS per 15cm plate and after the final wash cells were pooled in 15ml of

ice-cold PBS. Cell counts were determined by a Countess Cell Counter (Thermo Fisher). For dTAP lysis, 9×10^7 cells were lysed in 1ml Urea Buffer with Phosphate (UBP) (50mM Na_2HPO_4 , pH 8.0, 8M urea, 300mM NaCl, 0.5% NP40) at room temperature with end-over-end rotation for 20 minutes. For xdTAP, crosslinking of the harvested cells with paraformaldehyde (PFA) (spacer arm of 2.0 Å (262)) was in 1ml 2% formaldehyde solution (1g paraformaldehyde (Sigma, cat# P6148) in 50ml PBS) with incubation for nine minutes at room temperature with end-over-end rotation. Cross-linkers disuccinimidyl suberate (DSS, spacer arm 11.4 Å), disuccinimidyl glutarate (DSG, spacer arm 7.7 Å) and ethylene glycol bis(succinimidyl succinate) (EGS, spacer arm 16.1 Å)(262) were prepared as 25mM solutions in anhydrous dimethyl sulfoxide (DMSO) prepared fresh. Cell pellets were resuspended in either DSS, DSG or EGS cross-linking solution consisting of 10ul DMSO, 40ul of the 25mM cross linker solution (1mM final concentration) and 950ul of PBS followed by a 30 minute incubation at room temperature with end-over-end rotation. Cross-linking solution was removed by centrifugation at 800xg for one minute at room temperature, and the reaction was quenched with 1ml of ice-cold 125mM glycine (GE, cat# 17-1323-01) in PBS for five minutes at room temperature with end-over-end rotation. Quenched samples were centrifuged at 800xg for one minute at room temperature, and all supernatant was carefully removed before resuspending in 1ml of PBS. All cross-linked cells were then lysed in 1ml UBP for 20 minutes at room temperature with end-over-end rotation and homogenized using a QIAshredder (Qiagen, cat# 79656) by centrifuging at 10,000xg for one minute at room temperature. Alternatively, samples were sonicated with five pulses for 20 seconds each on a microsonic ultrasonic cell disruptor with a microtip probe (Mandel, cat# HS-Q500-

110). Samples were clarified by centrifugation for one hour at 16,000xg at room temperature. Soluble supernatants were stored at -80°C or processed immediately by the dTAP/xdTAP protocol.

2.4.2 dTAP/xdTAP Metal Chelate Chromatography and Streptavidin capture for the purification of HBH tagged proteins

dTAP/xdTAP metal chelate chromatography purifications were performed similarly to the nTAP metal chelate chromatography batch purifications with cobalt beads described in section 2.3.3 with the following modifications. Denatured and denatured/cross-linked protein lysates (section 2.4.1) were added to 50ul of packed cobalt-based His-Tag Isolation and Pull-down Dynabeads that had been washed twice with H₂O and conditioned twice with UBP buffer. Binding was for a total of two hours at room temperature. The binding supernatant was removed, and the cobalt beads with bound protein complexes were washed thrice with 1ml UBP. Denatured/cross-linked protein complexes were eluted from the cobalt beads by the addition of 1ml of UBP Elution buffer (50mM NaPO₄ pH 5.0, 8M urea, 300mM NaCl, 0.5% NP40, 500mM imidazole) and a 10-minute incubation. The elution was repeated and the eluates pooled. Cobalt purification was performed using a HisPur Cobalt Chromatography Cartridges (Pierce, cat# 90093) with loading performed with the aid of a syringe pump (kdScientific, cat# 78-0220V), where protein complexes were adsorbed to the 1ml column, washed thrice with 5ml UBP and eluted with 5ml of UBP Elution buffer. Eluted material from either method of cobalt capture was added directly to 150ul of packed Streptavidin T1 MyOne BSA coated Dynabeads previously washed twice with water and conditioned twice with

UBP Buffer, followed by an overnight capture at room temperature. The following day, the streptavidin bead and bound protein complexes were washed twice with UBP and twice with AB buffer, leaving the final pellet in 25ul of AB Buffer (50mM NH_4HCO_3) then stored at -80°C .

2.5 Digestion and Purification of Peptides for Mass Spectrometry Analysis

2.5.1 Reduction/Alkylation/Trypsin Digestion of Peptides from Streptavidin

Capture

Denatured protein complexes were resuspended in 100ul of Urea Exchange Buffer (UEB) (8M Urea (GE, cat#17-1319-01), 50mM Tris-HCl, pH 8.0) and allowed to denature at room temperature for 30 minutes. Reduction and alkylation of the proteins was accomplished by the addition of 1,4-Dithiothreitol (DTT) (Sigma, cat# 10197777001) to a final concentration of 5mM with a 30 minute incubation followed by the addition of iodoacetamide (IAA) (Sigma, cat# I6125) to a final concentration of 15mM in Ammonium Bicarbonate buffer (AB Buffer) (50mM NH_4HCO_3 (Sigma, cat# 09830) and a 30 minute incubation in the dark. The Urea concentration was adjusted to 1.6M with AB Buffer, before adding 1.0ug of trypsin (lyophilized protein reconstituted in 100ul 50mM acetic acid) (Promega, Porcine Sequencing Grade, cat#V5280-100ug) followed by an overnight incubation in a humidified chamber at 37°C .

2.5.2 Strong Cation Exchange (SCX) Purification of Peptides

Peptides as prepared in Section 2.5.1, peptides were separated from magnetic beads by magnetic rack separation and acidified with 2ul of 10% Trifluoroacetic acid (TFA) with a minimum final concentration of 0.2% TFA. Sample pH was determined by applying 1ul of the acidified peptides onto pH test strips ensured the pH was less than 3.5. Penta-SCX stage tips (312) used five layers of Empore SPE cation exchange disks (Sigma cat# 66889-U) in a 200ul unfiltered pipette tip which were conditioned by slowly passing 80ul of 0.1% TFA through the tip, three times. Tryptic digested peptides were adsorbed to the Penta-SCX stage tip by slow addition of the peptide solution. The Stage Tip was washed once with 80ul of 0.1% TFA and twice with 80ul of 50% Methanol (MeOH)/0.1% TFA. Peptides were eluted by adding 50ul of 5% Ammonium Hydroxide (NH₄-OH) /30% MeOH, twice, pooling both eluates. 100ul of acetonitrile (ACN) was added to the pooled eluates before the peptides were subsequently dried using vacuum centrifugation in a Savant Universal SpeedVac vacuum system (Thermofisher, Massachusetts, USA). Dried peptides were stored at -80°C. Prior to Mass Spectrometry, peptides were resuspended in 22ul of mass spectrometry grade H₂O and the concentration of the eluted peptides was estimated using a Nanodrop spectrophotometer (assuming 1 A₂₈₀ = 1ug/ml). The concentration was adjusted to 2ug/20ul using 0.1% FA/ 2% ACN.

2.6 Mass Spectrometry Analysis of TAP Purified Protein Complexes

2.6.1 Mass Spectrometry

Individual samples were injected via a nano-flow Easy nLC II HPLC (Proxeon Biosystems) connected in-line to an LTQ Orbitrap Velos mass spectrometer.

Approximately 1.5 ug of total peptide (15ul) was concentrated onto a C₁₈ reverse phase trap column (2cm long, 100ul inner diameter, 5um particles) with 100% Buffer A (2% Acetonitrile, 0.1% FA) at 3ul/min prior to injecting onto a C₁₈-reversed phase analytical column (10cm long, 75 um inner diameter, 3um particles). Columns were packed in-house with ReproSil-Pur C18-AQ resin (Dr. Maisch) and fritted with Kasil by the NML Mass Spectrometry core unit (NML Winnipeg). Peptides were eluted using a 120-minute linear gradient of 0-30% acetonitrile applied at a constant flow rate of 300nl/minute using nano-LC Buffer A (2% CAN) 0.1% FA) and B (98% ACN / 0.1% FA). Eluted peptides were injected into the LTQ Orbitrap Velos mass spectrometer using a nanoelectrospray ion source at 2.35 kV. Data from the mass spectrometer was collected as a data-dependent acquisition consisting of an initial survey scan ($m/z = 300$ to 1700 , resolution = 60000 at m/z 400) in the Orbitrap followed by selection of the top 10 most abundant precursor ion peaks containing a charge state greater than +1 for analysis on the linear ion trap ($2.0m/z$ isolation width). Peaks chosen for fragmentation were subjected to collision-induced dissociation (CID) (35% normalized collision energy), with ten millisecond activation time. Dynamic exclusion lists included 500 features, an m/z tolerance of 15 ppm, a repeat count of 1 and duration of 30 seconds with an exclusion period of 15 seconds, with early expiration disabled. A blank injection of H₂O was run between samples containing to limit potential cross-contamination. In some experiments, HCD was employed and the top 5 most abundant ions were selected prior to analysis on the Orbitrap.

2.6.2 Mass Spectrometry Data Analysis

Data files from the Orbitrap Velos mass spectrometer were acquired in .RAW format were searched utilizing the Mascot server 2.3 (Matrix Science) against the International Protein Index (IPI) Human database version 3.71 to which all HCV genotype 2A (JFH1) protein sequences were appended. Trypsin was selected as the digestion enzyme with a maximum allowance of two missed cleavages and carbamidomethylation of cysteine as a fixed modification and oxidation of methionine as a variable modification. Resulting files were loaded into Scaffold version 3.4.9 (Proteome Science, Oregon), and Peptide and Protein Prophet algorithms were set to Protein 99%, Peptide 80%, 2 peptides per protein minimum. Common contaminants (keratin/trypsin) were excluded from the final tables. Additionally, PEAKS 7.5 software (SBI Biosciences, Waterloo, Canada) was employed with settings as for the Mascot server searches described above. A false discovery rate of 1.0% at the peptide level was set for each search engine.

2.7 Confirmation of nTAP and xdTAP NS5A-2a Protein-Protein Interaction

Candidates

2.7.1 TAP Confirmation Expression Plasmids

FLAG or Myc-tagged expression vectors were created using the cloning strategy described in section 2.1.3. The source of tagged vector, insert, PCR primers and restriction enzymes for each construct are listed in Appendix Table A3.

2.7.2 Confirmation of TAP Interaction Candidates by Co-Immunoprecipitation

2.5×10^5 293TN cells were plated in a 35mm dish producing a 60% monolayer the following day. Cells were transfected with bait and prey protein expression vectors using the Xtreme gene cell culture transfection (section 2.1.4). To obtain similar gene expression levels from the FLAG and Myc-tagged vectors, different quantities of expression vector was transfected. For example, 1.5ug of FLAG-NS5A-2a, 0.1ug of FLAG-GFP, 1.0ug of Myc-FKBP38 and 2.0ug of each of the remaining Myc-tagged candidates. After a 48 hour incubation period, transfected cells were washed twice with 1ml of ice-cold PBS and lysed in either 0.5ml of Co-IP Lysis Buffer P (PBS pH 7.4, 0.5% NP40, Protease and Phosphatase Inhibitors) or Co-IP Lysis Buffer T (Tris-HCl pH 7.4, 0.5% Triton X-100, 150mM NaCl, Protease and Phosphatase Inhibitors) for 30 minutes on ice. Lysates were sheared with a 25½-gauge needle, ten times then clarified by centrifugation at 15,000xg, for 15 minutes at 4°C. Soluble protein lysates were precleared using 80ul of Protein A/G agarose (Thermo Fisher, cat#20421) for 45 minutes. Magnetic beads were used to capture the bait proteins: a forward Co-IP captured the FLAG-tagged protein using Anti-FLAG M2 magnetic beads (Sigma cat# M8823) whereas the reciprocal IP captured myc-tagged proteins with Anti-c-myc Magnetic Beads (Pierce cat# 88842). The methodology was identical regardless of the capture bead type. 10ul of packed beads were used and were recovered from 20ul of bead slurry by removing the storage buffer and washing twice with 1ml of Co-IP Buffer P or T. Beads were blocked for one hour in 20% FBS in Co-IP Buffer P or T and were washed twice with 1ml of Co-IP Lysis Buffer P or T. Soluble protein lysates were added to the blocked beads and binding allowed for a total of two hours after which the beads were washed

five times, three times with 1ml of Co-IP Lysis Buffer P or T, then twice with the same buffer without detergent. Protein complexes were eluted from the beads with 45ul of a 1X SDS load buffer then boiled for ten minutes at 90°C. Eluted protein complexes were subsequently removed from the beads using a magnetic rack and stored at -80°C.

2.8 Generation of SG JFH1 and SG JFH1-NS5A-HBH replicon Huh7.5 cell lines

The HCV JFH1 subgenomic replicon (SG JFH1) consisting of the HCV non-structural open reading frame (NS3-NS5B) driven by an EMCV IRES and a neomycin resistance cassette under the control of the HCV JFH1 IRES was provided as a kind gift from Dr. Takaji Wakita (150). SG JFH1-HBH was created by inserting the entire HBH tag after E420 and before G421 in the SG JFH1 plasmid. Primers 1098F and 1099R both containing an *AbsI* restriction site were used in the PCR to amplify the HBH tag from pHBH-NS5A-2a. This amplicon was cloned initially into a 2484bp *NsiI/BsrGI* subfragment of pJFH1 from NS3 base pair 5321 in JFH1 genomic numbering to NS5B base pair 7805. The pJFH1 subfragment with the HBH tag was subsequently transferred into full-length pJFH1 via the *NsiI/BsrGI* restriction sites to create the SG JFH1-NS5A-HBH plasmid.

2.8.1 *In vitro* RNA Synthesis

Sixteen micrograms of pSG JFH1 (150), or pSG JFH1-NS5A-HBH DNA plasmids were linearized using *XbaI* (NEB), for two hours at 37°C followed by treatment with one unit of Mung Bean Nuclease (NEB, cat# M0250S) for 30 minutes at 37°C. Plasmids were purified using QIAEXII resin and quantified using a Nanodrop spectrophotometry. 1.0ug

of the digested template plasmid was used as a template for RNA synthesis using a MEGAscript T7 kit (Ambion cat# AM1334) in a 30ul reaction as detailed by the manufacturer for three hours at 37°C. DNA was removed using 1ul of TURBO DNase (Ambion cat# AM1239) for 15 minutes at 37°C after which RNA transcripts were purified using the RNeasy Plus kit (Qiagen cat# 74136) according to the manufacturer's instructions. RNA concentrations were determined by NanoDrop spectrophotometry, and quality was assessed using 0.7% agarose gel electrophoresis and deemed acceptable by the presence of a single band a lack of smearing. Absence of template DNA was ensured by no amplification in a PCR reaction without reverse transcriptase.

2.8.2 Electroporation of RNA into Huh7.5 cells

15cm plates were seeded at 3.9×10^6 Huh7.5 three days prior to electroporation and cells were harvested by trypsinization and pelleted using a JS 7.5 swinging bucket rotor centrifuge for 15minutes at 500xg, 4°C. Cells were washed twice with ice-cold PBS and centrifuging each time for 15 minutes, 500xg at 4°C. Cell counts were determined using a Countess cell counter (Invitrogen) and were adjusted to 1.5×10^7 cells/ml with PBS. Five ug of RNA was added to 400ul of the cell suspension containing 6×10^6 cells and immediately transferred to a pre-chilled 0.2 cm gap Gene Pulser Electroporation Cuvette (BioRad, cat# 1652082). Electroporation used a ECM 830 Square Wave Electroporation system (BTX, cat# 45-0002, Massachusetts) with settings: 820V, 99us, pulses=5, interval 220ms (313). Electroporated cells were allowed to recover for 20 minutes at room temperature prior to addition of 600ul of pre-warmed DMEM and plating onto a 35mm dish containing 2 ml complete media. The plating amounts required to produce a full

monolayers at time of harvest were, 291ul for 4hpe, 251ul for 12 hpe, 200ul for 24 hpe, 158ul for 36 hpe, 125ul for 48 hpe and 90ul for 72hpe. Generation of the Huh7.5 cell line stably expressing SG JFH1 or SG JFH1-NS5A-HBH was done using selection with 0.75mg/ml G418 for 10 days. Replicon containing cells were maintained under selective pressure with 0.4mg/ml G418.

2.9 Purification of HBH-NS5A-2a from stable cell lines and HBH-tagged NS5A from SG JFH1 in Huh7.5 cells for phosphorylation site identification using dTAP

11.4×10^6 HBH-NS5A-2a GP2 293 cells or SG JFH1-HBH Huh7.5 cells were plated onto five 15cm plates and harvested according to the dTAP method (section 2.4).

2.10 Purification of JFH1 NS5A protein from SG JFH1 Huh7.5 cell line by continuous elution gel electrophoresis

NS5A-2a protein from the SG JFH1-Huh7.5 cell line was isolated utilizing continuous elution gel electrophoresis in a 491 Prep Cell (Bio-Rad) to obtain high-resolution molecular weight separation of total protein extract. Either a 7.5%, 8.5% or 9% separating gel was prepared by assembling the gel tube of 491 Prep Cell and adding degassed acrylamide gel solution (Acrylamide/Bis (37.5:1 Stock, 30%), 1.5M Tris-HCl, pH 8.8, 10% ammonium persulfate, Tetramethylethylenediamine (TEMED) to the 37mm gel tube until the 10.5cm mark, overlaying the gel with 2ml of water-saturated 2-butanol for two hours and replacing the butanol overlay with 491 Gel Buffer (0.375M Tris-HCl pH 8.8). The acrylamide core was allowed to solidify overnight. The following day, a 3.2% stacking gel (Acrylamide/Bis (37.5:1 Stock), 0.5M Tris-HCl, pH 6.8, 10% ammonium persulfate, TEMED) was added on top of the separating gel, overlaid with

2ml water-saturated 2-butanol and allowed to polymerize for two hours. Cell lysates were prepared in 6ml of a 3% SDS in PBS solution containing both protease and phosphatase inhibitors and boiled for 10 minutes at 90°C. Cellular lysates were passed through a Qiashredder to reduce viscosity then total protein concentrations were determined by a Pierce BCA assay (2.1.6.1). DTT was added to protein lysates to a final concentration of 20mM, boiled at 95°C for seven minutes and allowed to cool to room temperature. IAA was added to 60mM final concentration and incubated for 30 minutes at room temperature in the dark followed by the addition of 6X 492 Prep Load Buffer (0.5M Tris 6.8, 30% glycerol) to a final concentration of 1X. 600ml and 800ml of Running Buffer (Tris-Glycine, SDS) added to the upper buffer reservoir and upper buffer elution reservoir, with two liters of buffer used in the lower gel chamber. Elution tubing was connected to the FPLC (acting as an external fraction collector) and the protein sample was loaded onto the surface of the gel and resolved by electrophoresis at 12W constant power, 600V and 100mA for a total of 6-10 hours. Fractions were eluted in 2ml volumes, evaluated by SDS-PAGE (2.1.6.2) for size by silver staining (2.1.6.3), and presence of NS5A-2a was determined by Western blot (2.1.6.4). Fractions containing NS5A-2a protein were pooled and concentrated using an Amicon Ultra-4 Centrifugal Filter Unit with Ultracel-30 membrane with a 30kDa molecular weight cut-off (Millipore, cat# UFC801024). Samples were washed twice with 4ml UBP buffer before storage at -80°C.

2.11 Identification of phosphorylation sites in NS5A-2a using Mass Spectrometry

2.11.1 Sources of NS5A-2a for phosphoacceptor site identification

Purified NS5A-2a protein was generated from four separate sources. Both HBH-NS5A-2a from GP2 293 and SG JFH1-NS5A-HBH Huh7.5 cells were obtained using the dTAP and nTAP protocols described in sections 2.4.2 and 2.3. Non-tagged NS5A-2a from SG JFH1 was purified utilizing the continuous gel electrophoresis method described in section 2.10.

2.11.2 Peptide reduction/alkylation/digestion for nTAP and dTAP purified NS5A-2a phosphoacceptor site identification

HBH-NS5A-2a obtained using the nTAP or dTAP purification methods was reduced, alkylated and digestion according to section 2.5.1 with the caveat that alternative proteases to trypsin were used in different experiments including 1.0ug/ul AspN (Promega, cat# V1321) or GluC (Roche, cat# 11047817001). These proteases required overnight incubation at 20°C for AspN and 25°C for GluC.

2.11.3 Peptide reduction/alkylation/digestion for 491 prep cell purified NS5A-2a phosphoacceptor site identification

Purified NS5A-2a from continuous gel electrophoresis (2.10) was prepared for M/S using a modified Filter-Aided Sample Preparation method previously described (314,315). Proteins obtained in section 2.10 were absorbed using a Nanosep 30K centrifugal cartridge (Pall, cat# OD030C34) by centrifugation at 10,000xg until all the liquid had passed through and washed twice with UEB to remove SDS. DTT was added to a

100mM final concentration in UEB and removed by centrifugation at 10,000x for 15 minutes after a 20-minute incubation at room temperature. Proteins were alkylated by the addition of 100ul of 50mM IAA in UEB to the cartridge and placing in a thermomixer to shake at 600 rpm for one minute at room temperature, followed by a 20-minute incubation at room temperature in the dark, then removing the IAA solution centrifugation at 10,000xg for 15 minutes. Next, the cartridge was washed three times with 250ul of UEB, centrifuging until all the liquid had passed through. Proteins were washed twice with 150ul AB buffer by centrifuging at 10,000xg for 10 minutes. Fifty ul of AB buffer containing 2ul of 1.0ug.ul trypsin, AspN or GluC was mixed in a thermomixer at 600 rpm for one minute before and an overnight incubation in a humidified chamber at 37°C for trypsin, 20°C for AspN 25°C for GluC. The following day, 50ul of AB buffer was added to cartridge and the cartridge was mixed in a thermomixer at 600rpm for two minutes after which the digested peptide mixture was collected by inverting the cartridge and centrifuging for three minutes at room temperature, collecting the eluate, and repeating the elution again with 50ul of AB buffer. Eluted peptides were pooled and diluted in H₂O to a final volume of 240ul before adding TFA to a final concentration of 2%. Peptides were lyophilized using a SpeedVac vacuum system and resuspended in 50ul of 30% ACN/1% TFA (pH <2.8) before proceeding to C₁₈ stage tip clean up.

2.11.4 C₁₈ stage tip clean-up of peptides for phosphopeptide identification

C₁₈ stage tips were moistened with 50ul of 100% methanol and conditioned, once with 50ul of 0.5% FA/80% ACN and again with 50ul of 0.5% FA. Digested peptide sample

was absorbed by loading and re-loading the flow through. Absorbed peptides were washed thrice with 0.5% FA before double eluting the peptides using 50ul 0.5% FA/ 80% ACN and pooling the eluates. Peptides were lyophilized using the SpeedVac vacuum system and resuspended in 22ul of 0.1% FA/ 2% ACN.

2.11.5 Phosphopeptide Enrichment

2.11.5.1 Phosphopeptide Enrichment using TiO₂

Phosphorylated peptides were enriched from total digested peptide samples using TitanSphere TiO₂ beads (GL Sciences, cat# 13528500). Four ug of TiO₂ beads were resuspended in 1ml H₂O and centrifuged for one minute at 5,000xg and washed twice with 1ml of Lactic Acid Load Buffer (2M Lactic acid / 50% ACN). Digested peptides were rehydrated in 1ml of Lactic Acid Load Buffer then clarified by centrifugation at 16,000xg for 20 minutes, after which, the soluble material was transferred to the TiO₂ beads and vortexed at maximum for one hour. TiO₂ beads were centrifuged for one minute at 5,000xg, the supernatant removed and two washes with 200ul of Lactic Acid Load Buffer and two washes with 200ul of 0.1% TFA/50% ACN was performed. Peptides were eluted twice using 20ul Lactic Acid Elution Buffer (50mM K₂HPO₄ pH 10.0), pooled and acidified using 20ul of 5% FA to achieve a 2.5% final FA concentration. Phospho-enriched peptides were then desalted and concentrated using C18 stage tip clean up (section 2.11.4).

2.11.5.2 Phosphopeptide Enrichment using PolyMAC-Ti

Phosphopeptides were enriched using the PolyMAC-Ti Expedeon Phosphopeptide Enrichment Kit (Expedeon, cat# PMACTM02). Lyophilized peptides were resuspended in 100ul of the Loading Buffer provided in the PolyMAC kit, and 4ul of the PolyMAC reagent was added followed by mixing in a thermomixer for five minutes at 900rpm. Next, 200ul of Capture Buffer was added to the peptides to acidify the solution, (ensuring a pH between 5.5-6.5), and 50ul of the Magnetic Capture beads were added mixing the beads and samples for 10 minutes at 900rpm. Following mixing, samples were spun briefly for three seconds and placed on the magnetic separator rack for 30 seconds while the beads collected on the side of the tube and the supernatant was removed. The capture beads were washed once by adding 200ul of Loading Buffer then shaking at 900rpm for five minutes and finally washing twice more with 200ul Washing Buffer. Phosphoenriched peptides were eluted by incubating the beads twice in 100ul of Elution Buffer, shaking for five minutes and using the magnetic rack to harvest supernatants. Eluted peptides were lyophilized with the SpeedVac vacuum system and rehydrated in 10ul of 0.25% FA.

2.12 NS5A phosphoacceptor site mutagenesis

pJFH1, a kind gift from Dr. Takaji Wakita (151), was used as a template to mutagenize specific serine and threonine residues within the NS5A ORF using the Q5 site-directed mutagenesis kit (NEB, cat # E0554S) on a 2484bp NsiI/BsrGI subfragment of pJFH1 containing a region encompassing NS3 to NS5B (base pair 5321-7803 on the JFH1 genome). Primers used in mutagenesis are provided in Appendix Table A4 and were

generated by the NEBasechanger v1.2.6 (316). Briefly, for a 25ul reaction, 1X Q5 Hot Start High-Fidelity Master Mix, 10uM of both the mutagenic forward and reverse primers, 1ng template DNA and nuclease-free H₂O was subjected to the following cycling conditions: initial denaturation for 30 seconds at 98°C, 25 cycles of denaturation at 98°C for 10 seconds, annealing temperature as calculated by the NEBaschanger program for 10 seconds, extension at 72°C for 30 seconds per kilobase and a final extension at 72°C for two minutes. Following amplification, 1ul of the PCR product was added to a Kinase-Ligation DpnI (KLD) reaction containing 1X KLD reaction buffer, 1ul KLD enzyme mix, and nuclease-free H₂O and allowed to incubate at room temperature for five minutes. Mutagenic plasmids were transformed using the aforementioned “heat shock” transformation protocol (2.1.3) into chemically competent *E.coli* QD cells provided with the kit) and plated on LB plates containing 100µg/ml carbenicillin. Plasmids were isolated using a QIAprep Spin Miniprep Kit (Qiagen, cat # 27104), and the NsiI-BsrGI fragment was transferred into full-length pJFH1. All mutations were confirmed by Sanger sequencing. JFH1 phosphomutant *in vitro* RNA transcripts were generated as described in section 2.8.1 and were electroporated into Huh7.5 as described in section 2.8.2.

2.13 RNA Isolation and Quantitative real-time reverse transcriptase PCR

Huh7.5 cells were electroporated with 5ug of *in vitro* transcribed HCV RNA from wt, GND, or phosphomutants (section 2.8). At four and 72 hours, post-electroporation (hpe) cells were washed twice with PBS and RNA was isolated using the RNeasy Plus Mini Kit with genomic DNA removal (Qiagen, cat# 74136). RNA concentrations were

determined by Nanodrop spectrophotometry, and 50ng of RNA was reverse transcribed into cDNA utilizing the Quantitect Reverse Transcription Kit, Qiagen cat# 205313). Briefly, 1ul 7X gDNA wipe-out buffer was added to the RNA in a total volume of 7ul then incubated for two minutes at 42°. RNA was reverse transcribed into cDNA in a 20ul reaction volume containing 2.0ul of 5X Quantiscript RT buffer, 0.5ul of Rt-Primer mix and 0.5ul of reverse transcriptase master mix for 15 minutes at 42°C, and three minutes at 95°C. One ul of the cDNA reaction was used for SYBR Green (Biotools, cat# B21203) real-time PCR reaction containing 8.2ul of H₂O, 10.0ul of 2X SYBR Select Mix and 400 mM of each primer. The primers used for amplification were previously described by Matto et al., 2011 (313) and bind in the HCV 5' UTR (Forward: 5'-TCTGCGGAACCGGTGAGTA-3' and Reverse: 5'-TCAGGCAGTACCACAAGGC-3'). The cellular control GAPDH amplification primers (NCBI accession # Nm_002046) span exons two and three (Forward: 5'-ACATCGCTCAGACACCATG-3' and Reverse 5'-TGTAGTTGAGGTCAATGAAGGG-3') and served as a total RNA normalization control. Reactions took place in a 96 well MicroAmp FAST optical reaction plate (ThermoFisher, cat#4346906) sealed with MicroAmp optical adhesive film (ThermoFisher, cat# 4311971). Analysis was performed in triplicate for each sample, and the average of the three technical replicate values was reported. An HCV RNA standard was prepared by serially diluting known amounts of *in vitro* transcribed HCV RNA into 100ng total Huh 7.5 cellular RNA to determine the viral genome copy numbers in each experimental sample. Thermocycling consisted of a UDG activation step at 50°C for two minutes, an AmpliTaq polymerase activation step of two minutes at 95°C, 40 cycles each consisting of 95°C for three seconds, 60°C for 30 seconds and a final

dissociation step producing a melt curve. Amplification was performed on a StepOnePlus Real-Time PCR System (Applied Biosystems/Life Technologies) and evaluated using StepOnePlus Software version 2.3 (Applied Biosystems). Total viral RNA copy numbers were normalized to the average GAPDH value provided by each experimental plate. All mutant RNA samples were evaluated from a minimum of two independent electroporation experiments.

2.14 Western Blot Analysis of NS5A from Electroporated Huh7.5 Cells

Protein extracts from electroporated Huh 7.5 cells were harvested at 72hpe by washing twice with PBS before lysing in 100ul 2% SDS/PBS and immediately boiling the samples for 10 minutes at 85°C. Samples were passed through a Qias shredder. Total protein was quantified using a BCA protein assay (section 2.1.6.1). Twenty ug of total protein was resolved on a 7% SDS-Tris Acetate gel (Novex) at 4°C for four hours at 130V. Western blots proceeded as described in Section 2.1.6.5). All phosphomutant protein samples were evaluated from a minimum of two independent electroporation experiments.

2.15 TCID₅₀/ml Analysis of HCV Viral Titer

Following electroporation with the JFH1 phosphomutants, Huh7.5 cells were passaged according to cellular confluency every three days for a total of nine days. On the ninth day, cell culture supernatants were collected and clarified at 500xg for 10 minutes at 4°C and stored at 4°C up to one week. Naïve Huh7.5 cells were seeded into 96 well plate at 8,000/cells per well 24 hours before infection with a five-fold serial dilution of clarified viral supernatants diluted in DMEM without FBS or antibiotics. 100ul of inoculum

diluted in DMEM (no FBS) was added to the cells, and the infection was incubated for a total of four hours followed by the addition of 100ul complete DMEM containing 20% FBS. Infections proceeded for four days. On the fourth day, cells were fixed by submerging plates in 100% ice-cold methanol for 25 minutes at -20°C, removing methanol and allowing plates to completely dry. Plates were washed with PBS before the addition of 100ul IF Blocking Buffer (2% BSA, 2% FBS, 0.1% Tween 20 in PBS) and were blocked for one hour. Primary antibody consisting of 1:750 dilution of NS5A-Ab02 was added to IF blocking buffer and incubated overnight at 4°C. The following day, plates were washed three times with PBS-T before an hour-long incubation with the anti-rabbit Dylight 488 antibody (Thermo) (1:1000). Plates were again washed three times with PBS-T before a final addition of 100ul PBS. Individual wells were evaluated by an Axiovert 200M fluorescence microscope (Zeiss) and scored as positive or negative based on the presence of a minimum of at least one viral foci per well. TCID₅₀/ml was calculated by a Lindenbach et al. 2009, modified Reed & Muench method (317). TCID₅₀/ml values were expressed as a ratio of mean wt values obtained from the corresponding electroporation, and these wt values were set to be a value of one. All phosphomutant TCID₅₀/ml values were evaluated from a minimum of two independent electroporation experiments.

Chapter 3: Identification of host cell interacting proteins of hepatitis C virus nonstructural 5A protein by a novel tandem affinity purification, mass spectrometry based approach

3.1 Introduction and Rationale

Of the ten proteins encoded by hepatitis C virus (HCV), NS5A has emerged as a key regulator of viral propagation and pathogenesis although in both areas specific mechanisms remain poorly defined. NS5A has previously been shown to interact with a diverse set of host proteins including TRAF2/TRADD (apoptosis regulation) (219–221), FKBP8/38 (immunophilins) (232,234–237), TIPE2 (neoplasia) (245) and p53 (tumor suppressor) (224,225,318). Revealing the broader NS5A-host protein interactome using state of the art techniques should provide critical insight into the protein's function and role in HCV pathogenesis and replication. Recently, a new tandem affinity purification (TAP) tag was developed which utilizes a biotinylation signal sequence flanked by two hexahistidine sequences. In combination with two rounds of purification this TAP system provides exquisite recovery and purity (255,256). The HBH tag is functional even under denaturing conditions; protein samples can be cross-linked *ex vivo*, locking protein-protein interactions (PPIs) in their biologically relevant context then lysed and purified in denaturing buffer to enhance bait purity. This has particular relevance for NS5A, as it is a membrane bound protein and often extracts poorly in standard interaction lysis buffers.

3.2 Results

3.2.1 Creation GP2 293 cells stably expressing HBH-tagged NS5A

Efficient purification of a target protein is crucial for the identification of interacting proteins isolated by tandem affinity purification. The HBH tag was originally designed for use in yeast cell experiments, so the first task was to repurpose it for mammalian cell work. The tag encoding region was introduced into a retrovirus vector (pQCXIN) in order to generate stable cell lines expressing the tagged bait (NS5A-2a). Two versions of the vector were made differing only in the placement of the HBH tag; one creates an N-terminally tagged construct (HBH-NS5A-2a) and the other a C-terminal construct (NS5A-HBH-2a) (Fig.3.1.A displays the C-terminal tag HBH plasmid). The vector expresses a bicistronic transcript with a CMV promoter driving the transcription of the gene of interest (in this case NS5A-2a) fused with the HBH tag. A neomycin resistance marker (neoR) is located downstream of an internal ribosome entry sequence (IRES). Long terminal repeats (LTRs) flanking the expression region allow the generation of infectious retrovirus, which can be used to integrate the coding region into the genome of a host cell (Fig.3.1.A). The HBH tag is composed of two sets of hexahistidine residues (one containing an RGS motif) flanking a biotin recognition sequence that becomes biotinylated *ex vivo* by a host cell biotinylase (Fig.3.1.B). The NS5A-2a ORF (HCV strain JFH1) and Green Fluorescent Protein (GFP) were cloned into pQCXIN-HBH vectors as both N and C-terminally tagged constructs. GFP was used as a control as it is a moderately sized soluble protein (34kDa), and originates from jellyfish and therefore should be innocuous to a human cell.

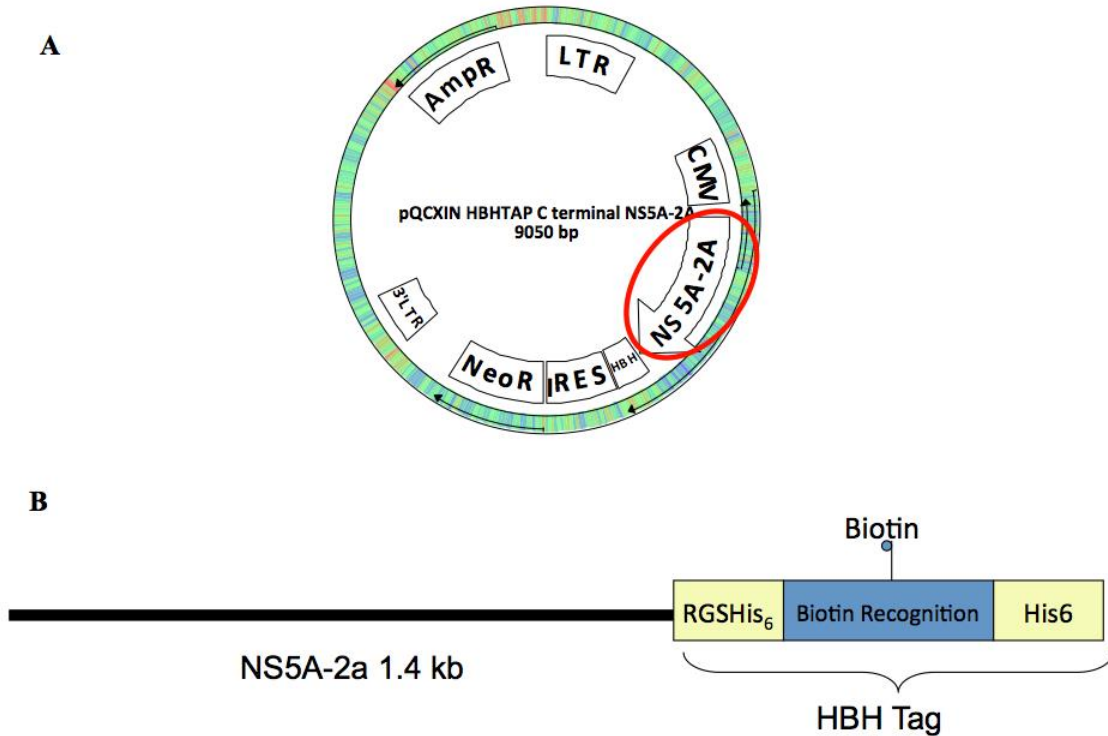


Figure 3. 1. Cloning of the HCV NS5A-2a ORF into the pQCXIN-HBH vector. **(A)** Schematic of the pQCXIN-HBH vector used for generation of the HBH C-terminally tagged NS5A protein (NS5A-HBH 2a, circled in red). A CMV promoter drives expression of a bicistronic transcript containing the gene of interest followed by an IRES and a neomycin resistance gene. **(B)** Schematic of C-terminally tagged NS5A-2a protein. The HBH tag is composed of two hexahistidine sequences, one of which contains an RGS motif upstream, flanking a biotinylation recognition sequence consisting of 75 amino acids. A single Lysine residue within this sequence becomes biotinylated by a host biotinylase when expressed *ex vivo* (255,256).

The expression clones were used to generate infectious retroviruses which were subsequently used to produce 293 cell lines stably expressing the relevant open reading frames (Fig 3.2). Verification of stable HBH-tagged protein expression was confirmed by Western blot analysis using the RGS_{H4} antibody (directed against the first hexahistidine motif in the HBH tag). Figure 3.3A shows HBH-NS5A-2a (lane 1) and NS5A-HBH-2a (lane 6) proteins are detected at 74/76 kDa consistent with the expected molecular weight (63/65 kDa for NS5A-2a and 11 kDa for the HBH tag). HBH-GFP (lane 2) produces a

protein of 38 kDa (27 kDa for GFP plus 11 kDa HBH tag). Previously generated HBH-HCV Core-1a and HBH-HCV Core-2a cells lines were used as positive controls (lanes 4-5), and a cells only negative control detected no protein (lane 3).

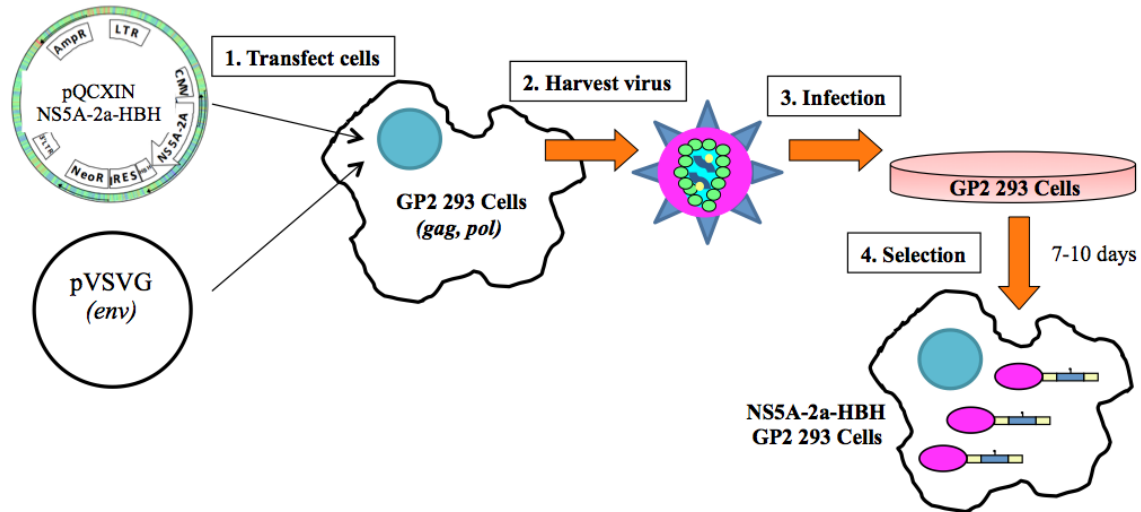


Figure 3. 2. Production of GP2 293 stable cell lines expressing HBH tagged proteins. pQCXIN-HBH vectors containing HBH-tagged NS5A-2a or GFP cassettes were dually transfected with the pVSVG plasmid containing vesicular stomatitis virus envelope glycoprotein (1) into GP2 293 cells that contain retroviral *gag* and *pol* genes. The Gag, Pol and Env proteins produce retroviral pseudoparticles containing the sequences within the long terminal repeats of the pQCXIN-HBH vector, and 48 hours post transfection (hpt) retrovirus was harvested from the cellular supernatants (2), and naïve GP2 293 were infected (3). GP2 293 cells with the successful incorporation of the retroviral genome were selected using the neomycin resistance cassette and placed under neomycin (G418) drug selection for 7-10 days (4). Surviving cells express HBH-tagged proteins (pink NS5A protein with yellow and blue HBH tag).

HBH-GFP (lane 2) produces a protein of 38 kDa (27 kDa for GFP plus 11 kDa HBH tag). Previously generated HBH-HCV Core-1a and HBH-HCV Core-2a cells lines were used as positive controls (lanes 4-5), and a cells only negative control detected no protein (lane 3). Full-length NS5A is located in the cell cytoplasm (128,171,190,191) and therefore, to verify the HBH tag had not interfered with the cellular distribution of NS5A, indirect immunofluorescence was performed. Figure 3.3.B upper panel shows detection of

cytoplasmic NS5A-2a-HBH while the lower panel is RGS4 antibody incubated with a cells only negative control exhibiting the antibody's specificity for the HBH tag. The same results were obtained with HBH-NS5A-2a construct (data not shown). HBH-tagged GFP (both N- and C-terminal tag forms) were confirmed by direct fluorescence of the GFP protein. In this case, HBH-tagged GFP variants were found in both the nucleus and cytoplasm, consistent with untagged GFP (not shown).

The quantity and quality of NS5A-HBH-2a expression from a stable versus a transient transfection was evaluated by Western blot. Total protein lysates were obtained from overnight cultures of the stable cells and protein from transient transfections were isolated 48 hours post transfection (hpt). In both cases, the monolayer density at time of collection was the same. In figure 3.3.C, total protein extracted from NS5A-HBH-2a stable cell lines (lanes 1 and 2) was compared to the equivalent protein isolated from transiently transfected cells (lanes 3-6). Even with the acknowledged limitations of chemiluminescence for quantification, the amount of tagged NS5A protein (red arrow) is equivalent but with a 5ug total protein load from the stable cell line sample (Fig.3.3.C, lane 1) compared with the 1.6ug total protein load from the transient transfection sample (Fig.3.3.C, lane 3) suggesting higher amounts of NS5A in the transient transfection sample. However, the transient transfection also produced additional lower molecular weight species suggesting more degradation or incomplete translation products. Results were the same for N-terminally tagged NS5A. More full-length NS5A-2a-HBH was desirable for PPI identification, and thus the stably integrated expressing system was chosen for subsequent experiments.

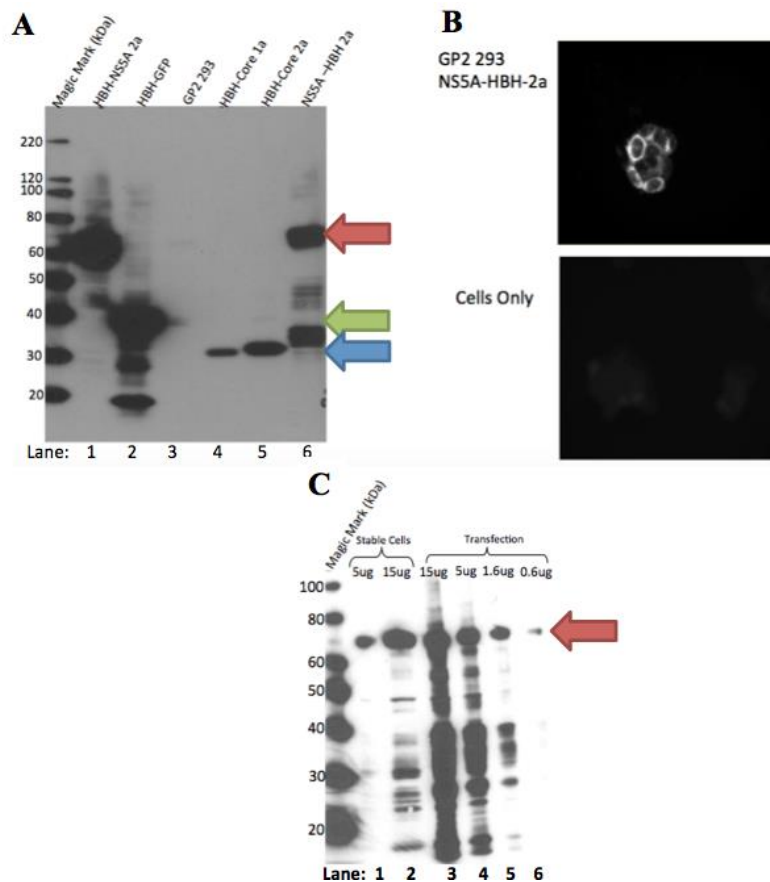


Figure 3. 3. Evaluation of HBH-tagged HCV proteins expressed in GP2 293 cells. **(A)** Confirmation of HBH-tagged protein expression. Total protein from cells stably expressing HBH-tagged clones was evaluated by Western blot with primary antibody anti-RGSH₄ antibody followed by anti-mouse HRP secondary antibody. The expression of HBH-NS5A-2a (74/76 kDa, red arrow, lane 1), HBH-GFP (38 kDa, green arrow, lane 2), and NS5A-2a-HBH (74/76 kDa, red arrow, lane 6) are indicated. A cells only negative control (GP2-293) (lane 3) produced no visible bands. Positive controls of previously verified HBH-Core 1a (lane 4) and HBH-Core 2a (lane 5) (31 kDa, blue arrow) were used to demonstrate RGSH₄ antibody detection and specificity. **(B)** Confirmation of cytoplasmic expression of NS5A-2a-HBH in stably transduced cells. Fixed cells were evaluated by indirect immunofluorescence with an RGSH₄ antibody. **(C)** Western blot of NS5A-2A HBH from stable cells and transient transfections. Total protein was extracted from overnight cultures of NS5A-2a-HBH cells and cells (lanes 1 and 2) or transfected with the NS5A-2a-HBH construct then isolated at 48 hpt (lanes 3-6). Total protein load amounts are indicated above the lanes. Magic Mark ladder indicated molecular weights in kDa. For the Western blot, anti-RGSH₄ antibody was used for NS5A-2a-HBH detection (indicated by red arrow).

3.2.2 Optimization of the TAP protocol

The HBH tag and corresponding TAP protocol were initially developed to study ubiquitination in yeast and follow a two-step sequential purification methodology (Fig.3.4)(255,256).

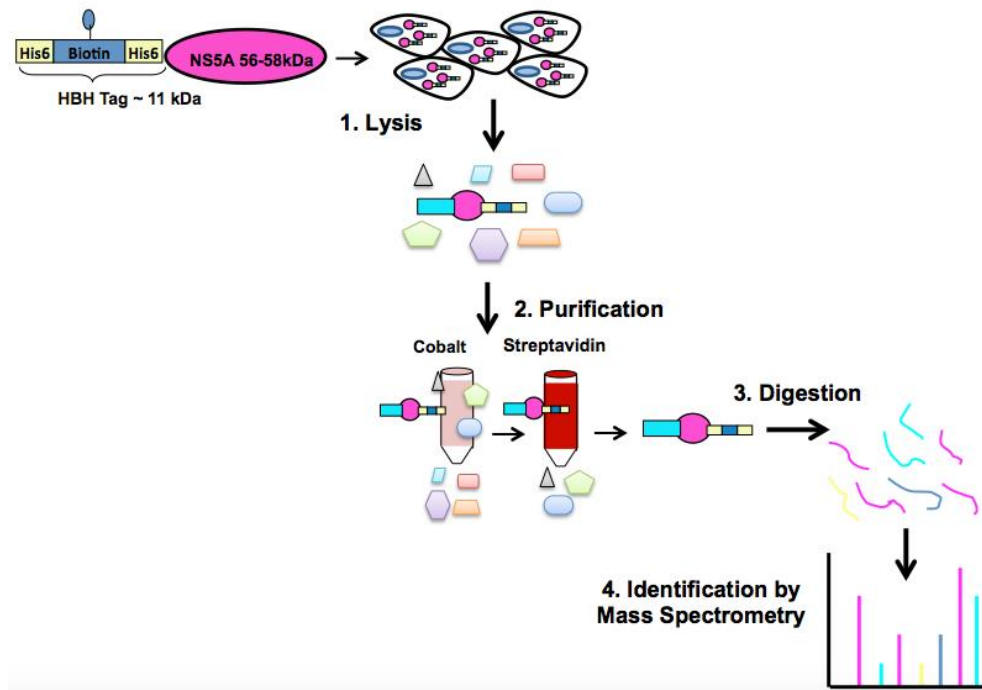


Figure 3. 4. Identification of host proteins interacting with HBH-tagged NS5A-2a using the HBH native state (n) TAP protocol. **(1)** HBH-NS5A-2a stable cells are lysed with a low detergent containing buffer to preserve protein interactions in their native state. **(2)** Soluble protein extracts are subjected to two purification steps. First, the hexahistidine motifs present on the HBH tag bind a metal chelate resin and are washed to remove unbound contaminants before eluting the target protein using imidazole. Streptavidin is then used to bind the endogenously biotinylated HBH tag and washed to remove contaminants. **(3)** Bound HBH-tagged NS5A and its interacting host proteins are digested to peptides using trypsin, cleaned of contaminants and **(4)** submitted to mass spectrometry to identify the NS5A-2a interacting proteins.

At the commencement of this project, the TAP protocol had no precedent for purification of proteins produced in human cells. In order to evaluate a number of conditions, an FPLC was employed to inject HBH-tagged protein sample onto a 1ml metal chelate cartridge (cobalt or nickel) in order to automate the loading, washing and elution steps of

the metal chelate portion of the purification. HBH-tagged NS5A-2a from a single 15cm culture dish was lysed, diluted in sodium phosphate buffer and injected onto a 1ml cobalt cartridge prior to washing and elution with 10mM, 150mM, and 500mM imidazole. The elution profile indicated that the majority of protein (and detergent which is also detected at A280) passed through the column during the loading and washing stages at 0-100ml (Fig.3.5). Elution with imidazole resulted in two peaks, both of which contained NS5A-2a-HBH protein (not shown) indicating that the FPLC coupled to the nickel cartridge method could be used as a starting point for further optimization.

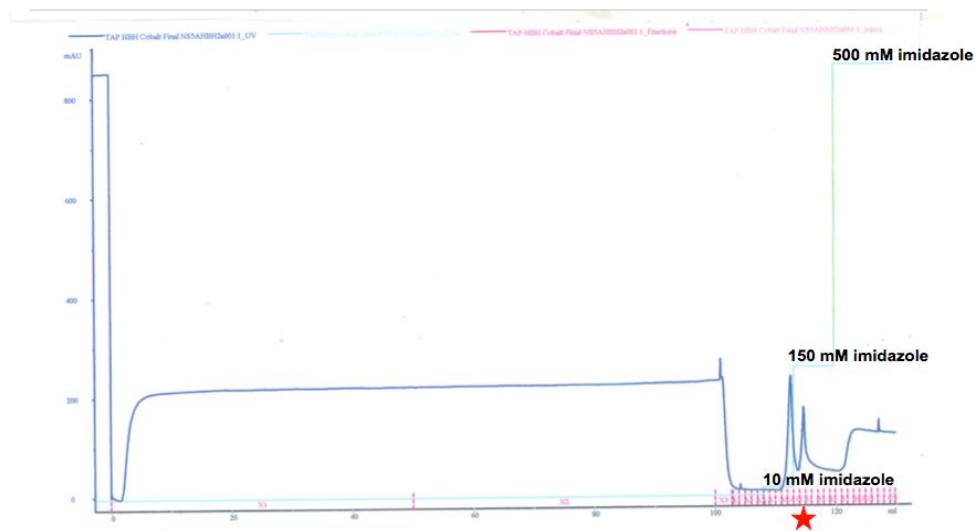


Figure 3. 5. Chromatogram of NS5A-2a-HBH protein purified with cobalt purification using an FPLC. The x-axis is time (minutes), and the y-axis is UV absorbance (A280). The concentration of imidazole (green line) in the step-elution is indicated. Elution fractions (pink) are indicated. A red star indicated fractions containing purified NS5A-2a-HBH protein.

Affinity purification lysis and purification buffers must balance the need to release cellular components but not denature proteins, disrupt native protein interactions or limit capture efficiency. Although Tris-based buffers have been used for metal chelate purifications, sodium phosphate-based buffers are generally preferred, as they contain no

primary amines that can interfere with capture. Salt concentrations should be near physiological (100-150mM) leaving choice of detergent as an important factor for the buffer (319). Two different extraction/purification buffers were chosen for comparison. A phosphate-based nTAP (native state TAP) lysis buffer (50mM NaPO₄ pH 8.0, 150mM NaCl, 0.5% NP40) was compared to the Tris-based RIPA buffer (50mM Tris, pH 8.0, 150mM NaCl, 1.0% NP40, 0.5% sodium deoxycholate, 0.1% SDS) for a cobalt purification with NS5A-2a-HBH (Fig 3.6.A).

Dot blot analysis demonstrated that the majority of NS5A-2a-HBH in the nTAP buffer purification was present in fractions A8 and A9 (Fig.3.6.A, upper). In contrast, purification with the RIPA lysed buffer identified NS5A-2a-HBH in 12 elution fractions (A7-B6) (Fig.3.6.A, lower panel). To evaluate the quality of purified protein using both buffer systems, Western blot analysis was performed. (Fig.3.6.B). Equivalent volumes of each FPLC cobalt purification step demonstrated that nTAP buffer FPLC fractions contained enough NS5A-2a-HBH to be detected on the Western blot in the diluted starting material (lane 4) and fraction A8 (lane 6) (Fig.3.6.B, left). RIPA buffer lysed and diluted starting material (lane 12), and fractions A3, A8, B1, B8 (lanes 13-16) were below the Western blot detection limit (Fig.3.6.B, right). RIPA treated NS5A-2a-HBH was however detected in FPLC fractions by dot blot (Fig.3.6.B, lower) but not in Western blots (Fig.3.6.B, right). This can be explained by differential protein loading (50ul for dot blot and 25ul of sample for the Western blot). The detection of NS5A-2a-HBH in the nTAP buffer starting material by Western blot and its absence in the RIPA lysis indicated

that the nTAP buffer was more efficient at extracting NS5A-2a-HBH and was therefore chosen for subsequent purifications.

Further comparison was made using the detergents NP40 and Triton X-100 using nickel resin purification of NS5A-2a-HBH (Fig.3.6.C). Both detergents were similar in their ability to extract NS5A-2a-HBH indicated by the intensity of NS5A-2a-HBH in the total lysis fraction (Fig.3.6.C, lane 1 vs. lane 13). NP40 and Triton X-100 also produced similar elution profiles with NS5A-2a-HBH being detected in fractions A1-A6 with peaks at A3 for NP40 and A4 for Triton X-100 detergents (Fig.3.6.C, lanes 6-12 vs. lanes 18-23). As the profiles were similar, lysis buffer (50mM NaPO₄ pH 8.0, 150mM NaCl,) containing 0.5% NP40 was chosen as the buffer for the subsequent nTAP protocol.

An important difference between purification with nickel and cobalt columns using nTAP lysis buffer also became apparent. With cobalt purification, elutions were tightly focused with the HBH tagged protein eluting in typically one or two fractions (Fig.3.6.B, elution in A8, lane 6). In contrast, nickel-based purifications exhibited a broader elution profile (Fig.3.6.C, elution in A1-A6, lanes 6-11). This suggests that cobalt binds the HBH tag with a higher affinity and that a higher concentration of imidazole is required to elute NS5A-2a-HBH compared to nickel. Interestingly even at 10mM imidazole, some but not all of the HBH-tagged protein was eluted from the nickel columns (Fig.3.6.C, lane 6). The data also suggests that the choice of detergent can have marked effects on cobalt (and possibly nickel) column purification as RIPA buffer, which contains additional low levels of detergents compared to nTAP, buffer also caused elution over a broader range

(Fig 3.6.A). The higher extraction efficiency and tighter elution profile of the Cobalt resin affirmed its use in subsequent purifications.

The recommended pH for a metal chelate extraction/purification buffer is pH 7.0-8.0 (319). Extracts were prepared in pH 7.4 and pH 8.0 phosphate buffer in nTAP lysis buffer then subjected to FPLC cobalt purification. Western blot analysis was performed and despite similar starting amounts (Fig.3.6.D, compare lanes 1 and 7), very little eluted protein was detected in the A8 and A9 fractions with pH 7.4 buffer compared to pH 8.0 buffer (Fig.3.6.D, compare lanes 5 and 6 to lanes 11 and 12). A likely explanation is that the lower pH did not allow as efficient binding of tagged NS5A to the resin. Buffers at pH 8.0 were used in all subsequent TAP purifications.

It was previously stated that stable cell lines had a greater ratio of full length products compared to transiently transfected cells (Section 3.2.1, Figure 3.3) however Figure 3.6.B and C contain significant amounts of lower MW products. This is primarily due to differences in X-ray film exposure for this blot compared to the one in figure 3.3.

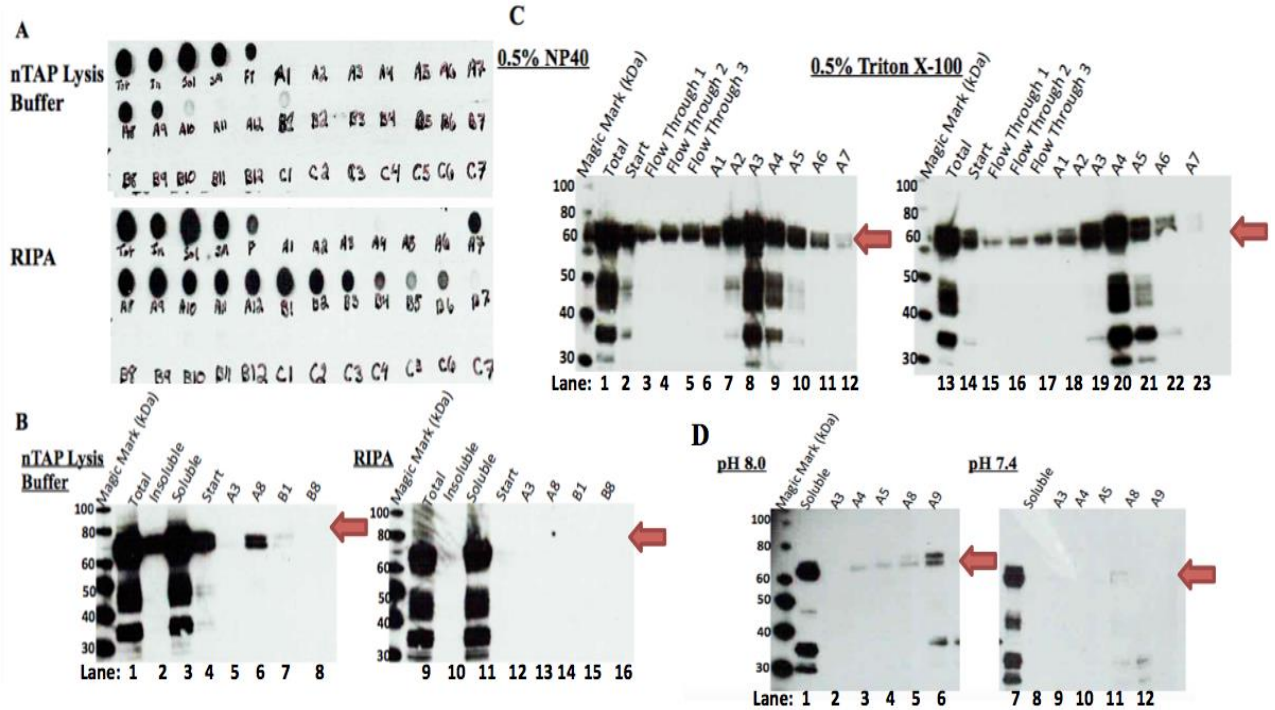


Figure 3. 6. Evaluation of different buffers for extraction and purification by native state TAP (nTAP). **(A, B, C)** Effects of detergent on purification of NS5A-2a-HBH. **(A)** nTAP lysis buffer versus RIPA. 50ul of each of the total protein extraction steps (Tot= total 10ml lysis, In = insoluble, Sol = soluble, SM = 1:10 diluted starting material) and FPLC cobalt elution fractions (A1-C7) were resolved by dot blot and NS5A-2a-HBH was visualized with the RGSH₄ antibody from nTAP (top) and RIPA (bottom) TAP purifications. **(B)** Western blot of 25ul each TAP purification step from (A) total (lane 1), insoluble (lane 2), soluble (lane 3), 1:10 diluted starting material (lane 4), FPLC cobalt elution fractions A3 (lane 5), A8 (lane 6), B1 (lane 7) and B8 (lane 8). HBH-tagged NS5A-2a protein was detected by the RGSH₄ antibody and chemiluminescence in nTAP (left) and RIPA (right) based purifications. NS5A-2a-HBH is indicated with a red arrow. **(C)** NP40 versus Triton X-100 detergents. Comparison of 18ul of total protein extracts (total, insoluble, soluble and 1:10 diluted starting material) and nickel FPLC 1ml elution fractions (A1-A7) resolved on chemiluminescent Western blot with the RGSH₄ antibody. nTAP lysis buffer samples extracted with 0.5% NP40 (left) or 0.5% Triton X-100 (right). **(D)** Effects of pH on nTAP lysis buffer. Western blot of 10ul of each TAP purification step from pH 8.0 buffer extracted/purified protein: Soluble (lane 1) FPLC elution fractions A3 (lane 2), A4 (lane 3), A5 (lane 4), A8 (lane 5) and A9 (lane 6) and pH 7.4 buffer extracted/purified protein: soluble (lane 7), FPLC elution fractions A3 (lane 8), A4 (lane 9), A5 (lane 10), A8 (lane 11) and A9 (lane 12). NS5A-2a-HBH protein was detected with anti-RGSH₄ antibody and chemiluminescence (indicated with red arrow).

The FPLC allows for automated purification of HBH-tagged proteins. However, there are several drawbacks associated with its use including labor-intensive set-up, larger

volumes of buffers required to prime pumps and equilibrate columns and the inability to purify multiple samples simultaneously. Therefore, batch purification using iron-core magnetic cobalt beads was evaluated. Magnetic cobalt beads are simple to manipulate; all binding, washing and elution steps make use of attraction of the iron core to rare earth magnets. As such, several different samples can be manipulated at once increasing efficiency and simplicity over the FPLC methodology.

The FPLC-based cobalt column purification was compared to cobalt bead magnetic capture. Cobalt column purification of NS5A-2a-HBH resulted in eight fractions containing NS5A-2a-HBH (A11-B6) with the majority present in three fractions B1-B3 (Fig.3.7.A, lanes 5-12). Due to the nature of the elution profile from a column, the FPLC column methodology produced a less concentrated NS5A-2a-HBH protein preparation eluting across these fractions. In contrast, a batch elution process resulted in a single fraction containing HBH-tagged protein (Fig.3.7.C, lane 7). For subsequent steps, elution in a smaller volume would be of distinct advantage. Silver staining SDS-PAGE gels assessed the purity of the FPLC column and batch elutions method for total protein content (Fig.3.7.B&D). The two FPLC-based purification elutions containing the majority of the NS5A-2a-HBH protein (B1-B2) contain substantial protein species, a problem often seen with metal chelate column purification where the target protein is present at low levels (Fig.3.7.B, lanes 6,7.). Although there may be less unique protein species in the magnetic cobalt bead batch elution method, (Fig.3.7.D, lane 7) compared to the FPLC column method, this purification procedure was also insufficiently pure, (although no worse than the FPLC method). The simplicity and reduced handling time

provided by the cobalt beads batch purification method allowed the FPLC purification methodology to be abandoned.

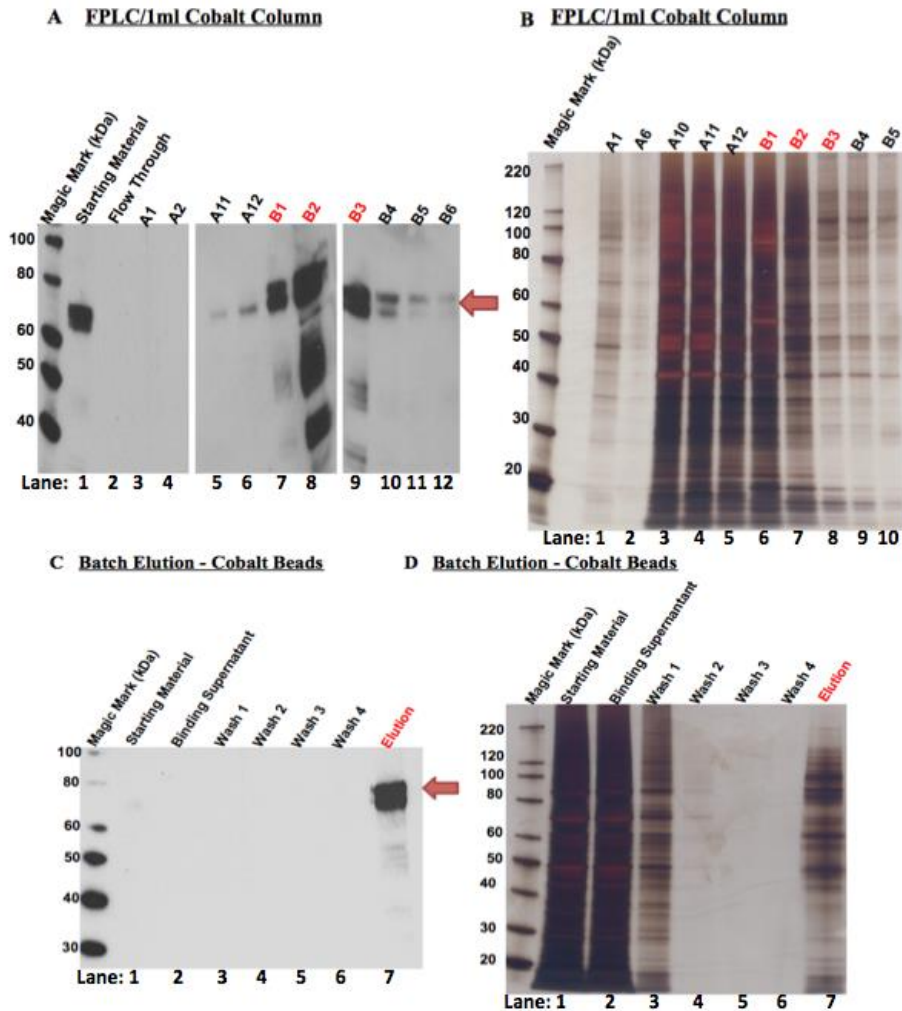


Figure 3. 7. Comparison of FPLC cobalt column and batch cobalt bead purifications of NS5A-HBH-2a tagged protein. A 15cm plate of cells expressing NS5A-2a-HBH was extracted using nTAP lysis buffer and subjected to either FPLC-1ml cobalt column purification (A, B) or a batch purification with magnetic cobalt beads (C, D). (A) Western blot analysis of FPLC-1ml cobalt column purified samples: starting material (lane 1), column flow through (lane 2) FPLC elution fractions A1, A2, A11-B6 (lanes 3-12). HBH-NS5A-2a was detected with RGSH4 antibody and chemiluminescence. (B) Samples from (A) evaluated by SDS-PAGE and silver stained to visualize total protein. (C) Western blot analysis of magnetic cobalt bead batch purification: starting material (lane 1), binding supernatant (lane 2), washes (lanes 3-6) and cobalt bead elution (lane 7) detected with anti-RGSH4 antibody and chemiluminescence. (D) Samples from (C) evaluated by SDS-PAGE and silver stained. Elution fractions s containing NS5A-2a-HBH are indicated with red text, and the size of NS5A-2a-HBH is shown with a red arrow.

With the need to further purify the HBH-tagged protein for subsequent use in identifying PPIs, attention was turned to streptavidin capture. One way to improve capture specificity is to optimize the amount of capture resin to protein amount used in purification. As such, 100ul and 25ul volumes of streptavidin beads were used to further purify HBH-tagged protein from cobalt bead batch elution (Fig.3.8). Western blots revealed that both 100ul and 25ul of streptavidin beads were sufficient to capture the NS5A-2a-HBH tagged protein (Fig.3.8.A, lane 7 and Fig.3.8.C, lane 6). Minimal HBH-tagged protein was detected in the binding supernatant (the supernatant left over following bead capture) of in either the 25 or 100 ul bead volumes (Fig.3.8.A, lane 2 versus Fig.3.8.C, lane 2). Silver stained SDS-PAGE gels showed a sharper delineation of total protein using 25ul of streptavidin beads than did the 100ul volume (Fig.3.8.B, lanes 7-10 versus Fig.3.8.D, lane 6). As 25ul of streptavidin beads was able to efficiently capture NS5A-2a-HBH protein and apparently with less confounding contaminating protein species, 25ul of streptavidin beads were used in all subsequent nTAP purifications.

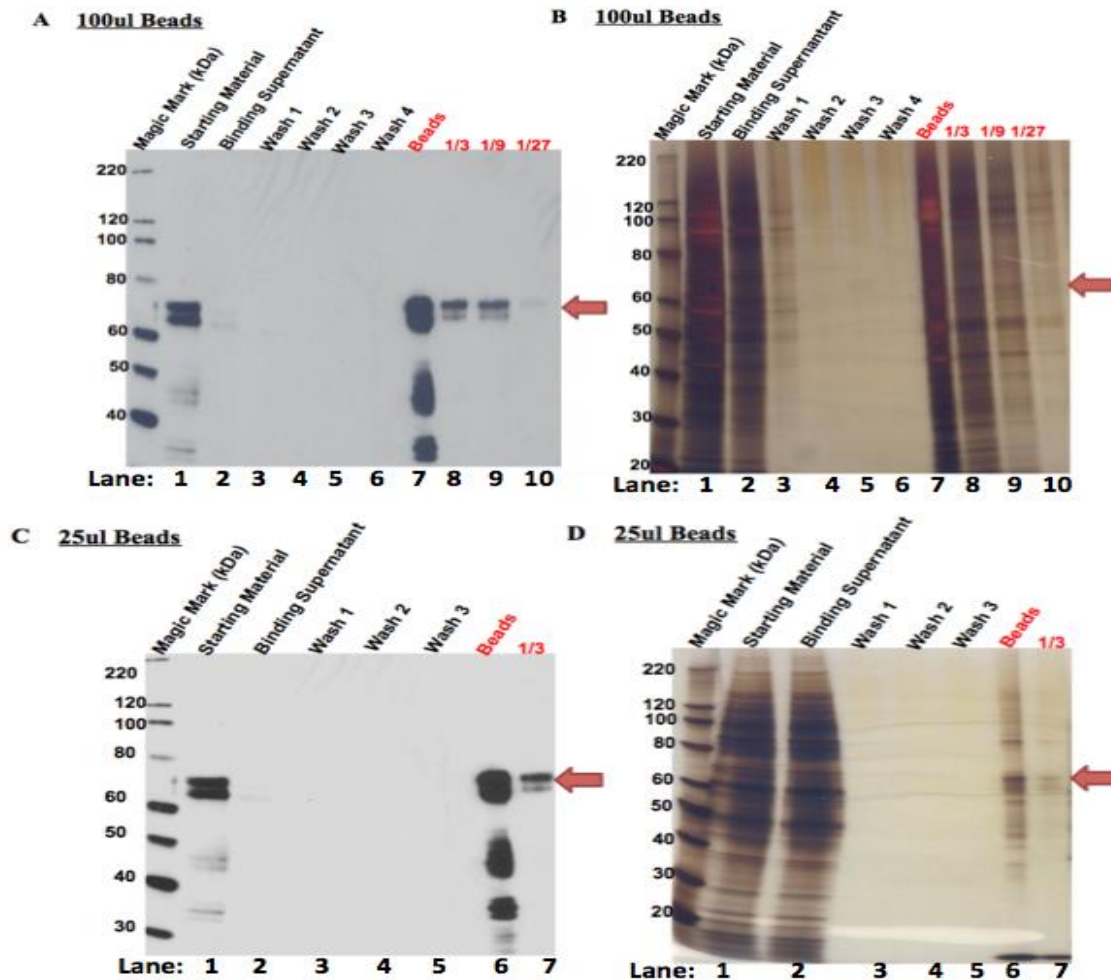


Figure 3. 8. Comparison of 100ul and 25ul of streptavidin magnetic beads in the purification of NS5A-HBH-2a protein. **(A, B)** NS5A-HBH-2a 100ul streptavidin bead purification fractions from: starting material (lane 1), streptavidin bead binding supernatant (lane 2), washes (lane 3-6) 5ul of streptavidin beads diluted in 100ul of PBS (lane 7) 1/3, 1/27 dilutions of streptavidin beads (lanes 9-10). **(A)** HBH-NS5A-2a was detected with RGSH₄ antibody and chemiluminescence. **(B)** Samples from (A) evaluated by SDS-PAGE and silver stained to visualize total protein. **(C, D)** NS5A-HBH-2a 25ul streptavidin bead purification fractions from: starting material (lane 1), streptavidin bead binding supernatant (lane 2), washes (lane 3-5) 5ul of streptavidin beads diluted in 100ul of PBS (lane 6) 1/3 (lanes 7). **(C)** HBH-NS5A-2a was detected with RGSH₄ antibody and chemiluminescence. **(D)** Samples from (C) evaluated by SDS-PAGE and silver stained to visualize total protein. NS5A-2a-HBH is indicated with a red arrow.

The final nTAP protocol consisted of lysis of a single plate of cells stably expressing an HBH-tagged protein in TAP lysis buffer (50mM NaPO₄ pH 8.0, 150mM NaCl, 0.5% NP40). The first purification used 100ul of cobalt beads and the second used 25ul of

streptavidin beads. A representative Western blot (Fig.3.9.A) demonstrates that NS5A-2a-HBH is effectively captured with minimal loss of target protein in the binding supernatants of both bead types (lanes 2 and 9) but a good recovery with minimal background bands in the final elution (lane 14) (Fig.3.9.A, lane 14 and 3.9.B, lane 14). Optimization of the nTAP protocol was demonstrated here with the C-terminal tagged NS5A-2a-HBH, but N-terminal tagged HBH-NS5A-2a behaved the same regarding capture and purity (data not shown).

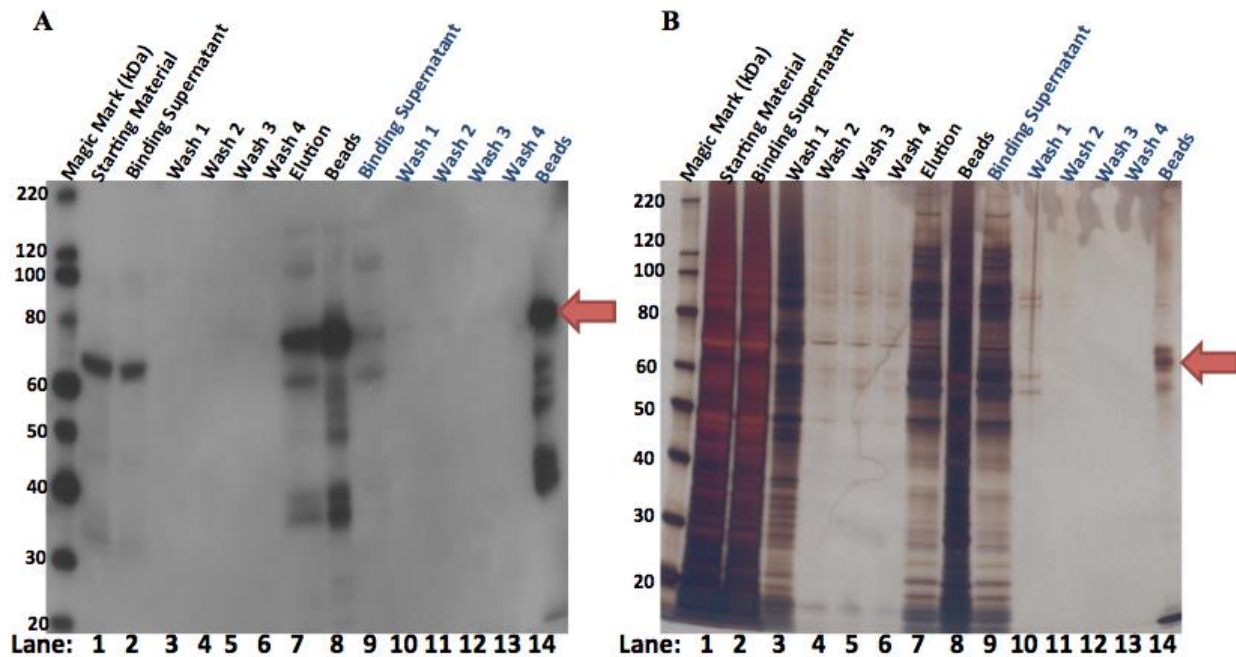


Figure 3. 9. Fully optimized nTAP protocol. **(A)** Protein from a 15cm plate of cells stably expressing NS5A-2a-HBH was extracted using an optimized nTAP lysis method. Cobalt magnetic bead purifications are indicated in black text and include: starting material (lane 1), binding supernatant (lane 2), washes (lanes 3-6), elution (lane 7) and 5ul of cobalt beads diluted in 100ul of PBS (lane 8). Streptavidin purification fractions are indicated in blue text and include: binding supernatant (lane 9), washes (lanes 10-13) and 5ul of streptavidin beads diluted in 100ul of PBS (lane 14) **(A)** Western blot, HBH-NS5A-2a was detected with anti-RGSH₄ antibody followed by chemiluminescence. **(B)** Samples from **(A)** evaluated by SDS-PAGE and silver stained to visualize total protein. NS5A-2a-HBH is indicated with a red arrow.

3.2.3 Identification of NS5A-2a interacting proteins by nTAP and mass spectrometry

Currently, there is an expansive list of NS5A-host PPIs identified by a multitude of techniques. However, every protein expression system suffers from limitations including appropriate protein expression levels and the absence of adequate controls. The nTAP protocol developed here was designed to address some of these limitations by: 1) stably expressing HBH-NS5A-2a at a moderate level to limit the potential for inducing overall stress to the cells and 2) by using, in addition to no bait protein expression controls, an HBH-tagged GFP construct to serve as an additional “irrelevant” protein negative control. To verify that the optimized nTAP methodology was capable of identifying NS5A-host PPIs, one 15cm plate each of HBH-NS5A-2a and HBH-GFP cells were subjected to the finalized nTAP purification protocol and the eluted samples were for each was subject to protein identification by mass spectrometry and database analysis.

The presence of the HBH-NS5A-2a and HBH-GFP proteins was tracked throughout the purification by Western blot and silver stain analysis (Fig 3.10). nTAP purification yielded highly purified HBH-NS5A-2a and HBH-GFP proteins with, as expected, a different profile of bands as seen in the silver stained gels (Fig 3.10.B, lane “elution” and D, lane “beads”).

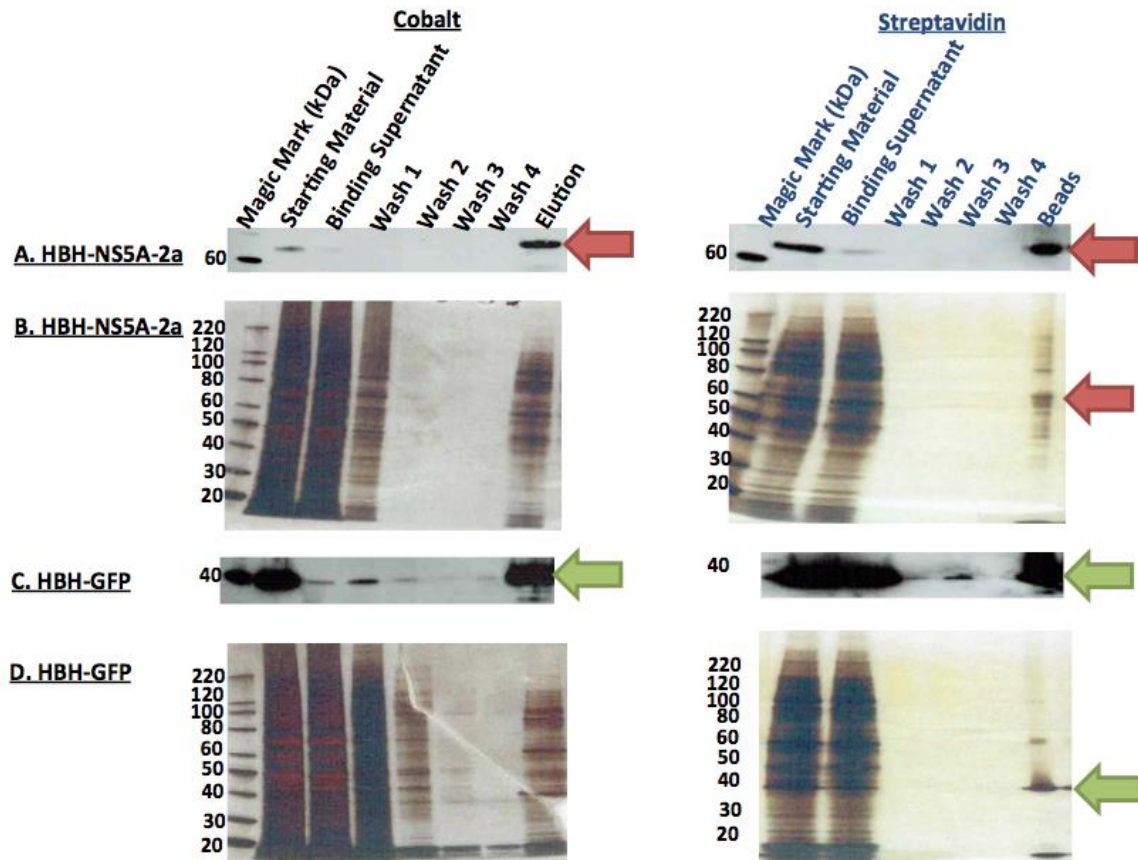


Figure 3. 10. nTAP purified HBH-NS5A-2a and HBH-GFP for the identification of interacting proteins. A single plate of HBH-NS5A-2a and HBH-GFP GP2 293 cells were subjected to the nTAP protocol. 15ul from each step of the nTAP procedure was resolved on SDS-PAGE for: (A, C) Western blots with the anti-RGSH₄ antibody and chemiluminescence, and (B, D) silver stain for total protein content. Cobalt purifications are on the left side and streptavidin on the right. Western blots appear directly above corresponding silver stained gels with HBH-NS5A-2a (red arrow) above the HBH-GFP samples (green arrow).

Purified HBH-NS5A-2a and HBH-GFP proteins were submitted for mass spectrometry with the resulting data queried against the IPI human custom database version 3.71 (appended to contain all JFH1 HCV protein sequences, GFP sequence and the HBH tag sequence). HBH-GFP served as an irrelevant expressed protein control to identify host proteins bound to the HBH tag or to any ectopically “irrelevant” expressed protein and the purification resins. Although wash cycles were performed between sample injections

during mass spectrometry, HBH-GFP samples were analyzed before HBH-NS5A-2a so proteins specific to HBH-NS5A-2a would not be mis-identified as false negatives.

Coverage of HBH-NS5A-2a by mass spectrometry and database searching yielded up to 70% coverage of the protein, a very high value considering that not all of NS5A peptides are amenable to trypsin digestion. Likewise, GFP coverage was 82% (Fig.3.11). Of a total of 558 proteins identified in the initial HBH-TAP, 87 proteins were found in common to both the HBH-NS5A-2a and HBH-GFP samples including: keratins (16 different types), desmoplakins, plakoglobin, transferrins, histones, HNRNP subunits (9 types), ribosomal proteins (50 types) and proline and glutamine rich proteins. Most of these are commonly seen contaminants. Of the 29 proteins found only in the HBH-GFP sample, histone subunits, topoisomerase 2, HNRNP subunits, Pinin and ribosomal protein subunits were present. There were no previously identified NS5A interacting proteins present in the HBH-GFP list. In the HBH-NS5A sample, 449 proteins were present, a number of which have been previously reported to be NS5A interacting proteins including: ArfGap (320), Nap1L (246) and p53 (224,225,318).

A NS5A-2a Coverage

```
1  S G S W L R D V W D W V C T I L T D F K N W L T S K L F P K L P G L P F F I S C Q K G Y K G V W A G T G I M T T R C P C G A N I S G N V R L G S M R I T G P K T C
81 M N T W Q G T F P I N C Y T E G Q C A P K P P T N Y K T A I W R V A A S E Y A E V T Q H G S Y S Y V T G L T T D N L K I P C Q L P S P E F F S W V D G V Q I H R
161 F A P T P K P F F R D E V S F C V G L N S Y A V G S Q L P C E P E P D A D V L R S M L T D P P H I T A E T A A R L A R G S P P S E A S S V S Q L S A P S L R
241 A T C T T H S N T Y D V D M V D A N L L M E G G V A Q T E P E S R V P V L D F L E P M A E E E S D L E P S I P S E C M L P R S G F P R A L P A W A R P D Y N P P
321 L V E S W R R P D Y Q P P T V A G C A L P P P K K A P T P P P R R R R T V G L S E S T I S E A L Q Q L A I K T F G Q P P S S G D A G S S T G A G A A E S G G P T
401 S P G E P A P S E T G S A S S M P P L E G E P G D P D L E S D Q V E L Q P P P Q G G G V A P G S G S G S W S T C S E E D D T T V C C
```

B GFP Coverage

```
1  M V S K G E E L F T G V V P I L V E L D G D V N G H K F S V S G E G E G D A T Y G K L T L K F I C T T G K L P V P W P T L V T T F S Y G V Q C F S R Y P D H M K
81  Q H D F F K S A M P E G Y V Q E R T I F F K D D G N Y K T R A E V K F E G D T L V N R I E L K G I D F K E D G N I L G H K L E Y N Y N S H N V Y I M A D K Q K N
161 G I K V N F K I R H N I E D G S V Q L A D H Y Q Q N T P I G D G P V L L P D N H Y L S T Q S A L S K D P N E K R D H M V L L E F V T A A G I T H G M D E L Y K
```

Figure 3. 11. Coverage of NS5A and GFP by mass spectrometry. Peptides detected by mass spectrometry from nTAP purified (A) HBH-NS5A-2a (70%) and (B) HBH-GFP (82%) proteins are highlighted in grey over the NS5A and GFP sequences.

To validate the nTAP methodology, one known NS5A interacting protein, p53 (224,225,318), identified by mass spectrometry was evaluated by Western blot analysis. Figure 3.12.A demonstrates that p53 is present throughout the nTAP purification of HBH-NS5A-2a including in the starting material (lane 1), cobalt bead elution (lane 7) and on the streptavidin beads (lane 14). In nTAP purified HBH-GFP (Fig 3.12.B), while p53 is detected in the starting material (lane 1) and the cobalt elution (lane 7) it is not recovered in the streptavidin elution (lane 14). This demonstrates the specificity of the nTAP procedure.

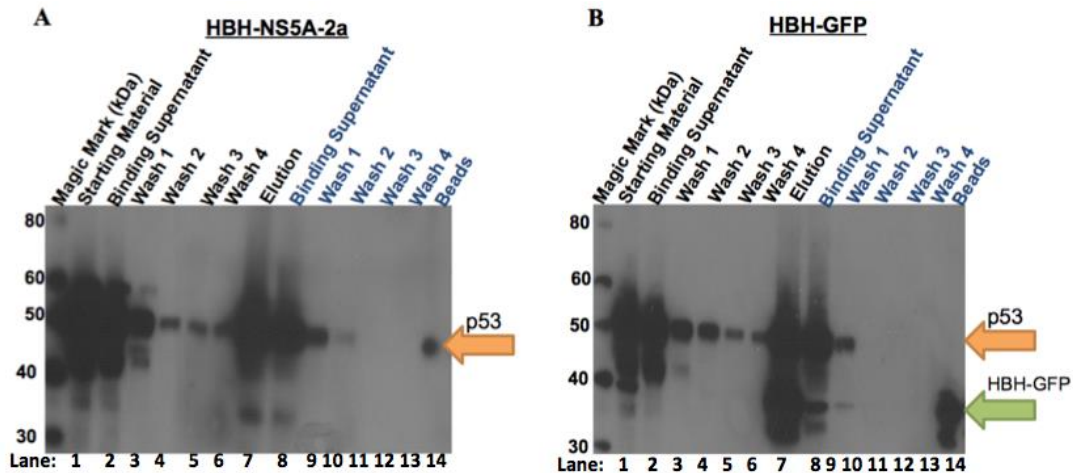


Figure 3. 12. Validation of a previously identified NS5A interacting protein, p53, by nTAP (cobalt-streptavidin). A single 15cm plate each of HBH-NS5A-2a and HBH-GFP expressing cells were subjected to nTAP purification and the resulting captured proteins were submitted for mass spectrometry and database searching. The presence of one interacting protein identified by this analysis, tumor suppressor protein p53, was assessed at various stages of nTAP purification. Cobalt purifications are identified by black text and streptavidin purifications by blue text. Western blot of: (A) HBH-NS5A-2a and (B) HBH-GFP. Sample types are indicated above the lanes. Detection used an anti- p53 specific antibody (A and B) and an RGS_{H4} antibody (B) followed by chemiluminescence. The RGS_{H4} antibody was not used on the HBH-NS5A Western blot as p53 and HBH-NS5A-2a have similar molecular weights. p53 (53 kDa) is indicated by an orange arrow and HBH-GFP by a green arrow.

To establish a candidate list of NS5A-2a interacting host proteins, three biological replicates each consisting of HBH-NS5A-2a, HBH-GFP, and GP2 293 cells were purified using the nTAP protocol. Mass spectrometry identified proteins were considered HBH-NS5A-2a interacting candidates by passing three requirements: 1) proteins identified had to be identified by a minimum of two peptides (false discovery rate= 0.01), 2) a candidate protein had to be identified in a minimum of two replicates and 3) a candidate protein had to be exclusively identified in the HBH-NS5A-2a sample and never in the HBH-GFP or cells only controls. In a total of 1015 protein contained within the 9 data sets, only 15 proteins were able to pass the harsh criteria outlined above and became the final candidates for NS5A host PPIs (Table 3.1).

Table 3. 1. HBH-NS5A-2a interacting candidates revealed by nTAP mass spectrometry/database searching. Proteins were identified by a minimum of two peptides in a minimum of two replicates and were present exclusively in the HBH-NS5A-2a sample and not HBH-GFP or GP2 293 controls. Protein functions were extracted from UniProt Protein Database (321). Proteins selected for further validation are indicated with an *.

Protein	Function (UniProt)
Cytochrome c1	This is the heme-containing component of the cytochrome b-c1 complex, which accepts electrons from Rieske protein and transfers electrons to cytochrome c in the mitochondrial respiratory chain.
*CCAR2 Cell Cycle and Apoptosis Regulator 2 - Isoform 1 - syn: KIAA1967, Deleted in Breast Cancer gene 1 protein	Core component of the DBIRD complex, a multiprotein complex that acts at the interface between core mRNP particles and RNA polymerase II (RNAPII) and integrates transcript elongation with the regulation of alternative splicing: the DBIRD complex affects local transcript elongation rates and alternative splicing of a large set of exons embedded in (A + T)-rich DNA regions. Inhibits SIRT1 deacetylase activity leading to increasing levels of p53/TP53 acetylation and p53-mediated apoptosis. Inhibits SUV39H1 methyltransferase activity.
Zinc Finger Protein 503	May function as a transcriptional repressor
*CDK12 Cyclin-dependent kinase 12	Cyclin-dependent kinase which displays CTD kinase activity and is required for RNA splicing. Has CTD kinase activity by hyperphosphorylating the C-terminal heptapeptide repeat domain (CTD) of the largest RNA polymerase II subunit RPB1, thereby acting as a key regulator of transcription elongation. Required for RNA splicing, possibly by phosphorylating SRSF1/SF2. Involved in regulation of MAP kinase activity, possibly leading to affect the response to estrogen inhibitors
*NKRF NF-Kappa-B-repressing factor	Interacts with a specific negative regulatory element (NRE) 5'-AATTCCTCTGA-3' to mediate transcriptional repression of certain NK-kappa-B responsive genes. Involved in the constitutive silencing of the interferon beta promoter, independently of the virus-induced signals, and in the inhibition of the basal and cytokine-induced iNOS promoter activity. Also involved in the regulation of IL-8 transcription.
ANT-1 Pre-mRNA-processing factor 6	Involved in pre-mRNA splicing. May act in the tri-snRNP complex as a bridging factor between U5 and U4/U6 snRNPs in the late step of spliceosome assembly. May be necessary for tri-snRNP formation. Enhances dihydrotestosterone-induced transactivation activity of AR, as well as dexamethasone-induced transactivation activity of NR3C1, but does not affect estrogen-induced

	transactivation
RPN-1 Dolichyl- diphosphooligosaccharide- protein glycosyltransferase subunit 1 precursor	Essential subunit of N-oligosaccharyl transferase enzyme which catalyzes the transfer of a high mannose oligosaccharide from a lipid-linked oligosaccharide donor to an asparagine residue within an Asn-X-Ser/Thr consensus motif in nascent polypeptide chains.
HDAC2 Histone deacetylase 2	Responsible for the deacetylation of lysine residues on the N-terminal part of the core histones (H2A, H2B, H3 and H4). Histone deacetylation gives a tag for epigenetic repression and plays an important role in transcriptional regulation, cell cycle progression and developmental events. Histone deacetylases act via the formation of large multiprotein complexes. Forms transcriptional repressor complexes by associating with MAD, SIN3, YY1 and N-COR. Interacts in the late S-phase of DNA-replication with DNMT1 in the other transcriptional repressor complex composed of DNMT1, DMAP1, PCNA, CAF1. Deacetylates TSHZ3 and regulates its transcriptional repressor activity. Component of a RCOR/GFI/KDM1A/HDAC complex that suppresses, via histone deacetylase (HDAC) recruitment, a number of genes implicated in multilineage blood cell development.
*SOD1 Superoxide dismutase [Mn] Mitochondrial	Destroys superoxide anion radicals which are normally produced within the cells and which are toxic to biological systems
PABP-1 Polyadenylate-binding protein	Binds the poly(A) tail of mRNA. May be involved in cytoplasmic regulatory processes of mRNA metabolism such as pre-mRNA splicing. Its function in translational initiation regulation can either be enhanced by PAIP1 or repressed by PAIP2. Can probably bind to cytoplasmic RNA sequences other than poly(A) in vivo. Involved in translationally coupled mRNA turnover. Implicated with other RNA-binding proteins in the cytoplasmic deadenylation/translational and decay interplay of the FOS mRNA mediated by the major coding-region determinant of instability (mCRD) domain. Involved in regulation of nonsense-mediated decay (NMD) of mRNAs containing premature stop codons; for the recognition of premature termination codons (PTC) and initiation of NMD a competitive interaction between UPF1 and PABPC1 with the ribosome-bound release factors is proposed.
NPL4 Nuclear complex protein 4 homolog	The ternary complex containing UFD1L, VCP and NPLOC4 binds ubiquitinated proteins and is necessary for the export of misfolded proteins from the ER to the cytoplasm, where they are degraded by the proteasome. The NPLOC4-UFD1L-VCP complex regulates spindle disassembly at the end of

	mitosis and is necessary for the formation of a closed nuclear envelope
Isoform 1 of Retinol dehydrogenase 11	Exhibits an oxidoreductive catalytic activity towards retinoids. Most efficient as an NADPH-dependent retinal reductase. Displays high activity towards 9-cis and all-trans-retinol. Also involved in the metabolism of short-chain aldehydes. No steroid dehydrogenase activity detected.
EF-1-gamma Elongation Factor 1-gamma	Probably plays a role in anchoring the complex to other cellular components. Response to virus.
MAGT1 Magnesium transporter Protein	May be involved in N-glycosylation through its association with N-oligosaccharyl transferase. May be involved in Mg ²⁺ transport in epithelial cells
*OGDH-2-oxoglutarate dehydrogenase	The 2-oxoglutarate dehydrogenase complex catalyzes the overall conversion of 2-oxoglutarate to succinyl-CoA and CO ₂ . It contains multiple copies of three enzymatic components: 2-oxoglutarate dehydrogenase (E1), dihydrolipoamide succinyltransferase (E2) and lipoamide dehydrogenase (E3)

The NF-Kappa-B repressing factor (NKRF or NRF) protein was one HBH-NS5A-2a interacting candidate that stood out in the list due to its regulatory functions. NKRF is a transcriptional repressor of NFKB responsive genes, regulates IFN β and iNOS promoters and is involved in IL-8 regulation (322–326). NS5A influences each of these processes by i) activating the iNOS promoter, ii) inhibiting IFN β production and iii) increasing expression of NFKB response genes and IL-8 (327–332). The potential correlation between NKRF functions and NS5A expression associated phenotypes made NKRF an attractive NS5A interacting candidate protein. NKRF association with HBH-NS5A-2a during nTAP was tracked throughout nTAP by Western blot analysis to monitor the presence of NKRF (Fig.3.13). Figure 3.13.A demonstrates that NKRF is present along with HBH-NS5A-2a in the final streptavidin bead elution (lane 13). The majority of the NKRF protein was in the binding supernatant and in the cobalt wash 1 (lane 3) suggesting that NKRF is in significant excess to NS5A or that the interaction properties are not robust.

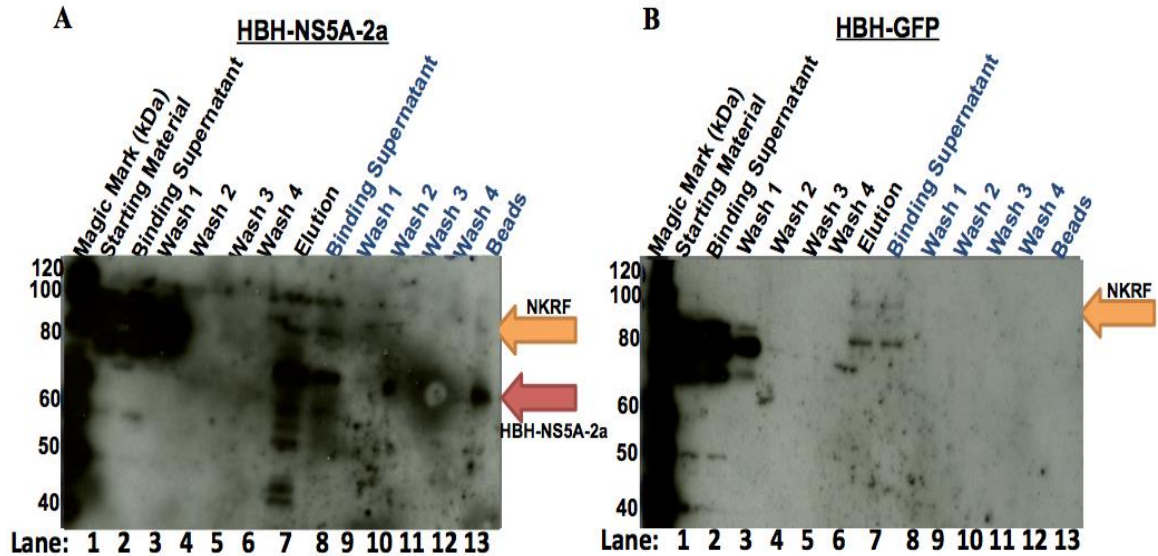


Figure 3.13. Specific interaction of NKRF with HBH-NS5A-2a throughout nTAP purification. A 15cm plate each of HBH-NS5A-2a and HBH-GFP cells were nTAP purified. All cobalt purifications are identified by black text and include starting material (lane 1), binding supernatant (lane 2), washes (lanes 3-6), elution (lane 7). Streptavidin purifications are demarcated by blue text and include binding supernatant (lane 8), washes (lanes 9-12) and 5ul of streptavidin beads diluted in 100ul PBS (lane 13). (A, B) NKRF was tracked throughout the nTAP purification of (A) HBH-NS5A-2a and (B) HBH-GFP. NKRF was detected by chemiluminescence with an NKRF antibody, and RGS4 detected HBH-NS5A-2a nTAP purifications (A only). NKRF (90/78 kDa) is indicated by an orange arrow and HBH-NS5A-2a with a red arrow.

3.2.4 Identification of NS5A-2a interacting proteins by xdTAP and mass spectrometry

nTAP uses non-denaturing lysis buffers and moderately stringent wash conditions that select for protein interactions that are robust and long-lived but as with most TAP methodologies, transient and weak interactions would not expect to be captured. An additional caveat of typical co-immunoprecipitation/affinity purification techniques is that there is the possibility for cellular compartments to mix inappropriately. As the HBH tag contains two affinity elements that are not affected by denaturing agents, chemical cross-linkers can be applied before cellular lysis and purification can proceed in

denaturing buffer. The denaturing buffer is required, as cross-linked proteins purified in non-denaturing buffers tend to be extremely dirty and viscous.

Cross-linking captures PPIs in their biologically relevant cellular location and improves recovery of weak and/or transiently interacting proteins. To cross-link two proteins, there must be two juxtaposed lysine residues situated within the length of the cross-linkers spacer arms used in this study: PFA: 2.0 Å spacer arm, DSS: 11.4 Å, DSG: 7.7 Å and EGS, 16.1 Å (262). This technique is termed cross-linked (x), denaturing (d) TAP purification (xdTAP) (255,256).

First, the cross-linking ability of paraformaldehyde (PFA) was evaluated in xdTAP. PFA concentrations must be high enough to cross-link interacting proteins, but low enough as to not create a large insoluble “protein mat” resulting in target protein loss during lysate clarification. HBH-NS5A-2a expressing cells were cross-linked with PFA at 0%, 0.5%, 1%, and 2% in PBS then incubated for 10 minutes at room temperature before quenching the reaction with glycine. After centrifugation, half the sample was boiled in an attempt to reverse the cross-links. Western blot analysis with the anti-RGSH₄ antibody directed toward the HBH tag on NS5A showed that inclusion of PFA at any percentage resulted in higher molecular weight smears in the unboiled samples (Fig.3.14.A). Boiled samples did not show much reversal of the cross-links although the definition of higher molecular weight species was better than in the unboiled samples. Interestingly, the HBH-NS5A-2a band was still clearly present even with increasing PFA concentration (Fig.3.14.A, lanes 4,6,8).

The 0%, 0.5%, 1% and 2% PFA cross-linked samples that were purified using the xdTAP methodology were each submitted for mass spectrometry analysis. The 0% PFA sample served as a negative control as no authentic PPIs should survive the xdTAP purification without prior cross-linking. Table 3.2 contains a list of host proteins identified in the different concentrations of PFA. As expected, 0% PFA yielded no confidently identified proteins by mass spectrometry other than NS5A-2A, after known contaminants such as keratin were removed. The number of proteins identified in PFA concentrations 0.5%, 1.0%, 2.0% were 8, 16 and 14, respectively, suggesting that 1% PFA could serve as optimal levels of cross-linker. Importantly, five previously published NS5A interacting proteins were identified: Hsp70 (333,334), Tubulin (335), Hsp90 (232), Hexokinase (244) and FKBP8 (232,234–237) (Table 3.2, yellow), increasing confidence in this methodology. 1% PFA was used in subsequent PFA xdTAP purifications.

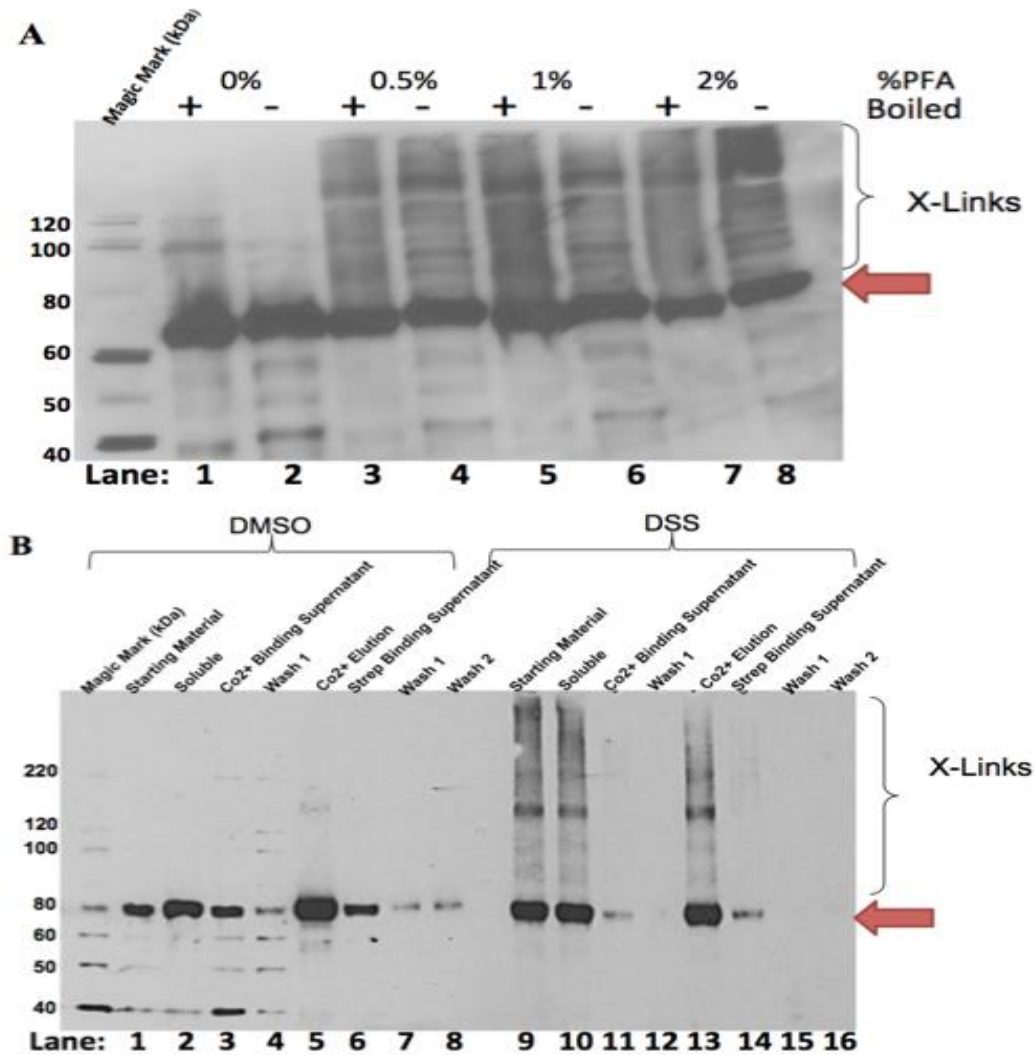


Figure 3.14. Chemical cross-linking and purification of samples expressing HBH-NS5A-2a. **(A)** Effects of increasing PFA concentration on HBH-NS5A-2a protein complex formation. Single 15cm plates of cells expressing HBH-NS5A-2a were cross-linked with increasing PFA concentrations: 0% (lanes 1,2), 0.5% (lanes 3,4), 1% (lanes 5,6) and 2% (lanes 7,8) for 10 minutes before quenching with glycine and lysis in urea denaturing buffer. Duplicate samples were boiled (1, 3, 5, 7) in an attempt to release cross-links prior to evaluation by Western blot analysis detecting HBH-NS5A-2a with the anti-RGSH₄ antibody and chemiluminescence. **(B)** DSS crosslinking of HBH-NS5A-2a complexes. HBH-NS5A-2a expressing cells were cross-linked with DSS in DMSO for 10 minutes or with DMSO as a control. Cells were quenched, lysed with UBP and processed using xdTAP to purify the HBH-NS5A-2a protein. HBH-NS5A-2a was visualized using Western blot analysis with the RGSH₄ antibody followed by chemiluminescence. Lanes 1-8 contain the DMSO control, and lanes 9-16 contain DSS cross-linked HBH-NS5A-2a. HBH-NS5A-2a uncomplexed 74 kDa form is indicated by a red arrow.

Table 3. 2. Mass spectrometry identified proteins from the xdTAP purification at different PFA concentrations to crosslink HBH-NS5A-2a protein interactions. Number of peptides identified at various PFA concentrations are indicated. Previously published NS5A interacting partners are highlighted in yellow.

Identified Proteins	MW	PFA 0.0%	PFA 0.5%	PFA 1.0%	PFA 2.0%	Published
cDNA FLJ54408, highly similar to Heat shock 70 kDa protein 1	64 kDa	0	8	12	13	(333,334)
Isoform DPI of Desmoplakin	332 kDa	0	2	2	2	
Mitochondrial import receptor subunit TOM70	67 kDa	0	2	5	4	
Hemoglobin subunit beta	16 kDa	0	2	2	1	
Tubulin alpha-1C chain	50 kDa	0	2	2	4	(335)
Elongation factor 1-alpha 2	50 kDa	0	2	1	0	
Heat shock protein HSP 90-beta	83 kDa	0	1	2	1	(232)
Isoform 2 of Voltage-dependent anion-selective channel protein 2	30 kDa	0	0	3	3	
Dermcidin	11 kDa	0	0	2	0	
Mitochondrial import receptor subunit TOM20 homolog	16 kDa	0	0	0	3	
60S ribosomal protein L8	28 kDa	0	0	2	0	
60S ribosomal protein L36	12 kDa	0	0	2	2	
Isoform 1 of Keratin, type I cytoskeletal 13	50 kDa	0	0	4	0	
Junction plakoglobin	82 kDa	0	0	0	2	

Isoform 1 of ATPase family AAA domain-containing protein 1	41 kDa	0	0	0	1	
WD repeat-containing protein 81 isoform 1	212 kDa	0	0	1	0	
Peroxiredoxin-1	22 kDa	0	0	0	1	
Isoform 1 of 14-3-3 protein epsilon	29 kDa	0	0	2	0	
Adenosylhomocysteinase	48 kDa	0	2	0	0	
Isoform 1 of Hexokinase-1	102 kDa	0	0	0	2	(244)
Keratin, type II cytoskeletal 1b	62 kDa	0	0	4	0	
Isoform 1 of Heat shock cognate 71 kDa protein	71 kDa	0	0	0	3	
FK506 binding protein 8	47 kDa	0	0	1	0	(232,234–237)

PFA is considered a zero length cross-linker meaning that juxtaposed lysines must be absolutely adjacent to allow cross-linking. In order to expand the range for potential PPIs, chemical cross-linkers with different spacer lengths including DSS (11.4 Å), DSG (7.7 Å) and EGS (16.1 Å) (262) were evaluated. Figure 3.14.B tracked the presence of a representative DSS cross-linked HBH-NS5A-2a protein complexes by Western blot analysis during xdTAP purification. In a DMSO no cross-linker control sample, HBH-NS5A-2a appeared predominantly as a single band with a few lower molecular weight bands, which were presumably degradation products (Fig.3.14.B, lanes 1-8). In contrast, DSS cross-linked HBH-NS5A-2a appears as a smear above the predominant 74 kDa protein band likely the result of forming a protein complex with one or more proteins (Fig.3.14.B, lanes 9,10,13). There is also a particularly prominent band featured in cross-linked samples, which would correspond with the MW of an NS5A dimer at 150 kDa. Cross-linked samples were subjected to xdTAP and mass spectrometry/database analysis.

Table 3.3 is a curated list of host proteins present within the samples for each cross-linker for which known contaminating proteins (keratins) and rare proteins identified in the DMSO negative control samples were removed. Not surprisingly, NS5A was the most predominant species in each of the samples, irrespective of whether the sample was cross-linked or not.

xdTAP purified HBH-NS5A-2a was cross-linked with the three extended length spacer arm cross-linkers. HBH-NS5A-2a samples cross-linked with EGS identified ten host protein interactions, DSS identified seven while DSG identified 11. (Table 3.3). Not

surprisingly, the cross-linkers did not identify the same subset of proteins most likely due to their different spacer arm lengths. This subset did also not directly match to the dataset for PFA cross linking (Table 3.2) Five previously published NS5A interacting proteins were identified in the cross-linker trials and included Hsp70 (333,334), ILF3 (synonym NF90) (336,337), CDK1 (338), FKBP8/38 (232,234–237), and hexokinase (244).

Perhaps most interestingly, there was no apparent overlap of the xdTAP and nTAP results. This strongly suggests that PPI discovery, at least for NS5A, may be far from complete and that the choice of affinity tags, purification methodologies, cell lines, etc. have a dramatic effect on PPI identification.

Table 3. 3. Proteins identified by mass spectrometry/database searching from xdTAP purification of HBH-NS5a-2a expressing cells using different chemical cross-linker prior to capture. Intensity corresponds to the total signal from all peptides for each protein in a single analysis. Previously published NS5A interacting partners are highlighted in yellow.

Identified Proteins	EGS	DSS	DSG	Published
HSPA9 Stress-70 (HSP70) protein, mitochondrial	20320	0	0	(333,334)
PRKDC Isoform 1 of DNA-dependent protein kinase catalytic subunit	8654	0	0	
TOMM70A Mitochondrial import receptor subunit TOM70	6864	15101	25687	
ILF3 interleukin enhancer-binding factor 3 isoform d	6057	0	0	(336,337)
CYB5R1 NADH-cytochrome b5 reductase 1	2489	6162	8387	
CDK1	1033	0	0	(338)
EIF3B Isoform 2 of Eukaryotic translation initiation factor 3 subunit B	963	0	0	
RHOA Transforming protein RhoA	732	0	0	
RAB7A Ras-related protein Rab-7a	716	0	3430	
RAB5C Uncharacterized protein	596	0	831	
FK506 binding protein 8, 38kDa (FKBP8)	0	9315	12689	(232,234–237)

TOMM20 Mitochondrial import receptor subunit TOM20 homolog	0	4162	13940	
RHOT2 Isoform 1 of Mitochondrial Rho GTPase 2	0	2064	0	
Hexokinase-1	0	1074	4553	(244)
PTPN1 Tyrosine-protein phosphatase non-receptor type 1	0	772	1084	
MTX2 Metaxin-2	0	0	431	
TOMM22 Mitochondrial import receptor subunit TOM22 homolog	0	0	2224	
TOMM5 Uncharacterized protein	0	0	458	

3.2.5 Confirmation of TAP candidate interactions with NS5A using Co-IP

To confirm that candidate host proteins identified by nTAP or xdTAP were bona fide NS5A-2a interacting proteins, select candidates were tested using co-immunoprecipitation (Co-IP) as an alternate technique. To eliminate the potential that the HBH tag had biased the results, NS5A-2a and GFP bait proteins were N-terminally FLAG-tagged. Candidate proteins were N-terminally myc-tagged and included: NKRF, TOM22, TOM40, RanGap1, CCAR2, CDK12, OGDH, and SOD1. Typically, Co-IP experiments reported in the scientific literature use a vector only control as the negative control, however, due to the size of FLAG tag (only nine amino acids in length), it would represent a limited negative control as there would be no chance of a non-relevant interaction occurring due to PPIs. A vector only negative control really only controls for the interaction of proteins with the affinity resin, and while an important control nonetheless, the additional negative control of GFP was also included in the experiments described here. Therefore, in a similar manner to the nTAP and dTAP HBH tag experiments, a FLAG-GFP construct was utilized as an additional negative control to verify that any interaction demonstrated between FLAG-NS5A-2a and a myc-tagged TAP candidate was highly specific to NS5A.

Surprisingly, despite repeated attempts with FLAG-NS5A-2a samples to specifically coprecipitate a myc-tagged TAP candidate, all attempts showed some level of non-relevant interaction with FLAG-GFP. Figure 3.15 shows a Co-IP with a FLAG pull-down of FLAG-NS5A-2a and FLAG-GFP from cells co-transfected candidate NS5A interacting protein myc-NKRF. Here, myc-NKRF is co-precipitated with either bait

protein (Fig.3.15.A, lane 3 and lane 6). Similar results were obtained using myc-tagged TOM22, TOM40, CHERP and RanGap1 (data not shown). It is important to note that in no case did a vector only control bait sample co-precipitate any candidate or control protein. Therefore, it appears that attaching a larger protein capture area (e.g. GFP as a non-relevant protein) to the tag was enough to cause an inappropriate interaction.

To evaluate this issue further, a well-established NS5A interacting protein, FKBP38 (232,234–237) was N-terminally myc-tagged to use as a positive control and a variety of technical optimizations were undertaken in an attempt to improve specificity including: detergents (RIPA versus NP40), pH (7.4 versus 8.0), DNA removal (needle shearing versus high-speed centrifugation), increasing the number of washes, substitution of FLAG antibody capture resins (protein A/G magnetic beads versus agarose), precoating the FLAG capture resin and differing the FLAG resin elution conditions (boiling versus FLAG peptide). Of all of these conditions, only adjusting the amount of protein expressed from the transient transfections (by lowering the amount of plasmid transfected) improved conditions (Fig.3.15.B, lanes 1, 2 and 3).

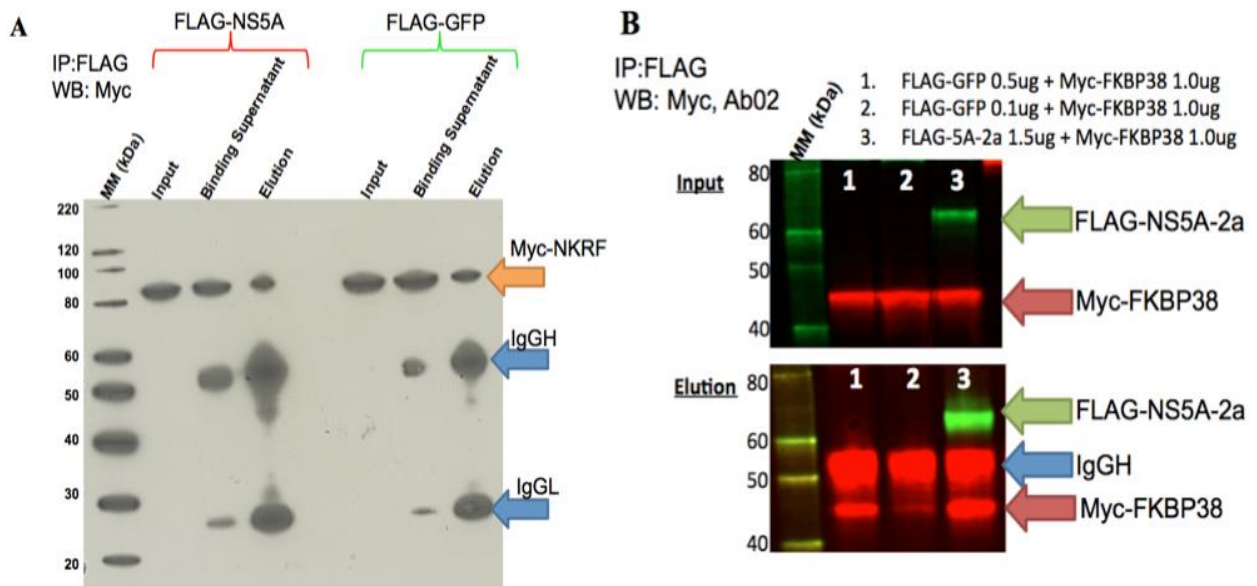


Figure 3.15. Non-specific capture of NS5A interacting TAP candidate proteins by FLAG antibody affinity resin co-precipitation. **(A)** FLAG-NS5A-2a or FLAG-GFP were transfected along with: **(A)** myc-NKRIF or **(B)** myc-FKBP38 into 293TN cells and harvested 48 hpt. Soluble proteins were precleared using protein A/G agarose for one hour then incubated with FLAG antibody overnight to capture FLAG-NS5A-2a or FLAG-GFP. Following addition of protein A/G agarose and one-hour incubation, complexes were washed four times with lysis buffer then eluted by boiling. **(A)** 15ul of the sample input, binding supernatant and elution were evaluated by Western blot analysis. myc-NKRIF was detected using an anti-myc antibody and chemiluminescence. Sample input, binding supernatant (post- antibody capture) and elution are shown. myc-NKRIF (78 kDa) is indicated by an orange arrow and immunoglobulin G (IgG) heavy (H) and light (L) chains (50 and 25 kDa) with blue arrows. **(B)** FLAG-coated magnetic beads were incubated with precleared lysates for one hour, washed six times with lysis buffer and eluted by boiling. 15ul of sample input (upper panel) and elutions (lower panel) were analyzed by Western blot. FLAG-NS5A-2a and myc-FKBP38 were detected with anti-NS5A-Ab02 and anti-myc antibodies. myc-FKBP38 (43 kDa) is indicated by a red arrow, FLAG-NS5A-2a (63/65 kDa) by a green arrow and IgG-Heavy chain (50 kDa) with a blue arrow. FLAG-GFP was run off the gel in order to separate myc-FKBP from IgGH.

So as not to deal with expression issues directly, an alternate strategy was employed to confirm PPIs using reciprocal affinity pull-downs i.e. capture myc-tagged TAP candidates directly and then determine if NS5A-2a or GFP was co-purified. Figure 3.16 shows a Western blot of doubly transfected FLAG-NS5A-2a/Myc-TAP candidates

precipitated with anti-myc antibodies. In all cases, NS5A-2a interacting candidates (lanes 2-10) and myc-FKBP38, as a positive control (lane 1), were precipitated using the anti-myc bead approach suggesting that this approach could next be evaluated for GFP specificity. FLAG-NS5A, when transfected on its own was not captured by myc antibody/resin purification. The strongest FLAG-NS5A-2a (63/65 kDa) band intensities were observed with the positive control myc-FKBP38 (lane 1), myc-CCAR2 (lane 2), myc-CDK12 (lane 3), myc-NKRF (lane 6), and myc-TOM22 (lane 10) (Fig. 3.16). Weaker FLAG-NS5A-2a band intensities were observed in myc-OGDH (lane 4), myc-SOD1 (lane 5), myc-CHERP (lane 7), myc-Rangap1 (lane 8), and Myc-TOM40 (lane 9) (Fig. 3.16). myc-CCAR2 and TOM22 were chosen for further myc-tag based purification validation.

Figure 3.17 shows a Western blot of myc Co-IPs evaluating the specificity of myc-CCAR2 and myc-TOM22 pull-down of FLAG-NS5A-2a and FLAG-GFP as prey proteins. FLAG-NS5A-2a was detected with both FLAG and NS5A-Ab02 antibodies in Figure 3.17, but a serial dilution of FLAG-NS5A-2a transfected 293TN cells revealed that the anti-FLAG antibody was more efficient at detecting the FLAG-NS5A-2a protein, however, in Fig.3.16 FLAG-NS5A-2a was detected using the NS5A-Ab02 antibody (channel 700, green) instead of the anti-FLAG antibody (channel 700, red) for clarity. myc-FKBP38 pull-down of FLAG-NS5A-2a was used as a positive control and demonstrated specific capture of FLAG-NS5A but not FLAG-GFP (compare lanes 3 and 6, Fig.3.17). The measles matrix protein (MeaslesM, a kind gift from Dr. Alberto Severini and Ms. Helene Schulz, NML) (35 kDa) was used as an additional negative

control protein as it is not believed to bind either NS5A or GFP and helps support the concept that the mere act of overexpressing a myc-tagged protein does not result in irrelevant/non-specific pull-down. Neither NS5A nor GFP were captured with myc-MeaslesM (Fig.3.17 lanes 9 and 12). FLAG-NS5A-2a and FLAG-GFP were also expressed in the absence of any myc-tagged proteins and neither FLAG-NS5A nor FLAG-GFP was captured by the myc-magnetic beads (Fig.3.17, lanes 15 and 18).

Interestingly, the specificity test with myc-TOM22 suggested that this bait protein was able to capture both FLAG-NS5A and FLAG-GFP (Fig.3.17, lanes 21 and 24). TOM22 was found to be a specific NS5A protein interaction candidate in xdTAP, so the Co-IP results differ from those of the TAP experiments. However, one function of TOM22 is to act as a chaperone (339) and therefore it may regularly interact with a number of proteins to assist with proper folding. The fact that these Co-IP experiments all involve transient expression, which tends to produce much higher amounts of protein compared to stable cell expression, may be a factor in the different results seen between nTAP/xdTAP. An additional candidate protein, myc-CCAR2 was able to co-precipitate FLAG-NS5A-2a and because it was the only protein to specifically co-precipitate FLAG-NS5A-2a and not FLAG-GFP, CCAR2 became a primary candidate for further function evaluation (Fig.3.17, lanes 27 and 30).

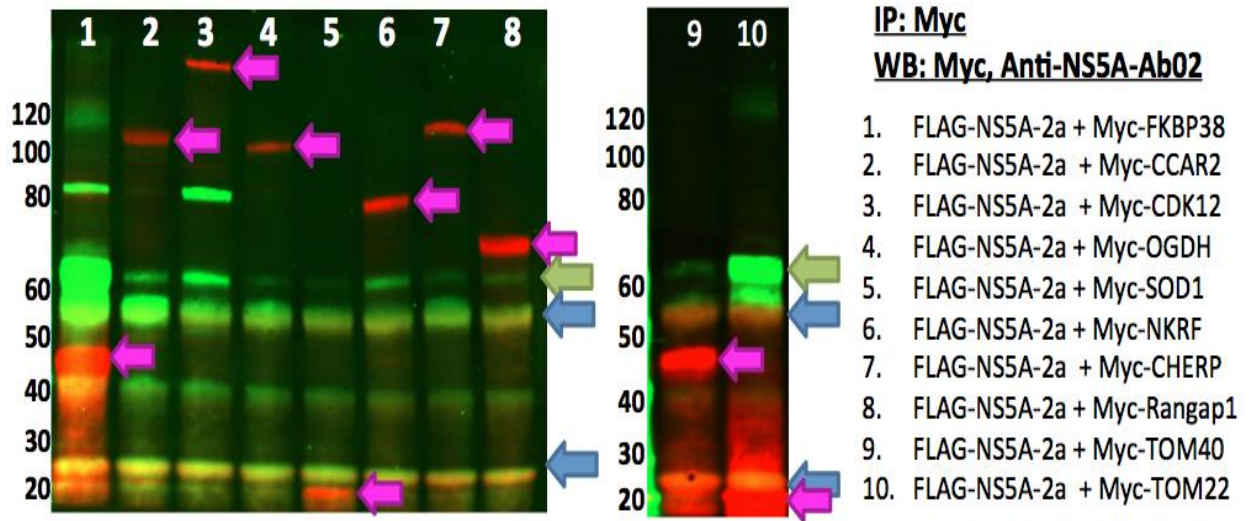


Figure 3. 16. Co-immunoprecipitation of FLAG-NS5A-2a with myc-tagged candidate proteins. Plasmid expression vectors were transfected into 293TN cells, harvested 48 hpt, subjected to anti-myc antibody coated magnetic bead purification and the final elution was evaluated by Western blotting with anti-NS5A-Ab02 and anti-myc antibodies. myc-FKBP38 (43kDa) (lane 1), myc-CCAR2 (103kDa) (lane 2), myc-CDK12 (160kDa) (lane 3), myc-OGDH (116kDa) (lane 4), myc-SOD1 (16kDa) (lane 5), myc-NKRF (78kDa) (lane 6), myc-CHERP (106kDa) (lane 7), myc-Rangap1 (64kDa) (lane 8), myc-TOM40 (42kDa) (lane 9), TOM22 (16kDa) (lane 10) are detected with the myc antibody as red bands (pink arrows). FLAG-NS5A-2a is detected as a green band using antibody NS5A-Ab02 at 63/65 kDa (green arrow). IgG heavy and light chain bands appear as 50 and 25 kDa yellow bands (blue arrow).

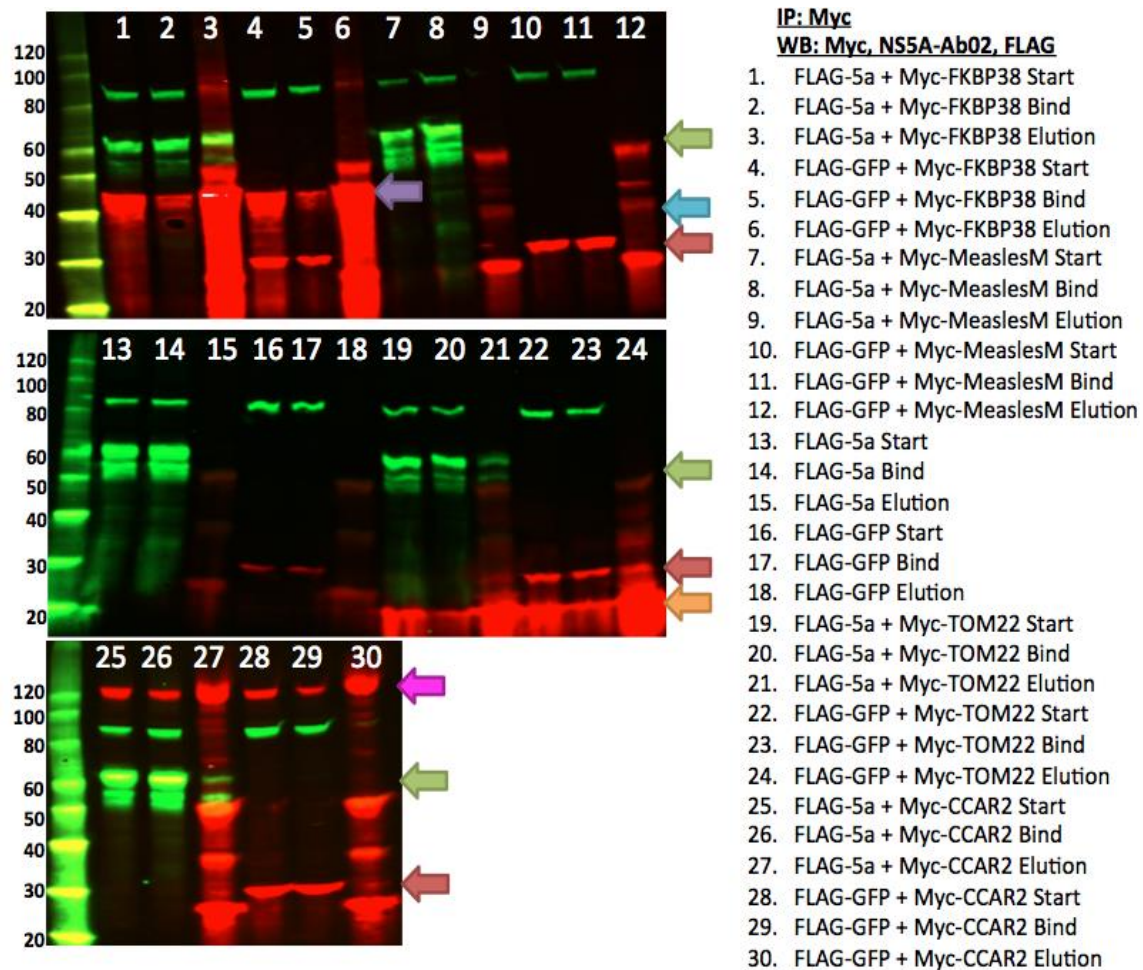


Figure 3. 17. Validation of myc co-immunoprecipitation using FLAG-NS5a-2a and FLAG-GFP as prey proteins. Plasmid expression vectors were transfected into cells, and harvested 48 hpt, subjected to anti-myc antibody coated beads and the final elutions obtained by boiling. Sample input (Start), binding supernatant (Bind) and elutions (Elution) were evaluated by Western blot analysis with anti-FLAG, anti-NS5A-Ab02, and anti-myc antibodies. myc-FKBP38 (43 kDa, purple arrow) (lanes 1-6) myc-MeaslesM (35 kDa, teal arrow) (lanes 7-12), myc-TOM22 (16 kDa, orange arrow) (lanes 19-24) and myc-CCAR2 (103 kDa, pink arrow) (lanes 25-30) are detected with the myc antibody as red bands. 24) FLAG-GFP (27 kDa, red arrow) (lanes 4-6, 10-12, 16-18, 22-24, 28-30) is detected by the FLAG antibody as a red band. FLAG-NS5A-2a (63/65 kDa, green arrow) (lanes 1-3, 7-9, 13-15, 19-21,25-27) is detected by FLAG and NS5A-Ab02 antibodies as a green-yellow band. IgG heavy and light chains appear as 50 kDa and 25 kDa red bands elutions (lanes 3,6,9,12,15,18,21,24,27,30). Western blots are representative of six separate biological replicates. Figure

As myc-CCAR2 provided a strong signal from co-precipitating FLAG-NS5A-2a and using a myriad of controls, proved that the interaction was specific, the CCAR2 docking

site on NS5A was investigated. To determine if a particular NS5A-2a protein domain was responsible for the interaction with CCAR2, five FLAG-tagged JFH1 NS5A domain mutants were constructed. Domain mutants consisted of domain D1, D2, D3, D1-D2, and D2-D3 with the corresponding low complexity sequence (LCS) regions as pictured in Fig.3.18.A. The upper panel of figure 3.18.B shows a Western blot of the myc Co-IP sample input with the full-length FLAG-NS5A-2a (63/65 kDa) (lane 1) and the domain mutants, D1 (30 kDa, lane 2), D2 (25 kDa, lane 3), D3 (28 kDa, lane 4), D1-D2 (45 kDa, lane 5) and D2-D3 (40 kDa, lane 6). No protein was detected for the FLAG-D2 construct but all the other constructs showed expression at the expected molecular weights and to a similar level to full-length NS5A. Only full-length FLAG-NS5A-2a protein was co-precipitated to any extent by myc-CCAR2 (Fig.3.18.B, Elution, lane 1) as none of the FLAG-NS5A-2a domain constructs were detected by either the anti-FLAG or NS5A-Ab02 antibodies in the myc-CCAR2 Co-IPs (Fig.3.18.B, lanes 2-6). Although improper folding and inappropriate subcellular localization issues were not explored further, it remains that only a full-length form of the NS5A protein was competent for capture by myc-CCAR2.

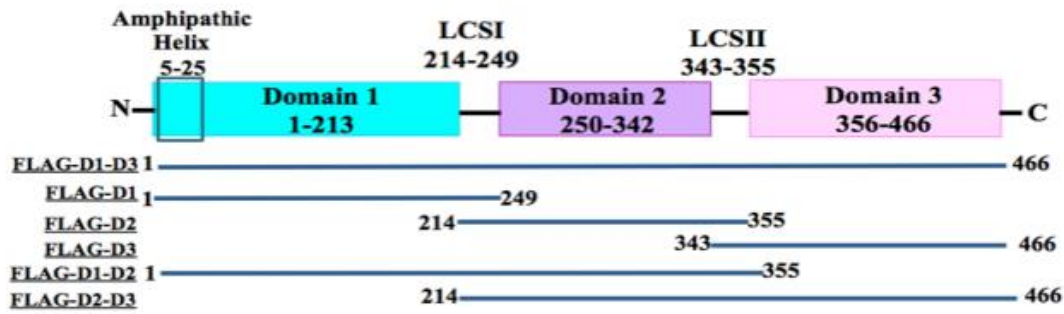
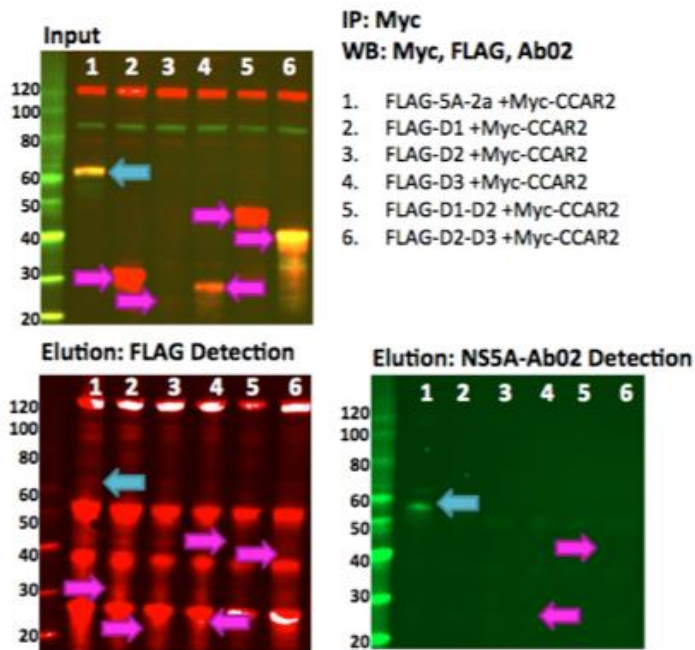
A**B**

Figure 3. 18. Evaluation of CCAR2 interaction with NS5A-2a domains. (A) Schematic of full-length NS5A and NS5A domain mutants constructed from JFH1 NS5A. FLAG-tagged domain mutants consisting of one or two neighboring domains and the corresponding LCS I region were created from full-length JFH1 NS5A. (B) myc-CCAR2 co-precipitation of FLAG-NS5A-2a domain mutants. Plasmid expression vectors were transfected into cells and harvested 48 hpt, subjected to anti-myc antibody coated beads, and final elutions were obtained by boiling. Sample input (Input, upper panel), and elutions (Elution, lower panel, FLAG antibody left, NS5A-AB02, right) were evaluated by Western blot analysis with anti-FLAG (detects FLAG tag at N-terminus, all domain mutants, lanes 1-6), anti-NS5A-Ab02 (detects NS5A-2a epitope in D3, only lanes 1, 4, 6), and anti-myc antibodies. Full-length FLAG-NS5A-2a (63/65 kDa) (lane 1) FLAG-D1 (30 kDa, lane 2), FLAG-D2 (25 kDa, lane 3), FLAG-D3 (28 kDa, lane 4), FLAG-D1-D2 (45 kDa, lane 5) and FLAG-D2-D3 (40 kDa, lane 6) are detected with FLAG and NS5A-Ab02 antibodies as green or yellow bands. Myc-CCAR2 (103 kDa) (lanes 1-6) is detected with the myc antibody as a red band. IgG heavy and light chains appear as 50 kDa and 25 kDa red bands in the elutions (lanes 1-6). Size of full-length FLAG-NS5A-2a indicated by a blue arrow and size of FLAG-tagged domain mutants indicated with a pink arrow.

3.2.6 Evaluation of NS5A-2a/CCAR2 cell colocalization

Co-localization of NS5A-2a and CCAR2 was first examined in 293TN and Huh7.5 cells doubly transfected with FLAG-NS5A-2a and myc-CCAR2. In mock transfections of 293TN and Huh7.5 cells, endogenous CCAR2 is found predominately in the nucleus, (Fig.3.19, A/C, Merge, pink shading). However, in either 293TN or Huh7.5 cells expressing both FLAG-NS5A-2a and Myc-CCAR2, CCAR2 is largely redistributed to the cytoplasm where FLAG-NS5A-2a is also located (Fig.3.19, B/D, merge = yellow pixels). Examples of cells expressing both FLAG-NS5A-2a and myc-CCAR2 where there is redistribution of CCAR2 to the cytoplasm are indicated with white arrows in the CCAR2 (593 channel) and the corresponding NS5A-2a (488 channel) (Fig.3.19, B/D, CCAR2, NS5A-2a). In cells not expressing NS5A, CCAR2 is located primarily in the nucleus as indicated by orange arrows (Fig.3.19, B/D, CCAR2). Therefore, a correlation between FLAG-NS5A-2a expression and CCAR2 redistribution from the nucleus to the cytoplasm is apparent.

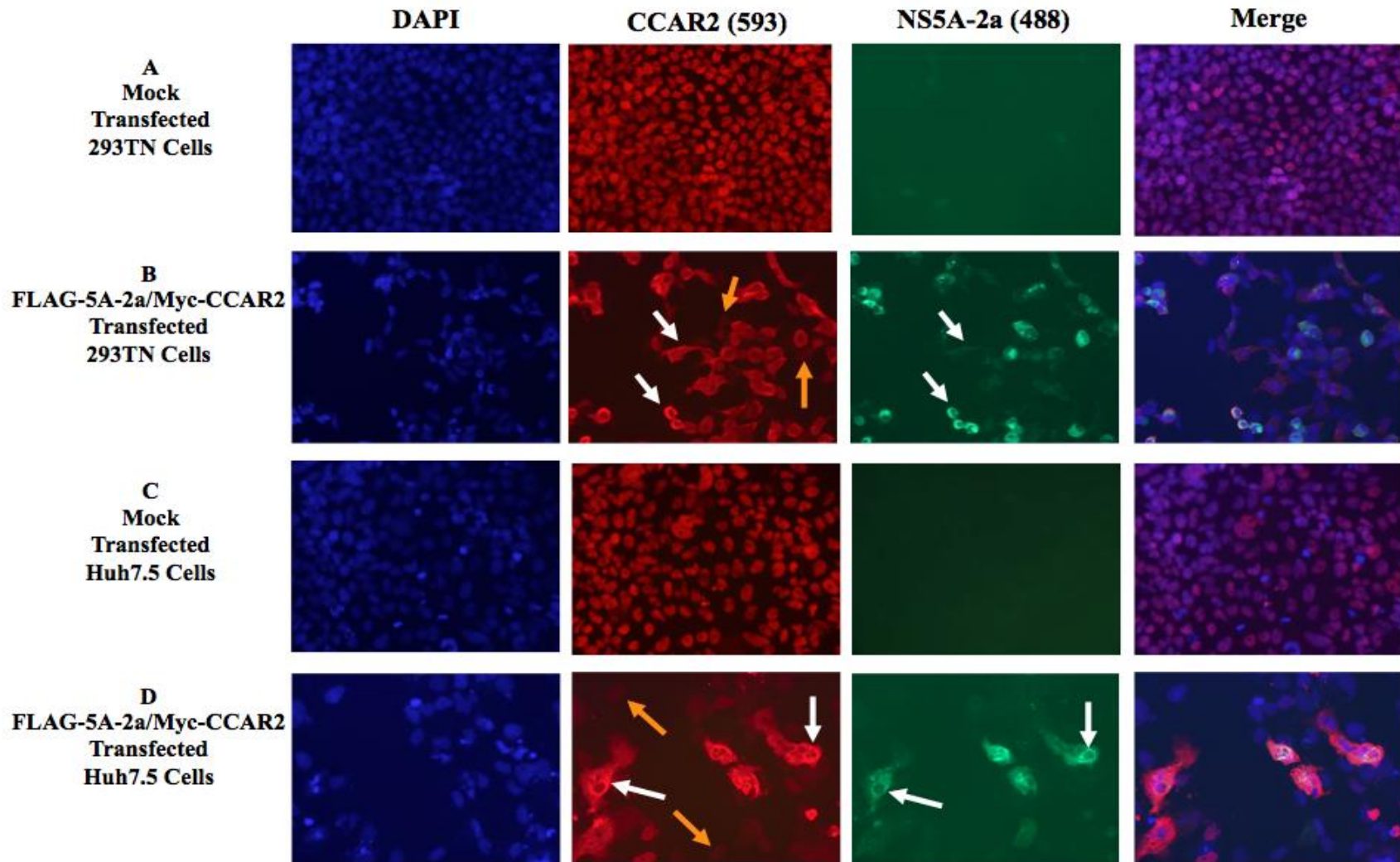


Figure 3. 19. Colocalization of FLAG-NS5A-2a and CCAR2 in co-transfected cells. 293TN and Huh7.5 cells were transfected with FLAG-NS5A-2a and myc-CCAR2 or mock transfected with a pUC19 plasmid (non-expressing control plasmid). 293TN and Huh7.5 cells were transfected with (A, C) pUC19, or (B, D) FLAG-NS5A-2a + myc-CCAR2. 48 hpt cells were fixed with 2% paraformaldehyde, permeabilized with Triton X-100 and anti-CCAR2 and NS5A-Ab02 antibodies were used for detection. Primary antibodies were detected with anti-mouse-593 and anti-rabbit-488 fluorescently conjugated secondary antibodies, and nucleic acids were stained with DAPI. Images were obtained with an Axiovert 200M fluorescence microscope (Zeiss) with the 20X and 32X and are representative images from three biological replicates. White arrows indicate CCAR2 cells with cytoplasmic localization of CCAR2 and FLAG-NS5A-2a and orange arrows indicate CCAR2 present in the nucleus in cells absent NS5A.

Evaluation of subcellular localization was also performed using a higher resolution LSM 700 laser scanning confocal microscope (Zeiss). In 293TN cells transfected with FLAG-GFP endogenous CCAR2 is mainly located in the nucleus (Fig.3.20.A, merge). While FLAG-GFP and CCAR2 are in similar areas of the cell, there is no yellow color that would be indicative of an overlap (Fig.3.20.A Merge-50X/100X). Alternatively, in the presence of FLAG-NS5A-2a, there is more cytoplasmic staining of CCAR2 (Fig.3.20.B, CCAR2). This is important as CCAR2 is often described as a nuclear protein (340–342). A zoomed in merge panel indicates that there are strong areas of overlap between NS5A and CCAR2 indicated by the yellow dots (Fig.3.20.B, Merge 50X/100X).

While majority of the CCAR2 protein remained in the nucleus in transfected cells, several cells expressing FLAG-NS5A-2a indicated CCAR2 cytoplasmic redistribution (Fig.3.20.C). In some 293TN cells containing FLAG-NS5A-2a (Fig.3.20.C), nucleic acids appear condensed, and CCAR2 no longer co-localizes with the nucleic acids but is present in the cytoplasm. There is a correlation between the presence of FLAG-NS5A-2a, condensed nucleic acids and CCAR2 cytoplasmic redistribution (Fig.3.20.C, Merge 50X/100X). This could highlight a moment in a cell's lifecycle (mitosis) when NS5A and CCAR2 interact strongly with one another. The strong interaction between NS5A-2a/CCAR2 is also demonstrated in 293TN cells doubly transfected with FLAG-NS5A-2a/Myc-CCAR2 (Fig.3.20.D). 293TN cells expressing the Myc-CCAR2 plasmid appear brighter red with broader total cell staining as opposed to endogenous CCAR2 levels that are lighter red with primarily nuclear staining (Fig.3.20.D, CCAR2). These colocalizations were repeated in Huh7.5 cells and yielded similar results (Fig.3.20.E-G).

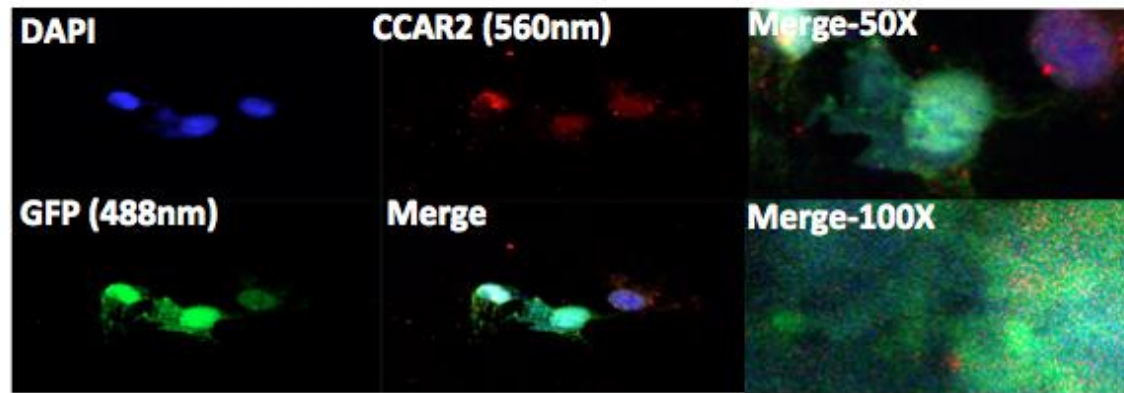
In Huh7.5 cells, CCAR2 was present in both the nucleus and cytoplasm, FLAG-NS5A-2a/CCAR2 colocalized in the cytoplasm and even more so in the FLAG-NS5A-2a/Myc-CCAR2 transfection (Fig.3.20.E-G).

Next, colocalization of NS5A-2a/CCAR2 was investigated with HBH tagged GFP and NS5A-2a stable GP2 293 cells used in the initial nTAP identification of the NS5A-2a/CCAR2 (Fig.3.21.A&B). Cytoplasmic expression of CCAR2 was confirmed in both HBH-tagged NS5A-2a and GFP cells lines (Fig.3.21.A&B, CCAR2). Discrete yellow puncta demonstrating an overlap between NS5A (488) and CCAR2 (593) were observed (Fig.3.21.B, merge). The yellow puncta do not represent a majority population suggesting that this interaction may represent a lower amount of interaction when HBH-NS5A-2a is expressed at a more moderate level compared to the transient transfection results presented above. It should be noted that GP2 293 cells have a minimal cytoplasm, thus providing a smaller area by which to discern low-level cytoplasmic interactions.

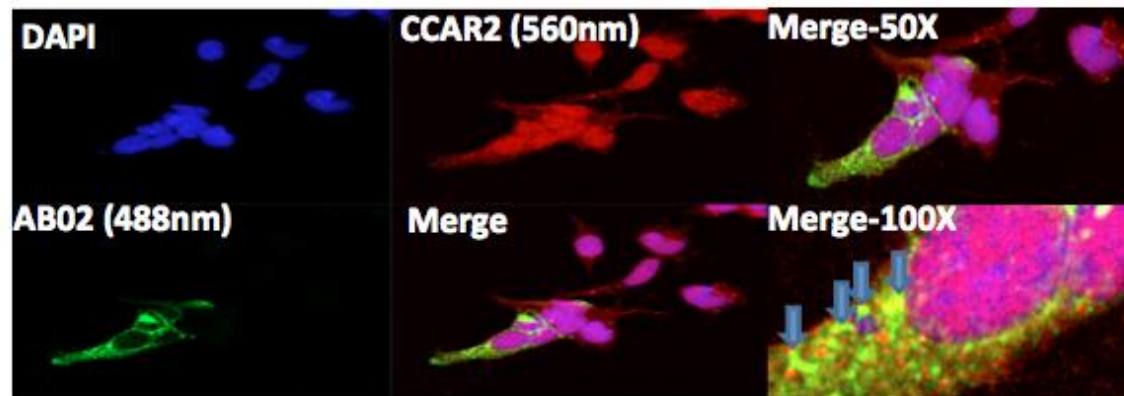
CCAR2-NS5A-2a co-localization was additionally evaluated in the SG JFH1 replicon and JFH1-HT infection models. SG JFH1 cells contain actively replicating HCV RNA of including the nonstructural HCV proteins and merging of the 488, and 593 fluorescence channels show regions of overlap between the CCAR2 and NS5A protein represented by discrete yellow puncta (Fig.3.21.C, merge). In SG JFH1 cells with condensed nuclei, there is an increase in the yellow overlap between CCAR2 (593) and NS5A-2a (488) indicating that the two proteins colocalize to a higher degree in cells with condensed nucleic acids that may be undergoing mitosis or cell death (Fig.3.21.C, merge). Huh7.5

cells infected with JFH1-HT virus reflect similar results as seen with the SG JFH1 model where NS5A-2a/CCAR2 colocalization is observed (Fig.3.21.D, merge). Taken together the indirect immunofluorescence experiments demonstrate that NS5A-2a and CCAR2 proteins interact.

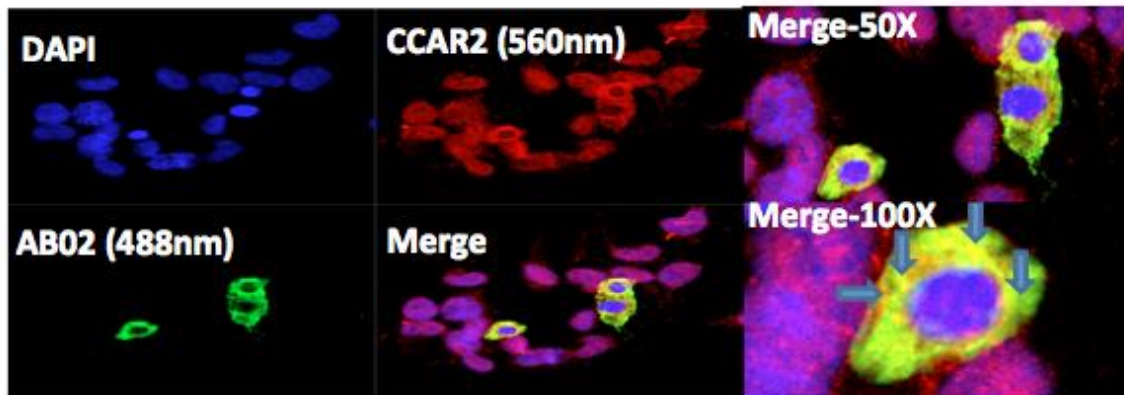
A
FLAG-GFP
Transfected
293TN Cells



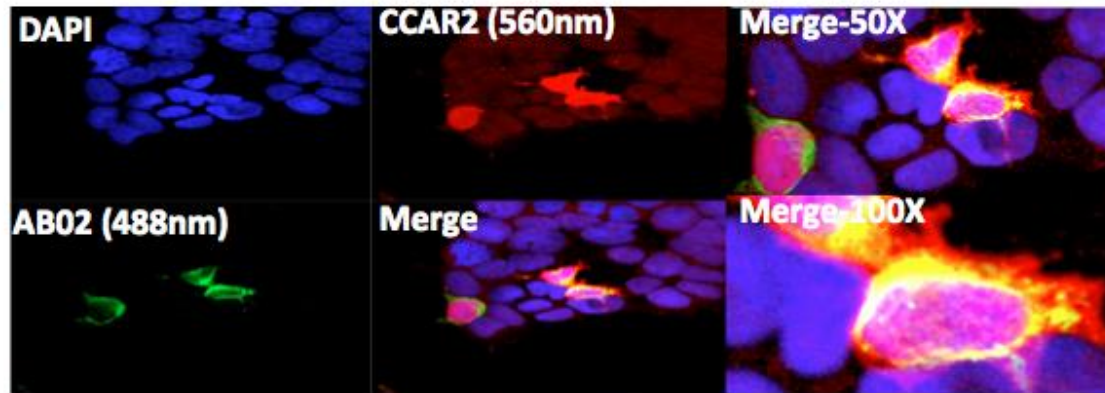
B
FLAG-NS5A-2a
Transfected
293TN Cells
Panel 1



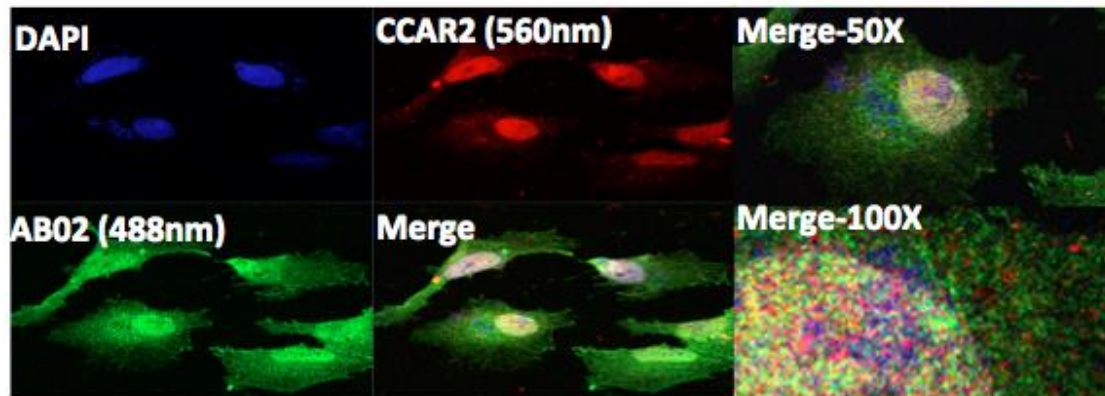
C
FLAG-NS5A-2a
Transfected
293TN Cells
Panel 2



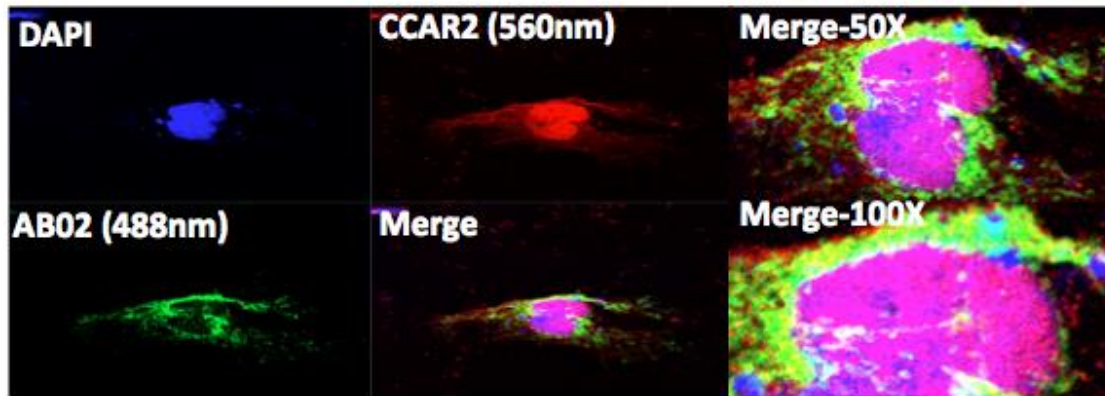
D
FLAG-NS5A-2a/Myc-CCAR2
Transfected
293TN Cells



E
FLAG-GFP
Transfected
Huh7.5 Cells



F
FLAG-NS5A-2a
Transfected
Huh7.5 Cells



G
FLAG-NS5A-2a/Myc-CCAR2
Transfected
Huh7.5 Cells

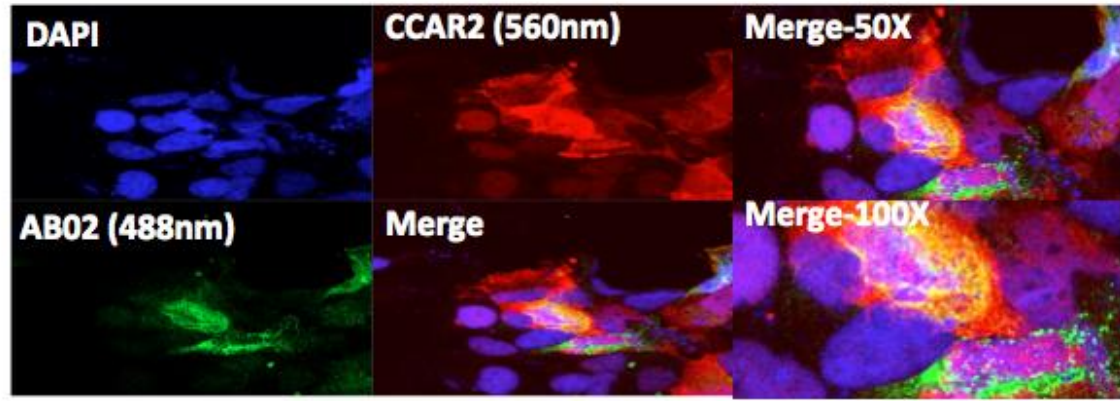
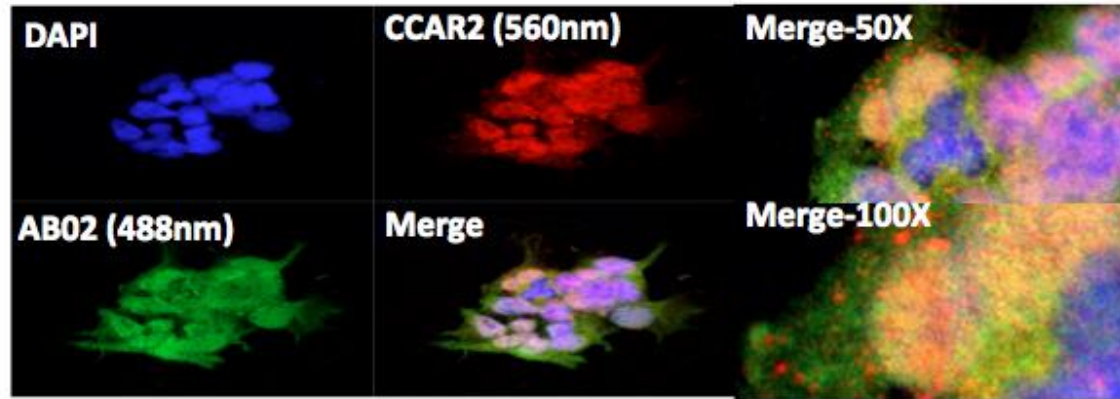
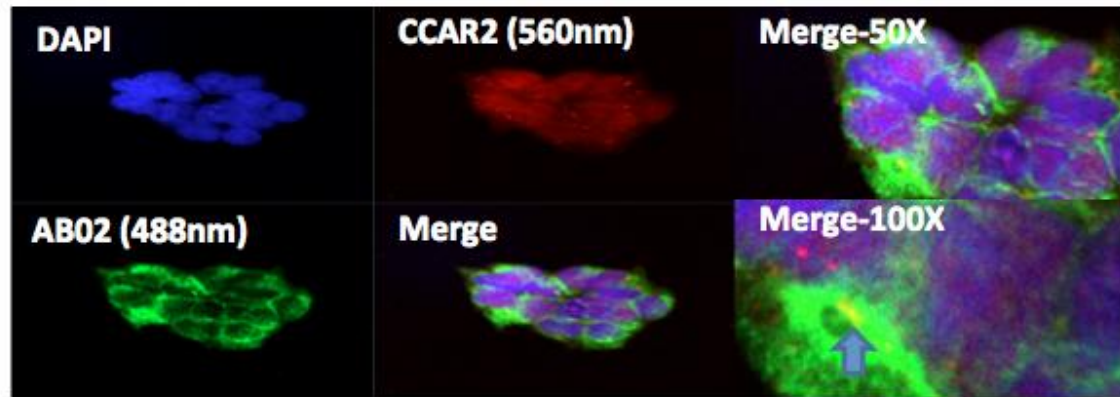


Figure 3. 20. Colocalization of FLAG-NS5A-2a and CCAR2 in transfected 293TN and Huh7.5 cells viewed with a laser scanning confocal microscope. 293TN and Huh7.5 cells were transfected with (A, E) FLAG-GFP, (B, C, F) FLAG-NS5A-2a or (D, G) FLAG-NS5A-2a/Myc-CCAR2. 48 hpt cells were fixed with paraformaldehyde, permeabilized with Triton X-100 and antibodies to CCAR2 and NS5A-Ab02 were used to detect proteins. Primary antibodies were detected with mouse-593 and rabbit-488 fluorescently conjugated secondary antibodies, and nucleic acids were stained with DAPI. Yellow overlapping puncta are indicated with a blue arrow. Images were obtained with an LSM 700 laser scanning confocal microscope (Zeiss) with the 40X objective and are representative of two biological replicates (cell transfections).

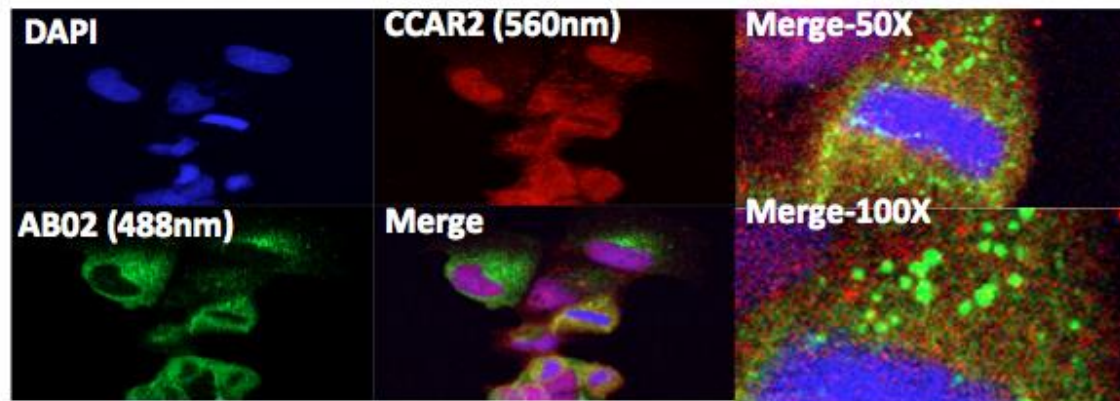
A
HBH-GFP
GP2 293 Cells



B
HBH-NS5A-2a
GP2 293 Cells



C
SG JFH1
Huh7.5 Cells



D
JFH1 infection
Huh7.5 Cells

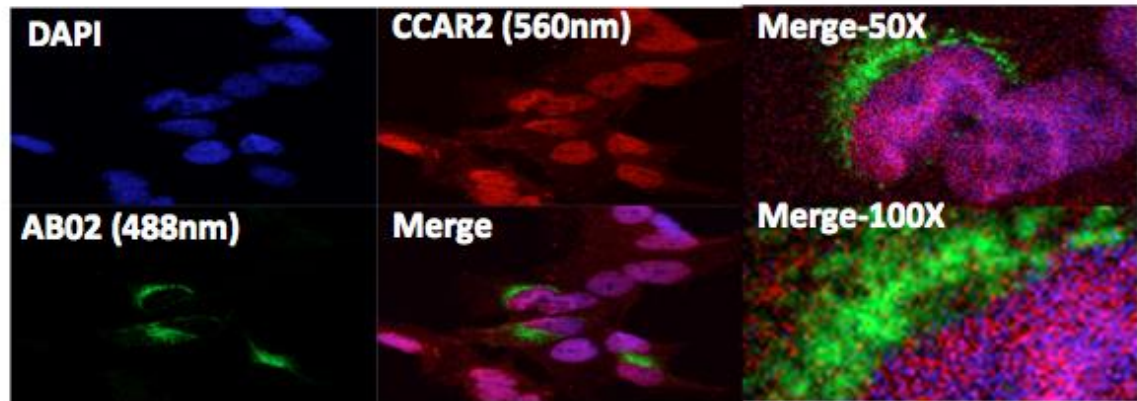


Figure 3. 21. Co-localization of NS5A-2a and CCAR2 in HBH-NS5A-2a GP2 293 cells, SG JFH1/Huh7.5 and JFH1-HT/Huh7.5 cells. (A) HBH-GFP, (B) HBH-NS5-2a GP2 293, SG (C) JFH1 Huh7.5 cells and (D) JFH1-HT infected Huh7.5 cells were fixed with paraformaldehyde, permeabilized with Triton X-100 and antibodies to CCAR2 and NS5A-Ab02 were used to detect proteins. Primary antibodies were detected with mouse-593 and rabbit-488 fluorescently conjugated secondary antibodies, and nucleic acids were stained with DAPI. Yellow overlapping puncta are indicated with a blue arrow. Images were obtained with an LSM 700 laser scanning confocal microscope (Zeiss) with the 40X objective and are representative of two biological replicates

3.2.7 Quantification of CCAR2 in NS5A-2a expressing cells

To determine whether expression of NS5A-2a influenced endogenous CCAR2 protein levels, CCAR2 was quantified in both HBH-NS5A-2a and HBH-GFP GP2 293 cells (Fig.3.22). Western blot serial dilution analysis of cell extract detected with the CCAR2 antibody showed a linear correlation ($r^2=0.986$) over a 5ug-40ug total protein load range (data not shown). 30ug of 2% SDS harvested total protein from GP2 293 stable HBH-NS5A-2a (lane 1), HBH-GFP (lane 2) cells and 293TN cells (lane 3) were evaluated by Western blot (Fig.3.22.A) and quantified (Fig.3.22.B). Actin was utilized as a load control to ensure equivalent protein loading, and CCAR2 protein abundance was expressed as a ratio of CCAR2/Actin signal (Fig.3.22.B). A two-tailed Student's t-test assuming unequal variance indicated that the quantity of CCAR2 was unaffected by HBH-NS5A-2a expression when compared to HBH-GFP controls with a p-value of 0.94 when the two means from three biological replicates were compared.

The colocalization studies from the previous section suggested a cytoplasmic redistribution of CCAR2 in at least a subset of cells expressing NS5A-2a (Fig.3.20&21). To test whether this observation could be quantified, GP2 293 cells expressing HBH-NS5A-2a and HBH-GFP were separated into cytoplasmic and nuclear fractions using the Rapid, Efficient And Practical (REAP) method (311). 40ug of total protein from the whole cell and cytoplasmic fractions and 35ug from the nuclear fraction was evaluated using Western blot analysis (Fig.3.22.C). GAPDH and Histone H3 (H3) were used as cytoplasmic and nuclear extraction specificity controls to produce ratios of CCAR2/GAPDH for whole cell and cytoplasmic fractions and CCAR2/H3 ratios for

nuclear fractions (Fig.3.22.D). The mean CCAR2 whole cell, cytoplasmic and nuclear ratios obtained from HBH-NS5A-2a cells were compared to HBH-GFP, but no significant difference was detected by a Student's t-test (p-values of 0.80, 0.67 and 0.64 for the whole cell, cytoplasm and nucleus abundance ratios respectively)(Fig.3.22.D). Therefore, NS5A-2a expression does not alter the CCAR2 protein levels in 293 cells.

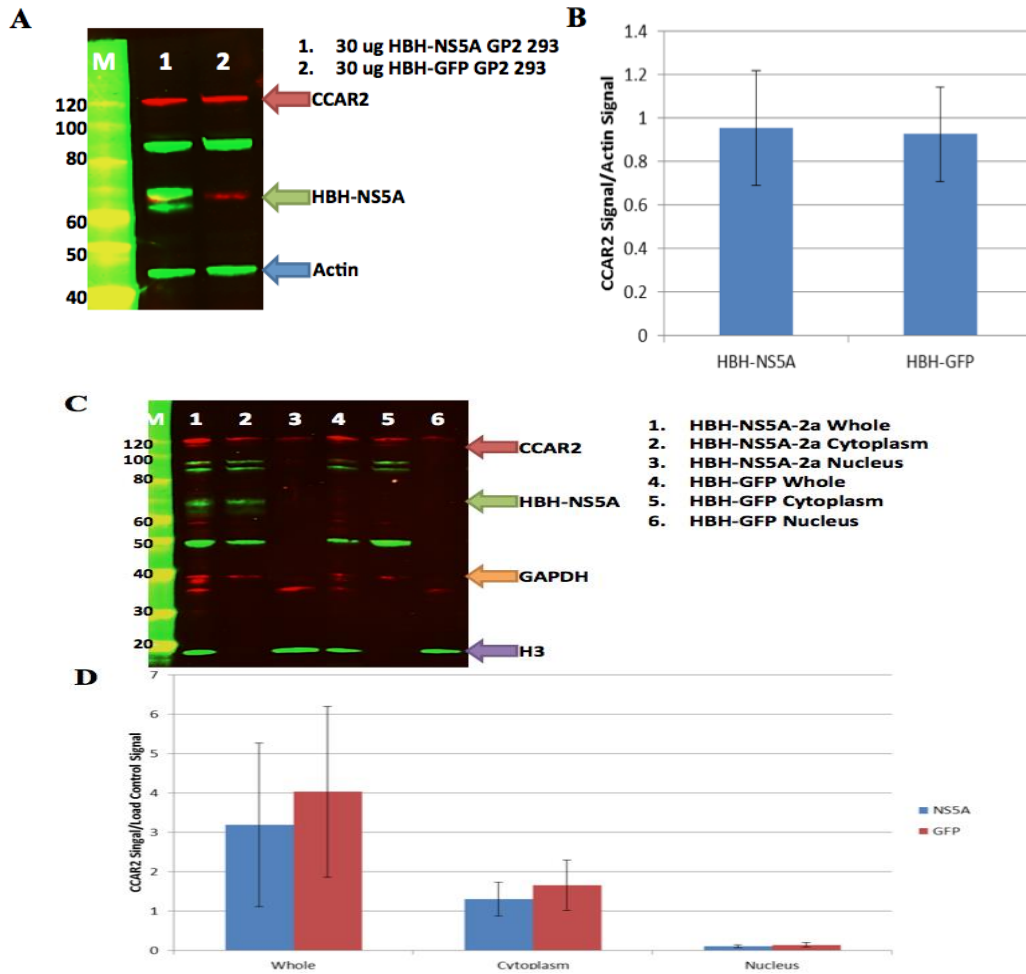


Figure 3. 22. Expression of NS5A-2a does not affect CCAR2 overall protein levels. **(A)** CCAR2 expression in HBH-tagged NS5A and GFP expressing cells. 30ug of total protein from HBH-NS5A-2a (lane 1) and HBH-GFP (lane 2), GP2 293 cells were evaluated by Western blot. CCAR2 (103 kDa, red arrow), HBH-NS5A-2a (63/65 kDa, green arrow) and Actin (42 kDa, blue arrow) are identified with anti-CCAR2, anti-NS5A-Ab02, and anti-Actin antibodies by near infrared detection. **(B)** Quantification of CCAR2 in HBH-tagged NS5A and GFP cells. Signal intensities of CCAR2 and actin were quantified using Image Lite software and presented as CCAR2/Actin ratios. Data presented are the mean CCAR2/actin ratios \pm SEM obtained from three biological replicates. **(C)** CCAR2 expression in REAP fractionated HBH-tagged NS5A and GFP cells. 40ug of whole cell lysate, 40ug cytoplasmic fraction and 35ug nuclear fraction from REAP separated HBH-NS5A-2a (lanes 1-3) and HBH-GFP (lanes 4-6) GP2 293 cells were evaluated by Western blot. CCAR2 (103 kDa, red arrow), HBH-NS5A-2a (63/65 kDa, green arrow), Histone H3(18 kDa, purple arrow) and GAPDH (37 kDa, orange arrow) are identified with anti-CCAR2, NS5A-Ab02, H3 and GAPDH antibodies by near infrared detection. **(D)** Quantification of CCAR2 in REAP fractionated HBH-tagged NS5A and GFP cells. Signal intensities of CCAR2, H3, and GAPDH were quantified using Image Lite. CCAR2 abundance is expressed as expressed as CCAR2/GAPDH for whole cell and cytoplasmic fractions and CCAR2/H3 for nuclear. Data presented are the mean CCAR2/Control ratios \pm SEM obtained three biological replicates.

3.3 Summary

nTAP and xdTAP methodologies were applied to stably expressed HBH-NS5A-2a samples and identified previously published and novel NS5A interacting candidates. While the FLAG-NS5A-2a immunoprecipitation did not provide the specificity required to confirm the TAP candidates when compared to a FLAG-GFP control protein, reciprocal myc-tagged Co-IPs established CCAR2 as a novel NS5A-2a interacting protein. Colocalization using indirect immunofluorescence provided further evidence of the NS5A-2a/CCAR2 interaction as both proteins colocalized intracellularly in several models of NS5A-2a expression. Expression of NS5A-2a does not affect the overall quantity of CCAR2 cellular protein in total protein lysates obtained from stable HBH-NS5A-2a GP2 293 or SG JFH1 replicon cells. While colocalization supports a model for CCAR2 cytoplasmic redistribution, it appears to occur in a subset of cells as this was not confirmed in REAP separated cytoplasmic and nuclear fractions of HBH-NS5A-2a GP2 293 cells possibly due to the limited number of cells that this occurs in.

Chapter 4: Mapping and characterization of phosphorylation sites on hepatitis C virus nonstructural 5A protein

4.1 Introduction and Rationale

The phosphorylation status of NS5A is believed to play a significant role in the replication and packaging of HCV. Different phosphorylation states affect NS5A's ability to bind host proteins and these interactions are required for successful completion of the viral life cycle (140,284). Several groups have attempted to identify phosphorylation sites within NS5A and the following NS5A residues: S146, S222, S225, S235, S238 and T348 have been unaided (303–306). Mass spectrometry analysis of HBH-tagged NS5A protein (Results, Chapter 3) indicated a number of phosphorylation sites had not been previously reported. Therefore, a more concerted effort was made to map any additional sites and determine if they had a biological phenotype in the context of an infectious virus clone.

4.2 Results

4.2.1 Expression of JFH1 NS5A to identify phosphoacceptor sites by mass spectrometry

During the course of this study, phospho-NS5A was isolated from several sources. Initially, the HBH-tagged protein expressed in 293 cells was used as a source of NS5A. dTAP purification of HBH-NS5A was enriched for phosphopeptides using titanium dioxide resin and subjected to mass spectrometry analysis. This source of NS5A identified 25 phosphorylation sites. (Table 4.1) While all of the peptides used for phosphorylation identification were confidently identified as being phosphorylated, in

two cases, the specific residue was not clear. For one peptide containing S381+S382 and for another peptide containing S414+S415, the specific serine residue could not be unambiguously assigned and therefore they are listed as S381/S382 and S414/S415 (Table 4.1 and Appendix 2). Additional proteases were also used in order to produce different peptides and thus provide different/greater coverage than trypsin could alone therefore GluC (cleaves after glutamate and aspartate residues) and AspN (cleaves after Asp and Cys residues) were incorporated in to the analysis. GluC digestion identified new phosphorylation sites in NS5A at S288, S381/S382, S401, T410, and S414/S415 and confirmed another phosphorylation site at T204. AspN digestion identified T210 and S272 (Table 4.1).

Table 4. 1. NS5A phosphorylation sites identified from each source where NS5A was expressed. NS5A sources: Expressed HBH-NS5A-2a (NS5A isolated from GP2 293 cells stably expressing HBH-tagged NS5A), wt SG JFH1 (NS5A isolated from cells harbouring a SG replicon JFH1 wt, genotype 2a), SG JFH1 NS5A-HBH (NS5A isolated from a modified wt SG JFH1 replicon where an HBH tag was incorporated into the NS5A coding sequence. Positively identified phosphorylated residues are indicated with a black box under the serine or threonine residue found to be modified by mass spectrometry analysis. Previously identified NS5A phosphorylation sites are highlighted in blue (289,303–306). Protein digestion enzymes used for site identification are indicated below (T=trypsin, G=GluC, A=AspN).

		NS5A Phosphorylation Sites																												
NS5A Source		S146	S151	T164	S201	T204	T210	T213	S222	S225	S228	S229	S230	S232	S235	S238	S272	S288	T334	T348	T356	S360	S362	T363	S365	S381/S382	S401	T410	S414/S415	
Expressed HBH-NS5A-2a																														
wt SG JFH1																														
SG JFH1-NS5A-HBH																														
Digestion Enzyme		T	T	T	T	T/G	A	T	T	T	T	T	T	T	T	T	A	G	T	T	T	T	T	T	T	G	G	G	G	

While the HBH-tagged NS5A protein platform provided large amounts of extremely pure product which is highly amenable to mass spectrometry identification, there was the

concern that additional phosphorylation sites may occur only when NS5A is expressed in the context of other viral proteins. Therefore, SG JFH1 replicon cells were used next as a source of NS5A protein. In order to reduce the proteome complexity, lysates were subjected to slab-gel SDS PAGE and the region corresponding to NS5A including the basally phosphorylated (p56) and the hyperphosphorylated form (p58) was isolated following electrophoresis. Unfortunately, this methodology is not optimal for mass spectrometry analysis as slab-gel SDS-PAGE can only resolve a limited amount of protein before resolution is compromised and the proteins migrate as an indistinguishable protein smear. Additionally, digestion and extraction of peptides from acrylamide slices is not an efficient process thereby limiting detection success during subsequent mass spectrometry interrogation. In order to alleviate the yield problems associated with standard slab gels, NS5A was isolated from SG JFH1 Huh7.5 replicon cells using a large format continuous high-resolution gel electrophoresis 491 prep cell (Bio-Rad). This system can circumvent the two most important issues mentioned above: 1) the system can successfully resolve up to 5mg of total protein and 2) protein is eluted from the gel as liquid fractions and therefore subsequent manipulations do not require digestion of the protein in acrylamide.

Figure 4.1.A depicts a silver stained SDS-PAGE gel of fractions collected from the 491 prep cells, demonstrating good separation of proteins by size. A Western blot probed with anti-NS5A-2a antibody (NS5A-Ab02) was used to identify the fractions containing NS5A-2a protein (Fig.4.1.B) and these fractions were concentrated and enriched for phosphopeptide identification. In this case, 12 sites were identified of which three were

new compared to the HBH-NS5A expressed and purified form (S381/S382, T410 and S414/S415). There were 16 sites seen in the HBH-tagged NS5A expressed source that were not seen in the SG replicon source of NS5A. A possible explanation is that yield and purity compromised detection of these species as numerous other host phosphorylated contaminating proteins were also detected in these samples. One potential advantage of the 491 prep cell size separation method was the ability to separate the two phospho-proteoforms of NS5A-2a. In Figure 4.1.B, eluted fraction lane 1 contains the equivalent of p56, whereas lanes 2 and 3 contain p56+p58, and lanes 4-9 contains p58.

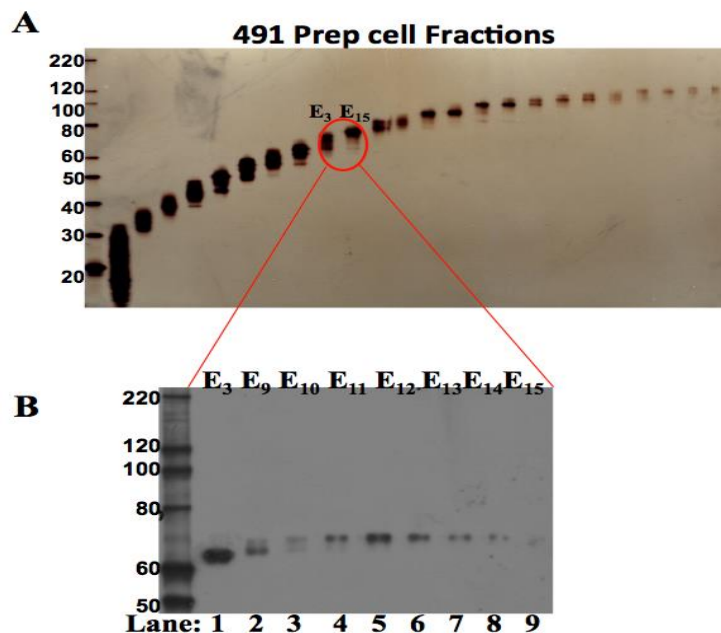


Figure 4. 1. Continuous gel electrophoretic separation of total protein from wt SG JFH1 replicon Huh7.5 cells. Five mg of total protein from wt SG JFH1 cells was separated on a 7.5% 491 prep cell (Bio-Rad), and fractions were eluted in 2ml volumes. **(A)** Separation of wt JFH1 replicon Huh7.5 491 by size using the 491 prep cell. 15ul of select 491 fractions were resolved on an SDS-PAGE gel and silver stained for total protein content. Fractions E3-E15 contained 60-70 kDa proteins. **(B)** Identification of NS5A-2a from 491 prep cell elution fractions. NS5A-2a was detected in the 491 elution fractions spanning the 60-70 kDa range E3 (lane 1) and E9-E15 (lanes 2-8) using the NS5A-Ab02 antibody and chemiluminescence.

Ultimately, the most valuable model to study NS5A phosphorylation would be one in which the HBH affinity tag was added to NS5A within the genome of a replication competent virus. This would allow expression of NS5A in the context of viral replication and provide a simple way to affinity purify the protein. To this end, the HBH tag was inserted into NS5A within the SG JFH1 replicon. The C-terminal region of NS5A-2a has been previously shown to tolerate insertion of foreign sequence while still allowing genome replication (141,181,304). The HBH tag was inserted between E420 and G421 within NS5A-2a at the site of an *AbsI* restriction site (Fig.4.2.A). Transcribed RNA was generated and used to establish a replicon cell line and the presence of NS5A-HBH in the cells was confirmed by Western blot and indirect immunofluorescence (Fig.4.2.B&C). In figure 4.2.B, lane 1, wt NS5A-2a is detected as two bands at 63/65 kDa, the two predominant phospho-proteoforms of NS5A. These forms will still be referred to as p56 (basally-) and p58 (hyperphosphorylated) even though NS5A from genotype 2a has a natural insertion that increases its size to 63 and 65 kDa. Bands at 80-85 kDa are unidentified host protein detected by NS5A-Ab02 in Huh7.5 cells as well as other cell lines tested (see Fig 3.17 for a 293 cells only control).

Increasing amounts of protein from the SG JFH1-NS5A-HBH replicon cell line evaluated by Western blotting are shown in lanes 2-5 and the bands detected at 74/76 kDa are the correct sizes for NS5A-2a-HBH. Indirect immunofluorescence using the NS5A-Ab02 revealed that SG JFH1-NS5A-HBH replicon cells displayed the same characteristic cytoplasmic NS5A staining as did wt SG JFH1 cells (Fig.4.2.C). The level of NS5A protein compared to wt suggested that the HBH tagged replicon was not as efficient as

the wt SG form (compare Fig.4.2.B, lanes 1 and 5). Nevertheless, viable subgenomic RNA replication and localization was taking place so SG JFH1-NS5A-HBH Huh7.5 replicon cells were used as a source of isolating phosphorylated NS5A from a replicon model.

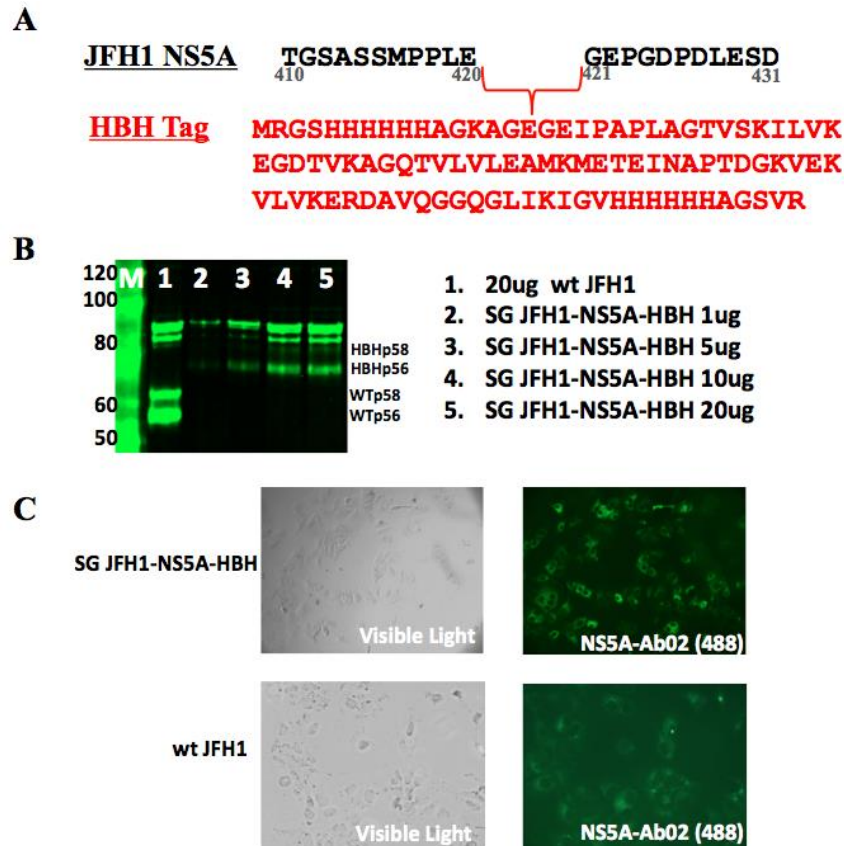


Figure 4. 2. Expression of NS5A-HBH-2a from SG JFH1-NS5A-HBH replicon Huh7.5 cells. **(A)** Schematic of HBH tag insertion into JFH1 NS5A-2a. The HBH tag was inserted utilizing an AbsI restriction site between E420 and G421 in NS5A within SG JFH1. **(B)** Western blot confirmation of NS5A-HBH-2a expression from SG JFH1-NS5A-HBH replicon cell lines. 20ug of protein from wt SG JFH1 (lane 1) and 1, 5, 10 and 20ug of SG JFH1-NS5A-HBH lysates (lanes 2-5) were detected using the NS5A-Ab02 antibody and near infrared detection. Wt NS5A-2a is indicated as wt p56/wt p58 and NS5A-HBH-2a as HBHp56/HBHp58. **(C)** Indirect immunofluorescence of SG JFH1-NS5A-HBH and wt SG JFH1 cells. NS5A-Ab02 was used to detect both wt, and HBH tagged NS5A-2a. The left panel shows cell under visible light, and the right panel shows indirect immunofluorescence detection of NS5A with NS5A-Ab02. Images were obtained with an Axiovert 200M fluorescence microscope (Zeiss) with the 20X objective.

In this case, HBH-tagged NS5A was isolated from the replicon cell model using the dTAP method. Mass spectrometry analysis identified 13 phosphorylation sites with eight being shared in common with the SG WT model with no affinity tag (Table 4.1). No new sites were identified compared to what the original HBH-NS5A protein expressed on its own saw.

As an example of typical phosphopeptide identification, phospho-threonine 164 is presented. Phospho-threonine 164 was detected as a phosphorylated residue within NS5A by each of the three different platforms and a spectrum (image generated in Scaffold Software, Proteome Sciences) is shown in Figure 4.3. Here, a doubly charged peptide of 1286.62 Da was selected and fragmented to produce a spectrum of fragment ions (tandem mass spectrometry spectrum). The peptide was identified as belonging to NS5A-2a with amino acid sequence “FAPTKPFFR” with phosphorylation at the threonine position 164 (T164) (Fig.4.3.A). There is a predominant parent ion species (parent +2H +1 -98), which is consistent with stripping of the phosphate group (H_3PO_4 , 98Da) from the parent ion during collisional induced dissociation (CID). This is a common feature of phosphopeptides detected by CID but causes decreased sequence information due to lack of fragmentation of the parent ion. Nevertheless, adequate sequence information was obtained for this species with six b-ions and seven y-ions detected (Fig.4.3.B). The fine-mapping of T164 as a phosphorylated residue is straightforward as the T+80 (HPO_3) Da ion species was identified in both the b and y-ion series, and peptide contains only a single phosphorylatable residue (T) (Fig 4.3). It should be noted that this peptide contained a missed cleavage at position K6. This was potentially a fortuitous event as cleavage at his site would have resulted in a smaller peptide with the sequence

“FAPTPK” which is just above the 600 Da minimum size window. More importantly, the peptide charge state would likely have been +1 rather than +2. The addition of a phosphate moiety results in a negative charge (even in acidic solution) and, combined with the positive charge from the N-terminus and the NH₃ side-chain on arginine (or lysine), a net charge of +1 results. Typically, when mass spectrometers are used for peptide interrogation, all +1 charged species are excluded from further (tandem) selection and fragmentation as they often represent chemical contaminants. However, due to the internal K, which was not cleaved during trypsin digestion, the peptide has an overall +2 charge and was selected for analysis (Fig.4.3).

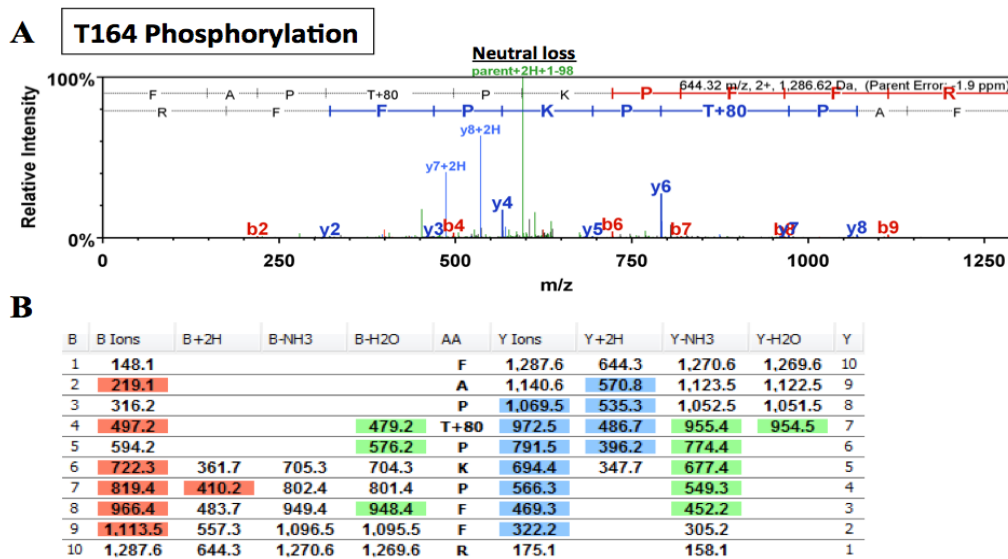


Figure 4. 3. Mass spectrometry spectrum of a peptide identifying phospho-T164 from NS5A peptide produced from dTAP purified HBH-NS5A-2a. **(A)** The mass spectrometry detected ion species are plotted as relative intensity vs. mass/charge (z) ratio. N-terminal (b-ions) are highlighted in red, C-terminal (y-ions) are highlighted in blue with numbers corresponding to the position along the peptide from N- or C- terminus. The m/z value, peptide charge, predicted mass and parent ion error (in ppm) is indicated in the upper left corner. The parent ion neutral loss (parent + 2H + 1-98Da) is indicated. **(B)** Ion fragmentation table b- and y-ions predicted to be present in the peptide spectra are indicated with detected species highlighted in color. Each column represents the anticipated mass of ions in the peptide. 98 Dalton parent ion corresponding to an 80 Dalton HPO₃ moiety and an H₂O molecule referred to as a neutral loss are indicative of a phosphorylation event is pictured in green. The phosphopeptide was incompletely digested by trypsin as evidenced by an internal Lysine (K) residue.

A comparison of the mass spectrometry phosphorylation site mapping from the various sources is depicted in figure 4.4 and the data supporting phosphorylation position site assignment is presented in Appendix 2. Figure 4.4 demonstrates that majority of the phosphoacceptor sites were identified within NS5A Domain 2, followed by Domain 3 and Domain 1. No phosphorylated residues were identified near the NS5A C-terminus due to the lack of protease cleavage sites available and thus the inability to produce appropriately sized peptides for mass spectrometry.

As the NS5A-2a protein is rich in lysines and arginines, the use of additional non-trypsin digestion enzymes was also included in order to more completely interrogate the phosphopeptide sites present. Using GluC provided the exclusive identification of phosphoacceptor sites S401, T410 and S414/S415 and AspN with T210, T213 and S272 from dTAP purified HBH-NS5A-2a samples. Therefore, inclusion of additional proteases can increase the coverage of interesting residues.

The majority of identifications were obtained using HBH-NS5A-2a in combination with the TAP protocol, most likely due to the high amount of protein recovered. Only three phosphopeptides were identified exclusively in the untagged SG JFH1 replicon, and those were peptides containing, “S381/S82”, “S414/S415” and “T410”. Fine mapping of the phosphorylation events was accomplished except the exact phosphorylated residues on peptides “S381/S82”, “S414/S415” could not be unambiguously assigned due to lack of defining ion species (Fig.4.4).

In all, 28 phosphorylated residues were identified from NS5A phosphopeptides of which 26 were mapped to a specific residue. The six previously unambiguously mapped NS5A phosphorylation sites (S146, S222, S225, S235, S238, T348 (303–306)) were confirmed in this thesis and 20 novel residues were identified (Fig.4.4).

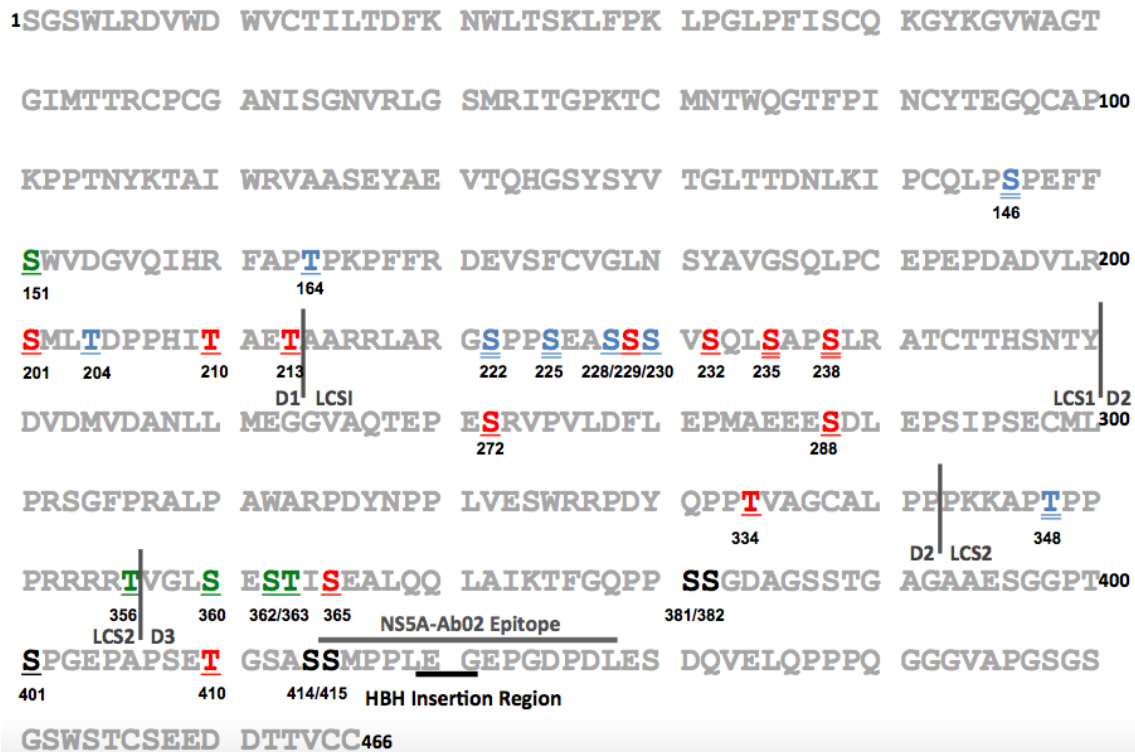


Figure 4. 4. Positively identified phosphoacceptor sites and residues identified on phosphopeptides from NS5A JFH1. Vertical lines separate the three NS5A-2a protein domains (D1, D2 and D3) and two low complexity sequences (LCS1 and LCS2). Serine and threonine residues identified by the search algorithms are bold-faced and colored, residues unequivocally assigned to a single residue are bold faced and underlined. Colors indicate the source material for the identified phosphorylation sites: blue (HBH-NS5A-2a, SG JFH1-NS5A-HBH, and SG JFH1), green (HBH-NS5A-2a, SG JFH1-NS5A-HBH), red (HBH-NS5A-2a) and black (SG JFH1). Previously published sites S146, S222, S225, S235, S238, and T348 (289,303–306) are double underlined.

As highly conserved residues between HCV genotypes may be indicative of the requirement of that particular amino acid, conservation of NS5A-2a identified

phosphoacceptor sites was evaluated using representative sequences from each of the seven HCV genotypes (343,344). Alignments were performed using CLUSTAL Omega 1.2.1 and conservation of the phosphorylated serine and threonine residues was evaluated (Appendix Fig. A1). Identified phosphoacceptor sites conserved in all seven HCV genotypes containing either a serine or threonine as the identified residue were: T204 (except R in 3a, a charge mimic), T210, S225, S229, S230, S232, S235, S414, and S415. Interestingly, T164 and T348, identified here as phosphorylation sites, were only present in JFH1, 2c and J6 strains respectively and T410 was found only in strain JFH1 (Appendix Fig.A1).

4.2.2 Phosphoblatant and mimetic mutations of phosphoacceptor sites in pJFH1

To determine the impact of the identified NS5A phosphoacceptor sites on the HCV life cycle, both alanine, and aspartic acid residues were substituted into the pJFH1 backbone at the sites identified by mass spectrometry and database analysis. The alanine mutations served to ablate phosphorylation, and aspartic acid residues were used to mimic the negative charge of a phosphate molecule. The JFH1 virus used in this study was the unmodified JFH1 strain devoid of any supplemental cell culture-adaptive mutations (151) as opposed to the commonly used Jc1 or J6/JFH1 chimeric strains. This choice was made to maintain the highest level of biological relevance and to avoid producing potentially synergistic mutations, despite JFH1's inferior production of infectious virus. Each RNA species was electroporated into Huh7.5 cells and plated to allow collection of RNA, protein and infectious supernatant from the same electroporated cells (Fig.4.5).

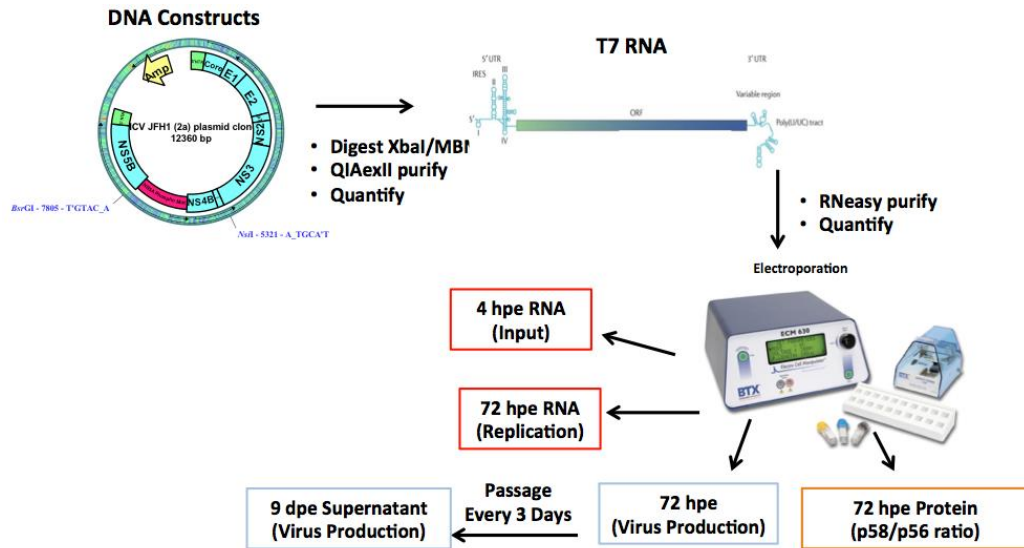


Figure 4. 5. Effects of NS5A-2a phosphomutants on the JFH1 HCV protein synthesis, RNA replication, and virus production. Nucleotide sequences of NS5A-2a serine and threonine residues identified as phosphoacceptor sites by mass spectrometry and database analyses were mutated to a phosphoblatant (alanine) or a phospho-charge mimetic (aspartate) within the HCV pJFH1 DNA plasmid. Following XbaI digestion, *in vitro* T7 RNA was synthesized and RNeasy purified. 5ug of RNA was electroporated into Huh7.5 cells and plated into separate 35 mm dishes. Samples were harvested for RNA (4 and 72 hours post electroporation (hpe), protein (72 hpe) and, following passaging of the cells, infectious supernatant (9 dpe).

4.2.3 Analysis of JFH1 RNA replication efficiency of phosphoblatant (alanine) and phosphomimetic (aspartate) mutation of positively identified NS5A phosphoacceptor sites

JFH1 genomic RNA levels were evaluated by qRT-PCR from samples harvested at four and 72 hours post-electroporation (hpe) (Fig.4.6). A non-replicative JFH1 GND mutant construct with an inactive NS5B polymerase was used as a replication null control. GND also served to define the rate of RNA degradation in the cells by comparing 4 hour “input” RNA to virus genomic RNA levels at 72 hours. Each RNA extract was adjusted to 100ng of total RNA prior to reverse transcription and JFH1 specific primers were employed along with a cellular loading control, GAPDH. JFH1 viral RNA levels were

determined by comparison to a 5-point log dilution standard of wt JFH1 RNA, and these values were further normalized to GAPDH levels. It is worthwhile noting that only very minor differences in the GAPDH values were seen between samples in any given experiment suggesting that the initial 100ng spectrophotometry values were essentially adequate for normalization (data not shown). However, the inclusion of this control also acted as general RNA quality control that could identify poor quality samples. JFH1 viral RNA fold change was determined by comparing the 72-hour RNA level to the 4-hour “input” RNA level then comparing to the values from wt JFH1 genome replication. Each qRT-PCR experiment incorporated duplicate wt JFH1 RNA species for each experiment. In this study, wt replication levels did not vary by more than 3-fold overall with respect to replicative capacity (comparing 4hpe to 72hpe values).

Most of the phosphoablatant or mimetic mutations produced phenotypes similar to wt (Fig.4.6) and none replicated with a greater capacity than wt JFH1 virus. The mutants that did not exhibit wt like replication could be classified as weak (3-10 fold less RNA levels at 72hpe/4hpe compared to wt), very weak (10-100 fold less RNA levels 72hpe compared to 4hpe) and extreme (>100 fold less RNA levels 72hpe compared to 4hpe). Mutant S229A showed the most severe decline in RNA at the 72 h time point, comparable to the GND mutant, which is RNA polymerase deficient. T210D, S229D, and S235A mutations displayed the “very weak” replication level phenotype (Fig.4.6.A&B). These mutants were unable to increase the RNA levels above the 4hpe input by 72 hpe but the RNA levels at 72 hpe were not as severely depressed as for S229A or GND. If RNA replication is occurring it is at very poor efficiency. Alternatively (or in

combination), RNA turnover may be adversely affected so that “input” RNA is being protected to a certain extent. Other studies have shown that mutations at these sites also adversely affect HCV replication (284,289,299,304,305). Several of the phosphomutants were hindered in their replicative capacity and are grouped into the “weak replication” category. These include T204D, T210A, S225D, S232A/D, S235D, S238A/D, T334A/D and T363A/D (Fig.4.6.). Here, replication showed a less than 10-fold increase in the amount of RNA compared to 72 hpe and suggests less than optimal replication levels for these mutants. T204D and T334D mutations had not been previously evaluated. An important caveat to this observation is that some of the mutants exhibited higher than wt input RNA levels at 4hpe (S232D, S235D and S238A/D). If a maximum “ceiling” exists for viral replication in these experiments, it could make the relative increase appear smaller than it could have been.

S222D has been suggested by Lemay et al., 2013 to be inhibited for replication capacity (303) but the results presented in this thesis are consistent with other reports suggesting that it replicates to wt levels (289,299,304). Mutant S229A’s extreme RNA replication phenotype was partially reversed with mutant S229D (now replicating like a “very weak” mutant phenotype). Mutant S235D likewise “rescued” the S235A phenotype to a weak RNA replication level. Mutant T210D (very weak phenotype) was rescued to a weak level with mutant T210A (Fig.4.6). Although additional experiments would need to be performed to determine if the altered phenotypes are due to changes in NS5A stability, localization or PPIs, the data points to the D1 and D2 domains as having the greatest influence relating phosphorylation to replication.

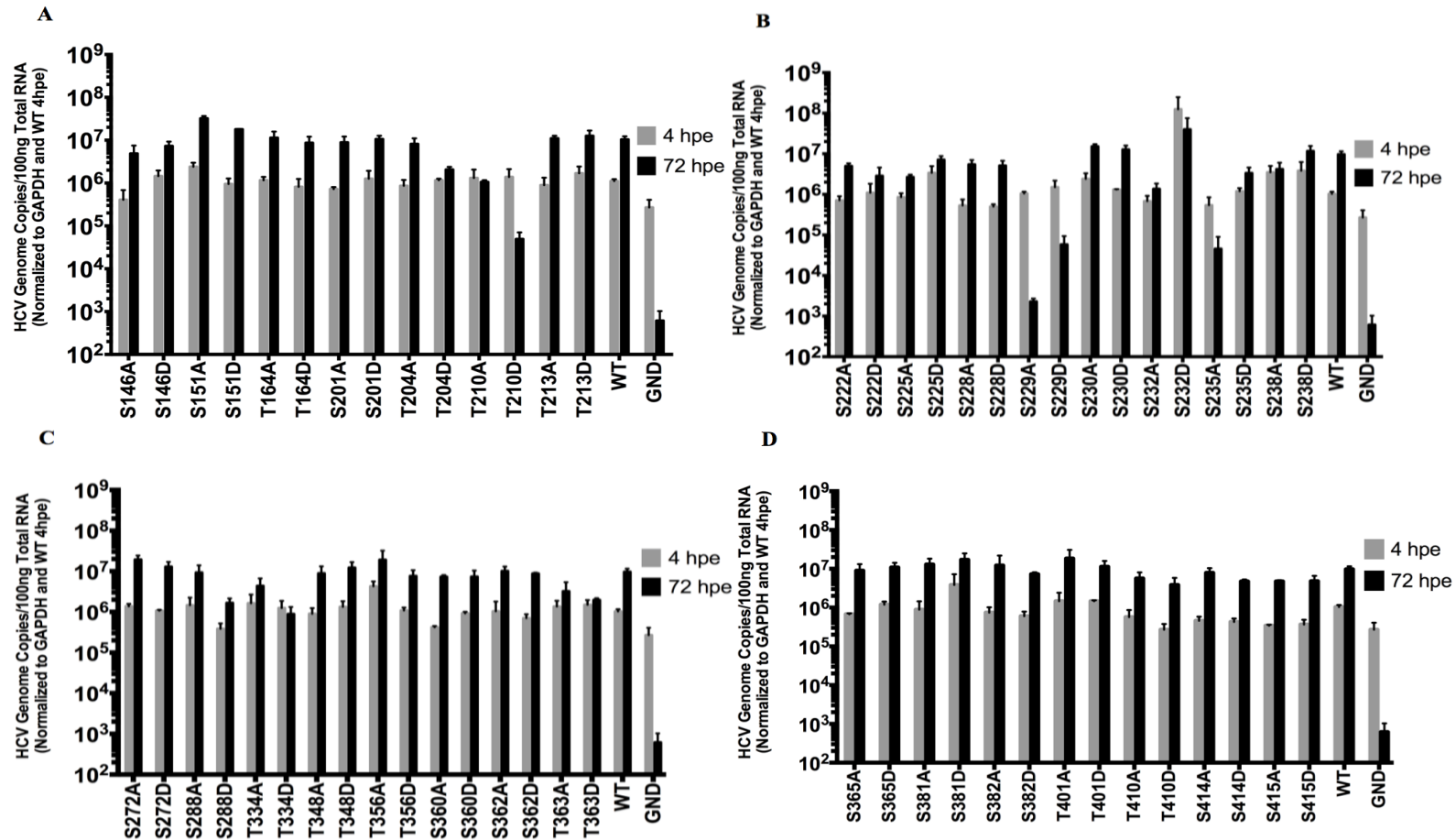


Figure 4. 6. Effects of mutating sequences of phosphoacceptor sites in HCV JFH1 NS5A-2a protein identified through mass spectrometry on RNA genome replication. Positively identified phosphoacceptor sites were mutated to either alanine (phosphoblatant) or aspartic acid (phosphomimetic) in a pJFH1 plasmid by site-directed mutagenesis. JFH1 wt and GND (non-replicative with a mutant NS5B polymerase) viruses were utilized as positive and negative controls. All plasmid constructs were subjected to T7 RNA synthesis, and 5ug of RNA was electroporated into Huh7.5 cells. Total cellular RNA was isolated at four (gray bars), and 72 hpe (black bars) to represent input RNA and replicated genome RNA respectively. JFH1 RNA and cell control GAPDH levels were determined by qRT-PCR. Data for each time point was normalized to GAPDH and then to four hpe wt input values. Results represent the mean \pm standard error of the mean (SEM) of a minimum of two independent electroporation experiments. **(A)** Normalized HCV JFH1 genome abundance of the serine-alanine and serine-aspartic acid mutations of positively identified phosphoacceptor sites of NS5A D1 **(B)** LCSII **(C)** D2/LCSI/N-terminus of D3 **(D)** C-terminus of D3 of JFH1-NS5A-2a.

4.2.4 Impact of NS5A phosphoacceptor site mutations on the abundance and ratio of basally and hyperphosphorylated NS5A protein

NS5A migrates as a doublet on SDS-PAGE gels with the faster migrating, basally phosphorylated band referred to as “p56” and the slower migrating hyperphosphorylated form referred to as “p58” (97). Although NS5A from JFH1 has additional sequence near the C-terminus making it a larger protein that migrates at 63 and 65kDA, the terms p56 and p58 are still used to refer to the two phospho-proteoforms (151). Earlier studies described in this thesis used chemiluminescence to evaluate Western blots. In order to improve quantitative accuracy, subsequent blots were assessed using near infrared detection quantitation (Li-Cor Biosciences).

To evaluate the quality of quantification on this platform, serial dilutions of a 72hpe wt JFH1 protein sample were applied as a 2-fold serial dilution to a Western blot and probed with antibody NS5A-Ab02 (Fig.4.7.A). The linearity of the NS5A-Ab02 antibody signal (r^2) was 0.997 when the signal from both p56 and p58 bands were evaluated (Fig.4.7.B). The Western blot in figure 3.7.A containing the serially diluted JFH1 protein was also used to determine whether the p58/p56 ratio of the NS5A-2a protein is affected by the percent of NS5A-2a protein occupying a total protein lysate (Fig.4.7.C). The p58/p56 ratio generated by the serially diluted JFH1 protein lysate showed less than 15% difference over a 5-fold serial dilution (Fig.4.7.C).

Next, NS5A-2a phospho-proteoform ratios were calculated from extracts of SG wt JFH1 Huh7.5 cells with different monolayer confluency (Fig.4.8). This was done to determine

if the density of a cellular monolayer significantly affected the NS5A-2a p58/p56 ratio. In figure 4.8.A NS5A-2a was detected from total protein extracts of SG JFH1 Huh7.5 cells at 60, 80,100 and >100% confluency (lanes 2-5). When quantified, the produced p58/p56 ratios from the different percent monolayers showed a decrease in the p56/58 proteoform ratio from 0.58 to 0.42 as the cell confluency went from 60% to >100%. Total NS5A-2a protein amounts also increased as the confluency increased (Fig.3.8.B). As such, the NS5A-2a phospho-proteoform ratio is moderately affected by cell confluency, and therefore all experiments were designed to result in plating densities that were similar throughout all experiments.

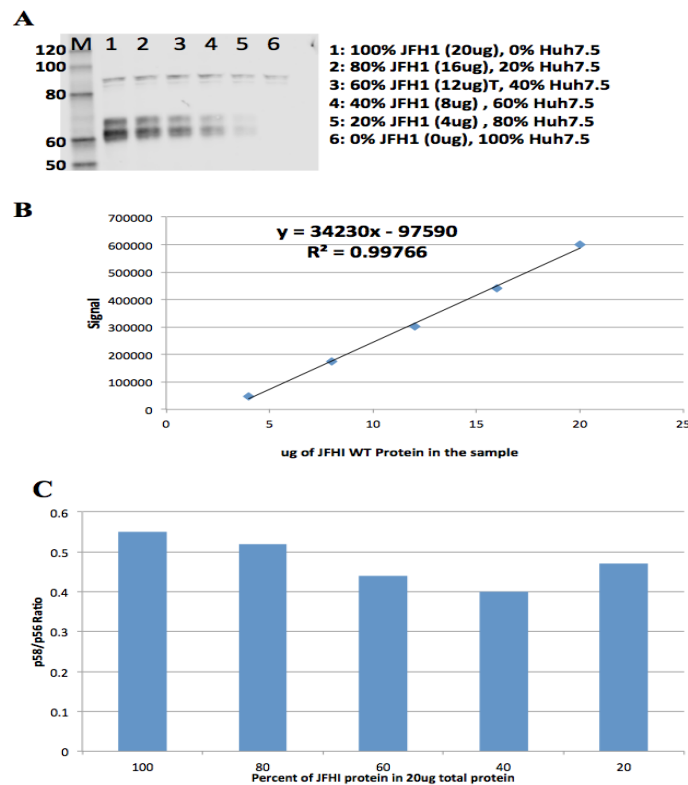


Figure 4. 7. Evaluation of NS5A antibody NS5A-Ab02 for quantitative detection of NS5A-2a by Western blot. **(A)** Western blot of total JFH1 electroporated Huh 7.5 cell protein extract (72 hpe) 2-fold serially diluted: 20-2ug. NS5A-2a was visualized using NS5A-Ab02 antibody and near infrared detection (Li-Cor Biosciences). **(B)** Plot of the relative signal intensity of detected NS5A protein versus total protein loaded. **(C)** p58/p56 NS5A phospho-proteoform signal ratios from serially 2-fold diluted JFH1 total protein lysate.

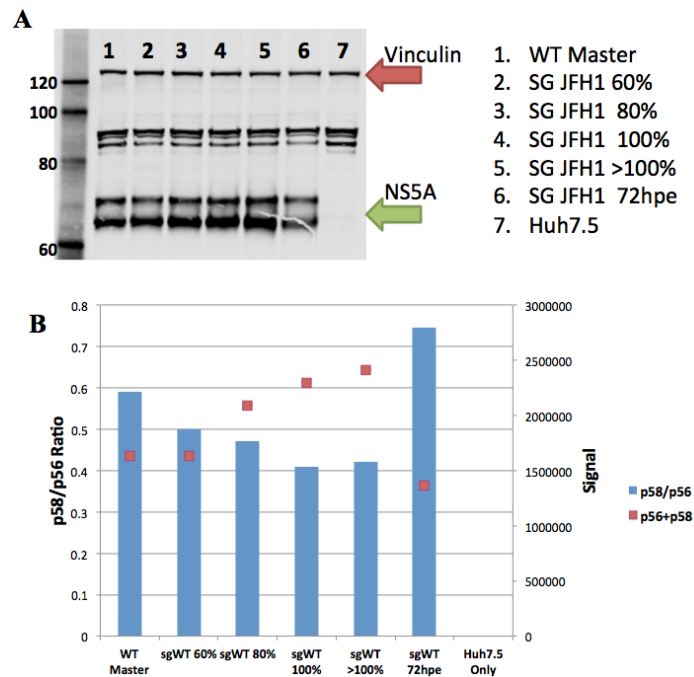


Figure 4. 8. Effects of cell confluency on NS5A-2a p58/p56 phospho-proteoform signal ratio in SG wt JFH1 Huh7.5 replicon cells. **(A)** Western blots of SG wt JFH1 total protein harvested at different cell confluencies. A wt master mix was created from pooled wt JFH1 total protein lysates to ensure consistency of the p58/p56 ratio between separate Western blots (lane 1). This Master sample was run on every Western blot where NS5A quantification was performed. Cell confluencies at the time of harvest were: 60% (lane 2), 80% (lane 3), 100% (lane 4) and >100% (lane 5), 72 hpe with 5ug of transcribed RNA (lane 6) and a Huh7.5 cells only control (lane 7). NS5A was visualized using the NS5A-Ab02 antibody (green arrow), and an anti-Vinculin antibody detected Vinculin (red arrow) as a load control in near infrared detection. **(B)** Quantification of the p58/p56 ratio from the Western blot in (A). NS5A signal intensity data was extracted using Image Studio Lite software (LI-COR Biosciences) and plotted against the cell confluency. The p58/p56 ratios are presented as blue bars, and total NS5A signals (p58+p56) are portrayed as red squares.

To determine the effects of the NS5A phosphoacceptor site mutations on the expression of each NS5A phospho-proteoform, total protein was collected from RNA electroporated Huh7.5 cells at 72hpe and subjected to Western blot analysis using NS5A-Ab02. The majority of phosphomutants displayed p58/p56 ratios within 20% of the mean wt ratio of 0.61, within the experimental variance noted earlier (Fig.4.9). NS5A protein from mutants S229A and S229D were below detectable levels and could not be quantified

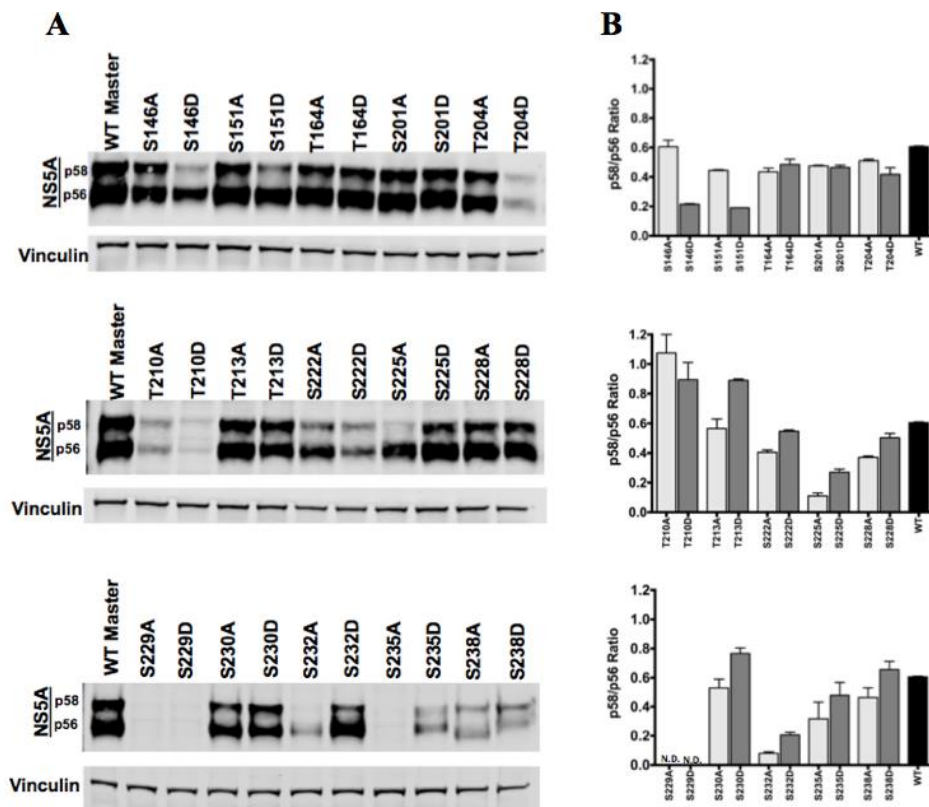
consistent with their extreme (SS229A) and very weak (S229D) RNA replication phenotypes discussed earlier (section 4.2.3). Interestingly, T210D which was also categorized as a very weak RNA replication mutant did have enough NS5A protein to allow quantification and although it was significantly reduced in total NS5A amount compared to wt NS5A levels. The p58/p56 ratio for this mutant was much higher than for wt at 1.01.

S151D, S225A, and S232A exhibited the lowest p58/p56 ratios of 0.19, 0.11 and 0.08 respectively (Fig.4.9). S151A expressed a closer to wt ratio of 0.44 indicating that phosphorylation at S151 may be detrimental to the production of p58 (Fig.4.9).

Interestingly, S225A and S232A were not fully rescued to wt level ratios by their phosphomimetic counterparts with S225D and S232D producing mean ratios of 0.28 and 0.24 (Fig.4.9). This suggests that the aspartic acid mimic at these residues may aid in charge compensation, but the full phosphate molecule may be required for optimal expression or that authentic phosphorylation at these sites are required to hinder migration in SDS-PAGE. This may also suggest that mutation of S225 and S232 has a destabilizing effect on the NS5A protein, a feature that was not further explored.

Several phosphomutants expressed moderately lower levels of p58 and include: S146D, S228A, S288D, S235A and T348D with mean p58/p56 ratios of 0.21, 0.37, 0.29, 0.35 and 0.35 respectively (Fig.4.9). The reduced abundance of p58 observed with phosphomutants S225A, S232A, S225D, S232D, S146D, S235A in this study is consistent with previous observations and is likely due to reduced replication capacity

(289,299,304,345). S235A phospho-proteoform abundance has been inconsistent between studies where previous investigations have reported no detectable protein (289,305), no discernable p58 expression (306) or, as was observed in this study, a lower p58/p56 ratio (299). Only three of the phosphomutants assessed produced decidedly more p58 than wt and included: T213D and T210A/D with mean p58/p56 ratios of 0.89, 1.08, 1.01, respectively (Fig.4.9). Several groups have reported the phosphomimetic mutations S232D, S235D and S238D result in the impeded mobility of p56 and thus an apparent increase in molecular weight was observed (289,299,304). The results presented here also indicate reduced mobility of the p56 species compared to the wt controls (Fig.4.9).



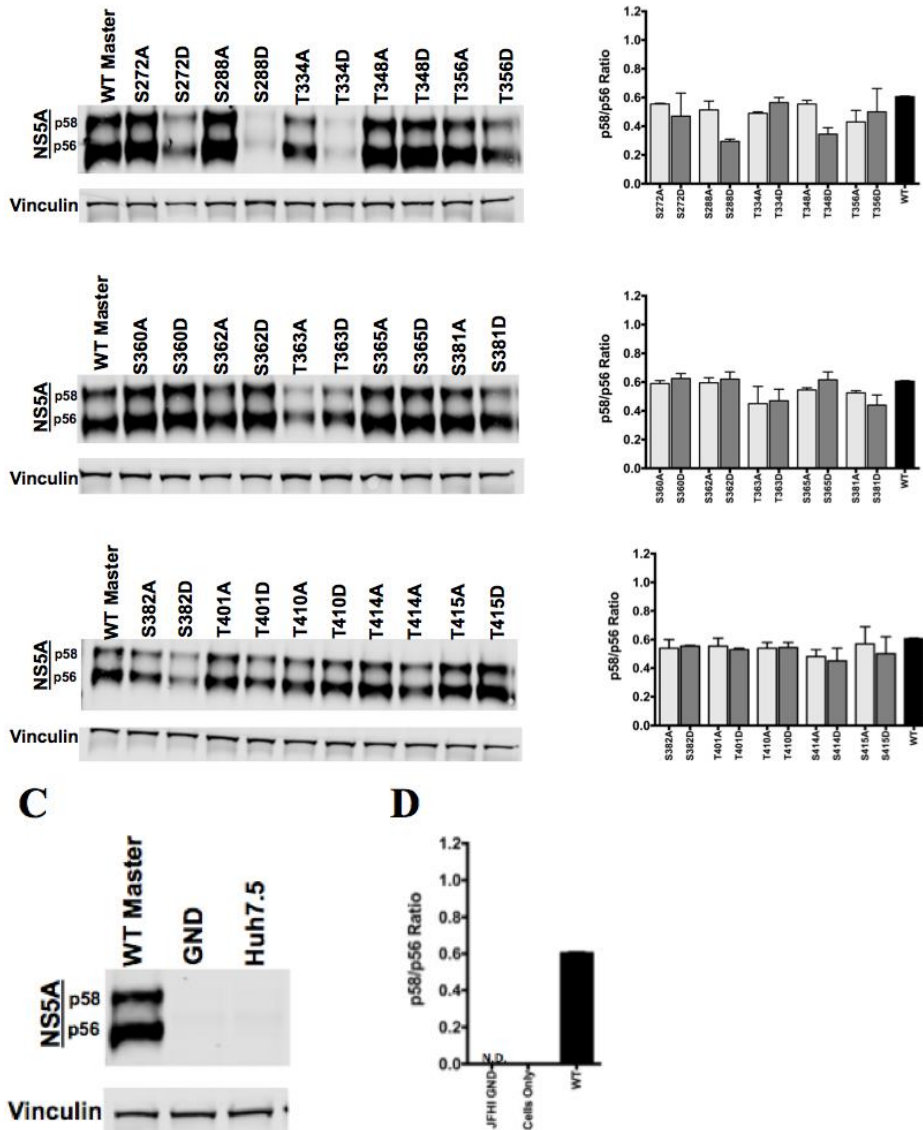


Figure 4.9. Impact of the phosphoblattant and phosphomimetic mutations of NS5A-2a on the abundance of the p58 and p56 phospho-proteoforms. (A) NS5A phosphomutants were evaluated by Western blot and near-infrared fluorescence detection. NS5A was detected using the NS5A-Ab02 antibody, and an anti-vinculin antibody detected Vinculin as a cellular load control. A wt master sample was included on each Western blot to ensure consistency between separate Western blots. (B) Quantification of the p58/p56 ratio from NS5A phosphomutants. Signal intensities produced by NS5A-2a phospho-proteoforms, p56, and p58, were quantified using Image Studio Lite software to determine p58/p56 ratios. Phosphoablattant mutations are displayed with white bars, phosphomimetic mutations are gray bars, and the wt levels are presented as black bars. N.D. indicates not determined where protein levels were below the minimum detection capabilities. (C) A replication defective virus (GND) and a Huh7.5 mock electroporation were utilized as negative controls. (D) Quantifications of (C). Data presented are the mean p58/p56 ratios \pm SEM obtained from a minimum of two independent experiments.

4.2.5 Determining the effects of phosphoablatant (alanine) and phosphomimetic (aspartate) mutations of positively identified phosphoacceptor sites on JFH1 infectious virus production.

The effects of the NS5A phosphoacceptor site mutations on infectious virus production were measured from Huh7.5 cell culture supernatants collected nine days after electroporation of 5ug of JFH1 RNA. Electroporated Huh7.5 cells were split every three days and seeded according to their confluency as to achieve near 100% confluency 72 hours later. At nine days post electroporation (dpe) infectious cell supernatants were serially diluted and plated onto naïve Huh7.5 cells and four days post infection were visualized using immunofluorescence. Infectious titers were based on the presence of positive wells, and TCID₅₀/ml values were calculated using the Reed and Muench method revised by Lindenbach, 2009 (317). Viral titer determination assays are known to produce inherent variability in repeat experiments (346). To combat this TCID₅₀/ml values were normalized to the mean wt TCID₅₀/ml value obtained from each individual electroporation experiment.

As was seen with the RNA and protein data, the majority of the phosphomutants produced titers akin to wt and with less than a two-fold change (Fig.4.10). Four of the phosphomutants were unable to produce detectable infectious virus nine days post electroporation (dpe) and included T210D, S229A/D and S235A (Fig.4.10.A, B). While T210D has not been previously assessed, the titer results obtained for S229A/D and S235A are in agreement with previous studies (289,305,345). Several phosphomutants produced less than three-fold the infectious virus of wt and included: S201D, T204D,

T210A and S225A with 4.7, 4.3, 3.2 and 3.1 fold reductions, respectively (Fig.4.10.A, B). Moderate reductions in viral titer between two and three fold from wt were observed in phosphomutants T164D, S222A, S230A/D, S238D, T334D and S381D with reductions of 2.3, 2.6, 2.7, 2.0, 2.7, 2.7 and 2.4 fold, respectively (Fig.4.10). While the majority of the phosphoacceptor site mutations have not had their titers previously evaluated, a reduction in the released infectious virus of the S225A is consistent with preceding reports (289,304,345). Several of the phosphomutants produced more infectious virus than wt including S151A, S151D, T213A, S228D, S232D, S238A, S382A and S415D with 1.86, 1.67, 1.33, 1.40, 1.25, 1.18, 1.62 and 1.26 fold increases above wt (Fig.4.10).

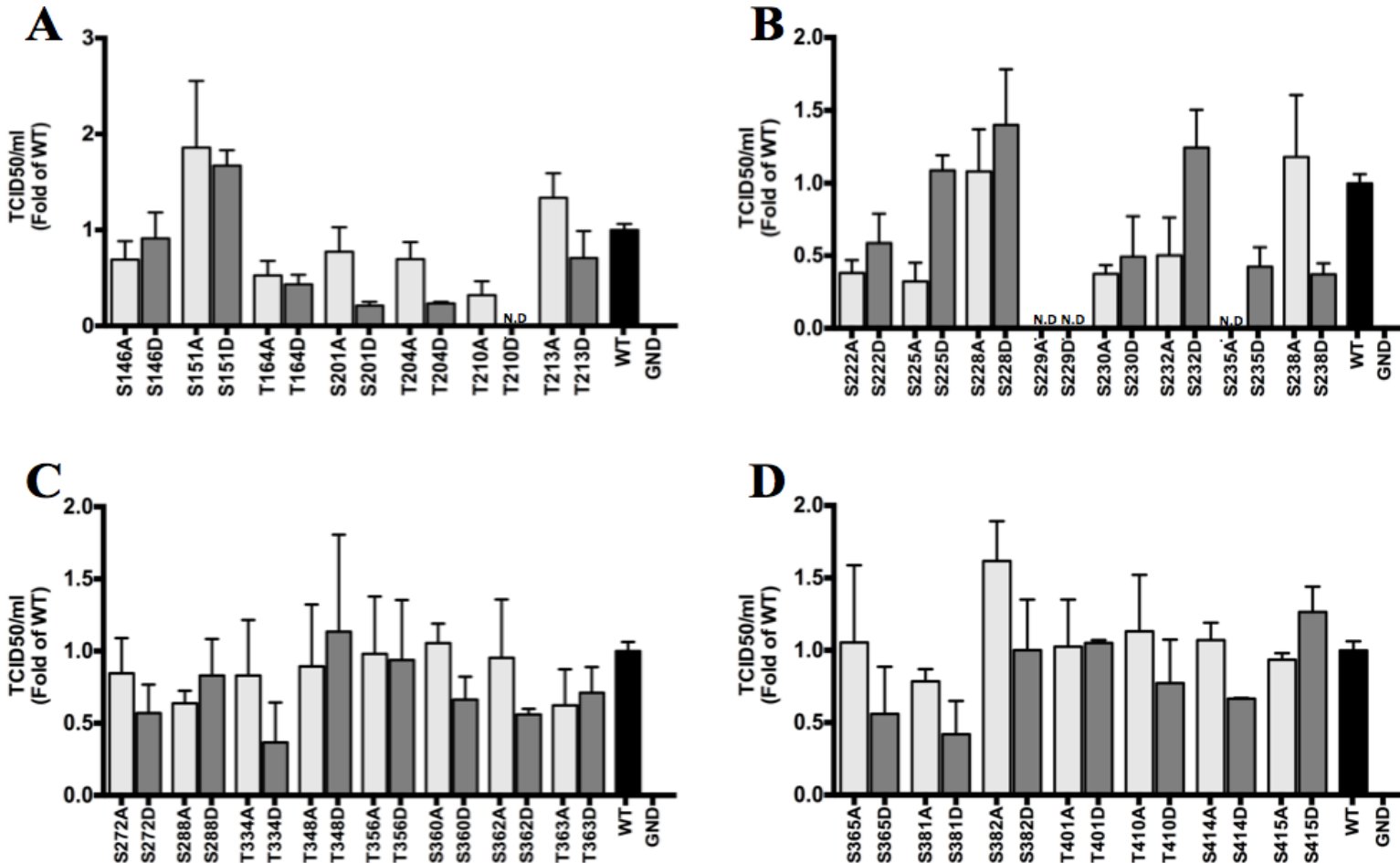


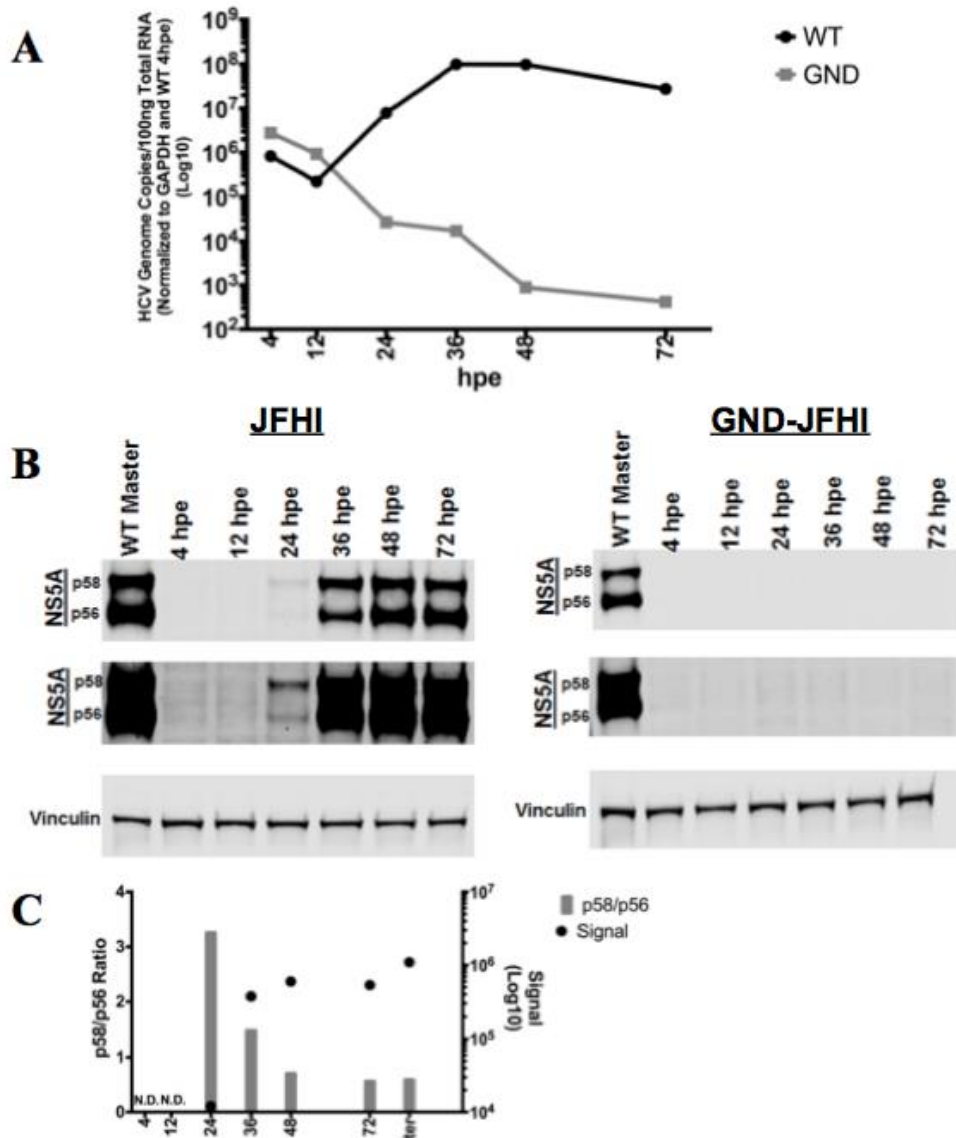
Figure 4. 10. NS5A phosphoacceptor site mutation effects on HCV JFH1 released infectious virus. *In vitro* synthesized RNA from mutant virus templates were electroporated into Huh 7.5 cells and cells were passaged every 72 hours based on cell confluency until cell supernatants were collected nine dpe. Five-fold serial dilutions of clarified infectious supernatant were plated onto naïve Huh7.5 cells and visualized by immunofluorescence with the NS5A-Ab02 antibody. TCID₅₀/ml values were calculated using the Lindenbach, 2009 revised Reed and Muench calculator (317) and expressed as a ratio of the mean TCID₅₀/ml values obtained from two independent wt TCID₅₀/ml values with each experiment. The GND mutant served as a nonviable negative control. Infectious titers were determined in at least two separate experiments and presented as mean fold changes ± SEM. N.D. indicates levels were below detection. (A) Normalized HCV JFH1 genome abundance of the serine-alanine and serine-aspartic acid mutations of positively identified phosphoacceptor sites of NS5A D1 (B) LCSII (C) D2/LCSII/N-terminus of D3 (D) C-terminus of D3 of JFH1-NS5A-2a.

4.2.6 NS5A from electroporated JFH1 is predominately hyperphosphorylated until 48 hpe

Most of the current understanding regarding NS5A biogenesis was obtained from studies using the HCV 1b genotype. It was concluded that NS5A is liberated from the HCV polyprotein, becomes basally phosphorylated creating the p56 form after which, hyperphosphorylation generates the p58 form (188,276,277). To track the development of NS5A-2a phospho-proteoforms over time, JFH1 RNA was electroporated into Huh7.5 cells, and total cellular RNA and proteins were obtained 4, 12, 24, 36, 48 and 72 hpe (Fig.4.11). JFH1 RNA samples were analyzed by qRT-PCR. JFH1 wt samples showed a continuous increase in genome copy number followed by a dip at 12 hpe. Maximum RNA quantity was seen at 36 and 48 hpe (Fig.4.11.A). As expected the non-replicative GND mutant showed a decrease in virus RNA over the time course (Fig.4.11.A).

Western blot analysis of JFH1 harvested protein samples showed no detectable NS5A protein until 24 hpe, at which point the p58/p56 ratio was 3.3 (Fig.4.11.B/C). Higher p58 levels were also sustained at the 36 hpe time-point with a p58/p56 ratio of 1.5 (Fig.4.11.B/C). At 48 hpe the p58/p56 ratio of wt NS5A was reversed, and p56 became the more abundant phospho-proteoform with a mean ratio of 0.71 followed by a ratio of 0.58 at 72hpe (Fig.4.11.B/C). GND protein data was not quantified as the protein signal was below the limits of detection at every time point. This same trend was seen in both the SG JFH1 replicon, and the SG JFH1-NS5A-HBH replicon (Fig.4.11.D) with the high p58/p56 ratio maintained at 24 hpe for SG JFH1 (Fig.4.11.D/E) but delayed until 48 hpe for the SG JFH1-NS5A-HBH (Fig.4.11.D/F). The delay for the HBH tagged replicon

would be consistent with its delayed kinetics of RNA replication in general compared to wt JFH1 (data not shown).



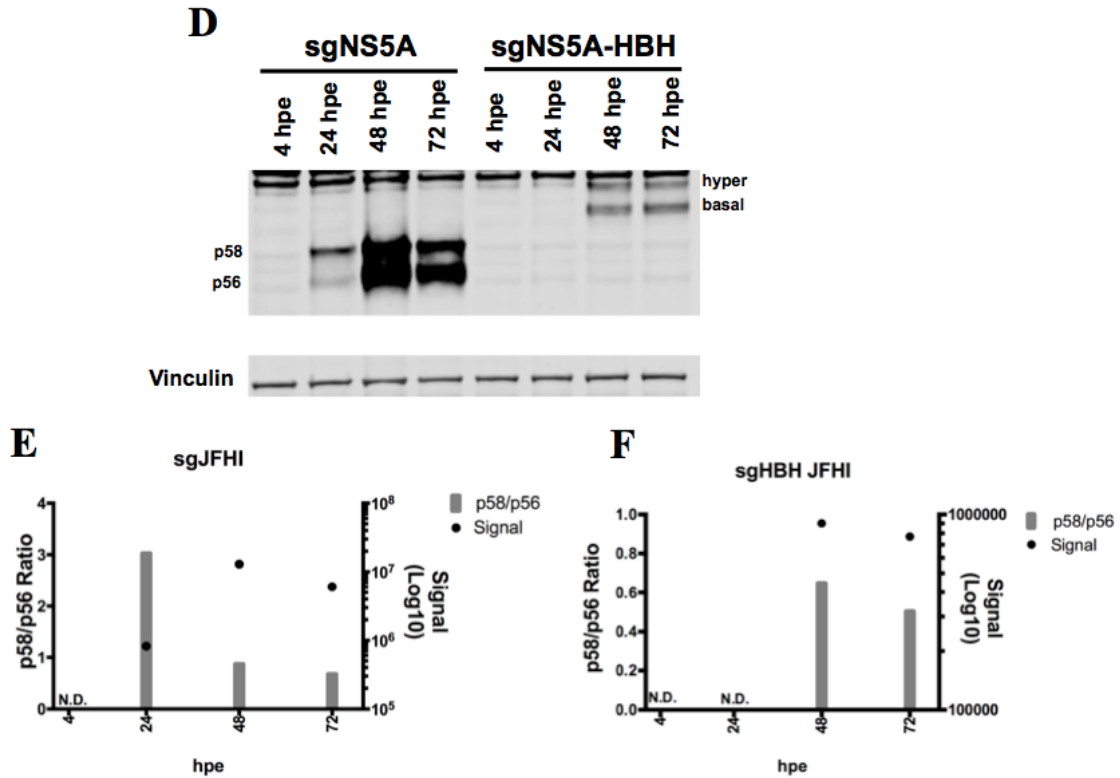


Figure 4. 11. Analysis of NS5A phospho-proteforms early time-points post electroporation of JFH1 RNA. JFH1 wt RNA was electroporated into Huh7.5 cells, and RNA and protein were isolated at the indicated time-points post electroporation. GND was used as a non-replicative negative control. **(A)** JFH1 wt and JFH1-GND genome copy numbers at 4, 24, 48 and 72 hpe. Viral RNA levels were determined by reverse transcription qRT-PCR and normalized to the housekeeping transcript GAPDH. **(B)** NS5A-2a from JFH1 and JFH1-GND evaluated by Western blot and near infrared fluorescence over 72 hpe. NS5A was detected using NS5A-Ab02 antibody, and an anti-vinculin antibody detected Vinculin as a cellular load control. **(C)** Quantification of the p58/p56 ratio and total NS5A signal intensity from JFH1 over time. Signal intensities produced by NS5A-2a phospho-proteforms, p56, and p58, were quantified using Image Studio Lite software and p58/p56 ratios were obtained. The p58/p56 ratio is displayed on the left y-axis, and the total NS5A-2a protein signal (p58+p56) is on the right y-axis. N.D. indicates levels below detection limits. **(D)** SG JFH1 and SG JFH1-NS5A-HBH NS5A phospho-proteform abundance post electroporation. Western blots were performed where NS5A was detected by the NS5A-Ab02 antibody, and anti-vinculin was used to detect Vinculin as a cellular load in near infrared imaging. **(E, F)** Quantification of NS5A phospho-proteform ratios and the total signal from SG JFH1 and SG JFH1-NS5A-HBH NS5A. The p58/p56 ratio is displayed on the left y-axis, and the total NS5A-2a protein signal (p58+p56) is on the right y-axis. N.D. indicates levels below detection limits.

4.2.7 Reduction of p58 in SG JFH1 overtime

Several groups have suggested that continued passaging of HCV replicons results in a decrease in p58 phospho-proteoform abundance (141,282,304). Based on these observations, Western blot analysis was performed on the SG JFH1 Huh7.5 cell lines produced and were carried longer term. Isolation of protein from cells three days post electroporation and from cells following ten weeks of passage was performed (Fig.4.12.A). Compared to short-term wt NS5A that produced a p58/p56 ratio of 0.592, NS5A from the ten-week-old SG JFH1 Huh7.5 cells produced a slightly lower ratio of 0.499. (Fig.4.12.B).

Although a 16% reduction in phospho-proteoform ratios is quite small, it is possible that passaging the SG JFH1 cells for a longer period would result in further loss of p58. For example, Ross-Thriepland and Harris. 2014, observed a 40% drop in the p58/p56 ratio after passaging SG JFH1 Huh-7 cells for 20 weeks (304). It could also be that confluencies may have partly confounded the previous studies as we have demonstrated that confluency affects the interpretation of p58/p56 ratios. To evaluate if any sequence changes had occurred in replicon form the 10-week old SG JFH1 cells, DNA sequencing was performed over the NS5A ORF. No changes in nucleotide sequence were detected (data not shown) and also argues that over the 10-week period of cell passage, no changes to NS5A (particularly at the phosphorylation sites) occurs.

It has also been suggested that kinase(s) specific for producing p58 may have reduced phosphorylation capacity in aged replicon cells. To test this possibility, wt SG replicons

were reintroduced into established 10-week-old SG JFH1-NS5A-HBH cell lines. HBH-NS5A is 11 kDa larger than wt NS5A, and therefore the HBH-tagged NS5A is distinct from wt NS5A-2a on a Western blot (Fig.4.13). The wt NS5A phospho-proteoform ratios produced by introduction 5ug of wt full-length JFH1 and SG JFH1 RNA into the SG JFH1-NS5A-HBH Huh7.5 cells at 24 hpe were 1.4 and 1.7, respectively (Fig.4.13.B/C). The NS5A phospho-proteoform ratios were slightly reduced when compared NS5A p58/p56 ratios produced by electroporation of the wt constructs into naïve Huh7.5 cells (3.0 and 3.3, Fig.4.11.E). However, at 72-hpe wt NS5A from full-length JFH1 and SG JFH1 provided ratios of 0.66 and 0.74, respectively (Fig.4.13.B/C). The 72hpe ratios are closer to the consistently observed 0.60 phospho-proteoform produced by NS5A at 72hpe from naïve Huh7.5 cells (Fig.4.11.E). This indicates that at least over the 10-week period during which cells were passaged, p58 phosphorylation capacities are not affected. It should be further noted that replicon cells used for any integral experiments were never passaged for longer than the 10-week period.

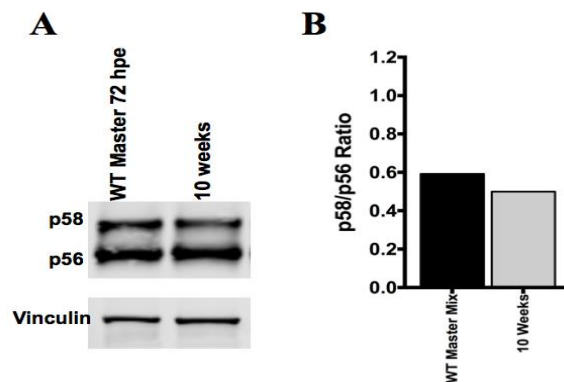


Figure 4. 12. NS5A-2a p58/p56 ratio in SG JFH1 replicons after extended passage in cell culture. (A)Western blot analysis of NS5A-2a from ten-week-old SG JFH1. Total protein was isolated from SG JFH1 replicon Huh7.5 cell lines 72 hpe and after ten weeks of cell culture passage. The NS5A-Ab02 antibody was used for NS5A-2a detection, and an anti-Vinculin antibody detected Vinculin as a cellular load control in near infrared detection. (B) Quantification of the p58/p56 ratio (A). Signal intensities produced by NS5A-2a phospho-proteoforms, p56, and p58, were quantified using Image Studio Lite software and p58/p56 ratios were obtained.

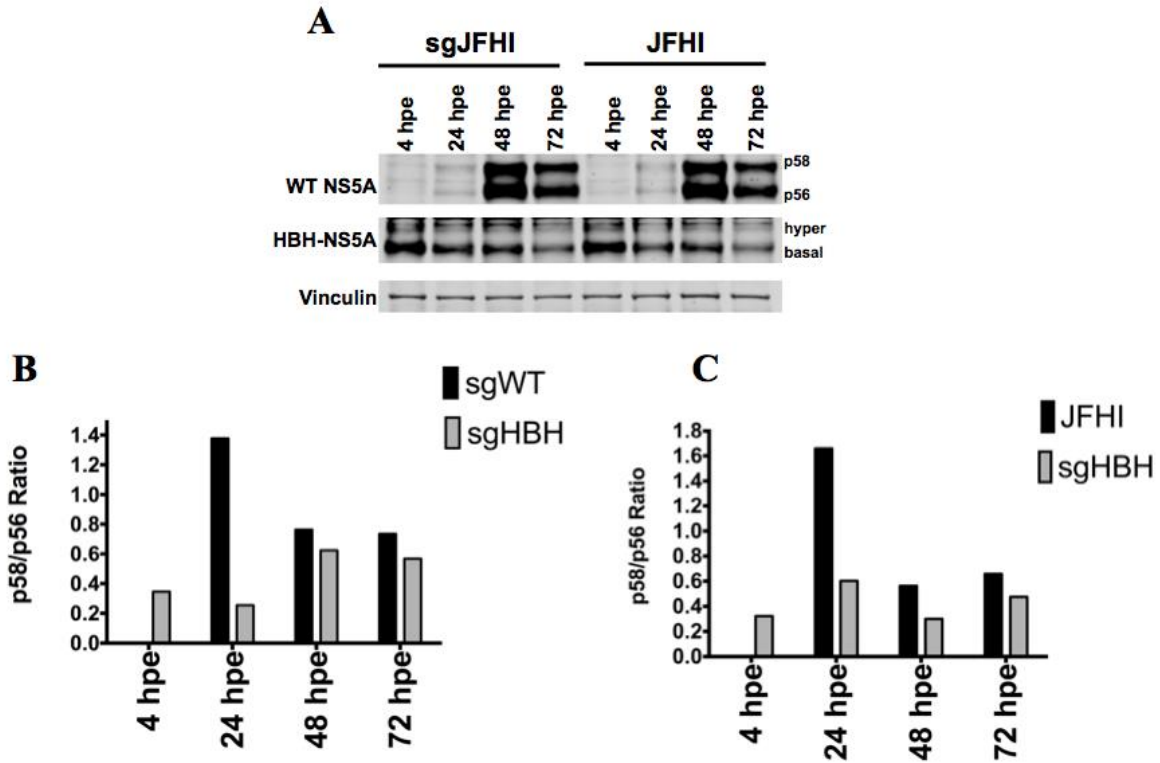


Figure 4.13. Introduction of wt SG JFH1 and JFH1 into SG JFH1-NS5A-HBH Huh7.5 cells. (A) Western blots of protein samples from electroporated SG JFH1 (left) and full-length JFH1 into SG JFH1-NS5A-HBH Huh7.5 cells. Total protein was harvested 4, 24, 48, 72 hpe. NS5A was detected with the NS5A-Ab02, and an anti-vinculin antibody detected Vinculin as a cellular load control. HBH-NS5A is approximately 11 kDa larger than wt NS5A and indicated as hyper and basal. NS5A wt is indicated as p58 and p56. (B) Quantification of NS5A phospho-proteoforms from electroporated SG JFH1 RNA into SG JFH1-NS5A-HBH Huh 7.5 cells. (C) Quantification of NS5A phospho-proteoforms from electroporated of full-length JFH1 RNA into SG JFH1-NS5A-HBH Huh 7.5 cells. Signal intensities produced by NS5A-2a phospho-proteoforms, p56, and p58, were quantified using Image Studio Lite software and p58/p56 ratios were obtained.

4.3 Summary

To extend the mapping of NS5A phosphorylation sites, NS5A-2a was isolated from both ectopically expressed NS5A and SG JFH1 replicons. Mass spectrometry and database searching identified phosphorylation sites within the NS5A-2a protein. In addition to previously identified S146, S222, S225, S235, S238, and T348 in NS5A (289,303–306), 20 new residues were additionally mapped. Phosphopeptides containing “S381/S382”

and “S414/S415” and T410 were identified exclusively from the unmodified SG JFH1 replicon. Relevant serine and threonine NS5A residues were mutated to either an alanine (phosphoablatant) or an aspartic acid (phosphomimetic) residue in the context of a JFH1 infectious virus clone. Phosphomutants were assessed for their effects on JFH1 genome replication, infectious titres, and NS5A p56/p58 ratios. While mutating most of NS5A phosphoacceptor sites did not affect virus genome replication and viral titre, T204D, T210A, T210D, S225D, S232A/D, S235D, S238A/D, T334A/D and T363A/D replicated weakly, T210D, S229D and S235A very weakly and S229A extremely weakly. Several phosphomutants produced NS5A phospho-proteoform ratios decidedly different than wt JFH1 with S151D, S225A and S232A producing the lowest and T213D and T210A/D producing the highest. T210D, S229A, S229D, and S235A JFH1 mutations were unable to produce infectious virus. Furthermore, NS5A was found to be predominantly hyperphosphorylated at early time-points post-electroporation but reaches a consistent, steady phospho-proteoform ratio at 72 hpe. This study reveals the highly phosphorylated nature of the NS5A protein and the impact of individual phosphorylated residues on the HCV life cycle.

Chapter 5: Discussion

5.1 Identification of host cell – hepatitis C virus NS5A protein-protein interactions (PPIs) by tandem affinity purification and mass spectrometry/database searching

Hepatitis C virus infection often leads to chronic disease that can result in severe liver damage including steatosis, fibrosis, cirrhosis, HCC, and death (2). Newly developed HCV direct acting antivirals (DAAs) can achieve SVR rates of 95% in infected individuals (56). However, accessibility and drug resistance remain points of concern.

The HCV NS5A protein directly regulates the HCV lifecycle and modulates the host cell to create an environment conducive to viral propagation (207,210). However, the exact molecular mechanisms dictating NS5A function remain elusive. This study used protein purification techniques combined with mass spectrometry/database searching to identify host cell-NS5A-2a PPIs. Additionally, a similar technical platform was used to identify and characterize phosphorylated residues within the NS5A-2a protein.

5.1.1 Generation of stable cell lines expressing HBH-tagged NS5A-2a

To identify host proteins interacting with NS5A, an HBH fusion affinity tag was employed. This tag/resin combination has a number of advantages: (1) the resin is relatively cheap compared to many immunoaffinity resins and therefore it is possible to economically scale up purification reactions and (2) the capture can be performed under high urea (denaturing conditions). As such, by first cross-linking PPIs in their native cellular compartments, then capturing under denaturing conditions, produces highly pure protein complexes.

In order to identify NS5A interacting proteins, polyclonal stable cell lines were generated which expressed HBH-tagged NS5A-2a (and HBH-tagged GFP as a control) at moderate levels (Fig.3.3.A). Stable expression, as opposed to transient transfections, may result in more manageable expression of cellular proteins allowing better/proper protein folding and appropriate post-translational modifications. This is key for NS5A as phosphorylation may be a critical factor in regulating its interactome (140,284,285). Overexpression can lead to protein aggregation as a result of overloading the cellular protein folding machinery. Moderate protein expression also helps circumvent issues such as over activation of chaperone and heat shock proteins (347). This phenomenon has been previously demonstrated in plasmid titration studies during transfection of NOD-like receptors into HEK293E cells. When expressed at too high a level, protein aggregation and reduced cellular viability were observed (348). Expression at a lower level improved protein solubility and also allowed improved capture by purification resins (348) thus demonstrating the value of moderate protein expression for use in interaction studies. Experiments in this thesis compared stable versus transient transfections of NS5A and demonstrated that transient transfections produced less full-length forms of the protein (Fig.3.3.C). It is plausible that the smaller bands were due to high over-expression of NS5A-2a-HBH creating degradation products and truncated proteins from incomplete translation.

One general concern with retroviral transduction is random integration of the viral genome into host genomic regions causing deleterious insertions. In some cases,

inappropriate insertions have led to leukemia in retrovirally transduced mice (349). Although this phenomenon would be difficult to discern in cell lines generated here, growth and viability were compared to non-transduced controls and did not appear to be affected.

Affinity epitope tagging a protein can potentially alter protein conformation, stability and/or sub-cellular localization. N- and C-terminally tagged NS5A and GFP were not affected at least with respect to their stability as immunoblots consistently produced proteins of the expected sizes even months after continuous cell passage (Fig.3.3.A and data not shown). HCV NS5A is present in the cytoplasm, with its N-terminal amphipathic helix causing the membrane association (168–171). HBH tagging NS5A did not interfere with localization either at either the C (Fig.3.3.B) or N-terminus (Fig.3.21.B) when stably expressed in cells. In all this suggested that the HBH tag could be used as an affinity epitope without severely altering NS5A stability and cellular localization.

5.1.2 TAP optimization

The original HBH-TAP protocol was designed for identifying yeast protein interactions (255,256), and as such, had to be optimized for human cell line work. However, the first consideration was to establish that the HBH tag was accessible. Purifications using a cobalt cartridge coupled to an FPLC alleviated this concern as NS5A-2a-HBH was recovered with high efficiency with little bait protein present in the flow through or wash fractions (Fig.3.6.A). N-terminal HBH-tagged NS5A-2a and GFP were also easily captured from total cellular proteins (Fig.3.10). Although both N and C-terminal tags

appeared similar in all respects, a decision was made to concentrate more on the N-terminal tag form, which many other groups studying HCV had also used for their positional tagging. An additional consideration to support N-terminal tagging of NS5A was to avoid potential processing by methionine aminopeptidases present in human cells that cleave terminal methionines and often add an acetyl group to the penultimate amino acid (350,351). Authentic NS5A is cleaved from the HCV polyprotein producing an N-terminal serine and addition of an acetyl-group could be inappropriate.

Lysis and wash buffer optimization tests evaluating different detergents and pH identified an optimal lysis/purification nTAP buffer to be 50mM NaPO₄ pH 8.0, 150mM NaCl, 0.5% NP40 (Fig.3.6). During detergent optimization tests, it became apparent that a discrepancy existed between cobalt- and nickel-based purification of HBH-tagged NS5A. Elution from nickel columns occurred earlier and over a broader elution volume compared to similarly sized cobalt column purification (Fig.3.6.C vs. Fig.3.6.B). Although it is stated that nickel-based metal chelate resins produce higher protein yields, cobalt has a higher specificity for histidine residues (352). Comparatively, cobalt elution of NS5A-2a-HBH produced a cleaner and more concentrated elution and therefore was used in the final TAP procedure.

While the FPLC was useful in defining the initial purification protocol, the effort for set-up, higher volumes of buffer, lack of parallel processing for multiple samples and limited scalability dictated a switch to a different technique. An additional concern was that dilution of the samples during FPLC purification might affect PPIs reliant on

macromolecular crowding. A cell is composed of a concentrated milieu of macromolecules and dilution influences the affinity of some PPIs where the interaction affinity negatively correlates with increased dilution (353,354). A batch method utilizing iron-cored cobalt beads used a more concentrated input sample and most importantly, improved elution quality (Fig.3.7). It is likely that the FPLC column resin (1ml packed volume) to input protein sample volume was too high resulting in a large amount of non-relevant capture. With the beads, much smaller resin volumes improved this ratio. This optimal ratio concept also applies to batch purification at the second stage of purification, where reducing the streptavidin bead volume from 100ul to 25ul still captured the majority of the NS5A-2a-HBH protein but with improved purity (Fig.3.8.A&C).

TAP purification experiments in mammalian cells often suffer from low recovery with yields as low as 5% (254). The number of cells required for TAP-tagged experiments is typically 4-15, 15cm plates of confluent cells (355–357). Rigorous optimization of the nTAP procedure in the experiments presented here allowed for the use of only a single 15cm plate, which considerably reduced costs and processing times. Figure 3.10.B is a silver-stained SDS-PAGE gel containing aliquots from each step of the nTAP purification of HBH-NS5A-2a with the presence of a band corresponding to the correct size of HBH-NS5A-2a (74/76 kDa) detected from a streptavidin bead elution. Assuming that 0.2-0.6ng of protein can be detected for a mid-sized protein (PlusOne Silver staining kit, GE) such as HBH-NS5A-2a and that the streptavidin beads were diluted 1/20 prior to silver stain analysis, there is a minimum of 4.0-12ng of HBH-NS5A-2a protein captured on streptavidin beads. Coupled with the consistent protein coverage of 70% for NS5A

during mass spectrometry analysis/database searching, it was decided that a single 15cm plate of cells was a sufficient amount of starting material for HBH-TAP experiments.

5.1.3 Mass spectrometry identification of nTAP HBH-NS5A-2a-host PPI

Evaluation of HBH-tagged proteins using an optimized protocol revealed several previously identified NS5A interacting partners exclusively in HBH-NS5A-2a thus providing confidence that the native TAP (nTAP) method was capable of recovering specific NS5A interacting proteins. To establish a more rigorous the candidate list of NS5A-2a interacting host proteins, three nTAP biological replicates were performed consisting of HBH-NS5A-2a, HBH-GFP, and cells only (no vector). Mass spectrometry identified proteins had to meet three criteria: 1) proteins had to be identified by a minimum of two peptides and have false discovery rate of $\leq 1\%$, 2) the protein had to be present in a minimum of two replicates and 3) the protein had to be exclusive to the HBH-NS5A-2a sample.

Several points should be addressed here. First, because initial TAP experiments showed a large number of potential interacting proteins, it was intentional that a smaller candidate list would be generated. Second, although most comparative experiments use the bait protein (NS5A) and an empty vector control to discern non-relevant resin interactions effectively, GFP was included here as a non-relevant bait protein to determine if capture could occur simply with any protein being present. Additionally, the HBH tag could interact with proteins that are not relevant to the study and so this control would eliminate those proteins. Finally, HBH-GFP expression was higher than HBH-NS5A-2a for an

equivalent amount of GP2 293 cells (Fig.3.10.A vs. C). Attempts were made to generate cell lines having more comparable levels of each protein, however, this was the closest that could be obtained. Comparative Western blotting using the HBH target suggested that GFP was expressed approximately four times higher than NS5A. Although comparable levels of protein abundance would have made quantitative capture comparisons simpler, the results here can be viewed as a “toughest case scenario.” In essence, the negative bait GFP protein being present in higher per cell concentration than NS5A provided a greater opportunity for non-relevant interactions to occur and thereby be detected.

Although p53 was identified in the initial PPI experiments with HBH-NS5A, it was not classified as a specific HBH-NS5A-2a interacting protein in the triplicate nTAP experiment, and this could be considered a weakness of the data analysis method, which is likely, too strict. Several other studies using NS5A affinity capture combined with mass spectrometry/database searching have also not identified the NS5A/p53 interaction (248,269,295). All TAP methodologies are biased towards strong and abundant protein interactions and previous studies detailing the NS5A/p53 interaction used GST-affinity captured bait proteins and Co-IP to demonstrate the interaction (224,225,318). These methodologies use a targeted approach and thus amplify weak or lower level protein interactions. As the affinity of the NS5A/p53 interaction has not been empirically determined it may be a weaker or transient PPI that does not always survive nTAP purification.

One caveat of using mass spectrometry/database searching to identify proteins is that not every peptide present in a sample can be identified. A protein must produce viable peptides with favourable attributes for identification; peptide sizes that fall outside of the analysis window, are hydrophobic or have charges incompatible with efficient capture are not identified (358). Ion suppression, whereby analytes in a sample compete for ionization and elute simultaneously, thus suppressing their signals is also a potential problem (359). Although given the higher degree of purification from TAP protocols, it should be of lesser concern.

Several of the nTAP interacting candidates present in the triplicate analysis (Table 3.1) stood out, as their functions were consistent with phenotypes previously associated with NS5A expression. NKR1F is a transcriptional repressor of NF κ B responsive genes, regulates IFN β and iNOS promoters and is involved in IL-8 regulation (322–326). NS5A is capable of activating the iNOS promoter, inhibiting IFN β production and increasing the expression of IL-8 and NF κ B response genes (327–332). In the studies presented here, NRKF was found to be specifically associated with the HBH-NS5A-2a during nTAP purifications (Fig.3.13). Cell division cycle and apoptosis regulator protein 2 (CCAR2) (deleted in breast cancer 1 (DCB1), KIAA1967) regulates many cellular processes by interacting with additional host proteins to modulate their functions. These include negatively affecting enzyme function (SIRT1, HDAC3, SUV39H1), co-activating receptors (estrogen receptor alpha, glucocorticoid and thyroid hormone receptors) and influencing mRNA elongation and processing as part of the DBIRD complex (360–365). SOD1 was previously correlated with decreased HCV protein and RNA production in SG

replicon cells when treated with acetylsalicylic acid (366). Increased oxidative stress has been consistently observed in cells expressing NS5A (328,367–369), and it is tempting to speculate that an NS5A/SOD1 interaction may influence the antioxidant response.

CDK12 is a kinase, and as NS5A is highly phosphorylated, the possibility exists that it serves as an NS5A kinase. OGDH is an oxidoreductase crucial to the cellular glycolysis pathway, and an NS5A/hexokinase interaction has been previously established that results in increased cellular glycolysis (244). Therefore, nTAP analysis was able to identify several proteins with functions that are consistent with the cellular perturbations observed with NS5A expression.

5.1.4 Mass spectrometry identification of xdTAP HBH-NS5A-2a-host PPI

Before moving on to additional characterization of NS5A candidate interacting host proteins found during the native state HBH tag experiments, cross-linking denaturing TAP (xdTAP) was evaluated as another mechanism of potentially uncovering additional NS5A interacting proteins. Besides the advantage of potentially detecting weak and transient interactions in the appropriate spatial and temporal context, xdTAP can cement interactions that rely on labile post-translational modifications before the modification may be lost during isolation/capture purification. For NS5A this may be particularly relevant as the interaction with hVAP3 appears to be dependent on the phosphorylation status of NS5A (140).

Paraformaldehyde (PFA) is considered a zero length spacer arm cross linker, so additional linkers of varying length were evaluated including: DSS (11.4 Å spacer arm),

DSG (7.7 Å spacer arm) and EGS (16.1 Å spacer arm) (262) (Tables 3.2 and 3.3). All told, a significant number of previously defined interacting NS5A proteins were confirmed including: Hsp70 (333,334), Tubulin (335), Hsp90 (232), Hexokinase (244) and FKBP8/38 (232,234–237), ILF3 (synonym NF90) (336,337), CDK1 (338) and IPO5 (196,370). Heat shock proteins are molecular chaperones that aid in the synthesis assembly and folding of the protein and may bind any overexpressed protein (347). Co-IP studies previously revealed NS5A's interaction with both Hsp70 (333) and Hsp90 (232), but a control with another irrelevant overexpressed protein was not utilized. Gonzalez et al., 2009 overexpressed GFP as a potential expression control in their FLAG Co-IP demonstrating an interaction between NS5A and Hsp90, but GFP was not FLAG-tagged and therefore would not have been captured (334). Mechanistically, there does appear to be a role for heat shock proteins in the HCV life cycle, but at best they must be regarded as general class interacting proteins meaning that they can likely interact with any protein that is expressed. In the case of the TAP methodology used here, because the levels of HCV proteins in an authentic setting is difficult to determine, it is unclear what the “appropriate” level of expression is given the half-lives of HCV proteins in the SG replicon range from 10-16 hours (277).

Identification of ILF3 (NF90) as an NS5A interacting partner further illustrates the need to demonstrate PPI specificity using the proper controls. Li et al. 2014, revealed an NS5A/ILF3 interaction which was reliant on the presence of HCV RNA suggesting that the interaction is RNA-mediated (337). In contrast, Isken et al. 2007, were able to Co-precipitate ILF3 and NS5A from RNase treated SG replicon Huh-7 cells but not from

expressing on NS5A on its own concluding that NS5A/ILF3 interaction is based on a cofactor present in HCV replicating cells which is not HCV RNA (336). An ILF3/NS5A interaction was seen here with the EGS cross-linker. It is possible, if the hypothesis of Isken et al. 2007, is correct that another molecule may be facilitating this interaction and was cemented in place by the cross-linking reaction. Direct interaction with NS5A would have to be confirmed using different methodology such as a pull-down using purified putative interaction partners.

Typically NS5A is reported as being cytoplasmic or more specifically bound to the Golgi/ER at the periphery of the nucleus (171,192). However, immunogold electron microscopy has shown that NS5A produced from SG replicons is present in both the mitochondrial matrix and membranes (191). Interestingly, a large number of mitochondrial or mitochondrial associated proteins were identified in the xdTAP screens including: TOM5, TOM20, TOM22, TOM70, VDAC2, FKBP8, CDK1, RHOT2, Hexokinase and Metaxin-2. Identification of the TOM proteins 5, 20, 22 and 70 is interesting as these proteins, along with TOM 6, 7 and 40, form the translocase of the outer mitochondrial membrane (TOM) complex. The TOM complex is responsible for importing cytosolic produced proteins into the mitochondria. TOM proteins 70, 22 and 20 are receptors that sense mitochondrial pre-target sequences, passing them through a channel composed of TOM40. TOM proteins 5, 6 and 7 provide essential scaffold functions maintaining the stability of the TOM complex (371). Virtually the entire TOM complex was isolated by xdTAP as an NS5A interacting candidate suggesting the NS5A contacts one or more of the TOM proteins and is a possible mechanism of NS5A

mitochondrial import. Unfortunately, despite the use of programs such as pLINK (372) or xQUEST (373) which are used to infer cross-linked PPIs, it was not possible to precisely identify direct peptide-peptide interactions.

5.1.5 Reproducibility of NS5A-host cell PPIs

The reported NS5A interactome is extremely large with approximately 130 host interacting partners having been reported (207). Unfortunately, there tends to be little overlap between these reports. This lack of overlap may not be surprising as large-scale analysis of interactome studies revealed a 0.03% overlap in yeast PPI studies and 0.1% overlap in human PPI studies (249,250). The most likely explanation for NS5A-host PPI identification discrepancies is differences in protein expression systems and experimental procedures. Many NS5A interacting proteins have been identified using the Y2H system including FKBP38 (235), karyopherin beta 3 (370) and TIP47 (374). The Y2H system is prone to generating false positives, is limited to detecting binary interactions and, until recently required that the expressed proteins transit and interacted in the yeast nucleus (252). A Y2H study using each HCV protein produced 278 HCV protein-host PPIs, but only 10 PPIs had been previously described in the literature resulting in a 3.6% overlap (246). With NS5A specifically, 97 PPIs were identified with 38 previously published (246). Another Y2H screen of HCV proteins resulted in 112 identified PPIs, but only 18 PPIs were previously reported; a 16% overlap to the previous literature (247).

A study by Dolan et al. 2013, also investigated whether there was any genotype or sub-genotype specificity regarding HCV-host PPIs for genotypes/sub-genotypes 1b, 1a, and

2a (247). 326 HCV-host PPIs were identified in HCVprot database and separated based on the HCV protein's genotypes. 160 PPIs were identified for genotype 1b HCV proteins, 81 from genotype 1a, and 85 from genotype 2a. Not one host protein was identified as an interacting partner for all three genotypes investigated. Only 19 PPIs were identified in common from HCV 1a and 1b sub-genotypes, 4 from 1a-2a and 14 between 1b-2a (247). Okamoto et al. 2006, was one of the few studies that confirmed a FKBP8/38-NS5A interaction with NS5A generated from genotypes 1a, 1b, 2a (232). However, the NS5A-1a protein in this study appeared to be larger than NS5A-2a protein on the Western blots. The 18 amino acid insertion within NS5A from JFH1 should make this impossible, so the results must be interpreted with caution (232). These studies do illustrate there is little agreement in interactome screens performed with HCV proteins from different genotypes.

Co-IP experiments identify PPIs in what is likely a more biologically relevant context. However, the results are reliant on the choice of protein expression system, the presence/absence of an affinity tag, cell lines, antibodies and affinity resins. A primary concern is that the lysis procedure destroys any spatial constraints (251). Germain et al. 2014, used affinity purification of FLAG-tagged HCV Core, NS2, NS3/4A, NS4B, NS5A and NS5B from 293 cells. They defined 98 host interacting proteins involved with the six HCV proteins chosen and compared these host proteins to a curated list of previously identified HCV interacting partners, (543 PPIs total) (248). The 74 overlapping PPIs from the author's study and the literature were identified leading to a 24.5% overlap (248). In the case of NS5A, 17 PPIs were identified of which eight were previously reported (248).

While hepatoma cells would be the preferred biological source for expressing HCV proteins for TAP, expression in these cells from a CMV promoter is quite weak. However, 293 cells have been used to propagate the SG JFH1 replicon (375) albeit inefficiently, and thus must contain the necessary cellular factors to support JFH1 replication justifying their use. Experimental manipulation of cell lines can also impact the reproducibility of a PPI study. Chung et al., 2003, identified Bax as an NS5A interacting protein. However, cells were always stimulated with sodium phenylbutyrate prior to performing interaction studies (205). The Grb2/NS5A often cited as a clear NS5A interacting partner, but is apparently only observed in HeLa cells stimulated with epidermal growth factor (201).

An interaction between NS5A and PKR was established using NS5A from genotype 1b, but studies using NS5A derived from genotypes 2a and 3a failed to confirm the NS5A-PKR interaction (240–243). While Bax, Grb2, and PKR may be bona fide NS5A interacting proteins, they would not be detected except under specific experimental conditions or with specific NS5A bait proteins. Expression levels of the NS5A protein may also impact its interactome. An Hsp70/90/NOD-like receptors protein interaction was identified when NOD-like receptors were highly expressed by transfection but was absent when evaluated from a moderately expressing lentiviral integrated stable cell line (348,376,377). The lack of reproducibility of NS5A-host PPIs across studies demonstrates the need to scrutinize the interaction by many methods using several model systems with negative controls addressing interaction specificity.

5.1.6 Confirmation of nTAP and xdTAP NS5A interacting candidates

In order to further confirm candidate PPIs, FLAG-myc Co-IPs were undertaken. FLAG-GFP was used as an irrelevant expressed negative control protein in tandem with FLAG-NS5A-2a to control for interaction specificity. Surprisingly, the Co-IPs using FLAG antibody and affinity resins all resulted in the co-precipitation of the myc-tagged TAP interaction candidate with FLAG-GFP as well as FLAG-NS5A-2a (Fig.3.15). This interaction did not occur when lysates were prepared from cells transfected with only the myc-expressing construct subjected to FLAG pull downs. Numerous technical optimizations were attempted, but no criteria seemed to improve the specificity, although lowering the GFP expression did help to some extent. However, even a 5-fold reduction of FLAG-GFP still allowed binding of the myc-FKBP38 positive control interaction (232,234–237) Fig.3.15.B. Additionally, EGLN1, another previously identified NS5A interacting protein (248), was evaluated as a control (a kind gift from Dr. Daniel Lamarre, University of Montreal). Unfortunately, EGLN1 co-elutes with the IgG heavy chain at approximately 50 kDa, and it was difficult to distinguish the two proteins by SDS-PAGE analysis (not shown).

It is unclear why the FLAG immunoprecipitation experiments did not give definitive results and why FLAG-GFP co-precipitated the TAP candidate proteins and myc-FKBP38 positive control. Other FLAG-tagged proteins (FLAG-NS5A-1b, 3XFLAG-NS5A-1b) (a kind gift from Dr. Daniel Lamarre, University of Montreal) were also able to indiscriminately co-precipitate the myc-tagged TAP candidate proteins (not shown). There appears to be a specificity issue with the FLAG antibody/resin when a FLAG-

tagged protein is expressed that is absent from the myc antibody/resin and thus interaction confirmations were only considered from the myc-Co-IPs.

5.1.6.1 Specificity of the NS5A-2a interactions with TOM22 and CCAR2 in Myc reciprocal Co-IP

As there was an issue with the FLAG Co-IP experiments, additional controls were evaluated to determine the specificity of the NS5A-2a/TOM22 and NS5A-2a/CCAR2 interactions by myc Co-IP (Fig.3.17). myc-FKBP38 was used as a positive control (232,234–237) (Fig.3.17, lanes 1-6) and a myc-tagged Measles Matrix protein was used as an additional negative control bait protein (Fig.3.17, lanes 7-12). FLAG-NS5A-2a but not FLAG-GFP was captured by myc-FKBP. Neither FLAG-NS5A-2a nor FLAG-GFP was captured by the myc-Measles matrix protein suggesting that not just any myc-tagged protein will result in non-specific binding. FLAG-NS5A-2a and FLAG-GFP, when expressed in the absence of a myc-tagged protein, were not detected with the myc-capture protocol suggesting they did not bind to the myc antibody or resin directly (Fig.3.17, lanes 13-18). While myc-TOM22 precipitated both FLAG-NS5A-2a and FLAG-GFP, myc-CCAR2 specifically precipitated FLAG NS5A (Fig.3.17, lanes 22-24 & 28-30). Therefore, the interaction between CCAR2/NS5A-2a was both reproducible and specific in the reciprocal myc-Co-IP.

The TOM22/NS5A interaction, while reproducible was not deemed specific to NS5A-2a as FLAG-GFP was also co-precipitated by Myc-TOM22 ((Fig.3.17, lanes 24). This may be due to the chaperone activity of TOM22 (339). TOM20/22/70 function as the TOM

complex receptors as they contain cytosolic tails with TOM20/22 recognizing N-terminal pre-sequences and TOM70 recognizing internal hydrophobic residues (378). In addition to their receptor function TOM20/22 also function as chaperones, binding to unfolded proteins to aid in folding preventing aggregation on the mitochondria (339). The high levels of FLAG-GFP and FLAG-NS5A-2a proteins resulting from the transient transfection experiments may be binding to TOM22 acting as a chaperone and not as a receptor in complex with the other TOM proteins. It is possible that FLAG-NS5A-2a and HBH-NS5A-2a are binding different pools of TOM22 protein. Figure 3.16 also used a reciprocal myc Co-IP to co-precipitate FLAG-NS5A-2a with Myc-TOM40, but without the use of FLAG-GFP as a specificity control. As TOM40 makes up part of the TOM complex channel, this possibly suggests that FLAG-NS5A-2a was in complex with at least one protein within the mitochondrial TOM complex. Therefore, it is possible that NS5A interacts with the TOM complex, but further studies would need to be performed to elucidate which member(s) of the TOM complex specifically interact with NS5A.

As it is often the case that many viruses utilize similar mechanisms for propagation in the host cell it is not surprising that the TOM proteins make additional appearances in the literature with other viral proteins. Interestingly, the mitochondrial import of Influenza A RNA polymerase PB1+1 alternative frame-shift protein appears to be reliant on the presence of TOM40 (379). However, siRNA reduction of TOM20 and TOM22 and mutation of the internal TOM70 recognition sequence did not impede import of PB1+1 into the mitochondria (379). This suggests that while PB1+1 requires TOM40 to enter mitochondria, it is by a non-canonical TOM import pathway not reliant on the

TOM20/22/70 receptors (379). It is not impossible to consider that NS5A binds TOM40 but uses a similar non-canonical pathway and that the TOM20/22 proteins detected act as chaperones. In another study, the HIV-1 protease was found to cleave TOM22 when associated with the mitochondria resulting in a reduction in mitochondrial membrane potential and apoptosis (380). As many studies have demonstrated the antiapoptotic effects of expressing NS5A (205,216,217,221), it could be that NS5A binding to TOM22 protects the protein from cleavage. Additional experiments would need to be performed to assess whether NS5A has a protective effect on TOM22 under induced apoptotic conditions.

5.1.6.1.1 NS5A-2a interaction with CCAR2

Deletion constructs of NS5A-2a were generated to identify the CCAR2 binding site within NS5A (Fig.3.18). Unlike full-length NS5A-2a, myc-CCAR2 failed to provide clear co-precipitation with any of the FLAG-NS5A-2a domain constructs. It may be that CCAR2 binds to multiple NS5A-2a domains requiring the full-length protein or that the presequence of more than one domain provides a tertiary structure that is necessary for CCAR2 interaction. Of the constructs tested, FLAG-D2 NS5A-2a (25 kDa) produced a weak signal in the input lane. This is likely a stability issue as increasing the plasmid transfection amount did not improve the signal substantially. Therefore it is possible that this low protein abundance was below the detection limit of the Western blot. However, it could be assumed that the other constructs D1-D2 and D2-D3, which both contain the domain 2, would have shown capture with the myc-CCAR2 protein (Fig.3.18). It is also

possible that CCAR2/NS5A interaction requires NS5A domain 1 dimerization but then binds elsewhere in the protein.

Colocalization studies using both fluorescent and confocal laser-scanning microscopy indicated that NS5A-2a and CCAR2 occupy a similar cellular location (Fig.3.19, 3.20,3.21). Demonstrating this NS5A-2a/CCAR2 co-localization was important as CCAR2 is often described as a nuclear protein (340–342). Interestingly, CCAR2 can be N-terminally deleted due to activated caspase cleavage, and in this case, it is found to be exclusively cytoplasmic (381). Confocal images of negative control 293TN and Huh7.5 cells (in which NS5A-2a was absent) demonstrate that while the majority of CCAR2 does align with the DAPI stained nucleic acids, CCAR2 is also detected in the cytoplasm (Fig.3.20.A.E, Fig.3.21.A). In NS5A/CCAR2 doubly transfected cells, yellow punctate fluorescence indicating NS5A-2a/CCAR2 co-localization are present in any NS5A-2a expression model evaluated (transient transfection or SG replicon, 293 or Huh7.5 cells), although the majority of NS5A-2a and CCAR2 proteins are not participating in this interaction. This is not surprising given the fact that both proteins likely have a role in interacting with other proteins in the host proteome.

Additionally, in FLAG-NS5A-2a (endogenous CCAR2 detection) and FLAG-NS5A-2a/myc-CCAR2 double transfections, there is a correlation between high FLAG-NS5A-2a expression, condensed nucleic acids, and CCAR2 cytoplasmic redistribution (Fig.3.20.C.D.F.G). One interpretation for the increase in co-localization could be that NS5A-2a is sequestering CCAR2 in the cytoplasm. CCAR2 interacts with mutated in

colorectal cancer (MCC) protein and MCC sequestered CCAR2 in the cytoplasm in a subset of RKO cells doubly transfected with tagged HA-CCAR2 and GFP-MCC (341). Nuclear/cytoplasmic fractionation of HBH-NS5A-2a 293 cells showed no increase in cytoplasmic redistribution of CCAR2 (Fig.3.22.C) however, the translocation may only occur in only a small population of cells as with MCC/CCAR2 (341). Fig.3.20&21 show that CCAR2 cytoplasmic redistribution does not happen in all NS5A-2a expressing cells and therefore may be diluted out when analyzed by subcellular fractionation. Another explanation for CCAR2 cytoplasmic redistribution, especially in NS5A-2a cells with condensed nuclei, is that these cells are undergoing apoptosis. Nucleic acid condensation is a hallmark of apoptotic cells, and DAPI stained images of FLAG-NS5A-2a transfected (Fig.3.20.C), FLAG-NS5A-2a/Myc-CCAR2 double transfected (Fig.3.20.D.G) 293 and Huh7.5 cells suggest cells with irregular nucleic acid components are coupled with virtually complete cytoplasmic redistribution of CCAR2. As such, cells high levels of NS5A-2a may be experiencing cellular stress and activating an apoptotic response thereby leading to N-terminal cleavage of CCAR2 and ultimately its cytoplasmic translocation (381). Whether NS5A-2a has higher/any affinity for truncated CCAR2 over the full-length protein remains unknown.

A specific protein interaction has the potential to increase a protein's stability or induce an increase in expression of that protein to compensate for the portion participating in the interaction. The result of either is an increase in protein abundance. The CCAR2 antibody used for CCAR2 quantification studies (abcam, 151190) specifically detected the full-length CCAR2 protein and was capable of producing a reliable, linear

quantifiable signal when analyzed using a five-point dilution curve (not shown). The anti-myc antibody and commercial anti-CCAR2 antibody (detecting the N-terminus of CCAR2) both detected expressed myc-CCAR2 but in the absence of a C-terminal target, it is unclear whether a truncated form is present at different levels in NS5A expressing cells. It may be that NS5A expression may increase quantities of the truncated CCAR2, but an antibody directed toward an epitope in the C-terminus of CCAR2 is required.

Quantitative western blotting performed on HBH-NS5A-2a, and HBH-GFP 293 cells determined that the expression of NS5A-2a did not affect the abundance of 130 kDa CCAR2 (Fig.3.22.A&B). One caveat to quantifying CCAR2 in GP2 293 cells is that these cells have neoplastic origins. 293 cells are a transformed embryonic kidney cells containing adenovirus type 5 DNA where portions of the viral genome integrated into the host genome and decreased cellular senescence resulting in continuous cell division (382). Bae et al. 2012, quantified the CCAR2 protein in both cancerous and noncancerous liver tissue of 10 HCC patients and revealed CCAR2 was only increased in the tumours (383). As such, CCAR2 expression may already be elevated in GP2 293 cell lines used in the studies described here, dampening any observable effects of NS5A on CCAR2 abundance. Demonstrating any CCAR2 expression changes in both an authentic *ex vivo* HCV infection and ectopic NS5A expression in primary liver cells could provide insight into NS5A effects on CCAR2 in a non-cancerous cell line. JFH1 infections of primary hepatocytes have recently been demonstrated (384).

While NS5A-2a expression may not have impacted CCAR2 abundance, the NS5A-2a/CCAR2 interaction could affect the HCV lifecycle. One of the best-characterized functions of CCAR2 is its ability to bind SIRT1 and interrupt its NAD⁺-dependent deacetylase functions (360,361,385). SIRT1 regulates several cellular functions including DNA repair, metabolism, rRNA transcription (386–391), and directly impacts p53 function by deacetylating p53 at K382 (392). SIRT1 deacetylation serves as a p53 antagonist as deacetylated p53 exhibits dampened p53 target gene expression (387,392). Furthermore, SIRT1 overexpression in cells containing wt p53 leads to increased resistance to genotoxic induced apoptosis (387,392). Deacetylation of p53 at K382 also allows for ubiquitination of K382 by the Mdm2 E3 ubiquitin-protein ligase and p53's subsequent degradation (393). CCAR2 is a direct negative regulator of SIRT1's antagonist effects on p53 as CCAR2 binds SIRT1's active site rendering SIRT1 unable to deacetylate p53 (360,361). siRNA depletion studies of CCAR2 revealed that such cells were more resistant to genotoxic-induced apoptosis and these effects were reversed by reducing both CCAR2 and SIRT1 protein abundance (360,361). Therefore, the interaction of NS5A-2a and CCAR2 could impact CCAR2's negative regulation of SIRT1 leading to either an increase or decrease in p53 K382 acetylation.

Using a quantitative Western blot with a K382 acetylation specific p53 antibody could determine any change in p53 K382 acetylation in the presence of NS5A-2a.

Interestingly, it was discovered that CCAR2 did not function as a negative regulator of SIRT1 mediated deacetylation of p53 in the liver cancer cell line SNU-182 (383). As well, siRNA mediated CCAR2 silencing led to a reduction in p53 acetylation in etoposide

treated A549 epithelial cells but not in etoposide treated SNU-182 liver cells (383). These results suggest that CCAR2 may not influence SIRT1 functions in SNU-182 cells and are perhaps indicative of CCAR2 function in HCC. However, the acetyl-p53 antibody used in this study was not well described, and it is not clear which acetylated-lysine the antibody targeted in p53. Without quantifying the pixel density on the Western blots, it is hard to conclude that acetylated p53 is not reduced in CCAR2 depleted SNU-182 cells as the results obtained from SNU-182 cells are not as dramatic when compared to reduced acetylated p53 levels in CCAR2 depleted controls (383). The author's themselves state that p53 is wt in A549 cells and is a mutant derivative in SNU-182, which may confound the results further (383). As such, studies determining on whether the NS5A-2a/CCAR2 interaction affects p53 K382 acetylation in an HCC cell lines are still warranted.

An additional function of SIRT1 in the liver that has links to HCV protein expression is protection against steatosis (394). CCAR2 is involved in the development of steatosis as mice depleted of CCAR2 were resistant to lipid accumulation, inflammation and injury in a steatosis induction model (394). The development of steatosis is a frequent complication of HCV infection that is linked to a Y164F mutation in the HCV Core protein (34,35). However, an interaction between NS5A-2a/CCAR2 may inhibit CCAR2 functions and lead to an increase in cellular lipid accumulation contributing to steatosis. The deacetylase activity of HDAC and the methyltransferase activity of SUV39H1 are also negatively impacted by their binding to CCAR2 (362,363), and these targets could be examined in the presence of NS5A-2a expression. CCAR2 is also a ligand dependent co-

activator of several receptors including the estrogen receptor alpha, glucocorticoid and the thyroid hormone receptors (364) and NS5A-2a may affect CCAR2's affinity and potentially downstream signaling. The DBIRD complex is composed of CCAR2/ZNF326/ZIRD and regulates mRNA elongation and splicing (365). The NS5A/CCAR2 interaction could influence the formation of the DBIRD complex. Given the important regulatory functions of CCAR2, interaction with NS5A may affect these processes and have multiple effects on cellular homeostasis.

5.1.6.1.3 Role of CCAR2 in viral infections

The role of CCAR2 has been investigated in viral infections. CCAR2 was evaluated in 199 HCC patients infected with hepatitis-related viruses by immunohistochemical staining and tissue microarray (395). 177/199 HCC cases displayed high reactivity to CCAR2 and were associated with unfavorable effects on recurrence-free survival (395). Twenty-two out of 199 patients were HCV positive, and 14 of those patients had high CCAR2 staining (395).

Cardiovirus leader proteins (L_X) belonging to viruses of the *Picornaviridae* family are known for halting nuclear import/export processes by binding Ran-GTP protein leading to perpetual activation (396). The RAN- L_X interaction results in NUP hyperphosphorylation thus terminating nucleocytoplasmic trafficking (397). Affinity purification coupled to mass spectrometry analysis revealed CCAR2 bound to the EMCV L_X protein (398). This is interesting as the both the EMCV L_X protein and HCV NS5A both interfere with the cellular distribution of the Ran GTPase (195,196). Majority of the

Ran protein is typically located in the nucleus, but in HCV infected cells Ran was observed in the cytoplasm in NS5A positive foci (195,196). The EMCV Lx protein and NS5A both disrupt the nuclear/cytoplasmic trafficking and also bind to CCAR2 suggesting the possibility of common functions. Mass spectrometry also identified CCAR2 as an interacting partner of Ebola virus (EBOV) VP24 by purification of VP24-EGFP using GFP-trap from 293 cells (399). VP24 is a multifunctional protein with an affinity for membranes that plays a role in EBOV replication, assembly, and packaging (400,401). VP24 aids in Ebola virus immune evasion by binding karyopherin-alpha blocking nuclear accumulation of STAT1, again interfering with the nuclear transport system (402). It is tempting to draw correlations between EBOV VP24 and NS5A in that both are multifunctional proteins involved in viral life cycle regulation and cellular trafficking and both interact with CCAR2. It is not surprising to find that many different virus proteins target a single host cellular protein, such as CCAR2, as a means to modulate host cell functions.

5.2 Mapping and characterization of phosphorylation sites on hepatitis C virus

NS5A protein

NS5A exists as two distinct phospho-proteoforms by SDS-PAGE analysis (97) and this has prompted initiatives to generate a comprehensive list of all the phosphorylated residues within NS5A. Several investigations have reported identifying NS5A phosphopeptides (289,303–305), but fine-mapping has only identified S146, S222, S225, S235, S238, and T348 as bona fide phosphoacceptor sites (303–306). In this investigation, NS5A was isolated for phosphoacceptor site identification by mass

spectrometry. In several isolation experiments, nTAP or dTAP was used to isolate highly purified HBH-NS5A-2a protein from GP2 293 cells, and NS5A-HBH-2a from SG JFH1-NS5A-HBH Huh7.5 cells. Continuous elution electrophoresis was also used as a purification technique in order to purify untagged NS5A derived from SG JFH1 protein in Huh7.5 cells. In all, 28 phosphoacceptor sites were identified in the NS5A protein (Table 4.1& Fig.4.4) across all experimental platforms. Twenty of these phosphorylated residues were novel, and six previously identified sites were confirmed (S146, S222, S225, S235, S238, and T348 (303–306) (Fig.4.4).

The identification of 28 phosphorylated residues within NS5A was aided by the use of multiple sources of NS5A, purification techniques, phosphopeptide enrichment and multiple proteases. Several phosphorylated residues were identified in samples obtained from expression of HBH-NS5A-2a, SG JFH1-NS5A-HBH, and SG JFH1 that included S146, T164, T204, S222, S225, S228, S230, and T348 (Table.4.1&Fig.4.4). Consistent identification of these residues could indicate that they are highly abundant or that these phosphopeptides have biochemical characteristics favourable for mass spectrometry identification. Phosphopeptides containing “S381/S382”, “S414/S415” and “T410” were identified exclusively from the unmodified SG JFH1 replicon (Table.4.1&Fig.4.4). As such, phosphorylation of these residues may require active RNA replication of the presence of the other HCV NS proteins. S201, T210, T213, S229, S232, S235, S238, S272, S288, T334, and, S365 were only identified in TAP purified HBH-NS5A-2a samples (Table.4.1&Fig.4.4).

TAP purified HBH-NS5A-2a is extremely pure and as such may have significantly improved detection sensitivity potentially leading to the identification of low-level phosphorylations. TAP purified HBH-NS5A-2a was digested with GluC and AspN in addition to trypsin producing alternative peptides. The expanded coverage led to the identification of S288, S381/S382, S401, T410, and S414/S415 from GluC digested peptides and T210, and S272 from AspN.

5.2.1 Phosphorylation requirements for NS5A from different genotypes

While clear that differential phosphorylation exists in NS5A, presence of the hyperphosphorylated form (p58) appears to differ between HCV genotypes even to the strain level. Expression of NS5A-1b in COS-1 cells showed that hyperphosphorylation was dependent on the expression of HCV-NS4A provided in trans (97). Deletion of the 1b polyprotein in Hep3B cells indicated that p58 production depends on NS5A being expressed in cis as an NS3-NS5A segment and that NS3 must contain an active protease (276). NS5A-1a requires the expression all of the nonstructural proteins for NS5A hyperphosphorylation (276). However, the findings were different when NS5A-1a was expressed in BHK-21 cells. Here, both phospho-proteoforms were observed without the need for additional HCV proteins (281). This study also demonstrated that NS5A-2a did not require other HCV proteins for the production of both phospho-proteoforms (281).

NS5A hyperphosphorylation requirements are further complicated when evaluated at the strain level. Several different HCV 1b strains were assessed independently, and each appeared to require a different set of HCV proteins to produce NS5A p58. Strain J

(genotype 1b) required NS4A supplied in trans (97), while a 102 amino acid deletion from the N-terminus no longer required NS5A to generate p58 (403). Strain BK (genotype 1b) required NS2 provided in cis (278) for p58 formation. NS5A derived from two patients (genotype 1b) required complete NS3-NS5A expression for p58 to be produced (279). It is possible that the use of different cell lines could explain many of these discrepancies. However, it is also probable that even subtle differences within the NS5A sequences used may lead to differences in phenotype. The effects these different requirements have on HCV biology remains unresolved.

5.2.2 Conservation of phosphoacceptor sites identified in NS5A JFH1

Typically highly conserved residues across multiple samples, or in this case genotypes/strains would suggest conservation of function. An alignment of the NS5A ORF from several different HCV genotypes indicated that T204, T210, S225, S229, S230, S232, S235, S414, and S415 were highly conserved across all seven genotypes (Appendix Fig. A1). Conservation of serines within the LCSII (S225, S229, S230, S232, S235) has been previously noted and modifications in this area have been shown to affect HCV life cycle kinetics indicating their importance in the virus life cycle (141). T204 and T210 are present in the PI4KIII α binding site on NS5A(284). T204 was conserved in genotypes 1-6 but with a negatively charged aspartic acid in two genotype 3a strains while T210 was conserved in all genotypes. Given the important role for PI4KIII α in HCV replication, they are of interest especially since work presented here has demonstrated that each can be phosphorylated. Reiss et al., 2013 revealed phosphoablatant alanine substitution of T204 was wt, but T210 lead to dramatic increases

in hyperphosphorylation, indicating that phosphorylation of these residues are repressive to p58 formation (284). T204A and T210A replicated to wt levels but T210E replication was severely reduced, T204E was not tested (284). The conservation of T204 and T210 among HCV genotypes may indicate that phosphorylation of these residues is detrimental to p58 production and negatively affects HCV replication.

Interestingly, T410 is exclusive to the JFH1 strain. JFH1 possesses the unique ability to grow in hepatoma cell culture without adaptive mutations (151) and identifying which viral sequences provide this capacity has been inconclusive. Sequences within Core, NS3, NS5A, and NS5B (100,152–155) have all been suggested. While it was demonstrated that T410A/D mutations produced near wt RNA replication levels and viral titers (Fig.4.10.D), the T410 residue may be a factor, in combination with an additional site that contributes to the unique features found in JFH1.

5.2.3 Phospho-proteoform effects on HCV life cycle

The phosphoacceptor sites identified in NS5A were systematically mutated in the JFH1 virus backbone to determine the effects of eliminating and constitutively mimicking phosphorylation charge at a single residue. The mutant viruses were then evaluated for their effects on RNA genome production, p58/p56 protein abundance ratios, and infectious virus particle production (Fig.4.5). While the majority of the mutants did not differ significantly from the wt control, others showed clear differences in one or more of the factors studied.

5.2.4 NS5A phosphomutant effects on HCV RNA replication

When comparing the four-hour (input) to 72-hour (replicated) viral RNA levels, most mutants showed no appreciable differences compared to wt, and none of the mutants exhibited higher levels of RNA production compared to wt. Mutants were considered of interest when their replicative capacity differed from wt by more than 5-fold as evaluating duplicate wt JFH1 RNA over multiple experiments revealed a variability in the wt of two-fold. Replication phenotypes differing from wt JFH1 were classified as weak (0- 10 fold less RNA levels 72hpe compared to 4hpe), very weak (10-100 fold less RNA levels 72hpe compared to 4hpe) and extreme (>100 fold less RNA levels 72hpe compared to 4hpe). A point to consider is that the input RNA levels at 4hpe for each mutant are relatively high and thus the genome replication may hit a “replication ceiling,” thus limiting the fold change observed. While this was not tested empirically, a replicative maximum may account for the smaller fold changes observed with the RNA data presented in this study.

S229A was the only mutant to display extremely weak replication levels comparable to that of the GND negative control. T210D, S229D and S235A mutants had very weak replication and the mutants that replicated weakly included T204D, T210A, S225D, S232A/D, S235D, S238A/D, T334A/D and T363A/D (Fig.4.6). Interestingly T210A and S235D mutants at least partially rescued the virus although not necessarily to wt levels, suggesting that the presence of a charged residue at T210 and the absence of one at S235 are tolerated. Alanine or aspartate substitutions at position S229 were both deleterious with S229A showing no RNA replication and S229D showing very weak

RNA replication capacity. It is interesting to speculate that this site represents a molecular “switch” such that at certain points in the genome replication cycle, the serine must be unphosphorylated while at other times it must be phosphorylated. The effect of these mutations on RNA replication is consistent with previously published data (284,289,299,304,305). Reduced RNA replication capacity for mutants T210A, S232A and T334A are consistent with earlier investigations (179,284,289,299,304). Whether the reduced replicative capacity observed with these mutants involves altering the stability of the NS5A protein, the efficiency of establishing replisomes or actual RNA replication remains unknown.

The small but consistent reduction in replication for mutant S222D is in line with previous results (303), but others found this mutant to behave more like wt JFH1 virus (289,304). Mutant S238A has also been reported to replicate at wt levels whereas this work suggests a weakened replication capacity (289,299,304). Considering how small the reduced replicative capacities are for S222D, and S238A compared to wt, these lower level fold changes are difficult to quantify and could be a reason for the discrepancy between studies. It is not believed that RNA synthesis and electroporation was a key factor in this investigation as different batches of RNA were prepared, measured and electroporated with each species behaving very consistently across experiments.

S229A and S235A both show decreases in replication compared to wt. In both cases, a phosphomimetic improves the replication capacity albeit not to the same levels as wt. This is not surprising. Besides the obvious possibility that the amino acids are simply

incompatible with the secondary/tertiary structure or stability of the protein at that site, there are inherent issues associated with attempting to mimic a phosphorylation event with a charged amino acid. The negative charge on a phosphate molecule at physiological pH is generally -1.5 while aspartate has a charge of -1, thereby, limiting the size of the ionic shell created by the replacement (297). Furthermore, if the phosphate residue contributes to an essential PPI, an aspartate mimic will not efficiently replicate the area needed to complete a proper interaction region (297).

The negative impact on RNA replication in NS5A Domain 3 mutants was unexpected. It was previously reported that this region was dispensable for genome replication and D3 is principally involved in viral assembly and virion production (98,178). T334A/D, T363A/D and T401D all negatively impacted HCV replication and indicate that these sites may play some role in maintaining optimal genome replication levels (Fig.4.6). Reduced T334A replication levels have been observed previously, but a potential link to phosphorylation was not made (179).

5.2.4.1 NS5A T356A Mutation

Cordek et al.,2013, utilized an *in vitro* kinase assay with protein kinase A and NS5A protein derived from the Con1b genotype combined with mass spectrometry to identify T360 as a phosphorylation site (175). 1b replicons with the S2204I replication enhancement mutation were established containing the phosphoablatant alanine mutation and the phosphomimetic glutamine mutation and revealed that tampering with T360, regardless of the mutation introduced reduced HCV genome copies levels approximately

10-fold, but only after multiple cell passages (175). However, the use of the Con1b replicon with the S2204I mutation may have interfered with NS5A phosphorylation studies as S2204I eliminates p58 NS5A hyperphosphorylated form (134). In order to verify the importance of this site in a replication model, T356 (the comparable residue in the JFH1 sequence) was mutated to either alanine or glutamate. These mutations were engineered into a JC1/Gluc2a luciferase reporter viruses (175). Both viral replication and infectivity were monitored and both assays indicated that the T356A mutation resulted in a non-replicative, non-infectious virus while T356E resulted in WT levels of replication and packaging (175).

However, these results were not confirmed in the study presented here. Replication (and infectivity) levels of both T356A and D were comparable to wt ((Fig.4.6)&4.10). In order to rule out a mix-up of testing samples, RNA from T356A/D electroporation experiments was converted to cDNA and directly sequenced. In all cases, the mutations were present as expected. Although the simplest explanation for the discrepancy in results is a mixed up sample, it is possible that T356A/D in the JC1/Gluc2a reporter virus exhibits different effects on genome replication compared to JFH1. If this were the case, it could substantially change the interpretation of data using reporter systems for their read-outs.

5.2.5 NS5A phosphomutant effects on NS5A phosphoform protein abundance

Determining the effect of mutations on phosphorylation status, particularly on p58 and p56 was also of interest as prior studies using 1b replicons suggested a correlation of this ratio with HCV replication (141,282). The average p58/p56 ratio produced by wt NS5A

was 0.61. Mutants S151D, S225A, and S232A produced the lowest levels of hyperphosphorylated NS5A with mean p58/p56 ratios of 0.19, 0.11 and 0.08 respectively (Fig.4.9). While S151D appeared to be wt, at least concerning RNA replication, S232A had lower replication levels compared to wt virus. Interestingly, S232D which showed impaired RNA replication levels had a p58/p56 ratio of 0.24. Mutant S151A expressed a near wt ratio of 0.44 whereas S146D was considerably lower 0.19 ratio suggesting that phosphorylation at this site decreases p58 amounts (Fig.4.9). S151D also produced a ratio 40% below wt although RNA replication was not affected. These findings appear to be consistent with previous observations involving sites within the N-terminus. Double mutant experiments have demonstrated that the S146D mutation is dominant and negatively affects NS5A hyperphosphorylation at secondary sites within the LCSII (304). Interestingly, deleting N-terminal portions of NS5A-1b resulted in p58 production whereas the full-length NS5A-1b, p58 was only produced when NS4A expression occurred suggesting a role for the NS5A N-terminus on NS5A hyperphosphorylation (403). One explanation for these findings is that phosphorylating residues at the NS5A N-terminus disrupts a recognition site that blocks phosphorylation or that the addition of a charge causes repulsion of an otherwise weak interaction at that site.

Studies involving mutations of NS5A S235A have been inconsistent. Both Masaki et al., 2014 and Eyre et al., 2016 were unable to detect any NS5A protein production from JFH1 or JC1 viruses with that mutation (289,305). Chong et al., 2015 expressed S235A NS5A in HEK293 cells under a CMV promoter and determined by Western blot that the p58 band was below their detection limits (306). In this thesis and in a study by Fridell et

al., 2013 (299), p58 is produced in the S235A background, albeit at a lower level than wt (Fig.4.9). The disparities could easily be explained as a consequence of immunoblot sensitivity or RNA input levels. Additionally, the difference in expression systems are likely significant; CMV-driven NS5A in HEK 293cells (306) compared JFH1 electroporation into Huh7.5 cells (this study). P58 generation from a S235A mutant may require expression in the context of a more appropriate replication system. In this study, the JFH1 virus without additional replication enhancing mutations was used in the Huh7.5 hepatoma cell culture providing a biologically relevant model that did produce low levels of p58 from S235A

Three mutants produced a slightly greater p58/p56 ratio compared to wt and included T210A, T210D, and T213D with mean p58/p56 ratios of 1.08, 1.01, and 0.89, respectively (Fig.4.9). Interestingly, T210A and T210D mutants replicated weakly and very weakly, respectively. High p58 levels generated by T210A/D suggest that modification of this site alone either favors p58 production or suppresses p56. Phosphorylation of T213 could be a major contributing residue to p58 production.

Several reports have suggested that NS5A proteins containing S232D, S235D, and S238D mutations impede the mobility of p56 by SDS-PAGE (289,299,304). That observation was also made in this study (Fig.4.9) suggesting that NS5A phospho-proteoform production may be more complicated than just p56 and p58. 2D gel electrophoresis has indicated a large number of species at both the p56 and p58 levels that may differ by only one phosphorylation event (404) (Fig.4.9).

5.2.6 NS5A phosphomutant effects on infectious JFH1 titers

Evaluating the effects of mutations on the quantity of released infectious JFH1 proved to be difficult due to the inherently low viral production of unaltered JFH1 virus (151). A time-course evaluation determined that the optimal day post electroporation for viral harvest was nine dpe and serial passage was thus necessary to keep cell monolayers below 80% confluency. WT titers averaged 8.96×10^2 TCID₅₀/ml at nine dpe. These observations were in contrast to the that of Ross-Thriepland et al., 2014 reporting WT JFH1 titers of approximately 2×10^4 ffu/ml (2.9×10^4 TCID₅₀/ml) at 72hpe (304). Such a high value in the latter case is surprising given that most reports using unaltered JFH1 report similarly poor titers (hence the reason that the J6/JFH1 or Jc1 recombinant viruses are often used for virus production studies). The most plausible explanation is that there are differences in the cell lines used. This study uses the standard Huh7.5 cell line (a gift obtained directly from Dr. Rice, Rockefeller University) whereas the other study uses a Huh-7 cell line. In these cells, there appears to be a difference in the JFH1 input RNA decay rates. Using the same amount of input RNA (5ug) after 72 hours, GND mutants levels (an indication of RNA decay in the absence of viral replication) drops approximately 1000-fold in contrast to the study of Ross-Thriepland where there is only a 100-fold reduction in RNA copy 72 hpe which they hypothesized was due to the stability provided by the 5' UTR (304).

What is clear from the study presented here is that any manipulation of S229, either to A or D, changing T210 to D or changing S235 to A all decreases JFH1 infectious virus

production (Fig.4.10). In each case, this is directly explained by the fact that each of these species also showed the largest negative effect on RNA replication.

Several other mutants produced less (2-5 fold) infectious virus than JFH1 wt. T204D, T210A, S230A/D and T334D all had reduced titers but also had reduced RNA replication levels (Fig.4.10). Interestingly, T164D, T210D, S238D and S381D produced 2.3, 4.7, 2.7 and 2.4 fold less released infectious virus than WT but had no difference in genome replication levels compared to wt (Fig.4.10). This observation suggests that phosphorylation at T164, T210, S238 and S381 could be involved in the replication process but may be deleterious to viral assemble or packaging. Conversely, S222A and S225A also exhibited wt RNA replication levels, but have a 2.6 and 3.1 fold reduction in released infectious titers (Fig.4.10), suggesting that phosphorylating S222 and/or S225 may be required for processes downstream of replication. Important to keep in mind that when dealing with small differences such as these along with high variances and low sampling that statistical significance was not reached and therefore these observations must be treated more as “suggestive observations.”

5.2.7 NS5A phospho-proteoform abundance impact on the HCV lifecycle

Reports using the Con1b SG replicon suggested that a low p58/p56 ratio promotes viral replication while a high ratio bolsters infectious virus production (141,282,283). In direct contrast with this, work by Fridell et al., 2013 suggested that in the JHF1 system, high levels of p58 promoted genome replication whereas low levels of p56 caused higher viral titers (299). Despite the detailed analysis of the sites identified in this study and the

extensive investigation into the associated phenotypes, the results are not supportive of the hypothesis that a differential abundance of NS5A phospho-proteoforms promotes replication over packaging or vice versa. The findings here do support the concept that phosphoablant mutations in the LCSi (which causes reduced p58 abundance levels) appear to have the largest impact on the overall HCV life cycle. The reduction is most apparent with S232A, and S235A as each mutant produced a p58/p56 ratio <0.35 accompanied by a greater than 10 fold decrease in genome replication and lower levels of released infectious virus. These sites are of particular interest as the serines of the LCSi are conserved across 40 HCV strains (141). It is tempting to conclude that phosphorylation in the LCSi is a major contributing factor to the creation of hyperphosphorylated NS5A, but this may require phosphorylation of more than one residue. P58 likely contains multiple species of phospho-proteoforms but it may be that only one type is crucial in the phenotypes examined here and as such is but one of several essential factors.

5.2.8 NS5A/PI4KIII α Interaction

NS5A constructs containing the T204A mutation replicated to essentially wt levels while the T204D mutant was reduced 5-fold. The replication of the T210A mutant was also 5-fold less than wt, but the T210D was severely impaired and considered replication dead. Reiss et al., 2013 had previously mapped the PI4KIII α binding region to Q187-A214 on NS5A and suggested that the NS5A/PI4KIII α interaction either favored the p56 form or suppressed p58 formation (284). Utilizing triple alanine mutations in the PI4KIII α binding region revealed the importance of this region to both HCV RNA replication and

p58 production. Mutations that altered T204 and T210 resulted in non-replicative phenotypes with higher p58/p56 ratios (284). Similar to this study, a single alanine substitution at T204 resulted in wt replication and wt p58/p56 levels, but a phosphomimetic mutant was not evaluated (284). However, T210 proved to be a critical site as alanine substitution resulted in a 100-fold reduction in genome replication a phosphomimetic substitution (T210E) reduced virus genome replication by 10,000-fold. It also abrogated PI4KIII α binding leading to the argument against T210 as a phosphoacceptor site (284).

In the study presented in this thesis, conclusive evidence of both T204 and T210 phosphorylation was provided as both sites were seen as phosphorylated in expressed NS5A while T204 phosphorylation was also identified in a replicon model. T204A/D and T210A/D produced similar phenotypes to those reported by Reiss et al., 2013 with T204A replication levels indistinguishable compared to wt and the T204D mutant reduced 5.6-fold (Fig.4.6.A). T210A/D mutant RNA replication levels were reduced 6.5-fold for T210A and were almost non-existent for T210D (Fig.4.6.A). This phenomenon may not be directly related to the predominance of one p56 or p58 forms directly, as the p58/p56 ratios produced by T204A/D were similar to wt (Fig.4.9). While more studies would be necessary, it is possible that phosphorylation of T204 and T210 may negatively influence the NS5A/PI4KIII α interaction. As such, when T204 and T210 are not phosphorylated PI4KIII α can bind successfully, and HCV replication proceeds but phosphorylation at these sites prevents PI4KIII α binding and reduces viral replication. Eyre et al., 2016 provided further evidence that PI4KIII α expression is required for

optimal HCV genome replication (305). It appears that PI4KIII α is also involved in events needed for successful phosphorylation of S235 in NS5A through an undetermined mechanism (305). In this scenario, PI4KIII α may block access of other kinases responsible for phosphorylation events leading to the production of p58 (305). While there is cumulating evidence suggesting that PI4KIII α influences NS5A phosphorylation (284,305), further investigation will be required to establish the mechanism.

5.2.9 NS5A tyrosine phosphorylation

This investigation, along with several others using mass spectrometry/database search based approaches (289,303,304,306), has yet to positively identify tyrosine phosphorylation in NS5A. However, two studies utilizing a phospho-tyrosine antibody have suggested that NS5A contains phosphorylated tyrosine(s). The first study employed myc-NS5A-1b deletion constructs expressed in COS cells stimulated with the tyrosine phosphatase inhibitor, pervanadate, and used a phosphotyrosine antibody, pY20, to reveal a phosphotyrosine present between amino acids 147-447 (405). Mutation of Y334 to phosphoablatant phenylalanine in myc-NS5A produced a much weaker Western blot signal than wt NS5A when probed with the pY20 antibody (405). In a follow-up study, the pY20 antibody was used to evaluate the phosphotyrosine status of NS5A immunoprecipitated from a J6/JFH1 infected Huh7.5 cells and suggested that p58 was preferentially phosphorylated (406). Y330 in JFH1 NS5A was reported to be the tyrosine that corresponds to Y334 from NS5A-1b, and Y330F was engineered into the J6/JFH1 virus and the SG JFH1 replicon. Y330F J6/JFH1 produced lower genomic RNA levels and reduced intra and extracellular infectious viral titers while the Y330F mutation did

not affect genome replication (406). The conclusion was that Y330 phosphorylation was involved in HCV particle assembly and that the effects may only be evident in cells producing infectious virus (406). The investigation performed in this thesis did not identify Y330 as a phosphorylated residue. The tryptic peptide, containing Y330 is “RPDYQPPTVAGCALPPPK,” and this study mapped T334 as a site of phosphorylation indicating that the peptide was seen by the methods employed here. It cannot be ruled out the possibility that a multi-phosphorylated peptide exists (and is not captured for analysis) but other possibilities need to be evaluated. The phosphotyrosine antibody, pY20, may not be performing optimally when recognizing the NS5A epitope containing Y330. Peptide microarray experiments evaluating pY20 specificity revealed optimal affinity when a proline residue is at position +3, and a leucine at -1 from the tyrosine and that charged residues in the -1 positions reduce antibody specificity (407). Y330 in the JFH1 sequence has an aspartic acid residue at the -1 position, and as such, pY20 specificity for this residue may be lacking. The stringency of pY20 for phosphorylated tyrosines has been brought into question. Immunoblots using pY20 compared 293 cells treated with insulin (induces phosphorylation of tyrosine residues) with untreated cells, and the number of bands identified between the two treatments was indistinguishable (407). Therefore, the presence and/or significance of tyrosine phosphorylation in the NS5A phenotype remains an open question and it was not surprising to not have identified phospho-tyrosine residues in this investigation

5.2.10 NS5A protein production from non-replicative phosphomutants versus GND

An interesting observation was made involving the production of NS5A protein from the JFH1 mutants defective in RNA replication. The S229A mutation results in no measurable JFH1 genome replication and S229D mutant exhibits extremely weak RNA replication. However, T210D and S235A, while also exhibiting very reduced levels of RNA replication (and undetectable titers of infectious virus), do exhibit very low levels of NS5A protein at 72hpe. Initially, this was believed to be the result of translating input RNA, but the absence of NS5A protein in the GND mutant experiments indicated that this was unlikely to be the case (Fig.4.9). Two possible mechanisms include: 1) the mutations in NS5A severely inhibit RNA replication competency, but a small amount of activity still exists albeit it extremely inefficiently. 2) NS5A is known to have the capacity to bind RNA and may still maintain a binding/protective mechanism shielding input RNA from degradation in the absence of replication.

5.2.11 NS5A phosphorylation at early-time points post electroporation

It is generally accepted that NS5A is basally phosphorylated following liberation from the HCV polyprotein. This species then serves as a scaffold for hyperphosphorylation (188,276,277). In support of this, ³⁵S Methionine pulse-chase experiments revealed trace amounts of NS5A detected at the end of the labeling period, but ³²P labeled NS5A was only detectable 20 minutes after the chase period (188). Neddermann et al., 1999, utilizing ³⁵S methionine pulse-chase experiments with NS5A from the pcD3-5A genotype 1b polyprotein expressed in Hep3B cells evaluated phospho-proteoform appearance. p56 was detected 15 minutes after labeling and p58 was of equal intensity following two

hours of incubation time, therefore, p56 is released from the polyprotein and used as a substrate for hyperphosphorylation (276). These observations were also confirmed in pulse-chase experiments utilizing the Con1b replicon where p56 was produced before p58 (277). While this explanation is plausible, the functional nature of the two phospho-proteoforms of NS5A at early times has not been heavily studied. In this thesis, with any of the model systems evaluated, hyperphosphorylated NS5A (p58) was present at higher levels (compared to p56) at early points post electroporation (Fig.4.11). The p58/p56 ratios from electroporation of infectious JFH1 were 3.3 and 1.5 at the earliest detectable time-points, 24 and 36 hpe (Fig.4.11.B&C). At 48 hpe the ratio switches and p56 becomes the more abundant form with a mean ratio of 0.71 followed by 0.58 at 72 hpe (Fig.4.11.B&C). These observations were confirmed in SG JFH1 and SG JFH1-NS5A-HBH replicons, albeit the HBH-tagged NS5A SG replicon displayed the trend at a delayed time point, consistent with its delay in RNA replication (Fig.4.11.D, E, F).

While this is a novel observation, there have been other cases of differential p58/p56 ratios being reported. McCormick et al., 2006 showed that HCV replicons containing the GND mutants delivered via baculovirus had higher levels of p58 protein than their wt counterparts and that hindering polyprotein translation correlated with p58 abundance (280). These observations may help to explain the high p58/p56 ratio obtained at early time-points post electroporation. To establish a productive replication, HCV must translate its polyprotein to produce functional NS proteins to establish the replisome. Therefore, the process of polyprotein translation preceding genome replication may explain the initially elevated levels of p58. Differential decay rates of p56 and p58 may

offer an alternative explanation as the p58 produced by JFH1 may have a longer half-life thereby appearing to be the dominant form. However, Pietschmann et al., 2001, established that the half-life of the p56 was 16 hours and p58 was seven hours when NS5A was produced by the Con1b replicon (277). A potential reconciliation is that the stability of NS5A phospho-proteoforms may differ by genotype.

On the contrary, an overabundance of p58 at early time-points post electroporation may indicate that p58 is required to establish HCV genome replication while p56 is needed for later steps, perhaps with virion production. Interestingly, Fridell et al., 2013 investigated phospho-proteoform levels in relation to JFH1 replication and packaging utilizing phosphoablatant and phosphomimetic mutations of the serines of the LCS1 and concluded that a large abundance of p58 results in higher replication levels while p56 promotes viral packaging (299). The results presented in this thesis are not at odds with this hypothesis.

5.2.12 Reduction of p58 levels in long-term passage of established SG JFH1 Huh7.5 replicon cells

Studies exist that report upon prolonged cell culture passage, HCV SG replicon cell lines show decreased p58 phospho-proteoform levels (141,282,304). Ross-Thriepland et al., 2014 using an established SG JFH1 Huh-7 cell line model showed that after 40 passages the percentage of total NS5A hyperphosphorylation dropped by 40% and that this change was not due to nucleotide changes in the NS5A sequence (304). This investigation also evaluated the consequences of longer-term passage and showed that the p58/p56 ratio drops by 16% over ten weeks following initial electroporation. As was observed by

Ross-Thriepland et al., 2014 there were no sequence alterations within NS5A, therefore, reduced p58 was not due to loss of a phosphoacceptor site (data not shown). One other hypothesis for decreased p58 levels is that a cellular kinase responsible for p58 becomes exhausted over time. To assess this, wt SG JFH1 or full-length JFH1 RNA was introduced into ten-week-old SG JFH1-HBH-NS5A Huh7.5 cell lines. As the HBH-tagged NS5A protein is 11 kDa larger, it was possible to evaluate the two species independently. While wt NS5A from SG JFH1 or full-length JFH1 introduced into the HBH-tagged NS5A SG replicon cells had a lower p58/p56 ratio than did RNA electroporated into naïve Huh7.5 cells at 24hpe (1.4 and 1.7 versus 3.0 and 3.3), by 72hpe the ratios were 0.74 and 0.66 comparable to the 0.59 ratio produced by wt. This suggests that the elements required for p58 production are available and therefore the kinase exhaustion is not the mechanism responsible for depleted p58 abundance at least in replicon cells passaged over a two and a half month period.

An alternative hypothesis to the exhaustion concept is the possibility that kinase accessibility to NS5A changes. The form of NS5A required for establishing functional replication may be freely accessible to the kinase(s) responsible for hyperphosphorylation, but after a replisome has been established, NS5A is no longer freely accessible, spatially, to the kinase(s).

5.2.13 Issues involving phosphorylation studies

The number of caveats associated with phosphorylation studies is tremendous. While it would be easy to dismiss phosphomutants that exhibit an altered phenotype as merely

“protein destabilizing mutants,” this is unlikely to be the case overall. The mutants presented here (and in fact all of the mutants discussed in the literature) do of course need to be evaluated for alterations in stability, localization, and interaction that could compromise analysis, but these studies do represent a start. What additionally needs to happen is a more quantitative understanding of the NS5A phosphorylation.

For example, in most studies utilizing mass spectrometry and database analysis for studying phosphorylation, minimal mention is made of site occupancy issues. In order to identify the phosphates present on the peptides, enrichment is applied for these species, and as a result, the non-phosphorylated peptides are lost. As such, the phosphorylated species may be present at a minuscule level compared to the non-phosphorylated. Direct comparisons are difficult as a phosphopeptide is chemically distinct from its non-phosphorylated counterpart and as such may affect its charge, ionization, and elution into the mass spectrometer and thus direct quantitative comparisons difficult (297).

Identifying phosphopeptides without the ability to determine their site occupancy could overemphasize spurious and/or biologically irrelevant phosphorylation events.

Conversely, the act of not observing a phosphorylation site does not necessarily imply that it does not exist. Factors already discussed such as peptide length, hydrophobicity and charge may have significant effects on chromatographic properties and ionization efficiency. These issues are of concern as few truly quantitative proteomics has been performed at this stage.

An additional level of complexity concerning NS5A is its diverse functions aiding in both HCV propagation and modulating the host cellular environment. Differentially phosphorylated NS5A may direct specific functions that require only a specific subset of NS5A phospho-proteoforms to elicit a particular function. At this point, total cellular protein is evaluated, and the ability to work at both a temporal and spatial level becomes a future step forward.

5.3 Conclusions

Elucidating the molecular mechanisms ultimately responsible for HCV pathogenesis is a premier step required in the development of therapeutic interventions and a protective vaccine. The purpose of this study was to understand fundamental aspects of the HCV NS5A protein by: 1) implement a novel tandem affinity purification technique to identifying host proteins interactions and 2) delineating the sites and functions of phosphorylated residues within NS5A. Chapter three successfully addressed the first hypothesis as NS5A interacting proteins were identified utilizing native state and denatured cross-linked TAP methodology. The optimization of the TAP methodology resulted in the creation of a protocol that could be easily applied to any protein expressed in mammalian cell culture. Using Co-IP and colocalization experiments, CCAR2 was confirmed for the first time as a specific NS5A interacting protein. The interaction with NS5A was shown to occur in the cytoplasm, as expected, even though CCAR2 is often referred to as a nuclear protein. Identification of CCAR2 as an NS5A interacting protein may further mechanistic insights into HCV pathogenesis. Given CCAR2's regulatory functions in both apoptosis and carcinogenesis identification of this PPI may resulting in

more thorough understand of HCV induction of HCC. Chapter four evaluated several NS5A purification strategies in combination with mass spectrometry/database searching to extend the mapping of NS5A phosphorylation. Phosphopeptides containing 28 phosphoacceptor sites were identified with the specific residues assigned for 26 of them. In addition to confirming the six previously identified NS5A phosphorylated residues, 20 novel phosphorylated sites were identified, several from SG replicons. Identification of so many phosphorylated residues in the NS5A protein reveals the highly phosphorylated nature of NS5A. The extensive number of phosphorylated residues furthers the hypothesis that phosphorylation regulates the functions of NS5A. A major hurdle to identifying the consequences of NS5A phosphorylation has been the lack of phosphorylated sites conclusively identified in an *ex vivo* model. By now having conclusively identified 28 sites these provide a much-needed scaffold for future studies such as the identification of the NS5A phosphorylating kinases or the role of phosphorylation in facilitating protein interactions essential to HCV propagation. Both the kinases and interacting host proteins could present themselves as viable anti-HCV targets not amenable to the mutative nature of the HCV genome. Mutation of these sites to alanine (phosphoablatant) or an aspartic acid (phosphomimetic) residue in the context of a JFH1 infectious virus clone revealed that the majority of mutations had no impact on the HCV life cycle with some exceptions. The replicative capacity of JFH1 mutants T204D, T210A/D, S225D, S229A/D, S232A/D, S235A/D, S238A/D, T334A/D, and T363A/D was reduced compare to wt JFH1. Furthermore, T210D, S229A, S229D, and S235A mutants did not produce infectious virus indicating that phosphorylation of T210 is deleterious to HCV propagation but phosphorylation of S235 is required. While it was

generally thought that the predomination of p56 or p58 represented a possible mechanistic switch between viral replication and packaging, this study revealed that this mechanism not reliant on phosphorylation status of a single site identified in this study. This revealed a regulation of the HCV life cycle by NS5A phosphorylation is likely very complicated and may be reliant on sequential, multiple, or redundant phosphorylation events. A novel observation was made that electroporated JFH1 RNA leads to production of NS5A predominately in its hyperphosphorylated (p58) form followed by a switch to mostly the basally phosphorylated (p56) form past 72 hpe. This observation may reveal that hyperphosphorylated NS5A is required in the early events of HCV infection and a further target to halt the commencement of HCV propagation.

5.4 Future Directions

In this investigation, a specific interaction was established between NS5A-2a and CCAR2 using multiple methodologies. Revealing the NS5A-2a binding site(s) on CCAR2 could reveal possible consequences of the interaction. The N-terminus of CCAR2 is critical to its functions; N-terminal cleavage of CCAR2 sensitizes cells to apoptosis (381) and SIRT1, HDAC3, and SUV39H1 bind near the N-terminus (360–363). CCAR2 negatively regulates acetylation of p53 by SIRT1, leaving p53 acetylated on K382 (360,361,392) and interference with p53 deacetylation increases p53 transactivation and apoptosis (360,361). Therefore, K382 p53 acetylation could be quantified in the presence and absence of NS5A-2a. This could reveal a relationship between NS5A expression and CCAR2 cellular functions and may reveal a mechanism of p53 regulation by NS5A. Given that tight regulation of p53 is so important to cellular transformation a

role for NS5A in the development of HCC could be established. Furthermore, studies involving the reduction and overexpression of the CCAR2 protein could be used to investigate loss or gain of function effects on the JFH1 life cycle and determine if the NS5A/CCAR2 interaction is a requirement for successful HCV propagation. These gain and loss experiments could reveal if CCAR2 and its functions could provide viable anti-HCV targets.

The specificity of NS5A-2a interactions with CDK12, OGDH, SOD1, NKRF, and the TOM complex should be followed up. xTAP revealed an interaction between NS5A-2a and the TOM complex. Although Co-IP results determined that the NS5A-2a/TOM22 interaction was not specific the caveat of TOM22 (339) acting as a chaperone may have influenced this result. Therefore, the interaction between NS5A-2a and the TOM complex could be further specified by using Co-IPs to determine if NS5A-2a specifically interacts with other members of the TOM complex. The NS5A-2a/TOM complex interaction could be involved in importing NS5A into the mitochondria or NS5A-2a may be influencing the import process of other proteins. Given that NS5A has been viewed in the mitochondria and mitochondrial dysfunction has been correlated with NS5A-2a expression (191), understanding the role of the TOM complex may provide insight into the underlying mechanisms.

CDK12 provides an interesting candidate given its kinase function and the highly phosphorylated nature of NS5A-2a. If an NS5A-2a/CDK12 interaction was deemed essential to HCV propagation, a CDK12 inhibitor was recently developed (408) and

targeting CDK12 could potentially provide a host protein target as an alternative to DAAs. The NS5A-2a/TOM complex interaction could be involved in importing NS5A into the mitochondria and explain the mitochondrial dysfunction that has been correlated with NS5A-2a expression (191). Further confocal microscopy experiments should be applied first.

Precise identification of the phosphorylated residues in NS5A here has provided the framework for quantification studies. By adding known quantities of isotopically labeled synthetic NS5A-2a phosphopeptides into a wt NS5A-2a sample would allow for selected reaction monitoring for quantitative mass spectrometry analysis (409). Determining site occupancy especially with key residues that affect RNA replication and genome packaging may provide formation on the biological mechanisms of replication and packaging. Furthermore, quantifying a specific NS5A phosphorylation event would provide more biological relevance to a phosphorylated residue and help to narrow down the 28 for targeted studies. Identification of a predominant phosphoacceptor site within NS5A-2a provides a substrate to evaluate the specific kinase responsible for phosphorylation. Many kinase inhibitors are currently utilized in cancer chemotherapy and could potentially be adapted as an already safe anti-HCV therapy.

The incomplete overlap of phosphorylation mapping between the three NS5A sources, particularly the two SG replicon models suggests that there is more to be discerned. In particular, the application of purified HBH-tagged SG NS5A in the SG model applied to 491 separation should be able to discern the biochemical identity of p56 versus p58.

Additionally, it should not be discounted that there could be differences in NS5A between a SG replicon model and an infectious virus model as viral packaging may be influenced by particular phosphorylation events. We have already shown that the HBH NS5A tag can be inserted into JFH1 to produce infectious virus.

The phosphorylation status of NS5A influences its ability to interact with host proteins as such as hVAP-A and PI4KIII α (140,284). The PI4KIII α binding site in NS5A-2a contains phosphoacceptor sites T204 and T210 (284). Phosphomutants T204A/D could be used to assess the impact of phosphorylation on the NS5A/PI4KIII α interaction and whether phosphorylation repels PI4KIII α acting as the molecular switch for HCV to move from genome replication to viral packaging.

A paramount goal of any study in the field of infectious disease is to use the obtained knowledge to aid in the generation new therapeutics to ameliorate the disease. An NS5A-host PPI, if deemed essential for HCV propagation, could be used to disrupt the host protein's function using an aptamer to interrupt the interaction. The phosphorylated residues of NS5A-2a also provide a potential therapeutic target through an NS5A aptamer or specific kinase inhibitors. HCV infection often leads to devastating disease and the vast genetic diversity the mutagenic potential of HCV demands continued investigation into its pathogenic mechanisms.

Chapter 6: References

1. Mohd Hanafiah K, Groeger J, Flaxman AD, Wiersma ST. Global epidemiology of hepatitis C virus infection: new estimates of age-specific antibody to HCV seroprevalence. *Hepatology*. 2013 Apr;57(4):1333–42.
2. Group GBOHCW. Global burden of disease (GBD) for hepatitis C. *J Clin Pharmacol*. 2004 Jan;44(1):20–9.
3. Perz JF, Armstrong GL, Farrington LA, Hutin YJF, Bell BP. The contributions of hepatitis B virus and hepatitis C virus infections to cirrhosis and primary liver cancer worldwide. *J Hepatol*. 2006 Oct;45(4):529–38.
4. Daniels D, Grytdal S, Wasley A. Surveillance for acute viral hepatitis - United States, 2007. *MMWR Surveill Summ*. 2009 May 22;58(3):1–27.
5. El-Serag HB. Epidemiology of hepatocellular carcinoma in USA. *Hepatol Res*. 2007 Sep;37 Suppl 2(s2 Fourth JSH S):S88–94.
6. Ehemann C, Henley SJ, Ballard-Barbash R, Jacobs EJ, Schymura MJ, Noone AM, et al. Annual Report to the Nation on the status of cancer, 1975-2008, featuring cancers associated with excess weight and lack of sufficient physical activity. Vol. 118, *Cancer*. 2012. p. 2338–66.
7. Klevens RM, Hu DJ, Jiles R, Holmberg SD. Evolving epidemiology of hepatitis C virus in the United States. *Clin Infect Dis*. 2012 Jul;55 Suppl 1:S3-9.
8. Rein DB, Wittenborn JS, Weinbaum CM, Sabin M, Smith BD, Lesesne SB. Forecasting the morbidity and mortality associated with prevalent cases of pre-cirrhotic chronic hepatitis C in the United States. *Dig Liver Dis*. 2011

Jan;43(1):66–72.

9. Smith BD, Jorgensen C, Zibbell JE, Beckett GA. Centers for Disease Control and Prevention initiatives to prevent hepatitis C virus infection: a selective update. *Clin Infect Dis*. 2012 Jul;55 Suppl 1:S49-53.
10. Canadian Task Force on Preventive Health Care CTF on PH. Recommendations on hepatitis C screening for adults. *Can Med Assoc J*. 2017 Apr 24;189(16):E594–604.
11. Averhoff FM, Glass N, Holtzman D. Global burden of hepatitis C: considerations for healthcare providers in the United States. *Clin Infect Dis*. 2012 Jul;55 Suppl 1:S10-5.
12. Zeuzem S, Berg T, Moeller B, Hinrichsen H, Mauss S, Wedemeyer H, et al. Expert opinion on the treatment of patients with chronic hepatitis C. *J Viral Hepat*. 2009 Feb;16(2):75–90.
13. Billerbeck E, de Jong Y, Dorner M, de la Fuente C, Ploss A. Animal models for hepatitis C. *Curr Top Microbiol Immunol*. 2013 Jan;369:49–86.
14. Fletcher NF, Humphreys E, Jennings E, Osburn W, Lissauer S, Wilson GK, et al. Hepatitis C virus infection of cholangiocarcinoma cell lines. *J Gen Virol*. 2015;96(Pt 6):1380–8.
15. Fletcher NF, Wilson GK, Murray J, Hu K, Lewis A, Reynolds GM, et al. Hepatitis C virus infects the endothelial cells of the blood-brain barrier. *Gastroenterology*. 2012;142(3):634–43.
16. Laskus T, Radkowski M, Bednarska A, Wilkinson J, Adair D, Nowicki M, et al. Detection and analysis of hepatitis C virus sequences in cerebrospinal fluid. *J*

- Viol. 2002 Oct;76(19):10064–8.
17. Deforges S, Evlashev A, Perret M, Sodoyer M, Pouzol S, Scoazec J-Y, et al. Expression of hepatitis C virus proteins in epithelial intestinal cells in vivo. *J Gen Virol.* 2004;85(Pt 9):2515–23.
 18. Ducoulombier D, Roque-Afonso A-M, Di Liberto G, Penin F, Kara R, Richard Y, et al. Frequent compartmentalization of hepatitis C virus variants in circulating B cells and monocytes. *Hepatology.* 2004 Mar;39(3):817–25.
 19. Durand T, Di Liberto G, Colman H, Cammas A, Boni S, Marcellin P, et al. Occult infection of peripheral B cells by hepatitis C variants which have low translational efficiency in cultured hepatocytes. *Gut.* 2010 Jul;59(7):934–42.
 20. Nakai M, Seya T, Matsumoto M, Shimotohno K, Sakamoto N, Aly HH. The J6JFH1 Strain of Hepatitis C Virus Infects Human B-Cells with Low Replication Efficacy. *Viral Immunol.* 2014 Aug;27(6):285–94.
 21. MacParland SA, Pham TNQ, Gujar SA, Michalak TI. De novo infection and propagation of wild-type Hepatitis C virus in human T lymphocytes in vitro. *J Gen Virol.* 2006;87(Pt 12):3577–86.
 22. Sarhan MA, Pham TNQ, Chen AY, Michalak TI. Hepatitis C virus infection of human T lymphocytes is mediated by CD5. *J Virol.* 2012 Apr;86(7):3723–35.
 23. Sarhan MA, Chen AY, Michalak TI, Michalak T, Louie A. Differential Expression of Candidate Virus Receptors in Human T Lymphocytes Prone or Resistant to Infection with Patient-Derived Hepatitis C Virus. Bartosch B, editor. *PLoS One.* 2013 Apr 23;8(4):e62159.
 24. Sarhan MA, Chen AY, Russell RS, Michalak TI. Patient-derived hepatitis C virus

- and JFH-1 clones differ in their ability to infect human hepatoma cells and lymphocytes. *J Gen Virol.* 2012;93(PART 11):2399–407.
25. Orland JR, Wright TL, Cooper S. Acute hepatitis C. *Hepatology.* 2001 Feb;33(2):321–7.
 26. Kanzaki H, Takaki A, Yagi T, Ikeda F, Yasunaka T, Koike K, et al. A case of fulminant liver failure associated with hepatitis C virus. *Clin J Gastroenterol.* 2014 Apr 18;7(2):170–4.
 27. Sarin SK, Kumar M. Natural history of HCV infection. *Hepatol Int.* 2012 Oct 9;6(4):684–95.
 28. Thimme R, Oldach D, Chang K-M, Steiger C, Ray SC, Chisari F V. Determinants of Viral Clearance and Persistence during Acute Hepatitis C Virus Infection. *J Exp Med.* 2001;194(10):1395–406.
 29. Freeman AJ, Dore GJ, Law MG, Thorpe M, Von Overbeck J, Lloyd AR, et al. Estimating progression to cirrhosis in chronic hepatitis C virus infection. *Hepatology.* 2001 Oct;34(4 I):809–16.
 30. Zampino R, Marrone A, Restivo L, Guerrera B, Sellitto A, Rinaldi L, et al. Chronic HCV infection and inflammation: Clinical impact on hepatic and extra-hepatic manifestations. *World J Hepatol.* 2013 Oct 27;5(10):528–40.
 31. Thein HH, Yi Q, Dore GJ, Krahn MD. Estimation of stage-specific fibrosis progression rates in chronic hepatitis C virus infection: A meta-analysis and meta-regression. *Hepatology.* 2008 Aug;48(2):418–31.
 32. Lemon SM, McGivern DR. Is hepatitis C virus carcinogenic? *Gastroenterology.* 2012;142(6):1274–8.

33. Bruno S, Crosignani A, Maisonneuve P, Rossi S, Silini E, Mondelli MU. Hepatitis C virus genotype 1b as a major risk factor associated with hepatocellular carcinoma in patients with cirrhosis: A seventeen-year prospective cohort study. *Hepatology*. 2007 Nov;46(5):1350–6.
34. Rubbia-Brandt L, Leandro G, Spahr L, Giostra E, Quadri R, Malé PJ, et al. Liver steatosis in chronic hepatitis C: A morphological sign suggesting infection with HCV genotype 3. *Histopathology*. 2001;39(2):119–24.
35. Hourieux C, Patient R, Morin A, Blanchard E, Moreau A, Trassard S, et al. The genotype 3-specific hepatitis C virus core protein residue phenylalanine 164 increases steatosis in an in vitro cellular model. *Gut*. 2007 Sep;56(9):1302–8.
36. Balik I, Yilmaz N, Turkcapar N, Yasa H. Association of diabetes mellitus and chronic hepatitis C virus infection. *Hepatology*. 1999 Feb;30(2):584.
37. Imazeki F, Yokosuka O, Fukai K, Kanda T, Kojima H, Saisho H. Prevalence of diabetes mellitus and insulin resistance in patients with chronic hepatitis C: comparison with hepatitis B virus-infected and hepatitis C virus-cleared patients. *Liver Int*. 2008;28(3):355–62.
38. E Davis BE TM, Davis ADEF WA, Jeffrey G, Davis T. Successful Withdrawal of Insulin Therapy After Post-Treatment Clearance of Hepatitis C Virus in a Man with Type 2 Diabetes. *Am J Case Rep*. 2017;18:414–7.
39. Giordano TP, Henderson L, Landgren O, Chiao EY, Kramer JR, El-Serag H, et al. Risk of non-Hodgkin lymphoma and lymphoproliferative precursor diseases in US veterans with hepatitis C virus. *JAMA*. 2007 May 9;297(18):2010–7.
40. Su T-H, Liu C-J, Tseng T-C, Chou S-W, Liu C-H, Yang H-C, et al. Hepatitis C

- viral infection increases the risk of lymphoid-neoplasms: A population-based cohort study. *Hepatology*. 2016 Mar;63(3):721–30.
41. Lunel F, Musset L, Cacoub P, Frangeul L, Cresta P, Perrin M, et al. Cryoglobulinemia in chronic liver diseases: role of hepatitis C virus and liver damage. *Gastroenterology*. 1994 May;106(5):1291–300.
 42. Lai T-S, Lee M-H, Yang H-I, You S-L, Lu S-N, Wang L-Y, et al. Hepatitis C Viral Load, Genotype, and Increased Risk of Developing End-stage Renal Disease: REVEAL-HCV Study. *Hepatology*. 2017 Apr;
 43. Forton DM, Allsop JM, Main J, Foster GR, Thomas HC, Taylor-Robinson SD. Evidence for a cerebral effect of the hepatitis C virus. *Lancet*. 2001;358(9275):38–9.
 44. Rotermann M, Langlois K, Andonov A, Trubnikov M. Seroprevalence of hepatitis B and C virus infections: Results from the 2007 to 2009 and 2009 to 2011 Canadian health measures survey. *Health Reports*. 2013 Nov;24(11):1–13.
 45. Poordad F, McCone J, Bacon BR, Bruno S, Manns MP, Sulkowski MS, et al. Boceprevir for untreated chronic HCV genotype 1 infection. *N Engl J Med*. 2011 Mar 31;364(13):1195–206.
 46. Jacobson IM, McHutchison JG, Dusheiko G, Di Bisceglie AM, Reddy KR, Bzowej NH, et al. Telaprevir for previously untreated chronic hepatitis C virus infection. *N Engl J Med*. 2011 Jun 23;364(25):2405–16.
 47. Wu S, Kanda T, Nakamoto S, Imazeki F, Yokosuka O. Hepatitis C virus protease inhibitor-resistance mutations: Our experience and review. *World J Gastroenterol*. 2013 Dec 21;19(47):8940–8.

48. Lamarre D, Anderson PC, Bailey M, Beaulieu P, Bolger G, Bonneau P, et al. An NS3 protease inhibitor with antiviral effects in humans infected with hepatitis C virus. *Nature*. 2003 Nov 13;426(6963):186–9.
49. Gitto S, Gamal N, Andreone P. NS5A inhibitors for the treatment of hepatitis C infection. *J Viral Hepat*. 2017 Mar;24(3):180–6.
50. Eltahla AA, Luciani F, White PA, Lloyd AR, Bull RA. Inhibitors of the hepatitis C virus polymerase; mode of action and resistance. *Viruses*. 2015 Sep 29;7(10):5206–24.
51. McCauley JA, Rudd MT. Hepatitis C virus NS3/4a protease inhibitors. Vol. 30, *Current Opinion in Pharmacology*. 2016. p. 84–92.
52. Pearlman BL, Traub N. Sustained virologic response to antiviral therapy for chronic hepatitis C virus infection: A cure and so much more. *Clin Infect Dis*. 2011 Apr 1;52(7):889–900.
53. Martell M, Esteban JI, Quer J, Genescà J, Weiner A, Esteban R, et al. Hepatitis C virus (HCV) circulates as a population of different but closely related genomes: quasispecies nature of HCV genome distribution. *J Virol*. 1992 May;66(5):3225–9.
54. Geller R, Estada Ú, Peris JB, Andreu I, Bou J-V, Garijo R, et al. Highly heterogeneous mutation rates in the hepatitis C virus genome. *Nat Microbiol*. 2016 Apr 18;1(7):16045.
55. Bagaglio S, Uberti-Foppa C, Morsica G. Resistance Mechanisms in Hepatitis C Virus: implications for Direct-Acting Antiviral Use. *Drugs*. 2017 May 12;1–13.
56. Li G, De Clercq E. Current therapy for chronic hepatitis C: The role of direct-acting antivirals. Vol. 142, *Antiviral Research*. 2017. p. 83–122.

57. Gaetano JN. Benefit-risk assessment of new and emerging treatments for hepatitis C: focus on simeprevir and sofosbuvir. *Drug Healthc Patient Saf.* 2014 Jan;6:37–45.
58. Iyengar S, Tay-Teo K, Vogler S, Beyer P, Wiktor S, de Joncheere K, et al. Prices, Costs, and Affordability of New Medicines for Hepatitis C in 30 Countries: An Economic Analysis. Basu S, editor. *PLoS Med.* 2016 May 31;13(5):e1002032.
59. Feinstone SM, Kapikian AZ, Purcell RH, Alter HJ, Holland P V. Transfusion-Associated Hepatitis Not Due to Viral Hepatitis Type A or B. *N Engl J Med.* 1975 Apr 10;292(15):767–70.
60. Choo QL, Kuo G, Weiner AJ, Overby LR, Bradley DW, Houghton M. Isolation of a cDNA clone derived from a blood-borne non-A, non-B viral hepatitis genome. *Science.* 1989 Apr 21;244(4902):359–62.
61. Simmonds P, Bukh J, Combet C, Deléage G, Enomoto N, Feinstone S, et al. Consensus proposals for a unified system of nomenclature of hepatitis C virus genotypes. *Hepatology.* 2005 Oct;42(4):962–73.
62. Smith DB, Bukh J, Kuiken C, Muerhoff AS, Rice CM, Stapleton JT, et al. Expanded classification of hepatitis C virus into 7 genotypes and 67 subtypes: updated criteria and genotype assignment Web resource. *Hepatology.* 2014 Jan;59(1):318–27.
63. Hajarizadeh B, Grebely J, Dore GJ. Epidemiology and natural history of HCV infection. *Nat Rev Gastroenterol Hepatol.* 2013 Sep;10(9):553–62.
64. Fafi-Kremer S, Fofana I, Soulier E, Carolla P, Meuleman P, Leroux-Roels G, et al. Viral entry and escape from antibody-mediated neutralization influence hepatitis C

- virus reinfection in liver transplantation. *J Exp Med.* 2010;207(9):2019–31.
65. Kapoor A, Simmonds P, Gerold G, Qaisar N, Jain K, Henriquez JA, et al. Characterization of a canine homolog of hepatitis C virus. *Proc Natl Acad Sci.* 2011 Jul 12;108(28):11608–13.
66. Pfaender S, Walter S, Todt D, Behrendt P, Doerrbecker J, Wölk B, et al. Assessment of cross-species transmission of hepatitis C virus-related non-primate hepacivirus in a population of humans at high risk of exposure. Vol. 96, *Journal of General Virology.* 2015. p. 2636–42.
67. Catanese MT, Uryu K, Kopp M, Edwards TJ, Andrus L, Rice WJ, et al. Ultrastructural analysis of hepatitis C virus particles. *Proc Natl Acad Sci U S A.* 2013 Jun 4;110(23):9505–10.
68. Thomssen R, Bonk S, Propfe C, Heermann KH, Köchel HG, Uy A. Association of hepatitis C virus in human sera with beta-lipoprotein. *Med Microbiol Immunol.* 1992;181(5):293–300.
69. André P, Komurian-Pradel F, Deforges S, Perret M, Berland JL, Sodoyer M, et al. Characterization of Low- and Very-Low-Density Hepatitis C Virus RNA-Containing Particles. *J Virol.* 2002 Jul;76(14):6919–28.
70. Lindenbach BD. Virion Assembly and Release. In Springer Berlin Heidelberg; 2013. p. 199–218.
71. Bradley D, McCaustland K, Krawczynski K, Spelbring J, Humphrey C, Cook EH. Hepatitis C virus: buoyant density of the factor VIII-derived isolate in sucrose. *J Med Virol.* 1991 Jul;34(3):206–8.
72. Hijikata M, Shimizu YK, Kato H, Iwamoto A, Shih JW, Alter HJ, et al.

- Equilibrium Centrifugation Studies of Hepatitis C Virus: Evidence for Circulating Immune Complexes. *J Virol.* 1993;1953–8.
73. Lindenbach BD. Complete Replication of Hepatitis C Virus in Cell Culture. *Science* (80-). 2005;309(5734):623–6.
74. Lindenbach BD, Rice CM. The ins and outs of hepatitis C virus entry and assembly. *Nat Rev Micro.* 2013 Sep 10;11(10):688–700.
75. Chang K-S, Jiang J, Cai Z, Luo G. Human apolipoprotein e is required for infectivity and production of hepatitis C virus in cell culture. *J Virol.* 2007 Dec;81(24):13783–93.
76. Veyres G, Dubuisson J, Pietschmann T. Incorporation of hepatitis C virus E1 and E2 glycoproteins: The keystones on a peculiar virion. Vol. 6, *Viruses*. Multidisciplinary Digital Publishing Institute; 2014. p. 1149–87.
77. Suzuki T, Aizaki H, Murakami K, Shoji I, Wakita T. Molecular biology of hepatitis C virus. *J Gastroenterol.* 2007 Jun;42(6):411–23.
78. Tsukiyama Kohara K, Iizuka N, Kohara M, Nomoto A. Internal Ribosome Entry Site within Hepatitis C Virus RNA. *J Virol.* 1992;66(3):1476–83.
79. Wang C, Sarnow P, Siddiqui A. Translation of Human Hepatitis C Virus RNA in Cultured Cells Is Mediated by an Internal Ribosome- Binding Mechanism. *J Virol.* 1993 Jun;67(6):3338–44.
80. Otto GA, Puglisi JD. The Pathway of HCV IRES-Mediated Translation Initiation. *Cell.* 2004;119:369–80.
81. Yanagi M, St Claire M, Emerson SU, Purcell RH, Bukh J. In vivo analysis of the 3' untranslated region of the hepatitis C virus after in vitro mutagenesis of an

- infectious cDNA clone. *Proc Natl Acad Sci U S A*. 1999;96(5):2291–5.
82. Song Y, Friebe P, Tzima E, Jünemann C, Bartenschlager R, Niepmann M. The hepatitis C virus RNA 3'-untranslated region strongly enhances translation directed by the internal ribosome entry site. *J Virol*. 2006 Dec;80(23):11579–88.
83. You S, Rice CM. 3' RNA elements in hepatitis C virus replication: kissing partners and long poly(U). *J Virol*. 2008 Jan 1;82(1):184–95.
84. Friebe P, Boudet J, Simorre JP, Bartenschlager R. Kissing-loop interaction in the 3' end of the hepatitis C virus genome essential for RNA replication. *J Virol*. 2005 Jan;79(1):380–92.
85. Romero-López C, Berzal-Herranz A. A long-range RNA-RNA interaction between the 5' and 3' ends of the HCV genome. *RNA*. 2009 Sep;15(9):1740–52.
86. Yasui K, Wakita T, Tsukiyama-Kohara K, Funahashi SI, Ichikawa M, Kajita T, et al. The native form and maturation process of hepatitis C virus core protein. *J Virol*. 1998 Jul;72(7):6048–55.
87. Xu Z, Choi J, Yen TS, Lu W, Strohecker A, Govindarajan S, et al. Synthesis of a novel hepatitis C virus protein by ribosomal frameshift. *EMBO J*. 2001 Jul 16;20(14):3840–8.
88. Vieyres G, Thomas X, Descamps V, Duverlie G, Patel AH, Dubuisson J. Characterization of the envelope glycoproteins associated with infectious hepatitis C virus. *J Virol*. 2010 Oct;84(19):10159–68.
89. Griffin SDC, Beales LP, Clarke DS, Worsfold O, Evans SD, Jaeger J, et al. The p7 protein of hepatitis C virus forms an ion channel that is blocked by the antiviral drug, Amantadine. *FEBS Lett*. 2003 Jan 30;535(1–3):34–8.

90. Steinmann E, Penin F, Kallis S, Patel AH, Bartenschlager R, Pietschmann T. Hepatitis C virus p7 protein is crucial for assembly and release of infectious virions. *PLoS Pathog.* 2007;3(7):0962–71.
91. Schregel V, Jacobi S, Penin F, Tautz N. Hepatitis C virus NS2 is a protease stimulated by cofactor domains in NS3. *Proc Natl Acad Sci U S A.* 2009 Mar 31;106(13):5342–7.
92. Bartenschlager R, Ahlborn-Laake L, Mous J, Jacobsen H. Nonstructural protein 3 of the hepatitis C virus encodes a serine-type proteinase required for cleavage at the NS3/4 and NS4/5 junctions. *J Virol.* 1993;67(7):3835–44.
93. Kim DW, Gwack Y, Han JH, Choe J. C-terminal domain of the hepatitis C virus NS3 protein contains an RNA helicase activity. *Biochem Biophys Res Commun.* 1995 Oct;215(1):160–6.
94. Brass V, Berke JM, Montserret R, Blum HE, Penin F, Moradpour D. Structural determinants for membrane association and dynamic organization of the hepatitis C virus NS3-4A complex. *Proc Natl Acad Sci U S A.* 2008 Sep 23;105(38):14545–50.
95. Einav S, Elazar M, Danieli T, Glenn JS. A nucleotide binding motif in hepatitis C virus (HCV) NS4B mediates HCV RNA replication. *J Virol.* 2004 Oct;78(20):11288–95.
96. Egger D, Wölk B, Gosert R, Bianchi L, Blum HE, Moradpour D, et al. Expression of Hepatitis C Virus Proteins Induces Distinct Membrane Alterations Including a Candidate Viral Replication Complex. *J Virol.* 2002 Jun;76(12):5974–84.
97. Kaneko T, Tanji Y, Satoh S, Hijikata M, Asabe S, Kimura K, et al. Production of

- two phosphoproteins from the NS5A region of the hepatitis C viral genome. *Biochem Biophys Res Commun.* 1994 Nov 30;205(1):320–6.
98. Appel N, Zayas M, Miller S, Krijnse-Locker J, Schaller T, Friebe P, et al. Essential role of domain III of nonstructural protein 5A for hepatitis C virus infectious particle assembly. *PLoS Pathog.* 2008 Mar;4(3):e1000035.
99. Kim S, Welsch C, Yi M, Lemon SM. Regulation of the production of infectious genotype 1a hepatitis C virus by NS5A domain III. *J Virol.* 2011 Jul;85(13):6645–56.
100. Simister P, Schmitt M, Geitmann M, Wicht O, Danielson UH, Klein R, et al. Structural and functional analysis of hepatitis C virus strain JFH1 polymerase. *J Virol.* 2009 Nov;83(22):11926–39.
101. Bartenschlager R, Lohmann V, Penin F. The molecular and structural basis of advanced antiviral therapy for hepatitis C virus infection. *Nat Rev Microbiol.* 2013 Jul;11(7):482–96.
102. Barth H, Schafer C, Adah MI, Zhang F, Linhardt RJ, Toyoda H, et al. Cellular binding of hepatitis C virus envelope glycoprotein E2 requires cell surface heparan sulfate. *J Biol Chem.* 2003 Oct 17;278(42):41003–12.
103. Monazahian M, Böhme I, Bonk S, Koch A, Scholz C, Grethe S, et al. Low density lipoprotein receptor as a candidate receptor for hepatitis C virus. *J Med Virol.* 1999 Mar;57(3):223–9.
104. Germe R, Crance J-M, Garin D, Guimet J, Lortat-Jacob H, Ruigrok RWH, et al. Cellular glycosaminoglycans and low density lipoprotein receptor are involved in hepatitis C virus adsorption. *J Med Virol.* 2002 Oct;68(2):206–15.

105. Owen DM, Huang H, Ye J, Gale M. Apolipoprotein E on hepatitis C virion facilitates infection through interaction with low-density lipoprotein receptor. *Virology*. 2009;394(1):99–108.
106. Scarselli E, Ansuini H, Cerino R, Roccasecca RM, Acali S, Filocamo G, et al. The human scavenger receptor class B type I is a novel candidate receptor for the hepatitis C virus. *Embo J*. 2002;21(19):5017–25.
107. Bartosch B, Dubuisson J, Cosset F-L. Infectious hepatitis C virus pseudo-particles containing functional E1-E2 envelope protein complexes. *J Exp Med*. 2003 Mar 3;197(5):633–42.
108. Zeisel MB, Koutsoudakis G, Schnober EK, Haberstroh A, Blum HE, Cosset FL, et al. Scavenger receptor class B type I is a key host factor for hepatitis C virus infection required for an entry step closely linked to CD81. *Hepatology*. 2007 Dec;46(6):1722–31.
109. Pileri P, Uematsu Y, Campagnoli S, Galli G, Falugi F, Petracca R, et al. Binding of hepatitis C virus to CD81. *Science*. 1998;282(5390):938–41.
110. Bertaux C, Dragic T. Different Domains of CD81 Mediate Distinct Stages of Hepatitis C Virus Pseudoparticle Entry. *J Virol*. 2006 May;80(10):4940–8.
111. Benedicto I, Molina-Jiménez F, Bartosch B, Cosset F-L, Lavillette D, Prieto J, et al. The tight junction-associated protein occludin is required for a postbinding step in hepatitis C virus entry and infection. *J Virol*. 2009 Aug;83(16):8012–20.
112. Ploss A, Evans MJ, Gaysinskaya VA, Panis M, You H, de Jong YP, et al. Human occludin is a hepatitis C virus entry factor required for infection of mouse cells. *Nature*. 2009 Feb 12;457(7231):882–6.

113. Martin DN, Uprichard SL. Identification of transferrin receptor 1 as a hepatitis C virus entry factor. *Proc Natl Acad Sci U S A*. 2013 Jun 25;110(26):10777–82.
114. Sainz B, Barretto N, Martin DN, Hiraga N, Imamura M, Hussain S, et al. Identification of the Niemann-Pick C1-like 1 cholesterol absorption receptor as a new hepatitis C virus entry factor. *Nat Med*. 2012;18(2):281–5.
115. Lupberger J, Zeisel MB, Xiao F, Thumann C, Fofana I, Zona L, et al. EGFR and EphA2 are host factors for hepatitis C virus entry and possible targets for antiviral therapy. *Nat Med*. 2011;17(5):589–95.
116. Evans MJ, von Hahn T, Tscherne DM, Syder AJ, Panis M, Wölk B, et al. Claudin-1 is a hepatitis C virus co-receptor required for a late step in entry. *Nature*. 2007 Apr 12;446(7137):801–5.
117. Farquhar MJ, Hu K, Harris HJ, Davis C, Brimacombe CL, Fletcher SJ, et al. Hepatitis C virus induces CD81 and claudin-1 endocytosis. *J Virol*. 2012 Apr;86(8):4305–16.
118. Meertens L, Bertaux C, Dragic T. Hepatitis C virus entry requires a critical postinternalization step and delivery to early endosomes via clathrin-coated vesicles. *J Virol*. 2006 Dec;80(23):11571–8.
119. Garry RF, Dash S. Proteomics computational analyses suggest that hepatitis C virus E1 and pestivirus E2 envelope glycoproteins are truncated class II fusion proteins. *Virology*. 2003;307(2):255–65.
120. Tong Y, Chi X, Yang W, Zhong J. Functional Analysis of Hepatitis C Virus (HCV) Envelope Protein E1 Using a trans-Complementation System Reveals a Dual Role of a Putative Fusion Peptide of E1 in both HCV Entry and

- Morphogenesis. *J Virol.* 2017 Apr 1;91(7):e02468-16.
121. Timpe JM, Stamatakis Z, Jennings A, Hu K, Farquhar MJ, Harris HJ, et al. Hepatitis C virus cell-cell transmission in hepatoma cells in the presence of neutralizing antibodies. *Hepatology.* 2008 Oct 16;47(1):17–24.
 122. Fan H, Qiao L, Kang K-D, Fan J, Wei W, Luo G. Attachment and Post-Attachment Receptors Important for Hepatitis C Virus Infection and Cell-to-Cell Transmission. *J Virol.* 2017 Apr 12;JVI.00280-17.
 123. Gosert R, Egger D, Lohmann V, Bartenschlager R, Blum HE, Bienz K, et al. Identification of the Hepatitis C Virus RNA Replication Complex in Huh-7 Cells Harboring Subgenomic Replicons. *J Virol.* 2003 May;77(9):5487–92.
 124. Boulant S, Montserret R, Hope RG, Ratinier M, Targett-Adams P, Lavergne JP, et al. Structural determinants that target the hepatitis C virus core protein to lipid droplets. *J Biol Chem.* 2006 Aug 4;281(31):22236–47.
 125. Counihan NA, Rawlinson SM, Lindenbach BD. Trafficking of hepatitis C virus core protein during virus particle assembly. Siddiqui A, editor. *PLoS Pathog.* 2011 Oct 20;7(10):e1002302.
 126. Masaki T, Suzuki R, Murakami K, Aizaki H, Ishii K, Murayama A, et al. Interaction of hepatitis C virus nonstructural protein 5A with core protein is critical for the production of infectious virus particles. *J Virol.* 2008 Aug 15;82(16):7964–76.
 127. Phan T, Beran RKF, Peters C, Lorenz IC, Lindenbach BD. Hepatitis C virus NS2 protein contributes to virus particle assembly via opposing epistatic interactions with the E1-E2 glycoprotein and NS3-NS4A enzyme complexes. *J Virol.* 2009 Sep

- 1;83(17):8379–95.
128. Miyanari Y, Atsuzawa K, Usuda N, Watashi K, Hishiki T, Zayas M, et al. The lipid droplet is an important organelle for hepatitis C virus production. *Nat Cell Biol.* 2007 Sep;9(9):1089–97.
 129. Dubuisson J, Hsu HH, Cheung RC, Greenberg HB, Russell DG, Rice CM. Formation and intracellular localization of hepatitis C virus envelope glycoprotein complexes expressed by recombinant vaccinia and Sindbis viruses. *J Virol.* 1994 Oct;68(10):6147–60.
 130. Wozniak AL, Griffin S, Rowlands D, Harris M, Yi M, Lemon SM, et al. Intracellular Proton Conductance of the Hepatitis C Virus p7 Protein and Its Contribution to Infectious Virus Production. Rice CM, editor. *PLoS Pathog.* 2010 Sep 2;6(9):e1001087.
 131. Gastaminza P, Cheng G, Wieland S, Zhong J, Liao W, Chisari F V. Cellular Determinants of Hepatitis C Virus Assembly, Maturation, Degradation, and Secretion. *J Virol.* 2008 Mar;82(5):2120–9.
 132. Lohmann V, Körner F, Koch J, Herian U, Theilmann L, Bartenschlager R. Replication of subgenomic hepatitis C virus RNAs in a hepatoma cell line. *Science.* 1999 Jul 2;285(5424):110–3.
 133. Woerz I, Lohmann V, Bartenschlager R. Hepatitis C virus replicons: dinosaurs still in business? *J Viral Hepat.* 2009 Jan 1;16(1):1–9.
 134. Blight KJ, Kolykhalov AA, Rice CM. Efficient initiation of HCV RNA replication in cell culture. *Science.* 2000 Dec 8;290(5498):1972–4.
 135. Krieger N, Lohmann V, Bartenschlager R. Enhancement of hepatitis C virus RNA

- replication by cell culture-adaptive mutations. *J Virol.* 2001 May;75(10):4614–24.
136. Guo J-T, Bichko V V, Seeger C. Effect of Alpha Interferon on the Hepatitis C Virus Replicon. *J Virol.* 2001 Sep;75(18):8516–23.
137. Lohmann V, Hoffmann S, Herian U, Penin F, Bartenschlager R. Viral and Cellular Determinants of Hepatitis C Virus RNA Replication in Cell Culture. *J Virol.* 2003 Mar;77(5):3007–19.
138. Lanford RE, Guerra B, Lee H, Averett DR, Pfeiffer B, Chavez D, et al. Antiviral Effect and Virus-Host Interactions in Response to Alpha Interferon, Gamma Interferon, Poly(I)-Poly(C), Tumor Necrosis Factor Alpha, and Ribavirin in Hepatitis C Virus Subgenomic Replicons. *J Virol.* 2003 Jan;77(2):1092–104.
139. Welker MW, Susser S, Welsch C, Perner D, Füller C, Kronenberger B, et al. Modulation of replication efficacy of the hepatitis C virus replicon Con1 by site-directed mutagenesis of an NS4B aminoterminal basic leucine zipper. *J Viral Hepat.* 2012 Nov;19(11):775–83.
140. Evans MJ, Rice CM, Goff SP. Phosphorylation of hepatitis C virus nonstructural protein 5A modulates its protein interactions and viral RNA replication. *Proc Natl Acad Sci U S A.* 2004;101(35):13038–43.
141. Appel N, Pietschmann T, Bartenschlager R. Mutational Analysis of Hepatitis C Virus Nonstructural Protein 5A : Potential Role of Differential Phosphorylation in RNA Replication and Identification of a Genetically Flexible Domain. *J Virol.* 2005;79(5):3187–94.
142. Bukh J, Pietschmann T, Lohmann V, Krieger N, Faulk K, Engle RE, et al. Mutations that permit efficient replication of hepatitis C virus RNA in Huh-7 cells

- prevent productive replication in chimpanzees. *Proc Natl Acad Sci U S A*. 2002 Oct 29;99(22):14416–21.
143. Pietschmann T, Lohmann V, Kaul A, Krieger N, Rinck G, Rutter G, et al. Persistent and transient replication of full-length hepatitis C virus genomes in cell culture. *J Virol*. 2002 Apr;76(8):4008–21.
144. Nakabayashi H, Taketa K, Miyano K, Yamane T, Sato J. Growth of Human Hepatoma Cell Lines with Differentiated Functions in Chemically Defined Medium. *Cancer Res*. 1982;42(September):3858–63.
145. Sainz B, Barretto N, Uprichard SL. Hepatitis C virus infection in phenotypically distinct Huh7 cell lines. *PLoS One*. 2009 Jan;4(8):e6561.
146. Blight KJ, McKeating JA, Rice CM. Highly permissive cell lines for subgenomic and genomic hepatitis C virus RNA replication. *J Virol*. 2002 Dec;76(24):13001–14.
147. Sumpter R, Loo Y-M, Foy E, Li K, Yoneyama M, Fujita T, et al. Regulating intracellular antiviral defense and permissiveness to hepatitis C virus RNA replication through a cellular RNA helicase, RIG-I. *J Virol*. 2005 Mar;79(5):2689–99.
148. Zhong J, Gastaminza P, Cheng G, Kapadia S, Kato T, Burton DR, et al. Robust hepatitis C virus infection in vitro. *Proc Natl Acad Sci U S A*. 2005 Jun 28;102(26):9294–9.
149. Kato T, Furusaka A, Miyamoto M, Date T, Yasui K, Hiramoto J, et al. Sequence analysis of hepatitis C virus isolated from a fulminant hepatitis patient. *J Med Virol*. 2001 Jul;64(3):334–9.

150. Kato T, Date T, Miyamoto M, Furusaka A, Tokushige K, Mizokami M, et al. Efficient Replication of the Genotype 2a Hepatitis C Virus Subgenomic Replicon. *Gastroenterology*. 2003 Dec;125(6):1808–17.
151. Wakita T, Pietschmann T, Kato T, Date T, Miyamoto M, Zhao Z, et al. Production of infectious hepatitis C virus in tissue culture from a cloned viral genome. *Nat Med*. 2005 Jul;11(7):791–6.
152. Murayama A, Date T, Morikawa K, Akazawa D, Miyamoto M, Kaga M, et al. The NS3 helicase and NS5B-to-3'X regions are important for efficient hepatitis C virus strain JFH-1 replication in Huh7 cells. *J Virol*. 2007;81(15):8030–40.
153. Shukla P, Faulk KN, Emerson SU. The entire core protein of HCV JFH1 is required for efficient formation of infectious JFH1 pseudoparticles. *J Med Virol*. 2010 May;82(5):783–90.
154. Schmitt M, Scrima N, Radujkovic D, Caillet-Saguy C, Simister PC, Friebe P, et al. A comprehensive structure-function comparison of hepatitis C virus strain JFH1 and J6 polymerases reveals a key residue stimulating replication in cell culture across genotypes. *J Virol*. 2011;85(6):2565–81.
155. Kaul A, Woerz I, Meuleman P, Leroux-Roels G, Bartenschlager R. Cell culture adaptation of hepatitis C virus and in vivo viability of an adapted variant. *J Virol*. 2007 Dec;81(23):13168–79.
156. Han Q, Xu C, Wu C, Zhu W, Yang R, Chen X. Compensatory mutations in NS3 and NS5A proteins enhance the virus production capability of hepatitis C reporter virus. *Virus Res*. 2009;145(1):63–73.
157. Kim CS, Keum SJ, Jang SK, Zhong J, Gastaminza P, Cheng G, et al. Generation of

- a Cell Culture-Adapted Hepatitis C Virus with Longer Half Life at Physiological Temperature. Sommer P, editor. PLoS One. 2011 Aug 4;6(8):e22808.
158. Liu S, Xiao L, Nelson C, Hagedorn C, Choo Q, Kuo G, et al. A Cell Culture Adapted HCV JFH1 Variant That Increases Viral Titers and Permits the Production of High Titer Infectious Chimeric Reporter Viruses. Jang SK, editor. PLoS One. 2012 Sep 13;7(9):1–12.
159. Jiang J, Luo G. Cell culture-adaptive mutations promote viral protein-protein interactions and morphogenesis of infectious hepatitis C virus. J Virol. 2012 Sep;86(17):8987–97.
160. Lindenbach BD, Meuleman P, Ploss A, Vanwolleghem T, Syder AJ, McKeating JA, et al. Cell culture-grown hepatitis C virus is infectious in vivo and can be recultured in vitro. Proc Natl Acad Sci U S A. 2006 Mar 7;103(10):3805–9.
161. Pietschmann T, Kaul A, Koutsoudakis G, Shavinskaya A, Kallis S, Steinmann E, et al. Construction and characterization of infectious intragenotypic and intergenotypic hepatitis C virus chimeras. Proc Natl Acad Sci U S A. 2006 May 9;103(19):7408–13.
162. Saeed M, Andreo U, Chung H-Y, Espiritu C, Branch AD, Silva JM, et al. SEC14L2 enables pan-genotype HCV replication in cell culture. Nature. 2015;524(7566):471–5.
163. Kolykhalov AA, Agapov E V., Blight KJ, Mihalik K, Feinstone SM, Rice CM. Transmission of Hepatitis C by Intrahepatic Inoculation with Transcribed RNA. Science (80-). 1997;277(5325):570–4.
164. Mercer DF, Schiller DE, Elliott JF, Douglas DN, Hao C, Rinfret A, et al. Hepatitis

- C virus replication in mice with chimeric human livers. *Nat Med.* 2001;7(8):927–33.
165. Dorner M, Horwitz JA, Robbins JB, Barry WT, Feng Q, Mu K, et al. A genetically humanized mouse model for hepatitis C virus infection. *Nature.* 2011 Jun 8;474(7350):208–11.
166. Dorner M, Horwitz JA, Donovan BM, Labitt RN, Budell WC, Friling T, et al. Completion of the entire hepatitis C virus life cycle in genetically humanized mice. *Nature.* 2013;501(7466):237–41.
167. Feng Y-M, Feng Y-M, Lu C, Han Y, Liu L, Sun X, et al. Tree shrew, a potential animal model for hepatitis C, supports the infection and replication of HCV in vitro and in vivo. *J Gen Virol.* 2017 Aug 1;98(8):2069–78.
168. Tellinghuisen TL, Marcotrigiano J, Gorbalenya AE, Rice CM. The NS5A protein of hepatitis C virus is a zinc metalloprotein. *J Biol Chem.* 2004 Nov 19;279(47):48576–87.
169. Brass V, Bieck E, Montserret R, Wölk B, Hellings JA, Blum HE, et al. An amino-terminal amphipathic alpha-helix mediates membrane association of the hepatitis C virus nonstructural protein 5A. *J Biol Chem.* 2002 Mar 8;277(10):8130–9.
170. Penin F, Brass V, Appel N, Ramboarina S, Montserret R, Ficheux D, et al. Structure and function of the membrane anchor domain of hepatitis C virus nonstructural protein 5A. *J Biol Chem.* 2004 Sep 24;279(39):40835–43.
171. Elazar M, Cheong KH, Liu P, Greenberg HB, Rice CM, Glenn JS. Amphipathic helix-dependent localization of NS5A mediates hepatitis C virus RNA replication. *J Virol.* 2003 May 15;77(10):6055–61.

172. Tellinghuisen TL, Marcotrigiano J, Rice CM. Structure of the zinc-binding domain of an essential component of the hepatitis C virus replicase. *Nature*. 2005 May 19;435(7040):374–9.
173. Love RA, Brodsky O, Hickey MJ, Wells PA, Cronin CN. Crystal structure of a novel dimeric form of NS5A domain I protein from hepatitis C virus. *J Virol*. 2009 May;83(9):4395–403.
174. Lambert SM, Langley DR, Garnett JA, Angell R, Hedgethorpe K, Meanwell NA, et al. The crystal structure of NS5A domain 1 from genotype 1a reveals new clues to the mechanism of action for dimeric HCV inhibitors. *Protein Sci*. 2014 Jun;23(6):723–34.
175. Cordek DG, Croom-Perez TJ, Hwang J, Hargittai MRS, Subba-Reddy C V, Han Q, et al. Expanding the proteome of an RNA virus by phosphorylation of an intrinsically disordered viral protein. *J Biol Chem*. 2014;
176. Feuerstein S, Solyom Z, Aladag A, Favier A, Schwarten M, Hoffmann S, et al. Transient structure and SH3 interaction sites in an intrinsically disordered fragment of the hepatitis C virus protein NS5A. *J Mol Biol*. 2012 Jul 20;420(4–5):310–23.
177. Solyom Z, Ma P, Schwarten M, Bosco ML, Polidori A, Durand G, et al. The disordered region of the HCV protein NS5A: Conformational dynamics, SH3 binding, and phosphorylation. *Biophys J*. 2015;109(7):1483–96.
178. Tellinghuisen TL, Foss KL, Treadaway JC, Rice CM. Identification of residues required for RNA replication in domains II and III of the hepatitis C virus NS5A protein. *J Virol*. 2008 Feb;82(3):1073–83.

179. Ross-Thriepland D, Amako Y, Harris M. The C terminus of NS5A domain II is a key determinant of hepatitis C virus genome replication, but is not required for virion assembly and release. *J Gen Virol*. 2013 May 1;94(Pt 5):1009–18.
180. Tellinghuisen TL, Foss KL, Treadaway J. Regulation of hepatitis C virion production via phosphorylation of the NS5A protein. *PLoS Pathog*. 2008;4(3).
181. Moradpour D, Evans MJ, Gosert R, Yuan Z, Blum HE, Goff SP, et al. Insertion of green fluorescent protein into nonstructural protein 5A allows direct visualization of functional hepatitis C virus replication complexes. *J Virol*. 2004 Jul;78(14):7400–9.
182. Schaller T, Appel N, Koutsoudakis G, Kallis S, Lohmann V, Pietschmann T, et al. Analysis of hepatitis C virus superinfection exclusion by using novel fluorochrome gene-tagged viral genomes. *J Virol*. 2007 May 1;81(9):4591–603.
183. McCormick CJ, Maucourant S, Griffin S, Rowlands DJ, Harris M. Tagging of NS5A expressed from a functional hepatitis C virus replicon. *J Gen Virol*. 2006 Mar 1;87(3):635–40.
184. Moradpour D, Brass V, Penin F. Function follows form: The structure of the N-terminal domain of HCV NS5A. *Hepatology*. 2005 Sep;42(3):732–5.
185. Huang L, Hwang J, Sharma SD, Hargittai MRS, Chen Y, Arnold JJ, et al. Hepatitis C virus nonstructural protein 5A (NS5A) is an RNA-binding protein. *J Biol Chem*. 2005 Oct 28;280(43):36417–28.
186. Quinkert D, Bartenschlager R, Lohmann V. Quantitative Analysis of the Hepatitis C Virus Replication Complex. *J Virol*. 2005 Nov;79(21):13594–605.
187. Suzuki T, Ishii K, Aizaki H, Wakita T. Hepatitis C viral life cycle. *Adv Drug Deliv*

Rev. 2007 Oct 10;59(12):1200–12.

188. Tanji Y, Kaneko T, Satoh S, Shimotohno K. Phosphorylation of hepatitis C virus-encoded nonstructural protein NS5A. *J Virol.* 1995;69(7):3980–6.
189. Reed KE, Gorbalenya a E, Rice CM. The NS5A/NS5 proteins of viruses from three genera of the family flaviviridae are phosphorylated by associated serine/threonine kinases. *J Virol.* 1998;72(7):6199–206.
190. Pawlotsky JM, Germanidis G. The non-structural 5A protein of hepatitis C virus. Vol. 6, *Journal of Viral Hepatitis.* Blackwell Science Ltd; 1999. p. 343–56.
191. Chu VC, Bhattacharya S, Nomoto A, Lin J, Zaidi SK, Oberley TD, et al. Persistent expression of hepatitis C virus non-structural proteins leads to increased autophagy and mitochondrial injury in human hepatoma cells. Deli MA, editor. *PLoS One.* 2011 Dec 2;6(12):e28551.
192. Lee C, Ma H, Hang JQ, Leveque V, Sklan EH, Elazar M, et al. The hepatitis C virus NS5A inhibitor (BMS-790052) alters the subcellular localization of the NS5A non-structural viral protein. *Virology.* 2011;414:10–8.
193. Tanimoto A, Ide Y, Arima N, Sasaguri Y, Padmanabhan R. The amino terminal deletion mutants of hepatitis C virus nonstructural protein NS5A function as transcriptional activators in yeast. *Biochem Biophys Res Commun.* 1997 Jul 18;236(2):360–4.
194. Ide Y, Zhang L, Chen M, Inchauspe G, Bahl C, Sasaguri Y, et al. Characterization of the nuclear localization signal and subcellular distribution of hepatitis C virus nonstructural protein NS5A. *Gene.* 1996 Dec 5;182(1–2):203–11.
195. Neufeldt CJ, Joyce MA, Levin A, Steenbergen RH, Pang D, Shields J, et al.

- Hepatitis C Virus-Induced Cytoplasmic Organelles Use the Nuclear Transport Machinery to Establish an Environment Conducive to Virus Replication. Siddiqui A, editor. *PLoS Pathog.* 2013 Oct 31;9(10):e1003744.
196. Levin A, Neufeldt CJ, Pang D, Wilson K, Loewen-Dobler D, Joyce MA, et al. Functional characterization of nuclear localization and export signals in hepatitis C virus proteins and their role in the membranous web. PECHEUR E-I, editor. *PLoS One.* 2014 Dec 8;9(12):e114629.
197. Enomoto N, Sakuma I, Asahina Y, Kurosaki M, Murakami T, Yamamoto C, et al. Comparison of full-length sequences of interferon-sensitive and resistant hepatitis C virus 1b: Sensitivity to interferon is conferred by amino acid substitutions in the NS5A region. Vol. 96, *Journal of Clinical Investigation.* American Society for Clinical Investigation; 1995. p. 224–30.
198. Enomoto N, Sakuma I, Asahina Y, Kurosaki M, Murakami T, Yamamoto C, et al. Mutations in the nonstructural protein 5A gene and response to interferon in patients with chronic hepatitis C virus 1b infection. *N Engl J Med.* 1996 Jan 11;334(2):77–81.
199. Shen C, Hu T, Shen L, Gao L, Xie W, Zhang J. Mutations in ISDR of NS5A gene influence interferon efficacy in Chinese patients with chronic hepatitis C virus genotype 1b infection. *J Gastroenterol Hepatol.* 2007 Nov;22(11):1898–903.
200. Hayashi K, Katano Y, Ishigami M, Itoh A, Hirooka Y, Nakano I, et al. Mutations in the core and NS5A region of hepatitis C virus genotype 1b and correlation with response to pegylated-interferon-alpha 2b and ribavirin combination therapy. *J Viral Hepat.* 2011 Apr;18(4):280–6.

201. Tan SL, Nakao H, He Y, Vijaysri S, Neddermann P, Jacobs BL, et al. NS5A, a nonstructural protein of hepatitis C virus, binds growth factor receptor-bound protein 2 adaptor protein in a Src homology 3 domain/ligand-dependent manner and perturbs mitogenic signaling. *Proc Natl Acad Sci U S A*. 1999 May 11;96(10):5533–8.
202. Macdonald A, Crowder K, Street A, McCormick C, Harris M. The hepatitis C virus NS5A protein binds to members of the Src family of tyrosine kinases and regulates kinase activity. *J Gen Virol*. 2004 Mar 1;85(3):721–9.
203. Nanda SK, Herion D, Liang TJ. Src homology 3 domain of hepatitis C virus NS5A protein interacts with Bin1 and is important for apoptosis and infectivity. *Gastroenterology*. 2006;130(3):794–809.
204. Shelton H, Harris M. Hepatitis C virus NS5A protein binds the SH3 domain of the Fyn tyrosine kinase with high affinity: mutagenic analysis of residues within the SH3 domain that contribute to the interaction. *Viol J*. 2008;5:24.
205. Chung Y-LL, Sheu M-LL, Yen S-HH. Hepatitis C virus NS5A as a potential viral Bcl-2 homologue interacts with Bax and inhibits apoptosis in hepatocellular carcinoma. *Int J Cancer*. 2003 Oct 20;107(1):65–73.
206. Huang Y, Staschke K, De Francesco R, Tan SL. Phosphorylation of hepatitis C virus NS5A nonstructural protein: A new paradigm for phosphorylation-dependent viral RNA replication? *Virology*. 2007;364(1):1–9.
207. Ross-Thriepland D, Harris M. Hepatitis C virus NS5A: enigmatic but still promiscuous 10 years on! *J Gen Virol*. 2015 Apr;96(Pt 4):727–38.
208. RCSB Protein Data Bank - RCSB PDB [Internet]. [cited 2017 Jun 27]. Available

from: <http://www.rcsb.org/pdb/home/home.do>

209. Berman HM, Westbrook J, Feng Z, Gilliland G, Bhat TN, Weissig H, et al. The Protein Data Bank. *Nucleic Acids Res.* 2000 Jan 1;28(1):235–42.
210. Macdonald A, Harris M. Hepatitis C virus NS5A: tales of a promiscuous protein. *J Gen Virol.* 2004 Sep;85(Pt 9):2485–502.
211. Aweya JJ, Tan Y-J. Modulation of programmed cell death pathways by the hepatitis C virus. *Front Biosci (Landmark Ed.)* 2011 Jan;16:608–18.
212. Deng L, Adachi T, Kitayama K, Bungyoku Y, Kitazawa S, Ishido S, et al. Hepatitis C virus infection induces apoptosis through a Bax-triggered, mitochondrion-mediated, caspase 3-dependent pathway. *J Virol.* 2008 Nov;82(21):10375–85.
213. Calabrese F, Pontisso P, Pettenazzo E, Benvegnù L, Vario A, Chemello L, et al. Liver cell apoptosis in chronic hepatitis C correlates with histological but not biochemical activity or serum HCV-RNA levels. *Hepatology.* 2000 May;31(5):1153–9.
214. Fischer R, Baumert T, Blum H-E. Hepatitis C virus infection and apoptosis. *World J Gastroenterol.* 2007 Sep 28;13(36):4865–72.
215. Wajant H, Pfizenmaier K, Scheurich P. Tumor necrosis factor signaling. *Cell Death Differ.* 2003;10(1350–9047 (Print)):45–65.
216. Ghosh AK, Majumder M, Steele R, Meyer K, Ray R, Ray RB. Hepatitis C virus NS5A protein protects against TNF-alpha mediated apoptotic cell death. *Virus Res.* 2000;67(2):173–8.
217. Miyasaka Y, Enomoto N, Kurosaki M, Sakamoto N, Kanazawa N, Kohashi T, et

- al. Hepatitis C virus nonstructural protein 5A inhibits tumor necrosis factor-alpha-mediated apoptosis in Huh7 cells. *J Infect Dis.* 2003 Nov 15;188(10):1537–44.
218. van Horssen R, Ten Hagen TLM, Eggermont AMM. TNF-alpha in cancer treatment: molecular insights, antitumor effects, and clinical utility. *Oncologist.* 2006 Apr 1;11(4):397–408.
219. Park K-J, Choi S-H, Lee SY, Hwang SB, Lai MMC. Nonstructural 5A Protein of Hepatitis C Virus Modulates Tumor Necrosis Factor -stimulated Nuclear Factor B Activation. *J Biol Chem.* 2002 Apr 12;277(15):13122–8.
220. Park K-J, Choi S-H, Choi D-H, Park J-M, Yie SW, Lee SY, et al. Hepatitis C Virus NS5A Protein Modulates c-Jun N-terminal Kinase through Interaction with Tumor Necrosis Factor Receptor-associated Factor 2. *J Biol Chem.* 2003 Aug 15;278(33):30711–8.
221. Majumder M, Ghosh AK, Steele R, Zhou XY, Phillips NJ, Ray R, et al. Hepatitis C virus NS5A protein impairs TNF-mediated hepatic apoptosis, but not by an anti-FAS antibody, in transgenic mice. *Virology.* 2002;294(1):94–105.
222. Pawlowski J, Kraft AS. Bax-induced apoptotic cell death. *Proc Natl Acad Sci U S A.* 2000 Jan 18;97(2):529–31.
223. Kruiswijk F, Labuschagne CF, Vousden KH. p53 in survival, death and metabolic health: a lifeguard with a licence to kill. *Nat Rev Mol Cell Biol.* 2015;16(7):393–405.
224. Majumder M, Ghosh AK, Steele R, Ray R, Ray RB. Hepatitis C Virus NS5A Physically Associates with p53 and Regulates p21/waf1 Gene Expression in a p53-Dependent Manner. *J Virol.* 2001 Feb;75(3):1401–7.

225. Lan K-H, Sheu M-L, Hwang S-J, Yen S-H, Chen S-Y, Wu J-C, et al. HCV NS5A interacts with p53 and inhibits p53-mediated apoptosis. *Oncogene*. 2002 Jul 18;21(31):4801–11.
226. Vanhaesebroeck B, Stephens L, Hawkins P. PI3K signalling: the path to discovery and understanding. *Nat Rev Mol Cell Biol*. 2012 Feb 23;13(3):195–203.
227. He Y, Nakao H, Tan S-L, Polyak SJ, Neddermann P, Vijaysri S, et al. Subversion of Cell Signaling Pathways by Hepatitis C Virus Nonstructural 5A Protein via Interaction with Grb2 and P85 Phosphatidylinositol 3-Kinase. *J Virol*. 2002 Sep;76(18):9207–17.
228. Street A, Macdonald A, Crowder K, Harris M. The Hepatitis C Virus NS5A Protein Activates a Phosphoinositide 3-Kinase-dependent Survival Signaling Cascade. *J Biol Chem*. 2004 Mar 26;279(13):12232–41.
229. Prokic I, Cowling BS, Laporte J. Amphiphysin 2 (BIN1) in physiology and diseases. Vol. 92, *Journal of Molecular Medicine*. Springer Berlin Heidelberg; 2014. p. 453–63.
230. Zech B, Kurtenbach A, Krieger N, Strand D, Blencke S, Morbitzer M, et al. Identification and characterization of amphiphysin II as a novel cellular interaction partner of the hepatitis C virus NS5A protein. *J Gen Virol*. 2003;84(3):555–60.
231. Masumi A, Aizaki H, Suzuki T, DuHadaway JB, Prendergast GC, Komuro K, et al. Reduction of hepatitis C virus NS5A phosphorylation through its interaction with amphiphysin II. *Biochem Biophys Res Commun*. 2005;336(2):572–8.
232. Okamoto T, Nishimura Y, Ichimura T, Suzuki K, Miyamura T, Suzuki T, et al. Hepatitis C virus RNA replication is regulated by FKBP8 and Hsp90. *EMBO J*.

- 2006;25(20):5015–25.
233. Kang C, Ye H, Chia J, Choi B-H, Dhe-Paganon S, Simon B, et al. Functional role of the flexible N-terminal extension of FKBP38 in catalysis. *Sci Rep.* 2013 Dec 22;3(1):2985.
234. Okamoto T, Omori H, Kaname Y, Abe T, Nishimura Y, Suzuki T, et al. A Single-Amino-Acid Mutation in Hepatitis C Virus NS5A Disrupting FKBP8 Interaction Impairs Viral Replication. *J Virol.* 2008 Apr;82(7):3480–9.
235. Wang J, Tong W, Zhang X, Chen L, Yi Z, Pan T, et al. Hepatitis C virus non-structural protein NS5A interacts with FKBP38 and inhibits apoptosis in Huh7 hepatoma cells. *FEBS Lett.* 2006 Aug 7;580(18):4392–400.
236. Peng L, Liang D, Tong W, Li J, Yuan Z. Hepatitis C virus NS5A activates the mammalian target of rapamycin (mTOR) pathway, contributing to cell survival by disrupting the interaction between FK506-binding protein 38 (FKBP38) and mTOR. *J Biol Chem.* 2010 Jul 2;285(27):20870–81.
237. Tani J, Shimamoto S, Mori K, Kato N, Moriishi K, Matsuura Y, et al. Ca²⁺/S100 proteins regulate HCV virus NS5A-FKBP8/FKBP38 interaction and HCV virus RNA replication. *Liver Int.* 2013 Aug;33(7):1008–18.
238. George A, Panda S, Kudmulwar D, Chhatbar SP, Nayak SC, Krishnan HH. Hepatitis C virus NS5A binds to the mRNA cap-binding eukaryotic translation initiation 4F (eIF4F) complex and up-regulates host translation initiation machinery through eIF4E-binding protein 1 inactivation. *J Biol Chem.* 2012 Feb 10;287(7):5042–58.
239. Panda S, Vedagiri D, Viveka TS, Harshan KH. A unique phosphorylation-

- dependent eIF4E assembly on 40S ribosomes co-ordinated by hepatitis C virus protein NS5A that activates internal ribosome entry site translation. *Biochem J.* 2014;462(2):291–302.
240. Gale Jr MJ, Korth MJ, Tang NM, Tan SL, Hopkins DA, Dever TE, et al. Evidence that hepatitis C virus resistance to interferon is mediated through repression of the PKR protein kinase by the nonstructural 5A protein. *Virology.* 1997 Apr 14;230(2):217–27.
241. Gale M, Blakely CM, Kwieciszewski B, Tan SL, Dossett M, Tang NM, et al. Control of PKR protein kinase by hepatitis C virus nonstructural 5A protein: molecular mechanisms of kinase regulation. *Mol Cell Biol.* 1998 Sep;18(9):5208–18.
242. Noguchi T, Satoh S, Noshi T, Hatada E, Fukuda R, Kawai A, et al. Effects of mutation in hepatitis C virus nonstructural protein 5A on interferon resistance mediated by inhibition of PKR kinase activity in mammalian cells. *Microbiol Immunol.* 2001 Dec;45(12):829–40.
243. Castelain S, Khorsi H, Roussel J, François C, Jaillon O, Capron D, et al. Variability of the nonstructural 5A protein of hepatitis C virus type 3a isolates and relation to interferon sensitivity. *J Infect Dis.* 2002 Mar;185(5):573–83.
244. Ramiere C, Rodriguez J, Enache LS, Lotteau V, Andre P, Diaz O. Activity of Hexokinase Is Increased by Its Interaction with Hepatitis C Virus Protein NS5A. *J Virol.* 2014 Mar;88(6):3246–54.
245. Wang Y, Jiang Y, Zhou J, Song W, Li J, Wang M, et al. Hepatitis C virus promotes hepatocellular carcinogenesis by targeting TIPE2, a new regulator of

- DNA damage response. *Tumor Biol.* 2016 Nov 30;37(11):15265–74.
246. de Chassey B, Navratil V, Tafforeau L, Hiet MS, Aublin-Gex A, Agaugué S, et al. Hepatitis C virus infection protein network. *Mol Syst Biol.* 2008;4(230):1–12.
247. Dolan PT, Zhang C, Khadka S, Arumugaswami V, Vangeloff AD, Heaton NS, et al. Identification and comparative analysis of hepatitis C virus–host cell protein interactions. *Mol Biosyst.* 2013 Dec;9(12):3199.
248. Germain M-A, Chatel-Chaix L, Gagne B, Bonneil E, Thibault P, Pradezynski F, et al. Elucidating novel hepatitis C virus-host interactions using combined mass spectrometry and functional genomics approaches. *Mol Cell Proteomics.* 2014 Jan 1;13(1):184–203.
249. von Mering C, Krause R, Snel B, Cornell M, Oliver SG, Fields S, et al. Comparative assessment of large-scale data sets of protein–protein interactions. *Nature.* 2002;417(6887):399–403.
250. Futschik ME, Chaurasia G, Herzel H. Comparison of human protein protein interaction maps. *Bioinformatics.* 2007 Mar;23(5):605–11.
251. Miernyk JA, Thelen JJ. Biochemical approaches for discovering protein-protein interactions. *Plant J.* 2008 Feb 4;53(4):597–609.
252. Brückner A, Polge C, Lentze N, Auerbach D, Schlattner U. Yeast two-hybrid, a powerful tool for systems biology. Vol. 10, *International Journal of Molecular Sciences*. Multidisciplinary Digital Publishing Institute (MDPI); 2009. p. 2763–88.
253. Lievens S, Lemmens I, Tavernier J. Mammalian two-hybrids come of age. Vol. 34, *Trends in Biochemical Sciences*. NIH Public Access; 2009. p. 579–88.
254. Berggård T, Linse S, James P. Methods for the detection and analysis of protein-

- protein interactions. *Proteomics*. 2007 Aug;7(16):2833–42.
255. Tagwerker C, Flick K, Cui M, Guerrero C, Dou Y, Auer B, et al. A tandem affinity tag for two-step purification under fully denaturing conditions: application in ubiquitin profiling and protein complex identification combined with in vivocross-linking. *Mol Cell Proteomics*. 2006 Apr;5(4):737–48.
256. Guerrero C, Tagwerker C, Kaiser P, Huang L. An integrated mass spectrometry-based proteomic approach: quantitative analysis of tandem affinity-purified in vivo cross-linked protein complexes (QTAX) to decipher the 26 S proteasome-interacting network. *Mol Cell Proteomics*. 2006 Feb;5(2):366–78.
257. Arnau J, Lauritzen C, Petersen GE, Pedersen J. Current strategies for the use of affinity tags and tag removal for the purification of recombinant proteins. Vol. 48, *Protein Expression and Purification*. 2006. p. 1–13.
258. Bramwell ME. Characterization of biotinylated proteins in mammalian cells using 125I-streptavidin. *J Biochem Biophys Methods*. 1987;15(3–4):125–32.
259. Chapman-Smith A, Cronan JE. The enzymatic biotinylation of proteins: a post-translational modification of exceptional specificity. *Trends Biochem Sci*. 1999 Sep;24(9):359–63.
260. Green N, Toms E. The properties of subunits of avidin coupled to sepharose. *Biochem J*. 1973;133(4):687–700.
261. Sutherland BW, Toews J, Kast J. Utility of formaldehyde cross-linking and mass spectrometry in the study of protein-protein interactions. Vol. 43, *Journal of Mass Spectrometry*. John Wiley & Sons, Ltd.; 2008. p. 699–715.
262. Fabris D, Yu ET. Elucidating the higher-order structure of biopolymers by

- structural probing and mass spectrometry: MS3D. Vol. 45, Journal of Mass Spectrometry. 2010. p. 841–60.
263. Dunham WH, Mullin M, Gingras AC. Affinity-purification coupled to mass spectrometry: Basic principles and strategies. *Proteomics*. 2012 May;12(10):1576–90.
264. Fenn JB, Mann M, Meng CK, Wong SF, Whitehouse CM. Electrospray ionization for mass spectrometry of large biomolecules. *Science* (80-). 1989 Oct 6;246(4926):64–71.
265. Aebersold R, Mann M. Mass spectrometry-based proteomics. *Nature*. 2003;422(6928):198–207.
266. Han X, Aslanian A, Yates JR. Mass spectrometry for proteomics. *Curr Opin Chem Biol*. 2008;12(5):483–90.
267. Choi YW, Tan YJ, Lim SG, Hong W, Goh PY. Proteomic approach identifies HSP27 as an interacting partner of the hepatitis C virus NS5A protein. *Biochem Biophys Res Commun*. 2004;318(2):514–9.
268. Chen YJ, Chen YH, Chow LP, Tsai YH, Chen PH, Huang CYF, et al. Heat shock protein 72 is associated with the hepatitis C virus replicase complex and enhances viral RNA replication. *J Biol Chem*. 2010 Sep 3;285(36):28183–90.
269. Salloum S, Wang H, Ferguson C, Parton RRG, Tai AAW, Appel N, et al. Rab18 Binds to Hepatitis C Virus NS5A and Promotes Interaction between Sites of Viral Replication and Lipid Droplets. Luo G, editor. *PLoS Pathog*. 2013 Aug 1;9(8):e1003513.
270. Ubersax J a, Ferrell JE. Mechanisms of specificity in protein phosphorylation. *Nat*

- Rev Mol Cell Biol. 2007;8(7):530–41.
271. Manning G, Plowman GD, Hunter T, Sudarsanam S. Evolution of protein kinase signaling from yeast to man. Vol. 27, Trends in Biochemical Sciences. 2002. p. 514–20.
 272. Vlastaridis P, Kyriakidou P, Chaliotis A, Van de Peer Y, Oliver SG, Amoutzias GD. Estimating the total number of phosphoproteins and phosphorylation sites in eukaryotic proteomes. *Gigascience*. 2017;6(2):1–11.
 273. Zha J, Harada H, Yang E, Jockel J, Korsmeyer SJ. Serine phosphorylation of death agonist BAD in response to survival factor results in binding to 14-3-3 not BCL-X(L). *Cell*. 1996 Nov 15;87(4):619–28.
 274. Kim E, Lee Y, Choi S, Song JJ. Structural basis of the phosphorylation dependent complex formation of neurodegenerative disease protein Ataxin-1 and RBM17. *Biochem Biophys Res Commun*. 2014;449(4):399–404.
 275. Kuropka B, Witte A, Sticht J, Waldt N, Majkut P, Hackenberger CPR, et al. Analysis of Phosphorylation-dependent Protein Interactions of Adhesion and Degranulation Promoting Adaptor Protein (ADAP) Reveals Novel Interaction Partners Required for Chemokine-directed T cell Migration. *Mol Cell Proteomics*. 2015 Nov 1;14(11):2961–72.
 276. Neddermann P, Clementi a, De Francesco R. Hyperphosphorylation of the hepatitis C virus NS5A protein requires an active NS3 protease, NS4A, NS4B, and NS5A encoded on the same polyprotein. *J Virol*. 1999;73(12):9984–91.
 277. Pietschmann T, Lohmann V, Rutter G, Kurpanek K, Bartenschlager R. Characterization of cell lines carrying self-replicating hepatitis C virus RNAs. *J*

- Viol. 2001 Feb 1;75(3):1252–64.
278. Liu Q, Bhat R a, Prince a M, Zhang P. The hepatitis C virus NS2 protein generated by NS2-3 autocleavage is required for NS5A phosphorylation. *Biochem Biophys Res Commun.* 1999;254(3):572–7.
279. Koch JO, Bartenschlager R. Modulation of hepatitis C virus NS5A hyperphosphorylation by nonstructural proteins NS3, NS4A, and NS4B. *J Virol.* 1999;73(9):7138–46.
280. McCormick CJ, Brown D, Griffin S, Challinor L, Rowlands DJ, Harris M. A link between translation of the hepatitis C virus polyprotein and polymerase function; possible consequences for hyperphosphorylation of NS5A. *J Gen Virol.* 2006;87(1):93–102.
281. Reed KE, Xu J, Rice CM. Phosphorylation of the hepatitis C virus NS5A protein in vitro and in vivo: properties of the NS5A-associated kinase. *J Virol.* 1997;71(10):7187–97.
282. Neddermann P, Quintavalle M, Pietro C Di, Clementi A, Cerretani M, Altamura S, et al. Reduction of Hepatitis C Virus NS5A Hyperphosphorylation by Selective Inhibition of Cellular Kinases Activates Viral RNA Replication in Cell Culture. *J Virol.* 2004;78(23):13306–14.
283. Fridell R a, Qiu D, Valera L, Wang C, Rose RE, Gao M. Distinct functions of NS5A in hepatitis C virus RNA replication uncovered by studies with the NS5A inhibitor BMS-790052. *J Virol.* 2011;85(14):7312–20.
284. Reiss S, Harak C, Romero-Brey I, Radujkovic D, Klein R, Ruggieri A, et al. The Lipid Kinase Phosphatidylinositol-4 Kinase III Alpha Regulates the

- Phosphorylation Status of Hepatitis C Virus NS5A. *PLoS Pathog.* 2013;9(5).
285. Xiong W, Yang J, Wang M, Wang H, Rao Z, Zhong C, et al. Vinexin β Interacts with Hepatitis C Virus NS5A, Modulating Its Hyperphosphorylation To Regulate Viral Propagation. *J Virol.* 2015;89(14):7385–400.
286. Kim J, Lee D, Choe J, Kim Jiyun, Daeyoup Lee and JC. Hepatitis C virus NS5A protein is phosphorylated by casein kinase II. *Biochem Biophys Res Commun.* 1999;257(3):777–81.
287. Coito C, Diamond DL, Neddermann P, Korth MJ, Katze MG. High-Throughput Screening of the Yeast Kinome : Identification of Human Serine / Threonine Protein Kinases That Phosphorylate the Hepatitis C Virus NS5A Protein High-Throughput Screening of the Yeast Kinome : Identification of Human Serine / Threonine Pro. *Society.* 2004;78(7):3502–13.
288. Dal Pero F, Di Maira G, Marin O, Bortoletto G, Pinna L a., Alberti A, et al. Heterogeneity of CK2 phosphorylation sites in the NS5A protein of different hepatitis C virus genotypes. *J Hepatol.* 2007;47(6):768–76.
289. Masaki T, Matsunaga S, Takahashi H, Nakashima K, Kimura Y, Ito M, et al. Involvement of Hepatitis C Virus NS5A Hyperphosphorylation Mediated by Casein Kinase I- α in Infectious Virus Production. *J Virol.* 2014;88(13):7541–55.
290. Quintavalle M, Sambucini S, Di Pietro C, De Francesco R, Neddermann P. The alpha isoform of protein kinase CKI is responsible for hepatitis C virus NS5A hyperphosphorylation. *J Virol.* 2006;80(22):11305–12.
291. Quintavalle M, Sambucini S, Summa V, Orsatti L, Talamo F, De Francesco R, et al. Hepatitis C virus NS5A is a direct substrate of casein kinase I-??, a cellular

- kinase identified by inhibitor affinity chromatography using specific NS5A hyperphosphorylation inhibitors. *J Biol Chem.* 2007;282(8):5536–44.
292. Qiu D, Lemm J a., O’Boyle DR, Sun JH, Nower PT, Nguyen V, et al. The effects of NS5A inhibitors on NS5A phosphorylation, polyprotein processing and localization. *J Gen Virol.* 2011;92(11):2502–11.
293. Chen Y-C, Su W-C, Huang J-Y, Chao T-C, Jeng K-S, Machida K, et al. Polo-like kinase 1 is involved in hepatitis C virus replication by hyperphosphorylating NS5A. *J Virol.* 2010;84(16):7983–93.
294. Ide Y, Tanimoto A, Sasaguri Y, Padmanabhan R. Hepatitis C virus NS5A protein is phosphorylated in vitro by a stably bound protein kinase from HeLa cells and by cAMP-dependent protein kinase A- α catalytic subunit. *Gene.* 1997;201(1–2):151–8.
295. Meistermann HH, Gao J, Golling S, Lamerz J, Le Pogam S, Tzouros M, et al. A novel immuno-competitive capture mass spectrometry strategy for protein-protein interaction profiling reveals that LATS kinases regulate HCV replication through NS5A phosphorylation. *Mol Cell Proteomics.* 2014 Nov;13(11):3040–8.
296. Lee KK-Y, Chen YY-H, Hsu SS-C, Yu M-J, Scheel T. Phosphorylation of Serine 235 of the Hepatitis C Virus Non-Structural Protein NS5A by Multiple Kinases. Ho Y-S, editor. *PLoS One.* 2016 Nov 22;11(11):e0166763.
297. Dephoure N, Gould KL, Gygi SP, Kellogg DR. Mapping and analysis of phosphorylation sites: a quick guide for cell biologists. *Mol Biol Cell.* 2013 Mar;24(5):535–42.
298. Steen H, Jebanathirajah JA, Rush J, Morrice N, Kirschner MW. Phosphorylation

- analysis by mass spectrometry: myths, facts, and the consequences for qualitative and quantitative measurements. *Mol Cell Proteomics*. 2006 Jan;5(1):172–81.
299. Fridell R a, Valera L, Qiu D, Kirk MJ, Wang C, Gao M. Intragenic complementation of hepatitis C virus NS5A RNA replication-defective alleles. *J Virol*. 2013;87(4):2320–9.
300. Reed KE, Rice CM. Identification of the major phosphorylation site of the hepatitis C virus H strain NS5A protein as serine 2321. *J Biol Chem*. 1999;274(39):28011–8.
301. Katze MG, Kwieciszewski B, Goodlett DR, Blakely CM, Neddermann P, Tan SL, et al. Ser(2194) is a highly conserved major phosphorylation site of the hepatitis C virus nonstructural protein NS5A. *Virology*. 2000;278(2):501–13.
302. Gilliver AN, Griffin S, Harris M. Identification of a novel phosphorylation site in hepatitis C virus NS5A. *J Gen Virol*. 2010;91(10):2428–32.
303. Lemay KL, Treadaway J, Angulo-Herrera I, Tellinghuisen TL. A Hepatitis C Virus NS5A Phosphorylation Site that Regulates RNA Replication. *J Virol*. 2013;87(2):1255–60.
304. Ross-Thriepland D, Harris M. Insights into the complexity and functionality of hepatitis C virus NS5A phosphorylation. *J Virol*. 2014;88(3):1421–32.
305. Eyre NS, Hampton-Smith RJ, Aloia AL, Eddes JS, Simpson KJ, Hoffmann P, et al. Phosphorylation of NS5A Serine-235 is essential to hepatitis C virus RNA replication and normal replication compartment formation. *Virology*. 2016 Feb 10;491:27–44.
306. Chong WM, Hsu S-C, Kao W-T, Lo C-W, Lee K-Y, Shao J-S, et al.

- Phosphoproteomics Identified an NS5A Phosphorylation Site Involved in Hepatitis C Virus Replication. *J Biol Chem*. 2016 Dec 23;291(8):3918–31.
307. Hsu S-C, Lo C-W, Pan T-C, Lee K-Y, Yu M-J. Serine 235 Is the Primary NS5A Hyper-Phosphorylation Site Responsible for HCV Replication. *J Virol*. 2017 Apr 26;JVI.00194-17.
308. Liu S, Xiao L, Nelson C, Hagedorn C. A Cell Culture Adapted HCV JFH1 Variant That Increases Viral Titers and Permits the Production of High Titer Infectious Chimeric Reporter Viruses. *PLoS One*. 2012;7(9):1–12.
309. Double Digest Finder | NEB [Internet]. [cited 2016 Dec 18]. Available from: <https://www.neb.com/tools-and-resources/interactive-tools/double-digest-finder>
310. Janes K. Microplate BCA Protein Assay [Internet]. 2009 [cited 2016 Dec 18]. Available from: <http://bme.virginia.edu/janes/protocols/index.html>
311. Suzuki K, Bose P, Leong-Quong RY, Fujita DJ, Riabowol K. REAP: A two minute cell fractionation method. *BMC Res Notes*. 2010;3(1):294.
312. Rappsilber J, Ishihama Y, Mann M. Stop and go extraction tips for matrix-assisted laser desorption/ionization, nanoelectrospray, and LC/MS sample pretreatment in proteomics. *Anal Chem*. 2003 Feb 1;75(3):663–70.
313. Matto M, Sklan EH, David N, Melamed-Book N, Casanova JE, Glenn JS, et al. Role for ADP ribosylation factor 1 in the regulation of hepatitis C virus replication. *J Virol*. 2011 Jan;85(2):946–56.
314. Stein DR, Hu X, Mccorrister SJ, Westmacott GR, Plummer FA, Ball TB, et al. High pH reversed-phase chromatography as a superior fractionation scheme compared to off-gel isoelectric focusing for complex proteome analysis.

- Proteomics. 2013 Aug;13(20):2956–66.
315. Wiśniewski JR, Zougman A, Nagaraj N, Mann M. Universal sample preparation method for proteome analysis. *Nat Methods*. 2009;6(5):359–62.
 316. NEBaseChanger [Internet]. [cited 2016 Dec 18]. Available from: <http://nebasechanger.neb.com/>
 317. Lindenbach BD. Measuring HCV infectivity produced in cell culture and in vivo. *Methods Mol Biol*. 2009 Jan;510:329–36.
 318. Qadri I, Iwahashi M, Simon F. Hepatitis C virus NS5A protein binds TBP and p53, inhibiting their DNA binding and p53 interactions with TBP and ERCC3. *Biochim Biophys Acta - Mol Cell Res*. 2002;1592(2):193–204.
 319. Wong JW, Albright RL, Wang N-HL. Immobilized Metal Ion Affinity Chromatography (IMAC) Chemistry and Bioseparation Applications. *Sep Purif Methods*. 1991 Jan 24;20(1):49–106.
 320. Li H, Yang X, Yang G, Hong Z, Zhou L, Yin P, et al. Hepatitis C Virus NS5A Hijacks ARFGAP1 To Maintain a Phosphatidylinositol 4-Phosphate-Enriched Microenvironment. *J Virol*. 2014 Jun 1;88(11):5956–66.
 321. Consortium U. UniProt: the universal protein knowledgebase. *Nucleic Acids Res*. 2017 Jan 4;45(D1):D158–69.
 322. Nourbakhsh M, Hauser H. Regression of NF- κ B The Transcriptional Silencer Protein NRF: A Repressor of NF- κ B Enhancers Inducible and constitutive activity of NF- κ B/rel enhancers. *Immunobiology*. 1997;198:65–72.
 323. Nourbakhsh M, Hauser H. Constitutive silencing of IFN- β promoter is mediated by NRF (NF- κ B-repressing factor), a nuclear inhibitor of NF- κ B. *EMBO J*.

- 1999;18(22):6415–25.
324. Nourbakhsh M, Hoffmann K, Hauser H. Interferon-beta promoters contain a DNA element that acts as a position-independent silencer on the NF-kappa B site. *EMBO J.* 1993;12(2):451–9.
325. Nourbakhsh M, Kälble S, Dörrie A, Hauser H, Resch K, Kracht M. The NF-κB Repressing Factor Is Involved in Basal Repression and Interleukin (IL)-1-induced Activation of IL-8 Transcription by Binding to a Conserved NF-κB-flanking Sequence Element. *J Biol Chem.* 2001 Feb 9;276(6):4501–8.
326. Feng X, Guo Z, Nourbakhsh M, Hauser H, Ganster R, Shao L, et al. Identification of a negative response element in the human inducible nitric-oxide synthase (iNOS) promoter: The role of NF-kappa B-repressing factor (NRF) in basal repression of the iNOS gene. *Proc Natl Acad Sci U S A.* 2002 Oct 29;99(22):14212–7.
327. Chen WC, Tseng CK, Chen YH, Lin CK, Hsu S, Wang SN, et al. HCV NS5A up-regulates COX-2 expression via IL-8-mediated activation of the ERK/JNK MAPK pathway. Polyak SJ, editor. *PLoS One.* 2015 Jul 31;10(7):e0133264.
328. García-Mediavilla MV, Sánchez-Campos S, González-Pérez P, Gómez-Gonzalo M, Majano PL, López-Cabrera M, et al. Differential contribution of hepatitis C virus NS5A and core proteins to the induction of oxidative and nitrosative stress in human hepatocyte-derived cells. *J Hepatol.* 2005 Oct;43(4):606–13.
329. Machida K, Cheng KT-H, Sung VM-H, Lee KJ, Levine AM, Lai MMC. Hepatitis C virus infection activates the immunologic (type II) isoform of nitric oxide synthase and thereby enhances DNA damage and mutations of cellular genes. *J*

- Virol. 2004 Aug;78(16):8835–43.
330. Moriyama M, Kato N, Otsuka M, Shao R-X, Taniguchi H, Kawabe T, et al. Interferon-beta is activated by hepatitis C virus NS5B and inhibited by NS4A, NS4B, and NS5A. *Hepatol Int*. 2007 Jun;1(2):302–10.
331. Girard S, Vossman E, Misek DE, Podevin P, Hanash S, Bréchet C, et al. Hepatitis C virus NS5A-regulated gene expression and signaling revealed via microarray and comparative promoter analyses. *Hepatology*. 2004 Sep 1;40(3):708–18.
332. Polyak SJ. Hepatitis C Virus Nonstructural 5A Protein Induces Interleukin-8 , Leading to Partial Inhibition of the Interferon-Induced Antiviral Response
Hepatitis C Virus Nonstructural 5A Protein Induces Interleukin-8 , Leading to Partial Inhibition of the Interfero. *J Virol*. 2001;75(13):6095–106.
333. Khachatoorian R, Ganapathy E, Ahmadi Y, Wheatley N, Sundberg C, Jung CL, et al. The NS5A-binding heat shock proteins HSC70 and HSP70 play distinct roles in the hepatitis C viral life cycle. *Virology*. 2014 Apr;454–455(1):118–27.
334. Gonzalez O, Fontanes V, Raychaudhuri S, Loo R, Loo J, Arumugaswami V, et al. The heat shock protein inhibitor quercetin attenuates hepatitis C virus production. *Hepatology*. 2009 Dec 1;50(6):1756–64.
335. Lai C-K, Jeng K-S, Machida K, Lai MMC. Association of Hepatitis C Virus Replication Complexes with Microtubules and Actin Filaments Is Dependent on the Interaction of NS3 and NS5A. *J Virol*. 2008 Sep 1;82(17):8838–48.
336. Isken O, Baroth M, Grassmann CW, Weinlich S, Ostareck DH, Ostareck-Lederer A, et al. Nuclear factors are involved in hepatitis C virus RNA replication. *RNA*. 2007 Oct 1;13(10):1675–92.

337. Li Y, Masaki T, Shimakami T, Lemon SM. hnRNP L and NF90 Interact with Hepatitis C Virus 5'-Terminal Untranslated RNA and Promote Efficient Replication. *J Virol*. 2014 Jul 1;88(13):7199–209.
338. Arima N, Kao CY, Licht T, Padmanabhan R, Sasaguri Y, Padmanabhan R. Modulation of cell growth by the hepatitis C virus nonstructural protein NS5A. *J Biol Chem*. 2001 Apr 20;276(16):12675–84.
339. Yano M, Terada K, Mori M. Mitochondrial Import Receptors Tom20 and Tom22 Have Chaperone-like Activity. *J Biol Chem*. 2004 Mar 12;279(11):10808–13.
340. Hiraike H, Wada-Hiraike O, Nakagawa S, Koyama S, Miyamoto Y, Sone K, et al. Identification of DBC1 as a transcriptional repressor for BRCA1. *Br J Cancer*. 2010 Mar 16;102(6):1061–7.
341. Pangon L, Mladenova D, Watkins L, Van Kralingen C, Currey N, Al-Sohaily S, et al. MCC inhibits beta-catenin transcriptional activity by sequestering DBC1 in the cytoplasm. *Int J Cancer*. 2015 Jan 1;136(1):55–64.
342. Sakurabashi A, Wada-Hiraike O, Hirano M, Fu H, Isono W, Fukuda T, et al. CCAR2 negatively regulates nuclear receptor LXR α by competing with SIRT1 deacetylase. *J Steroid Biochem Mol Biol*. 2015;149:80–8.
343. Scheel TKH, Prentoe J, Carlsen THR, Mikkelsen LS, Gottwein JM, Bukh J. Analysis of functional differences between hepatitis C virus NS5A of genotypes 1-7 in infectious cell culture systems. *PLoS Pathog*. 2012 Jan;8(5):e1002696.
344. Wose Kinge CN, Espiritu C, Prabdial-Sing N, Sithebe NP, Saeed M, Rice CM. Hepatitis C virus genotype 5a subgenomic replicons for evaluation of direct-acting antiviral agents. *Antimicrob Agents Chemother*. 2014 Sep;58(9):5386–94.

345. Ross-Thriepland D, Mankouri J, Harris M. Serine phosphorylation of the hepatitis C virus NS5A protein controls the establishment of replication complexes. *J Virol*. 2015;89(6):3123–35.
346. LaBarre DD, Lowy RJ. Improvements in methods for calculating virus titer estimates from TCID₅₀ and plaque assays. *J Virol Methods*. 2001 Aug;96(2):107–26.
347. De Maio. Heat shock proteins: facts, thoughts, and dreams. *Shock*. 1999 Jan;11(1):1–12.
348. Half EF, Versteeg M, Brondijk THC, Huizinga EG. When less becomes more: Optimization of protein expression in HEK293-EBNA1 cells using plasmid titration - A case study for NLRs. *Protein Expr Purif*. 2014;99:27–34.
349. Li Z, Düllmann J, Schiedlmeier B, Schmidt M, von Kalle C, Meyer J, et al. Murine leukemia induced by retroviral gene making. *Science* (80-). 2002;296:497.
350. Kendall RL, Bradshaw RA. Isolation and characterization of the methionine aminopeptidase from porcine liver responsible for the co-translational processing of proteins. *J Biol Chem*. 1992;267(29):20667–73.
351. Xiao Q, Zhang F, Nacev BA, Liu JO, Pei D. Protein N-terminal processing: Substrate specificity of escherichia coli and human methionine aminopeptidases. *Biochemistry*. 2010;49(26):5588–99.
352. ThermoFisherScientific. HisPur™ Cobalt Resin [Internet]. Vol. 747. 2012 [cited 2017 Aug 22]. Available from: <https://www.thermofisher.com/order/catalog/product/89964>
353. Kozer N, Schreiber G. Effect of Crowding on Protein-Protein Association Rates:

- Fundamental Differences between Low and High Mass Crowding Agents. *J Mol Biol.* 2004;336(3):763–74.
354. Zhou YL, Liao JM, Chen J, Liang Y. Macromolecular crowding enhances the binding of superoxide dismutase to xanthine oxidase: Implications for protein-protein interactions in intracellular environments. *Int J Biochem Cell Biol.* 2006;38(11):1986–94.
355. Tsai A, Carstens RP. An optimized protocol for protein purification in cultured mammalian cells using a tandem affinity purification approach. *Nat Protoc.* 2006;1(6):2820–7.
356. Kaiser P, Meierhofer D, Wang X, Huang L. Tandem affinity purification combined with mass spectrometry to identify components of protein complexes. *Methods Mol Biol.* 2008;439:309–26.
357. Maine GN, Gluck N, Zaidi IW, Burstein E. Bimolecular affinity purification (BAP): Tandem affinity purification using two protein baits. *Cold Spring Harb Protoc.* 2009 Nov;4(11):pdb.prot5318.
358. Mallick P, Schirle M, Chen SS, Flory MR, Lee H, Martin D, et al. Computational prediction of proteotypic peptides for quantitative proteomics. *Nat Biotechnol.* 2007;25(1):125–31.
359. Furey A, Moriarty M, Bane V, Kinsella B, Lehane M. Ion suppression; A critical review on causes, evaluation, prevention and applications. Vol. 115, *Talanta.* 2013. p. 104–22.
360. Zhao W, Kruse J-P, Tang Y, Jung SY, Qin J, Gu W. Negative regulation of the deacetylase SIRT1 by DBC1. *Nature.* 2008 Jan 31;451(7178):587–90.

361. Kim JE, Chen J, Lou Z. DBC1 is a negative regulator of SIRT1. *Nature*. 2008 Jan 31;451(7178):583–6.
362. Chini CCS, Escande C, Nin V, Chini EN. HDAC3 is negatively regulated by the nuclear protein DBC1. *J Biol Chem*. 2010 Dec 24;285(52):40830–7.
363. Li Z, Chen L, Kabra N, Wang C, Fang J, Chen J. Inhibition of SUV39H1 methyltransferase activity by DBC1. *J Biol Chem*. 2009 Apr 17;284(16):10361–6.
364. Ji Yu E, Kim S-H, Heo K, Ou C-Y, Stallcup MR, Kim JH. Reciprocal roles of DBC1 and SIRT1 in regulating estrogen receptor α activity and co-activator synergy. *Nucleic Acids Res*. 2011 Sep 1;39(16):6932–43.
365. Close P, East P, Dirac-Svejstrup AB, Hartmann H, Heron M, Maslen S, et al. DBIRD complex integrates alternative mRNA splicing with RNA polymerase II transcript elongation. *Nature*. 2012;484(7394):386–9.
366. Rivas-Estilla AM, Bryan-Marrugo OL, Trujillo-Murillo K, Pérez-Ibave D, Charles-Niño C, Pedroza-Roldan C, et al. Cu/Zn superoxide dismutase (SOD1) induction is implicated in the antioxidative and antiviral activity of acetylsalicylic acid in HCV-expressing cells. *Am J Physiol Gastrointest Liver Physiol*. 2012;302(11):G1264-73.
367. Ivanov A V, Smirnova OA, Ivanova ON, Masalova O V, Kochetkov SN, Isaguliantz MG. Hepatitis C virus proteins activate NRF2/ARE pathway by distinct ROS-dependent and independent mechanisms in HUH7 cells. *PLoS One*. 2011 Jan;6(9):e24957.
368. Smirnova OA, Ivanova ON, Bartosch B, Valuev-Elliston VT, Mukhtarov F, Kochetkov SN, et al. Hepatitis C Virus NS5A Protein Triggers Oxidative Stress by

- Inducing NADPH Oxidases 1 and 4 and Cytochrome P450 2E1. *Oxid Med Cell Longev.* 2016 Apr 20;2016:1–10.
369. Gong G, Waris G, Tanveer R, Siddiqui A. Human hepatitis C virus NS5A protein alters intracellular calcium levels, induces oxidative stress, and activates STAT-3 and NF-kappa B. *Proc Natl Acad Sci U S A.* 2001 Aug 14;98(17):9599–604.
370. Chung KM, Lee J, Kim J-E, Song O-K, Cho S, Lim J, et al. Nonstructural Protein 5A of Hepatitis C Virus Inhibits the Function of Karyopherin beta 3. *J Virol.* 2000 Jun 1;74(11):5233–41.
371. Becker T, Böttinger L, Pfanner N. Mitochondrial protein import: From transport pathways to an integrated network. *Trends Biochem Sci.* 2012;37(3):85–91.
372. Yang B, Wu Y-J, Zhu M, Fan S-B, Lin J, Zhang K, et al. Identification of cross-linked peptides from complex samples. *Nat Methods.* 2012 Sep;9(9):904–6.
373. Rinner O, Seebacher J, Walzthoeni T, Mueller LN, Beck M, Schmidt A, et al. Identification of cross-linked peptides from large sequence databases. *Nat Methods.* 2008 Apr;5(4):315–8.
374. Vogt DA, Camus G, Herker E, Webster BR, Tsou CL, Greene WC, et al. Lipid Droplet-Binding Protein TIP47 Regulates Hepatitis C Virus RNA Replication through Interaction with the Viral NS5A Protein. Siddiqui A, editor. *PLoS Pathog.* 2013 Apr 11;9(4):e1003302.
375. Kato T, Date T, Miyamoto M, Zhao Z, Mizokami M, Wakita T. Nonhepatic cell lines HeLa and 293 support efficient replication of the hepatitis C virus genotype 2a subgenomic replicon. *J Virol.* 2005 Jan;79(1):592–6.
376. Mo J, Boyle JP, Howard CB, Monie TP, Davis BK, Duncan JA. Pathogen sensing

- by nucleotide-binding oligomerization domain-containing protein 2 (NOD2) is mediated by direct binding to muramyl dipeptide and ATP. *J Biol Chem.* 2012 Jun 29;287(27):23057–67.
377. Askari N, Correa RG, Zhai D, Reed JC. Expression, purification, and characterization of recombinant NOD1 (NLRC1): A NLR family member. *J Biotechnol.* 2012;157(1):75–81.
378. Brix J, Dietmeier K, Pfanner N. Differential recognition of preproteins by the purified cytosolic domains of the mitochondrial import receptors Tom20, Tom22, and Tom70. *J Biol Chem.* 1997 Aug 15;272(33):20730–5.
379. Yoshizumi T, Ichinohe T, Sasaki O, Otera H, Kawabata S-I, Mihara K, et al. Influenza A virus protein PB1-F2 translocates into mitochondria via Tom40 channels and impairs innate immunity. *Nat Commun.* 2014 Aug 20;5:4713.
380. Rumlová M, Křížová I, Keprová A, Hadravová R, Doležal M, Strohalmová K, et al. HIV-1 protease-induced apoptosis. *Retrovirology.* 2014;11(1):37.
381. Sundararajan R, Chen G, Mukherjee C, White E. Caspase-dependent processing activates the proapoptotic activity of deleted in breast cancer-1 during tumor necrosis factor-alpha-mediated death signaling. *Oncogene.* 2005;24(31):4908–20.
382. Graham FL, Smiley J, Russell WC, Nairn R. Characteristics of a human cell line transformed by DNA from human adenovirus type 5. *J Gen Virol.* 1977 Jul 1;36(1):59–72.
383. Bae HJ, Chang YG, Noh JH, Kim JK, Eun JW, Jung KH, et al. DBC1 does not function as a negative regulator of SIRT1 in liver cancer. *Oncol Lett.* 2012 Nov;4(5):873–7.

384. Yang D, Liu N, Zuo C, Lei S, Wu X, Zhou F, et al. Innate host response in primary human hepatocytes with hepatitis C virus infection. Jhaveri R, editor. PLoS One. 2011 Nov 8;6(11):e27552.
385. Langley E, Pearson M, Faretta M, Bauer UM, Frye RA, Minucci S, et al. Human SIR2 deacetylates p53 and antagonizes PML/p53-induced cellular senescence. EMBO J. 2002;21(10):2383–96.
386. Wang RH, Sengupta K, Li C, Kim HS, Cao L, Xiao C, et al. Impaired DNA Damage Response, Genome Instability, and Tumorigenesis in SIRT1 Mutant Mice. Cancer Cell. 2008;14(4):312–23.
387. Luo J, Nikolaev AY, Imai S-I, Chen D, Su F, Shiloh A, et al. Negative control of p53 by Sir2alpha promotes cell survival under stress. Cell. 2001;107(2):137–48.
388. Imai S, Armstrong CM, Kaerberlein M, Guarente L. Transcriptional silencing and longevity protein Sir2 is an NAD-dependent histone deacetylase. Nature. 2000;403(6771):795–800.
389. Rodgers JT, Lerin C, Haas W, Gygi SP, Spiegelman BM, Puigserver P. Nutrient control of glucose homeostasis through a complex of PGC-1a and SIRT1. Nature. 2005;434(7029):113–8.
390. Yuan Z, Zhang X, Sengupta N, Lane WS, Seto E. SIRT1 Regulates the Function of the Nijmegen Breakage Syndrome Protein. Mol Cell. 2007 Jul 6;27(1):149–62.
391. Murayama A, Ohmori K, Fujimura A, Minami H, Yasuzawa-Tanaka K, Kuroda T, et al. Epigenetic Control of rDNA Loci in Response to Intracellular Energy Status. Cell. 2008 May;133(4):627–39.
392. Vaziri H, Dessain SK, Eaton EN, Imai SI, Frye RA, Pandita TK, et al.

- hSIR2SIRT1 functions as an NAD-dependent p53 deacetylase. *Cell*. 2001 Oct;107(2):149–59.
393. Li M, Luo J, Brooks CL, Gu W. Acetylation of p53 inhibits its ubiquitination by Mdm2. *J Biol Chem*. 2002;277(52):50607–11.
394. Escande C, Chini CCS, Nin V, Dykhouse KM, Novak CM, Levine J, et al. Deleted in breast cancer-1 regulates SIRT1 activity and contributes to high-fat diet-induced liver steatosis in mice. *J Clin Invest*. 2010 Feb;120(2):545–58.
395. Ha SY, Kim JH, Yang JW, Bae H, Cho HY, Park C-KK. Expression of DBC1 is associated with poor prognosis in hepatitis virus-related hepatocellular carcinoma. *Pathol Res Pract*. 2016;212(7):616–21.
396. Porter FW, Bochkov YA, Albee AJ, Wiese C, Palmenberg AC. A picornavirus protein interacts with Ran-GTPase and disrupts nucleocytoplasmic transport. *Proc Natl Acad Sci U S A*. 2006 Aug 15;103(33):12417–22.
397. Porter FW, Palmenberg AC. Leader-Induced Phosphorylation of Nucleoporins Correlates with Nuclear Trafficking Inhibition by Cardioviruses. *J Virol*. 2009 Feb 15;83(4):1941–51.
398. Ciomperlik JJ, Basta HA, Palmenberg AC. Cardiovirus Leader proteins bind exportins: Implications for virus replication and nucleocytoplasmic trafficking inhibition. *Virology*. 2016;487:19–26.
399. García-Dorival I, Wu W, Dowall S, Armstrong S, Touzelet O, Wastling J, et al. Elucidation of the ebola virus VP24 cellular interactome and disruption of virus biology through targeted inhibition of host-cell protein function. *J Proteome Res*. 2014;13(11):5120–35.

400. Mateo M, Carbonnelle C, Martinez MJ, Reynard O, Page A, Volchkova VA, et al. Knockdown of Ebola virus VP24 impairs viral nucleocapsid assembly and prevents virus replication. *J Infect Dis.* 2011 Nov 1;204(SUPPL. 3):S892–6.
401. Watt A, Moukambi F, Banadyga L, Groseth A, Callison J, Herwig A, et al. A Novel Life Cycle Modeling System for Ebola Virus Shows a Genome Length-Dependent Role of VP24 in Virus Infectivity. *J Virol.* 2014 Sep 15;88(18):10511–24.
402. Reid SP, Leung LW, Hartman AL, Martinez O, Shaw ML, Carbonnelle C, et al. Ebola virus VP24 binds karyopherin alpha1 and blocks STAT1 nuclear accumulation. *J Virol.* 2006 Jun 1;80(11):5156–67.
403. Asabe SI, Tanji Y, Satoh S, Kaneko T, Kimura K, Shimotohno K. The N-terminal region of hepatitis C virus-encoded NS5A is important for NS4A-dependent phosphorylation. *J Virol.* 1997;71(1):790–6.
404. Hirota M, Satoh S, Asabe S, Kohara M, Tsukiyama-Kohara K, Kato N, et al. Phosphorylation of nonstructural 5A protein of hepatitis C virus: HCV group-specific hyperphosphorylation. *Virology.* 1999;257(1):130–7.
405. Nakashima K, Takeuchi K, Chihara K, Horiguchi T, Sun X, Deng L, et al. HCV NS5A Protein Containing Potential Ligands for Both Src Homology 2 and 3 Domains Enhances Autophosphorylation of Src Family Kinase Fyn in B Cells. *PLoS One.* 2012;7(10):1–8.
406. Yamauchi S, Takeuchi K, Chihara K, Sun X, Honjoh C, Yoshiki H, et al. Hepatitis C Virus Particle Assembly Involves Phosphorylation of NS5A by the c-Abl Tyrosine Kinase. *J Biol Chem.* 2015 Jul 22;290(36):21857–64.

407. Tinti M, Nardoza AP, Ferrari E, Sacco F, Corallino S, Castagnoli L, et al. The 4G10, pY20 and p-TYR-100 antibody specificity: profiling by peptide microarrays. *N Biotechnol.* 2012 Jun 15;29(5):571–7.
408. Zhang T, Kwiatkowski N, Olson CM, Dixon-Clarke SE, Abraham BJ, Greifenberg AK, et al. Covalent targeting of remote cysteine residues to develop CDK12 and CDK13 inhibitors. *Nat Chem Biol.* 2016;12(10):876–84.
409. Jin LL, Tong J, Prakash A, Peterman SM, St-Germain JR, Taylor P, et al. Measurement of protein phosphorylation stoichiometry by selected reaction monitoring mass spectrometry. *J Proteome Res.* 2010;9(5):2752–61.

Chapter 7: Appendix 1

Table A 1. Cloning primer nucleotide sequences. Included are the target amplification sequence, primer codes, primer nucleotide sequences and applicable restriction sites.

Amplification Target	Primer Code	Nucleotide sequence (5'→3')	Restriction site
NS5A -2a (JFH1) into pQCXIN-HBH-TAP-N-ter vector	650F	TGTGCGTACGCTCCGGATCCTGGCTCC	BsiWI
	651R	TAGAGAATTCCTAGCAGCACACGGTGGTAT	EcoRI
NS5A -2a (JFH1) into pQCXIN-HBH-TAP-C-ter vector vector	652Fr	TGTTGCGGCCGCATGTCCGGATCCTGGCTCCG	NotI
	653Rr	GTGTCGTACGGCGCAGCACACGGTGGTATC	BsiWI
GFP into pQCXIN-HBH-TAP-N-ter vector	616F	ACTAGGATCC ATGGTGAGCA AGGGCGA	BamH1
	617R	TGATGAATTCTTACTTGTACAGCTCGTCC	EcoRI
GFP into pQCXIN-HBH-TAP-C-ter vector	618F	ACTA GCGGCCGC ATGGTGAGCA AGGGCGAG	NotI
	619R	TGATACCGGTTT CTTGTACAGCTCGTCCATG	AgeI
GFP into N-terminal pFLAG-	770F	TGATGAATTCCATGGTGAGCAAGGGCGA	EcoRI

CMV-4	771R	GTATAGATCTTTACTTGTACAGCTCGTCC	BglII
NS5A-2a domain mapping into pFLAG-CMV-4	764F	TGATGAATTCCGGATCCTGGCTCCG	EcoRI
	765F	TGATGAATTCACGGCGCTTGGCACGGG	EcoRI
	766F	TGATGAATTCCCCCCCCAAGAAGGCCCC	EcoRI
	767R	GTATAGATCTCTAGCAGCACACGGTGG	BglII
	768R	CATCAGATCTCTATCTCCTTGGGGGAGGCG	BglII
	769R	TCAGAGATCTCTAGGTGTTGCTGTGGGTGGTG	BglII
NKRF N-terminally into pCMV-myc	824F	CCGCAGATCTCTATGGAAAAATTCTCCAAATGGC	BglII
	825R	TTATGCGGCCGCTCAATTTGCTTGAGGCATAACAAG	NotI
Rangap1 N-terminally into pCMV-myc	826F	TGCGGAATTCGGATGGCCTCGGAAGACATTG	EcoRI
	827R	GACTCTCGAGCTAGACCTTGTACAGCGTCTG	XhoI
CHERP N-terminally into pCMV-myc	828F	ATTCGTCGACCATGACTATGGAGAAGCAGAAGGAC	SalI
	829R	CGAAGGTACCCTACTTACACTCGTCCCTG	KpnI
TOM40 N-terminally into pCMV-myc	830F	GTCTGAAT TCGGATGGGG AACGTGTTGG CTG	EcoRI
	831R	TTACCTCGAGTCAGCCGATGGTGAGGCC	XhoI
TOM22 N-terminally into	832F	TCCAGAATTCGGATGGCTGCCGCCGTCGC	EcoRI

pCMV-myc	833R	TGTACTCGAGCTAGATCTTTCCAGGAAGTG	XhoI
FKBP38 N-terminally into	1023F	AGACGAATTCGGATGGGACAACCCCCGGC	EcoRI
pCMV-myc	1024R	ATCTGCGGCCGCTCAGTTCCTGGCAGCGAT	NotI
CCAR2 N-terminally into	1212F	GATCGAATTCGGATGTCCCAGTTTAAGCGCCAG	EcoRI
pCMV-myc	1213R	TCTACTCGAGTCAGTTGCTAGGTGCCGGCTC	XhoI
CDK12 N-terminally into	1216F	GTAGGTCGACCATGCCCAATTCAGAGAGACA	Sall
pCMV-myc	1217R	TACTGCGGCCGCTTAGTAAGGAACTCCTCTCC	NotI
OGDH N-terminally into	1220F	GATCGAATTCGGATGTTTCATTTAAGGACTTG	EcoRI
pCMV-myc	1221R	TCTACTCGAGCTACGAGAAGTTCTTGAAGAC	XhoI
HBH tag into NS5A SG JFH1	1098F	ACACCCTCGAGGCAAGGGGTTACATCATCACC	AbsI
	1099R	CTCTCCTCGAGGCGTACGGAGCCGGCG	AbsI

Table A 2. Primary antibodies. Antibody concentrations utilized in immunoblots and immunofluorescent microscopy. Described are the protein targets, antibody concentration used in Western blot (WB) and immunofluorescent microscopy (IF), company and catalogue numbers.

Antibody	Concentration	Company	Catalogue Number
Actin	1:2000 WB	Abcam	ab8226
BUB3	1:1000 WB	Epitomics	S2663
c-myc	1:1000 WB	Santa Cruz	sc-40
CCAR2 (KIAA1967)	1:1000 WB 1:200IF	abcam	ab151190
CHERP	1:1000 WB	abcam	ab15951
FLAG "THE DYKDDDDK Tag"	1:1000 WB	GenScript	A00187-200
FLAG M2	1:2000 WB	Sigma	F1804
GAPDH Clone 71.1	1:10,000 WB	Sigma	G8795
GFP	1:1000 WB	Santa Cruz	sc-9996
Histone H3	1:1000 WB	abcam	Ab8580
IGF2BP2	1:1000 WB	abcam	ab124930
MCM2	1:1000 WB	epitomics	2901 1
NKRF	1:1000 WB	Abcam	Ab168829
NS5A-2a-Ab01	1:4000 WB	Genscript	Custom Epitope:

			PPPKKAPTPPPRRR
NS5A-2a-Ab02	1:4000 WB 1:750 IF	Genscript	Custom Epitope: SSMPPLEGEPGDPDL
p53 (DO-1)	1:1000 WB	Santa Cruz	sc-126
RanGAP1	1:1000 WB	epitomics	01-71
RGS-HIS₄	1:1000 WB 1:200 IF	Qiagen	34610
tetra-HIS	1:1000 WB	Qiagen	34670
TOMM20	1:1000 WB	abcam	ab56783
TOMM22	1:1000 WB	abcam	ab57523
TOMM40	1:1000 WB	abcam	ab51884
Vinculin	1:2000 WB	abcam	ab18058

Table A 3. FLAG and myc-tagged expression vector cloning. Listed are the name of the construct, source of the vector, source of the insert, PCR amplification primers (see Appendix Table A1 for nucleotide sequence) and restriction enzymes facilitating the cloning.

Construct Name	Source of tagged vector	Source of insert	PCR amplification Primers	Restriction Enzymes
FLAG-GFP	pFLAG-CMV4 (Sigma cat# E7158)	pEGFP-N1 (Clontech cat# 6085-1)	770F/771R	EcoRI/BglII
FLAG-NS5A	pFLAG-CMV4 (Sigma cat# E7158)	pJFH1 plasmid (151) (NCBI # AB047640)	764F/767R	EcoRI/BglII
FLAG-D1-NS5A	pFLAG-CMV4 (Sigma cat# E7158)	pJFH1 plasmid (151) (NCBI # AB047640)	764F/769R	EcoRI/BglII
FLAG-D2-NS5A	pFLAG-CMV4 (Sigma cat# E7158)	pJFH1 plasmid (151) (NCBI # AB047640)	765F/768R	EcoRI/BglII
FLAG-D3-NS5A	pFLAG-CMV4 (Sigma cat# E7158)	pJFH1 plasmid (151) (NCBI # AB047640)	766F/767R	EcoRI/BglII
FLAG-D1-D2-NS5A	pFLAG-CMV4 (Sigma cat# E7158)	pJFH1 plasmid (151) (NCBI # AB047640)	764F/768R	EcoRI/BglII

	E7158)	AB047640)		
FLAG-D2-D3-NS5A	pFLAG-CMV4 (Sigma cat# E7158)	pJFH1 plasmid (151) (NCBI # AB047640)	765F/767R	EcoRI/BglII
myc-NKRF	pCMV-myc (Clontech cat#635689)	MGC Human NKRF Sequence- Verified cDNA (CloneId:5299667) NCBI#:BC068514	824F/825R	BglII/NotI
myc-Rangap1	pCMV-myc (Clontech cat#635689)	MGC Human RANGAP1 Sequence-Verified cDNA (CloneId:3506039) NCBI# BC014044	826F/827R	EcoRI/XhoI
myc-CHERP	pCMV-myc (Clontech cat#635689)	MGC Human CHERP Sequence- Verified cDNA (CloneId:4053575) NCBI# BC021294	828F/829R	Sall/KpnI
myc-TOM40	pCMV-myc (Clontech cat#635689)	MGC Human TOMM40 Sequence- Verified cDNA (CloneId:4549825) NCBI# BC012134	830F/831R	EcoRI/XhoI

myc-TOM22	pCMV-myc (Clontech cat#635689)	MGC Human TOMM22 Sequence- Verified cDNA (CloneId:4302531) NCBI# BC009363	832F/833R	EcoRI/XhoI
myc-FKBP38	pCMV-myc (Clontech cat#635689)	MGC Human FKBP8 Sequence- Verified cDNA (CloneId:4299915) NCBI# BC009966	1023F/1024R	EcoRI/NotI
myc-EGLN1	pcDNA3.1+N-myc	EGLN1 cDNA ORF clone, Homo sapiens (ConeID: OHu22997) NCBI# NM_022051NM_000454	Purchased directly	
myc-SOD1	pcDNA3.1+N-myc	SOD1 cDNA ORF clone, Homo sapiens (ConeID: OHu24018) NCBI# NM_000454	Purchased directly	
myc-CCAR2	pCMV-myc (Clontech cat#635689)	MGC Human CCAR2 Sequence- Verified cDNA (CloneId:5496068) NCBI# BC065495	1212F/1213R	EcoRI/XhoI
myc-CDK12	pCMV-myc (Clontech	MGC Human CDK12 Sequence-	1216F/1217R	Sall/NotI

	cat#635689)	Verified cDNA (CloneId:9021722) NCBI# BC140854		
myc-OGDH	pCMV-myc (Clontech cat#635689)	MGC Human OGDH Sequence- Verified cDNA (CloneId: 3010095) NCBI# BC014617	1220F/1221R	EcoRI/XhoI
myc-MeaslesMatrix		Kind gift from Helene Schultz		

Table A 4. NS5A phosphoacceptor site mutagenesis primers. Included are the target amplification sequence, primer codes, primer nucleotide sequences and applicable restriction sites.

NS5A phosphoacceptor site	Primer code	Nucleotide sequence (5'→3')
S146A	856F	CCAACTACCTGCCCCAGAGTTTTTC
	857R	CAAGGAATTTTCAGATTGTCAG
S146D	858F	CCAACTACCTGACCCAGAGTTTTTCTC
	859R	CAAGGAATTTTCAGATTGTCAG
S222A	860F	GGCACGGGGAGCCCCTCCATCTGAGG
	861R	AAGCGCCGCGCCGCAGTC
S222D	862F	GGCACGGGGAGACCCTCCATCTGAGGCGAGCTCCTCAGTG
	863R	AAGCGCCGCGCCGCAGTC
S225A	864F	ATCACCTCCAGCCGAGGCGAGCTCCTCAGTG
	865R	CCCCGTGCCAAGCGCCGC
S225D	866F	ATCACCTCCAGACGAGGCGAGCTCCTCAGTGAGCCAG
	867R	CCCCGTGCCAAGCGCCGC

S230A	868F	GGCGAGCTCCGCCGTGAGCCAGC
	869R	TCAGATGGAGGTGATCCCCG
S230D	870F	GGCGAGCTCCGACGTGAGCCAGCTATC
	871R	TCAGATGGAGGTGATCCC
T348A	872F	GAAGGCCCCGGCCCCTCCCCAAG
	873R	TTGGGGGGGGGGAGAGCA
T348D	874F	GAAGGCCCCGGACCCTCCCCAAGGAGACG
	875R	TTGGGGGGGGGGAGAGCA
T356A	876F	GAGACGCCGGGCCGTGGGTCTGAG
	877R	CTTGGGGGAGGCGTCGGG
T356D	878F	GAGACGCCGGGACGTGGGTCTGAGCGAGAGC
	879R	CTTGGGGGAGGCGTCGGG
S360A	880F	AGTGGGTCTGGCCGAGAGCACCATATCAG
	881R	GTCCGGCGTCTCCTTGGG
S360D	882F	AGTGGGTCTGGACGAGAGCACCATATCAG
	883R	GTCCGGCGTCTCCTTGGG

S457A	884F	GTCTACTTGCGCCGAGGAGGAC
	885R	CAAGACCCCGAGCCCGAA
S457D	886F	GTCTACTTGCGACGAGGAGGACGATAACC
	887R	CAAGACCCCGAGCCCGAA
T164A	939F	GTTTGCACCCGCCCAAAGCCGT
T164D	940F	GTTTGCACCCGACCCAAAGCCGTTTTTC
	941R	CTATGGATCTGCACACCG
S201A	942F	CGTATTGAGGGCCATGCTAACAGATC
S201D	943F	CGTATTGAGGGACATGCTAACAGATCCGCC
	944R	TCTGCGTCGGGCTCAGGT
T204A	945F	GTCCATGCTAGCCGATCCGCCCC
T204D	946F	GTCCATGCTAGACGATCCGCCCCAC
	947R	CTCAATACGTCTGCGTCG
S228A	948F	ATCTGAGGCGGCCTCCTCAGTGAGCC
S228D	949F	ATCTGAGGCGGACTCCTCAGTGAGCC
	950R	GGAGGTGATCCCCGTGCC

S229A	951F	TGAGGCGAGCGCCTCAGTGAGCC
	951R	GATGGAGGTGATCCCCGTGC
S229D	952F	TGAGGCGAGCGACTCAGTGAGCC
	953R	GATGGAGGTGATCCCCGT
S232A	954F	CTCCTCAGTGGCCCAGCTATCAGC
S232D	955F	CTCCTCAGTGGACCAGCTATCAGC
	956R	CTCGCCTCAGATGGAGGT
S235A	957F	GAGCCAGCTAGCCGCACCGTCGC
	957R	ACTGAGGAGCTCGCCTCAG
S235D	958F	GAGCCAGCTAGACGCACCGTCGCTGCG
	959R	ACTGAGGAGCTCGCCTCA
S238A	960F	ATCAGCACCGGCCCTGCGGGCCA
	960R	AGCTGGCTCACTGAGGAGCTC
S238D	961F	ATCAGCACCGGACCTGCGGGCCACC
	962R	AGCTGGCTCACTGAGGAG
S272A	963F	AGAGCCTGAGGCCAGGGTGCCCG

	963R	GTCTGAGCCACACCGCCCTCC
S272D	964F	AGAGCCTGAGGACAGGGTGCCCG
	965R	GTCTGAGCCACACCGCCC
S288A	966F	CGAGGAAGAGGCCGACCTTGAGC
S288D	967F	CGAGGAAGAGGACGACCTTGAGC
	968R	GCCATTGGCTCGAGAAAG
S362A	969Fr	TCTGAGCGAGGCCACCATATCAGAAGCCC
S362D	970Fr	TCTGAGCGAGGACACCATATCAGAAGCCC
	971R	CCCACTGTCCGGCGTCTC
T363A	972F	GAGCGAGAGCGCCATATCAGAAGC
T363D	973F	GAGCGAGAGCGACATATCAGAAGCCCTCC
	974R	AGACCCACTGTCCGGCGT
S365A	975F	GAGCACCATAGCCGAAGCCCTCC
S365D	976F	GAGCACCATAGACGAAGCCCTCCAGCAACTG
	977R	TCGCTCAGACCCACTGTC
S381A	1029F	CCAGCCCCCGCCAGCGGTGATG

	1030R	CCAAAGGTCTTGATGGCCAGTTG
S381D	1031F	CCAGCCCCCGACAGCGGTGATGC
	1032R	CCAAAGGTCTTGATGGCC
S382A	1033F	GCCCCCTCGGCCGGTGATGCAG
S382D	1034F	GCCCCCTCGGACGGTGATGCAG
	1035R	TGGCCAAAGGTCTTGATGG
T410A	1036F	CCCCTCAGAGGCCGGTCCGCCTC
T410D	1037Fr	CCCCTCAGAGGACGGTCCGCCTCCTCTATGCC
	1038R	GCCGGCTCACCAGGGGAC
S414A	1039F	AGGTTCCGCCGCCTCTATGCCCC
S414D	1040F	AGGTTCCGCCGACTCTATGCCCCCC
	1041R	GTCTCTGAGGGGGCCGGC
S415A	1042F	TTCCGCCTCCGCCATGCCCCCC
S415D	1043F	TTCCGCCTCCGACATGCCCCCC
	1044R	CCTGTCTCTGAGGGGGCC
S151A	1045F	AGAGTTTTTCGCCTGGGTGGACG

S151D	1046F	AGAGTTTTTCGACTGGGTGGACGG
	1047R	GGAGAAGGTAGTTGGCAAG
S210A	1048F	GCCCCACATCGCCGCGGAGACTG
	1049R	GGATCTGTTAGCATGGACCTC
S210D	1050F	GCCCCACATCGACGCGGAGACTG
	1051R	GGATCTGTTAGCATGGAC
T213A	1052F	CACGGCGGAGGCCGCGGCGCGGC
	1053R	ATGTGGGGCGGATCTGTTAGCATGGACCTC
T213D	1054F	CACGGCGGAGGACGCGGCGCGGC
	1055R	ATGTGGGGCGGATCTGTTAGC
T334A	1056F	CCAACCGCCCGCCGTTGCTGGTT
	1057R	TAATCTGGCCTCCTCCACGATTCCAC
T334D	1058F	CCAACCGCCCGACGTTGCTGGTT
	1059R	TAATCTGGCCTCCTCCAC

2b.JP.HC-J8.D10988	SGSWLQDIWDWVCSILTDfKNWLSskllPKMPGIPFIScQkGyKGVWAGTgVMTTRCPCG	60
2c. .BEBE1.D50409	SGSWLRDVWDWVCSILIDfKNWLSAKLFPRLPGIPFIScQkGyRGTWAGTgIMTTRCPCG	60
Ref.2a.JP.x.JFH-1.AB047639	SGSWLRDVWDWVCTILTDFKNWLTskLFPKLPGLPFIScQkGyKGVWAGTgIMTTRCPCG	60
Ref.2a.JP.x.HC-J6.D00944	SGSWLRDVWDWVCTILTDFKNWLTskLFPKMPGLPFIScQkGyKGVWAGTgIMTTRCPCG	60
Ref.7a.CA.x.QC69.EF108306	AGSWLREVVDWVCMVLSDFASWLKAKVLPslPGIPFLScQkGyKGEWRNDgIMNTKcPCG	60
4a. .02C.DQ418784	ADSWLWEVVDWVCTVLSDFKTWlKAKLLPLMPGVPFLScQRgyRGEWRGEGIMHTKcPCG	60
Ref.4a.EG.x.ED43.Y11604	AESWLWEVVDWVlHVLSDfKTCLKAKFVPLMPGIPLLSWPRgyKGEWRGDgVMHTTcPCG	60
5a.GB.EUH1480.Y13184	DGTWLRAlIWDWVCTAlTDFKAWLQAKLLPQLPGVPPFFScQkGyKGVWRGDgVNSTKcPCG	60
5a.ZA.SA13.AF064490	DGTWLRAlIWDWVCTAlTDFKAWLQAKLLPQLPGVPPFLScQRgyRgVWRGDgVNSTKcPCG	60
3a. .K3A.D28917	SGDwLRlIWDWVCSVVSDFKTWLSAKIMPALPGLPFIScQkGyKGVWRGDgVMSTRcPCG	60
3a. .NZL1.NC_009824	SDDwLRtIWDWVCSVLADfKAWLSAKIMPALPGLPFIScQkGyKGVWRGDgVMSTRcPCG	60
6a.HK.6a63.DQ480514	ATSWLRDVWDWVCTVLSDFKvWlQAKLFPRLPGIPFLScQTgyRgVWAGDgVCHTTCTCG	60
1b.JP.JK1-full.X61596	SGSWLRDVWDWICTVLTDFKTWlQskLLPRLPGDPFFScQRgyRgVWRGDgVMQTTcPCG	60
1b. .pCV-J4L10.AF054259	SGSWLRDVWDWICTVLTDFKTWlQskLLPRLPGVPPFLScQRgyKGVWRGDgIMQTTcPCG	60
1b.JP.JT.D11355	SGSWLRDVWDWICTVLTDFKTWlQskLLPQLPGVPPFFScQRgyKGVWRGDgIMQTTcPCG	60
Ref.1a.US.x.HCV-1.M62321	SGSWLRDIWDWICEVLSDFKTWlKAKLMPQLPGIPFVScQRgyKGVWRVDgIMHTRCHCG	60
1a. .H77.NC_004102	SGSWLRDIWDWICEVLSDFKTWlKAKLMPQLPGIPFVScQRgyRgVWRGDgIMHTRCHCG	60
1a.US.HC-TN.EF621489	SGSWLRDIWDWICEVLSDFKTWlKAKLMPQLPGIPFVScQRgyKGVWRGDgIMHTRCHCG	60
1a.JP.HC-J1.D10749	SGSWLRDIWDWICEVLSDFKTWlKTKLMPHLPGIPFVScQHgyKGVWRGDgIMHTRCHCG	60
	** :***: : ** * :...* :** *:. * ** * *	
2b.JP.HC-J8.D10988	ANISGHVrMGTMKITGPKTCLNLWQGTfPInCYTEgPCVpKPPpNYKTAIWRVAASEYVE	120
2c. .BEBE1.D50409	ANITGNVRLGTMRISGPKTCLNTWQGTfPInCYTEgScVpKpAPNFkTAIWRVAASEYAE	120
Ref.2a.JP.x.JFH-1.AB047639	ANISGNVRLGSMRITGPKTCMNTWQGTfPInCYTEgQcAPkPPTNYKTAIWRVAASEYAE	120
Ref.2a.JP.x.HC-J6.D00944	ANISGNVRLGSMRITGPKTCMNIWQGTfPInCYTEgQcVpKpAPNFkIAIWRVAASEYAE	120
Ref.7a.CA.x.QC69.EF108306	ALIAGHVKNgSMRIVGPKTCrNTWwGTfPInSHTTgPSSpVpSxCYQRALWRVsxTEYVE	120
4a. .02C.DQ418784	AELAGHIKNGSMRITGPKTCSNTWHGtFPIInAYTTgPgvPvPAPNYKfALWRVSAEEYVE	120
Ref.4a.EG.x.ED43.Y11604	ADLAGHIKNGSMRITGPKTCSNTWHGtFPIInAYTTgPgvPIpAPNYKfALWRVSAEDYVE	120
5a.GB.EUH1480.Y13184	ATISGHVKNgTMRIvGPKLCSNTWQGTfPInATTTgPsvPAPAPNYKfALWRVGAADYAE	120
5a.ZA.SA13.AF064490	ATISGHVKNgTMRIvGPKLCSNTWHGtFPIInATTTgPsvPAPAPNYKfALWRVGAADYAE	120
3a. .K3A.D28917	ASIAGHVKNgSMRLAGPrTCANMCHGtFPIInEYTTgPstPcPppNYTRAlWRVAANSYVE	120
3a. .NZL1.NC_009824	AAITGHVKNgSMRLAGPrTCANMWHGtFPIInEYTTgPstPcPspNYTRAlWRVAANSYVE	120
6a.HK.6a63.DQ480514	AVIAGHVKNgTMKITGPrTCSNTWwGTfPInATTTgPCTPrPAPNYQRALWRVSAEDYVE	120
1b.JP.JK1-full.X61596	AQITGHVKNgSMRIVGPKTCSNTWHGtFPIInAYTTgPCTPSPAPNYSRALWRVAEEYVE	120
1b. .pCV-J4L10.AF054259	AQIAGHVKNgSMRIVGPrTCSNTWwGTfPInAYTTgPCTPSPAPNYSRALWRVAEEYVE	120
1b.JP.JT.D11355	AQITGHVKNgSMRIVGPKTCSNMWHGtFPIInAYTTgPCTPSPAPNYSRALWRVAEEYVE	120
Ref.1a.US.x.HCV-1.M62321	AEITGHVKNgTMRIvGPrTCrNMwSGtFPIInAYTTgPCTPLPAPNYTFALWRVSAEEYVE	120
1a. .H77.NC_004102	AEITGHVKNgTMRIvGPrTCKNMwSGtFFInAYTTgPCTPLPAPNYKfALWRVSAEEYVE	120
1a.US.HC-TN.EF621489	AEITGHVKNgTMRIvGPKTCrNMwSGtFPIInAYTTgPCTPLPAPNYTFALWRVSAEEYVE	120

1a.JP.HC-J1.D10749	AEITGHVKNGTMRIVGPKTCRNMWSGTFPINAYTTGPCTPLPAPNYTFALWRVSAEEYVE * :*:*.:: *::*: *::: ** : * * *** * * * * * * : *::***. .*.*	120
2b.JP.HC-J8.D10988	VTQHGSFSYVTGLTSDNLKVPQVPAPEFFSWVDGVQIHRFAPVPGPFFRDEVTFTVGLN	180
2c._.BEBE1.D50409	VTQHDSHAYVTGLTADNLKVPQVPAPEFFSWVDGVQIHRFAPTPKAFMRDEVSFSVGLN	180
Ref.2a.JP.x.JFH-1.AB047639	VTQHGSYSYVTGLTTDNLKIPQVPAPEFFSWVDGVQIHRFAPTPKPFRRDEVSFCVGLN	180
Ref.2a.JP.x.HC-J6.D00944	VTQHGSYHYITGLTTDNLKVPQVPAPEFFSWVDGVQIHRFAPIPKPFRRDEVSFCVGLN	180
Ref.7a.CA.x.QC69.EF108306	ILRHNDQHXVVGVTAEADLKPCQVPSPEFFSFDVGVRIHRFAPEPKPMIREEAAFVVGLH	180
4a._.02C.DQ418784	VRRVGFDFHYVTGVTQDNIKPCQVPAPEFFTEVDGIRLHRHAPKCKPLLRDEVTFSVGLN	180
Ref.4a.EG.x.ED43.Y11604	VRRVGFDFHYVTGVTQDNIKPCQVPAPELFFTEVDGIRIHRHAPKCKPLLRDEVSFSVGLN	180
5a.GB.EUH1480.Y13184	VRRVGDYHYITGVTQDNLKPCQVPSPEFFTELDGVRIHRFAPPCNPLLRREEVTFVGLH	180
5a.ZA.SA13.AF064490	VRRVGDYHYITGVTQDNLKPCQVPSPEFFTELDGVRIHRYAPPCNPLLRREEVCFVGLH	180
3a._.K3A.D28917	VRRVGFDFHYITGATEDGLKPCQVPAPEFFTEVDGVRIHRYAPPCRPLLRDEITFMVGLN	180
3a._.NZL1.NC_009824	VRRVGFDFHYITGATEDGLKPCQVPAPEFFTEVDGVRLHRYAPPCPKPLLRDDITFMVGLH	180
6a.HK.6a63.DQ480514	VRLGDCHYVVGVTAEGLKPCQVPAPEFFTEVDGVRIHRYAPPCPKPLLRDEVTFSVGLS	180
1b.JP.JK1-full.X61596	VTRVGFDFHYVTGTTDNLKPCQVPAPEFFTEVDGVRLHRYAPACKPLLRDEVTFQVGLN	180
1b._.pCV-J4L10.AF054259	VTRVGFDFHYVTGITDNLKPCQVPAPEFFTEVDGVRLHRYAPACKPLLRREDVAFQVGLN	180
1b.JP.JT.D11355	ITRVGFDFHYVTGTTDNLKPCQVPAPEFFTELDGVRLHRYAPACRPLLRREDVTFQVGLN	180
Ref.1a.US.x.HCV-1.M62321	IRQVGFDFHYVTGTTDNLKPCQVPSPEFFTELDGVRLHRFAPPCPKPLLRREEVSRVGLH	180
1a._.H77.NC_004102	IRRVGFDFHYVSGTTDNLKPCQVPSPEFFTELDGVRLHRFAPPCPKPLLRREEVSRVGLH	180
1a.US.HC-TN.EF621489	IRQVGFDFHYVTGTTDNLKPCQVPSPEFFTELDGVRLHRFAPPCPKPLLRREEVSRVGLH	180
1a.JP.HC-J1.D10749	IRRVGFDFHYVTGTTDNLKPCQVPSPEFFTELDGVRLHRFAPPCPKPLLRREEVSRVGLH : : . : * * : : * ***:*. *::: *:::***. * * * :::: * * *	180
2b.JP.HC-J8.D10988	SFVVGSQQLPCDPEPDTEVLASMLTDPSHITAEEAARLARGS--PPSQASSASQLSAPS	238
2c._.BEBE1.D50409	SYVVGSQQLPCEPEPDTEVLASMLTDPSHITAEEAARLARGS--PPSAASSASQLSAPS	238
Ref.2a.JP.x.JFH-1.AB047639	SYAVGSQQLPCEPEPDADVLRSMMLTDPPHITAETAARLARGS--PPSEASSSVSLSAPS	238
Ref.2a.JP.x.HC-J6.D00944	SFVVGSQQLPCDPEPDTEVLASMLTDPSHITAETAARLARGS--PPSEASSASQLSAPS	238
Ref.7a.CA.x.QC69.EF108306	SYVVGSQQLPCEPEPDVQTVSOLLTDPSHITAETAARLRRGS--PPSNASSASQLSAPS	238
4a._.02C.DQ418784	SFVVGSQQLPCEPEPDVAVLTSMLTDPSHITAETASRRLARGS--PPSLASSASQLSAPS	238
Ref.4a.EG.x.ED43.Y11604	SFVVGSQQLPCEPEPDVAVLTSMLTDPSHITAESARRLARGSR--PSLASSASQLSAPRL	238
5a.GB.EUH1480.Y13184	SYVVGSQQLPCEPEPDVTVLTSMMLSDPAHITAETAKRRLNRGS--PPSLANSSASQLSAPS	238
5a.ZA.SA13.AF064490	SFVVGSQQLPCEPEPDVTVLTSMMLSDPAHITAETAKRRLDRGS--PPSLASSASQLSAPS	238
3a._.K3A.D28917	SYAIGSQQLPCEPEPDVSVLTSMLRDPHITAETAARLARGS--PPSEASSASQLSAPS	238
3a._.NZL1.NC_009824	SYTIGSQQLPCEPEPDVSVLTSMLRDPHITAETAARLARGS--PPSEASSASQLSAPS	238
6a.HK.6a63.DQ480514	NYAIGSQQLPCEPEPDVTVVTSMMLTDPMHITAETAARLKRGS--PPSLASSASQLSAPS	238
1b.JP.JK1-full.X61596	QFPVGSQQLPCEPEPDVTVLTSMMLTDPSHITAETAKRRLARGS--PPSLASSASQLSAPS	238
1b._.pCV-J4L10.AF054259	QYLVGSQQLPCEPEPDVTVLTSMMLTDPSHITAETAKRRLARGS--PPSLASSASQLSAPS	238
1b.JP.JT.D11355	QYLVGSQQLPCEPEPDVAVLTSMLTDPSHITAETAKRRLARGS--PPSLASSASQLSAPS	238
Ref.1a.US.x.HCV-1.M62321	EYPVGSQQLPCEPEPDVAVLTSMLTDPSHITAEEAGRRLARGS--PPSVASSASQLSAPS	238
1a._.H77.NC_004102	EYPVGSQQLPCEPEPDVAVLTSMLTDPSHITAEEAGRRLARGX-XPPSMASSASQLSAPS	239

1a.US.HC-TN.EF621489	EYPVGSQLPCEPEPDVAVLTSM L TDP S HIT A E A AG R RL L ARG S --PP S MA S SS S AS Q LS A PS	238
1a.JP.HC-J1.D10749	DYPVGSQLPCEPEPDVAVLTSM L TDP S HIT A AA A AG R RL L ARG S --PP S E A SS S AS Q LS A PS	238
	.: :*****:****. .: .:* ** ***** :* *** ** ** *.***.***	
2b.JP.HC-J8.D10988	LKATCTT----HKTAY-DCDMVDANLF----MGG-DVTRIESDSK V IVLDSLD-SMTE-V	286
2c._.BEBE1.D50409	LRATCTT----HAKCP-DIDMVDANLFCWCTMGG-NMTRIESES K VLMVDSFD-PVVD-K	290
Ref.2a.JP.x.JFH-1.AB047639	LRATCTT----HSNTY-DVDMVDANLL----MEG-GVAQTEPES R VPVLD F LE-PM A EEE	287
Ref.2a.JP.x.HC-J6.D00944	LRATCTT----HGKAY-DVDMVDANLF----MGG-DVTRIESES K VVVVLD S LD-PM V EER	287
Ref.7a.CA.x.QC69.EF108306	LKATHTT---L-PQHP-DAELIEANLMW-EHKVG-AIRMETDT K VII L DSFD-SASS X E	290
4a._.02C.DQ418784	LKATCTA----RHGSP-GTDLLEANLLW----GS-AATRVETDER V II L DSFE-PC V AES	287
Ref.4a.EG.x.ED43.Y11604	LQATCTA----PHDSP-GTDLLEANLL----WGS-TATRVETDE K VII L DSFE-SC V AEQ	287
5a.GB.EUH1480.Y13184	LKATCTI----QGHHP-DADLIKANLLWRQCMGG-NITRVEAEN K VEILDC F K-PL K E-E	290
5a.ZA.SA13.AF064490	LKATCTT----QGHHP-DADLIEANLLWRQCMGG-NITRVEAEN K VVILDSFE-PL K A-D	290
3a._.K3A.D28917	LKATCQT----HRPHP-DAELVDANLLWRQEMGS-NITRVESE T KVVILDSFE-PL R A-E	290
3a._.NZL1.NC_009824	LKATCQT----HRPHP-DAELVDANLLWRQEMGS-NITRVESE T KVVVILDSFE-PL R A-E	290
6a.HK.6a63.DQ480514	LKATCTT----SKDHP-DMELIEANLLWRQEMGG-NITRVESE N KVVVILDSFE-PL T A-E	290
1b.JP.JK1-full.X61596	LKATCTT----RHDSP-DADLIEANLLWRQEMGG-NITRVESE N KVVILDSFE-PL R A-E	290
1b._.pCV-J4L10.AF054259	LKATCTT----HHDSP-DADLIEANLLWRQEMGG-NITRVESE N KVVILDSFE-PL H A-D	290
1b.JP.JT.D11355	LKATCTT----HHDSP-DADLIEANLLWRQEMGG-NITRVESE N KVVILDSFD-PL R A-E	290
Ref.1a.US.x.HCV-1.M62321	LKATCTA----NHDSP-DAELIEANLLWRQEMGG-NITRVESE N KVVILDSFD-PL V AEE	291
1a._.H77.NC_004102	LKATCTAX---XHXXPDAELIEANLLWRQEMGG-NITRVESE N KVVILDSFXX P LVA-E	294
1a.US.HC-TN.EF621489	LRATCTT----NHDSP-DAELIEANLLWRQEMGG-NITRVESE N KVVILDSFD-PL V A-E	290
1a.JP.HC-J1.D10749	LKATCTI----NHDSP-DAELIEANLLWRQEMGG-NITRVESE N KVVILDSFD-PL V A-E	290
	*:** ** ::::***: .* : * : :* ::* :	
2b.JP.HC-J8.D10988	EDDREPSVPSEYL-IK-RRKFPPALPPWARPDYNPVL I ETW K RPGYEP P T V LGCALPPTP	344
2c._.BEBE1.D50409	EDEREPSIPSEYL-LP-KSRFPPALPPWARPDYNP L LETW K RPDYQPPV V AGCALPPPG	348
Ref.2a.JP.x.JFH-1.AB047639	- S DLEPSIPSECM-LP-RSGFPRALPAWARPDYNP L VESW R RPDYQ P PT V AGCALPPPK	344
Ref.2a.JP.x.HC-J6.D00944	- S DLEPSIPSEYM-LP-KKRFPALPAWARPDYNP L VESW K RPDYQ P AT V AGCALPPPK	344
Ref.7a.CA.x.QC69.EF108306	-DDMEPSTAAECLRTR--KVFPAMPIWARPDYNP V VENW K DPEYAPPQ V SGCALPPAQ	347
4a._.02C.DQ418784	DDDKEVSVAEAIL-RP-TKKFPPALPIWARPDYNP L TETW K Q R DYCP P T V YGCALPPSK	345
Ref.4a.EG.x.ED43.Y11604	NDDREVSVAEILRPT--KKFPPALPIWARPDYNP L TETW K Q Q DYQ A PT V HGCALPPAK	345
5a.GB.EUH1480.Y13184	EDDREISVSADCF-KK-GPAFPPALPVWARPGYD P LLETW K RPDYD P PP V WGCP I PPAG	348
5a.ZA.SA13.AF064490	DDDREISVSADCF-RR-GPAFPPALPIWARPGYD P LLETW K Q P DYD P PP V SGCPLPPAG	348
3a._.K3A.D28917	TDDAELSAAAECF-KK-PPKYPPALPIWARPDYNP L LD R W K SPDYV P P T VHGCALPPKG	348
3a._.NZL1.NC_009824	TDDVEPSVAEFCF-KK-PPKYPPALPIWARPDYNP L LD R W K APDYV P P T VHGCALPPRG	348
6a.HK.6a63.DQ480514	YDEREISVSAECH-RPPRQKFPPALPVWARPDYNP L LQ A W Q MPGYE P PP V SGCAVAPPK	349
1b.JP.JK1-full.X61596	EDEREVSVAEAIL-RK-SRKFPALPIWARPSYNP L LESW K KDPDYV P PP V HGCPLPPTM	348
1b._.pCV-J4L10.AF054259	GDEREISVAEAIL-RK-SRKFPSALPIWARPDYNP L LESW K KDPDYV P PP V HGCPLPPTK	348
1b.JP.JT.D11355	EDEREVSVAEAIL-RK-SKKFPPALPIWARPDYNP L LESW K SPDYV P PP V HGCPLPPTT	348
Ref.1a.US.x.HCV-1.M62321	-DEREISVPAEILRKS--RRFAQALPVWARPDYNP L VETW K KPDYEP P V V HGCPLPPPK	348

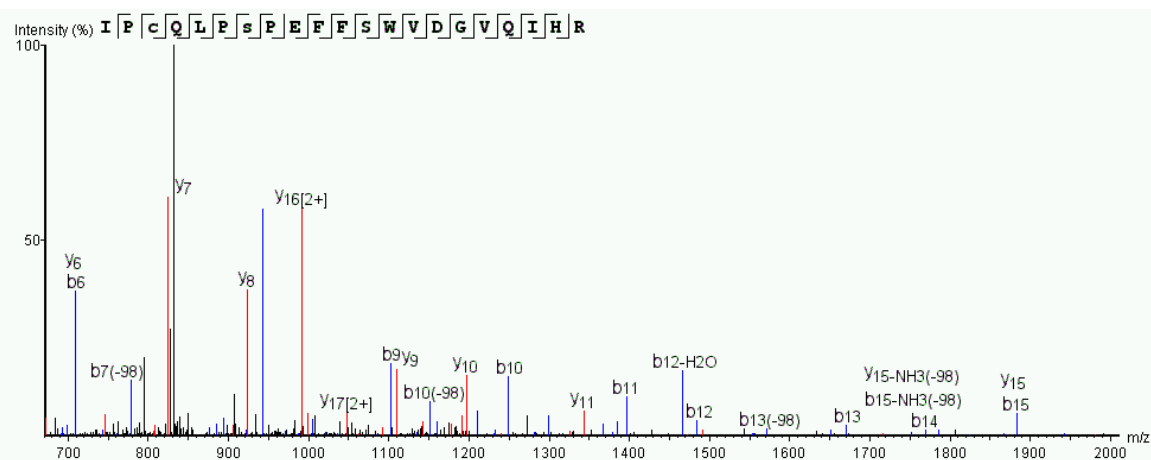
1a. .H77.NC_004102	EDEREVSVPAEIL-RXVSEXFAPALPVWARPDYNPLLVETWKKPDYEPVHVHCPLPPPR	353
1a.US.HC-TN.EF621489	EDEREVSVPAEIL-RK-SRKFTPALPIWARPDYNPLVPEPWKKPDYEPVHVHCPLPPPQ	348
1a.JP.HC-J1.D10749	EDEREISVPAEIL-RK-SRRFTQALPIWARPDYNPLIETWKKPNYEPVHVHCPLPPPQ	348
	.: * * : : : * : * * * * * * : : * : * * * : *	
2b.JP.HC-J8.D10988	QTPVPPP-RRRRAKV--LTQDNVEGVLREMADKVLSP--QDNNDGHS---TGAD--TG	394
2c. .BEBE1.D50409	TTPVPPP-RRRRAVV--LDQSNVGEALKELAIKSF--GCPPPSGDPGHS---TGGG--TT	398
Ref.2a.JP.x.JFH-1.AB047639	KAPTTPPPRR-RR-TVG-LSESTISEALQQLAIKTF--GQPPSSGDAGSSTGA-GAA--ES	396
Ref.2a.JP.x.HC-J6.D00944	KTPTTPPPRR-RR-TVG-LSESTIADALQQLAIKSF--GQPPSSGDSGLSTGA-DAA--DS	396
Ref.7a.CA.x.QC69.EF108306	TPPVPPRR-KR-AVIQLTESAVSTALAEALERSF--PKEEAPPSDSAI--SLD-SPAAN	400
4a. .02C.DQ418784	QPPVPPP-RRKRX--VQLTESVASAALAEALAAKTFGQPELGS DSGAD-----LT	391
Ref.4a.EG.x.ED43.Y11604	QPPVPSRR-KR-TVQ-LTESVSTALAEALAAKTF--GQSEPSSDRDT---DL-----TT	392
5a.GB.EUH1480.Y13184	PPPVPLPRRKRK--MELSDSTVSQVMADLADARFKVDTPSIEGQDS----AL-----	395
5a.ZA.SA13.AF064490	LPPVPPRRRKRK--VVLSDSNVSQVLADLAHARFKADTQSIIEGQDS----AV-----	395
3a. .K3A.D28917	APPVPPP-RRKRT--IQLDGSNVSAALAALAEKSFSSKQPEENSSS---SGVDTQSSTA	402
3a. .NZL1.NC_009824	APPVPPP-RRKRT--IQLDGSNVSAALAALAEKSFSSKQPEENSSS---SGVDTQSSTT	402
6a.HK.6a63.DQ480514	PAPIPPP-RRKR--LVHLDESTVSHALAQADKVFVSSSDPGPSSDS---GL--S--IT	399
1b.JP.JK1-full.X61596	APPVPPP-RRKRT--VVLTESTVSSALAEALATKTFGSSGSS-AVDSGT----A-----TA	395
1b. .pCV-J4L10.AF054259	APPVPPP-RRKRT--VVLTESTVSSALAEALATKTFGSSGSS-AVDSGT----A-----TA	395
1b.JP.JT.D11355	GPVPPP-RKKRT--VVLTESTVSSALAEALATKTFGSSGSS-AVDSGT----A-----TA	395
Ref.1a.US.x.HCV-1.M62321	SPPVPPPRK-KR-TVV-LTESTLSTALAEALATRSF----GSSS-TSGIT-GDN-----TT	394
1a. .H77.NC_004102	SPPVPPP-RKKRT--VVLTESTLPTALAEALATKSFSSGSS-----STSGIT-GDN-----TT	399
1a.US.HC-TN.EF621489	SPPVPPP-RKKRT--VILTESTLPTALAEALATKSFSSGSS-----STSGIT-GDD-----TT	394
1a.JP.HC-J1.D10749	SPPVPPP-RKKRT--VVLTESTLSTALAEALAAKSFSSGSS-----STSGIT-GDN-----TT	394
	* * * : : : * . . : : * : :	
2b.JP.HC-J8.D10988	GDIVQQP----SDETAASEAG----SLSSMPPLEGEPGDPDLFEFEPVGSAPPSEGECEVI	446
2c. .BEBE1.D50409	GETSKSP----PDEP--DDSEAG--SVSSMPPLEGEPGDPDLPEQVEHPAPPQEGGAAP	450
Ref.2a.JP.x.JFH-1.AB047639	GGP--TS-----PGEPA-----SETGSASSMPPLEGEPGDPDLSDQVELQPPPQGGVAP	446
Ref.2a.JP.x.HC-J6.D00944	GSR--TP-----PDELAL----SETGSISSMPPLEGEPGDPDLPEQVELQPPPQGGVVT	446
Ref.7a.CA.x.QC69.EF108306	DP----PSDCDQ-----SEI-SFSSMPPLEGEPGDPDL-----S-	430
4a. .02C.DQ418784	TPTETTHSGPILADDASDN--G---SYSSMPPLEGEPGDPDLTSD-----	431
Ref.4a.EG.x.ED43.Y11604	-PTETTDGSPIVVDDA-----SDDGSYSSMPPLEGEPGDPDL-----T-	429
5a.GB.EUH1480.Y13184	GTSSQHDSGPEEKRD--DNSDAA--SYSSMPPLEGEPGDPDLSSG-----	436
5a.ZA.SA13.AF064490	GTSSQPDGSGPEEKRD--DDSDAA--SYSSMPPLEGEPGDPDLSSG-----	436
3a. .K3A.D28917	SKVLPSPG-----EESDSE-SCSSMPPLEGEPGDPDLSCD-----	436
3a. .NZL1.NC_009824	SKVPPSPG-----GESDSE-SCSSMPPLEGEPGDPDLSCD-----	436
6a.HK.6a63.DQ480514	SPVPPAP---TTSDD--ACSEAE--SYSSMPPLEGEPGDPDLSSG-----	437
1b.JP.JK1-full.X61596	PPDQPSDDGD-RGSD--DE-----SYSSMPPLEGEPGDPDLSDG-----	431
1b. .pCV-J4L10.AF054259	LPDQASDDGD-KGSD--VE-----SYSSMPPLEGEPGDPDLSDG-----	431

1b.JP.JT.D11355	PPDQTSDDGD-KESD--VE-----SYSSMPPLEGEPGDPDLSDG-----	431
Ref.1a.US.x.HCV-1.M62321	TSSEPAPSGCPPD-----SDAESYSSMPPLEGEPGDPDL-----S-	429
1a._.H77.NC_004102	TSSEPAPSGCPPDSD--VE-----SYSSMPPLEGEPGDPDLSDG-----	436
1a.US.HC-TN.EF621489	TSPEPASSSCPPDSD--AE-----SYSSMPPLEGEPGDPDLSDG-----	431
1a.JP.HC-J1.D10749	TSSEPAPSGCSPDSD--AE-----SYSSMPPLEGEPGDPDLSDG-----	431
	* *****	
2b.JP.HC-J8.D10988	DSDSKSWSTVSDQ----EDSVICC	466
2c._.BEBE1.D50409	GSDSGSWSTCSDV----DDSVVCC	470
Ref.2a.JP.x.JFH-1.AB047639	GSGSGSWSTCSE----EDDTTVCC	466
Ref.2a.JP.x.HC-J6.D00944	GSGSGSWSTCSE----EDDSVVCC	466
Ref.7a.CA.x.QC69.EF108306	---DGSWSTVST-----RSDVICC	446
4a._.02C.DQ418784	-----SWSTVSGS----ED-VVCC	445
Ref.4a.EG.x.ED43.Y11604	---SDSWSTVS-----GSEDVVCC	445
5a.GB.EUH1480.Y13184	-----SWSTVSGE----DN-VVCC	450
5a.ZA.SA13.AF064490	-----SWSTVSDE----DS-VVCC	450
3a._.K3A.D28917	-----SWSTVSDS---EEQSVVCC	452
3a._.NZL1.NC_009824	-----SWSTVSDS---EEQSVVCC	452
6a.HK.6a63.DQ480514	-----SWSTVSDQ----DD-VVCC	451
1b.JP.JK1-full.X61596	-----SWSTVSEEAS-ED--VACC	447
1b._.pCV-J4L10.AF054259	-----SWSTVSEEAS--ED-VVCC	447
1b.JP.JT.D11355	-----SWSTVSGEAS-DD--IVCC	447
Ref.1a.US.x.HCV-1.M62321	---DGSWSTVSSEANAED--VVCC	448
1a._.H77.NC_004102	-----SWSTVSSGADTED--VVCC	453
1a.US.HC-TN.EF621489	-----SWSTVSSEADKED--VVCC	448
1a.JP.HC-J1.D10749	-----SWSTVSSEAGTED--VVCC	448
	**** * **	

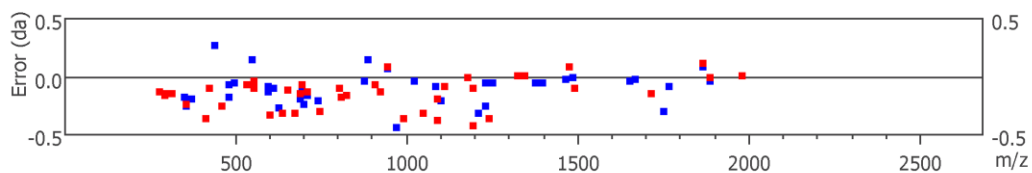
Figure A 1. Conservation of NS5A phosphoacceptor sites. HCV amino acid sequences from 19 strains were chosen based on providing representation of the HCV genotypes 1-6 and were previously identified as such from investigations performed by Scheel et al., 2012 and Wose King et al., 2014 (343,344) and were retrieved from the Los Alamos Database (<http://hcv.lanl.gov/content/index>). Alignments were performed using CLUTAL Omega software. Serines identified as NS5A phosphoacceptors in our study and their conserved corresponding serines in the other HCV strains are highlighted in light grey and threonines are highlighted in dark grey.

Chapter 8: Appendix 2: NS5A Phosphorylation Site Evidence

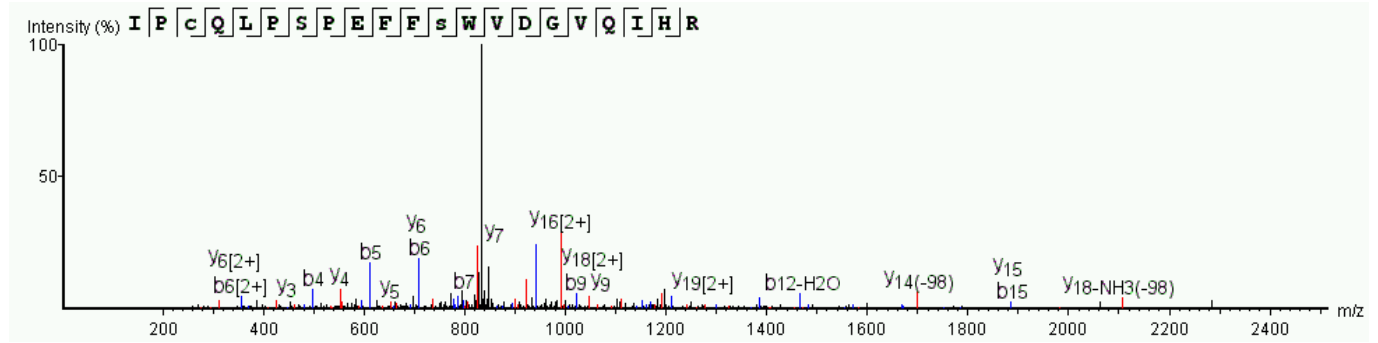
S146 (Trypsin digestion, A-Score = 77.53)



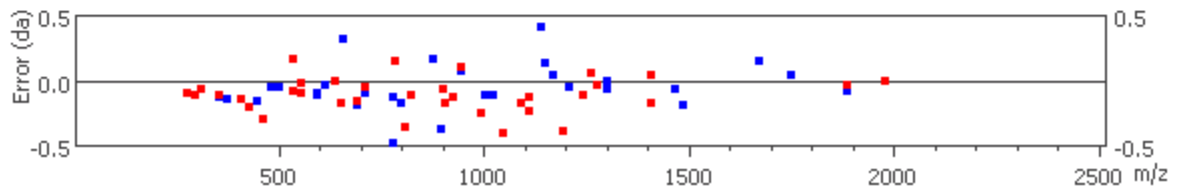
#	b	b-H2O	b-NH3	b (2+)	Seq	y	y-H2O	y-NH3	y (2+)	#
1	114.09	96.08	97.06	57.55	I					21
2	211.14	193.13	194.12	106.07	P	2479.13	2461.12	2462.10	1240.42	20
3	371.36	353.34	354.15	186.09	C(+57.02)	2382.07	2364.06	2365.05	1191.96	19
4	499.29	481.40	482.28	250.12	Q	2222.04	2204.03	2205.02	1111.52	18
5	612.42	594.43	595.38	306.66	L	2093.98	2075.97	2076.96	1047.81	17
6	709.54	691.55	692.45	355.44	P	1980.87	1962.89	1963.87	991.31	16
7	876.40	858.36	859.34	438.40	S(+79.97)	1883.84	1865.84	1866.69	942.32	15
8	973.42	955.41	956.39	487.21	P	1717.00	1698.84	1699.82	858.92	14
9	1102.68	1084.45	1085.52	551.58	E	1619.80	1601.79	1602.77	810.40	13
10	1249.59	1231.78	1232.56	625.54	F	1490.85	1472.64	1473.73	746.18	12
11	1396.66	1378.64	1379.57	699.03	F	1343.67	1325.66	1326.66	672.65	11
12	1483.62	1465.64	1466.61	742.52	S	1196.72	1178.60	1179.59	599.15	10
13	1669.74	1651.74	1652.69	835.36	W	1109.68	1091.95	1092.75	555.39	9
14	1768.86	1751.08	1751.75	884.73	V	923.64	905.57	906.48	462.50	8
15	1883.84	1865.80	1866.69	942.32	D	824.59	806.52	807.59	413.08	7
16	1940.83	1922.82	1923.80	971.35	G	709.54	691.55	692.45	355.44	6
17	2039.90	2021.89	2022.87	1020.48	V	652.50	634.38	635.68	326.69	5
18	2167.96	2149.95	2150.93	1084.48	Q	553.36	535.38	536.29	277.29	4
19	2281.04	2263.03	2264.01	1141.02	I	425.36	407.25	408.23	213.13	3
20	2418.10	2400.09	2401.07	1209.87	H	312.33	294.33	295.29	156.59	2
21					R	175.12	157.11	158.09	88.06	1



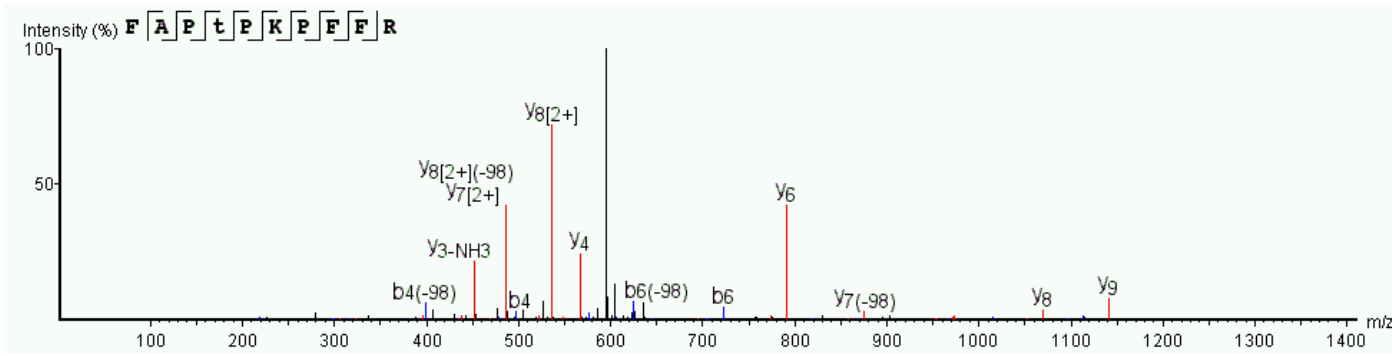
T151 (Trypsin digestion, CID, A-Score =8.39)



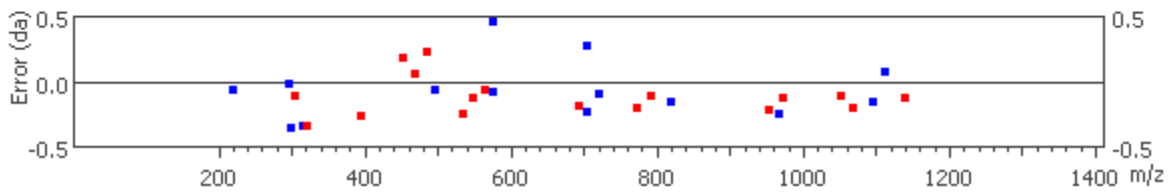
#	b	b-H2O	b-NH3	b (2+)	Seq	y	y-H2O	y-NH3	y (2+)	#
1	114.09	96.08	97.06	57.55	I					21
2	211.14	193.13	194.12	106.07	P	2479.13	2461.12	2462.10	1240.18	20
3	371.32	353.16	354.15	186.09	C(+57.02)	2382.07	2364.06	2365.05	1191.94	19
4	499.28	481.22	482.26	250.12	Q	2222.04	2204.03	2205.02	1111.77	18
5	612.35	594.41	595.41	306.66	L	2093.98	2075.97	2076.96	1047.91	17
6	709.46	691.56	692.34	355.31	P	1980.91	1962.89	1963.87	991.21	16
7	796.58	778.53	779.86	398.70	S	1883.89	1865.84	1866.82	942.31	15
8	893.83	875.44	876.26	447.39	P	1796.82	1778.81	1779.79	898.98	14
9	1022.61	1004.61	1005.47	511.75	E	1699.76	1681.75	1682.74	850.38	13
10	1169.51	1151.41	1152.54	585.28	F	1570.72	1552.71	1553.69	785.71	12
11	1316.63	1298.69	1299.60	658.48	F	1423.65	1405.58	1406.80	712.33	11
12	1483.83	1465.69	1466.61	742.32	S(+79.97)	1276.62	1258.57	1259.48	638.79	10
13	1669.56	1651.70	1652.69	835.36	W	1109.72	1091.57	1092.74	555.39	9
14	1768.78	1750.77	1751.71	884.89	V	923.64	905.67	906.48	462.56	8
15	1883.89	1865.80	1866.78	942.31	D	824.56	806.79	807.41	412.72	7
16	1940.83	1922.82	1923.80	970.91	G	709.46	691.56	692.38	355.31	6
17	2039.90	2021.89	2022.87	1020.45	V	652.57	634.38	635.35	326.69	5
18	2167.96	2149.95	2150.93	1084.48	Q	553.34	535.40	536.11	277.25	4
19	2281.04	2263.03	2264.01	1140.60	I	425.47	407.25	408.38	213.13	3
20	2418.10	2400.09	2401.07	1209.61	H	312.24	294.17	295.27	156.59	2
21					R	175.12	157.11	158.09	88.06	1



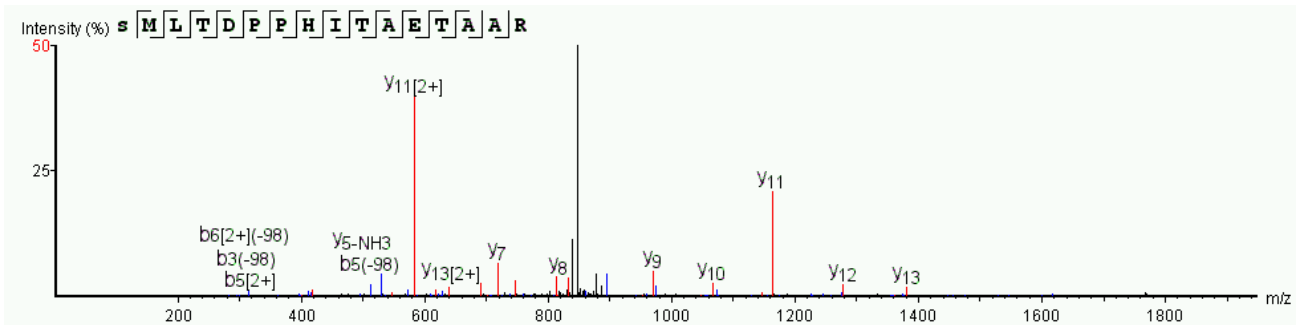
T164 (Trypsin digestion, CID, A-Score =1000)



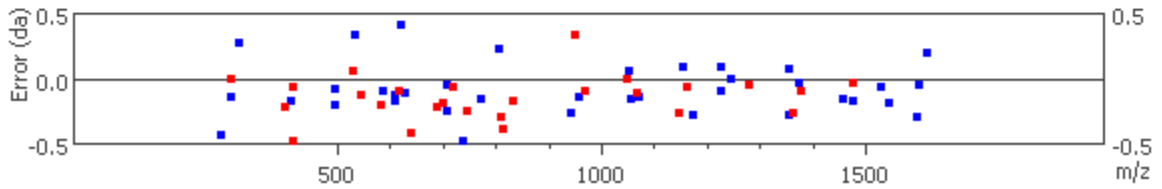
#	b	b-H2O	b-NH3	b (2+)	Seq	y	y-H2O	y-NH3	y (2+)	#
1	148.08	130.07	131.05	74.54	F					10
2	219.18	201.10	202.09	110.06	A	1140.69	1122.55	1123.53	570.78	9
3	316.51	298.18	299.51	158.58	P	1069.73	1051.51	1052.61	535.51	8
4	497.24	479.17	480.15	249.09	T(+79.97)	972.60	954.68	955.44	486.49	7
5	594.23	575.76	577.30	297.62	P	791.57	773.66	774.43	396.50	6
6	722.42	704.03	705.54	361.66	K	694.59	676.39	677.38	347.70	5
7	819.55	801.37	802.35	410.19	P	566.37	548.43	549.28	283.65	4
8	966.70	948.44	949.42	483.72	F	469.18	451.25	452.04	235.13	3
9	1113.43	1095.51	1096.66	557.26	F	322.54	304.18	305.28	161.59	2
10					R	175.12	157.11	158.09	88.06	1



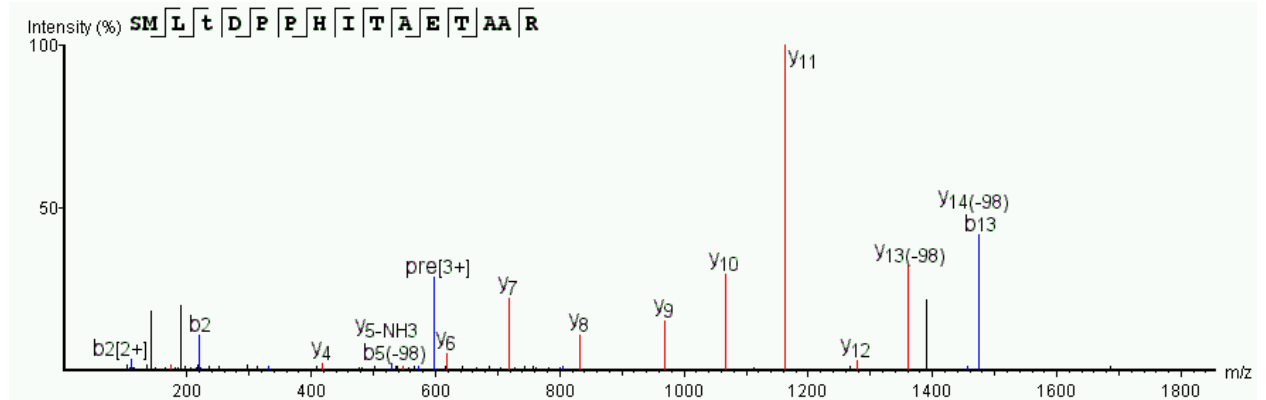
S201 (Trypsin digestion, CID, A-Score =32.97)



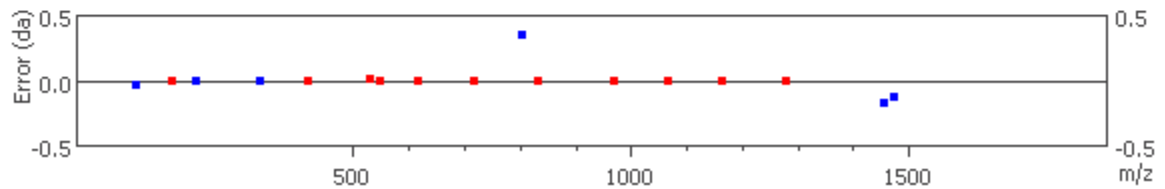
#	b	b-H2O	b-NH3	b (2+)	Seq	y	y-H2O	y-NH3	y (2+)	#
1	168.01	150.00	150.98	84.50	S(+79.97)					16
2	299.20	281.04	282.46	150.02	M	1623.82	1605.81	1606.79	812.71	15
3	412.31	394.12	395.10	206.57	L	1492.78	1474.81	1475.75	747.14	14
4	513.18	495.38	496.23	257.09	T	1379.79	1361.96	1362.66	690.57	13
5	628.32	610.33	611.35	314.32	D	1278.70	1260.63	1261.62	640.24	12
6	725.26	707.30	708.49	363.13	P	1163.69	1145.87	1146.59	582.52	11
7	822.31	804.30	805.28	411.66	P	1066.67	1048.56	1049.54	533.78	10
8	959.52	941.62	942.34	480.18	H	969.62	951.50	952.14	485.26	9
9	1072.60	1054.37	1055.59	536.38	I	832.62	814.44	815.81	417.22	8
10	1173.79	1155.39	1156.47	587.36	T	719.43	701.55	702.34	360.18	7
11	1244.55	1226.64	1227.41	622.35	A	618.42	600.31	601.29	309.66	6
12	1373.62	1355.85	1356.47	687.29	E	547.41	529.27	530.18	274.14	5
13	1474.81	1456.78	1457.60	738.30	T	418.32	400.23	401.44	209.62	4
14	1545.86	1527.66	1528.71	773.50	A	317.19	299.20	300.17	159.10	3
15	1616.49	1599.00	1599.73	808.61	A	246.16	228.15	229.13	123.58	2
16					R	175.12	157.11	158.09	88.06	1



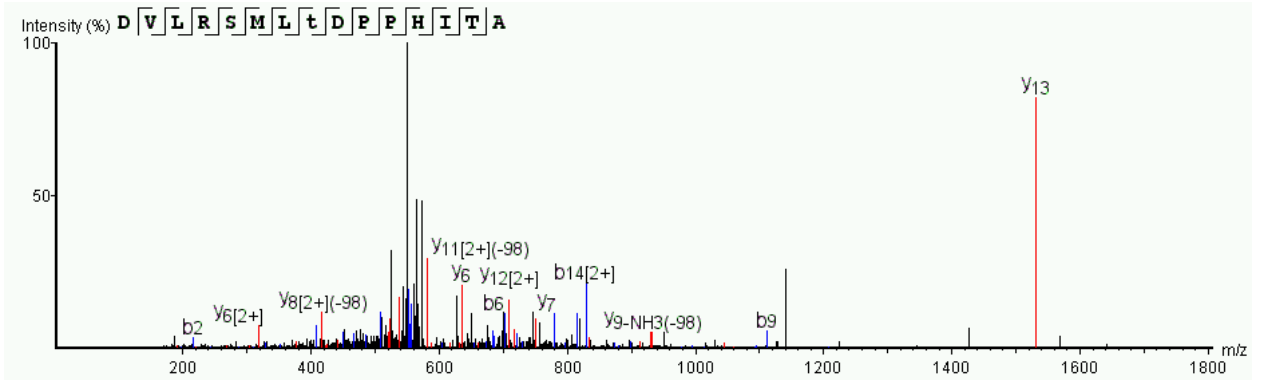
T204 (Trypsin Digestion, HCD, A-Score =19.05)



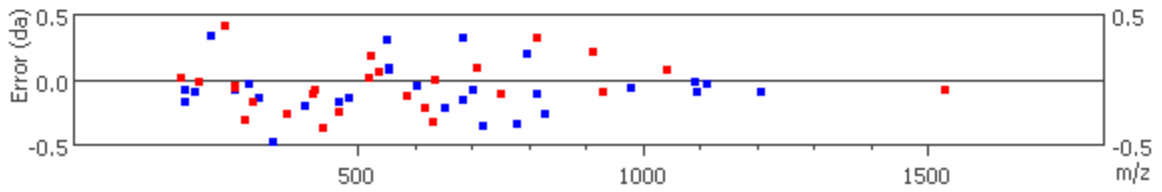
#	b	b-H2O	b-NH3	b (2+)	Seq	y	y-H2O	y-NH3	y (2+)	#
1	88.04	70.03	71.01	44.52	S					16
2	219.08	201.07	202.05	110.07	M	1703.78	1685.77	1686.76	852.39	15
3	332.17	314.15	315.14	166.58	L	1572.74	1554.73	1555.71	786.87	14
4	513.18	495.17	496.15	257.09	T(+79.97)	1459.66	1441.65	1442.63	730.33	13
5	628.21	610.19	611.18	314.60	D	1278.64	1260.63	1261.62	639.82	12
6	725.26	707.25	708.23	363.13	P	1163.62	1145.61	1146.59	582.31	11
7	822.31	803.94	805.28	411.66	P	1066.57	1048.55	1049.54	533.78	10
8	959.37	941.36	942.34	480.18	H	969.51	951.50	952.48	485.26	9
9	1072.45	1054.44	1055.43	536.73	I	832.45	814.44	815.43	416.73	8
10	1173.50	1155.49	1156.47	587.25	T	719.37	701.36	702.34	360.18	7
11	1244.54	1226.53	1227.51	622.77	A	618.32	600.31	601.29	309.66	6
12	1373.58	1355.57	1356.55	687.29	E	547.29	529.27	530.23	274.14	5
13	1474.76	1456.80	1457.60	737.81	T	418.24	400.23	401.21	209.62	4
14	1545.67	1527.66	1528.64	773.33	A	317.19	299.18	300.17	159.10	3
15	1616.70	1598.69	1599.68	808.85	A	246.16	228.15	229.13	123.58	2
16					R	175.12	157.11	158.09	88.06	1



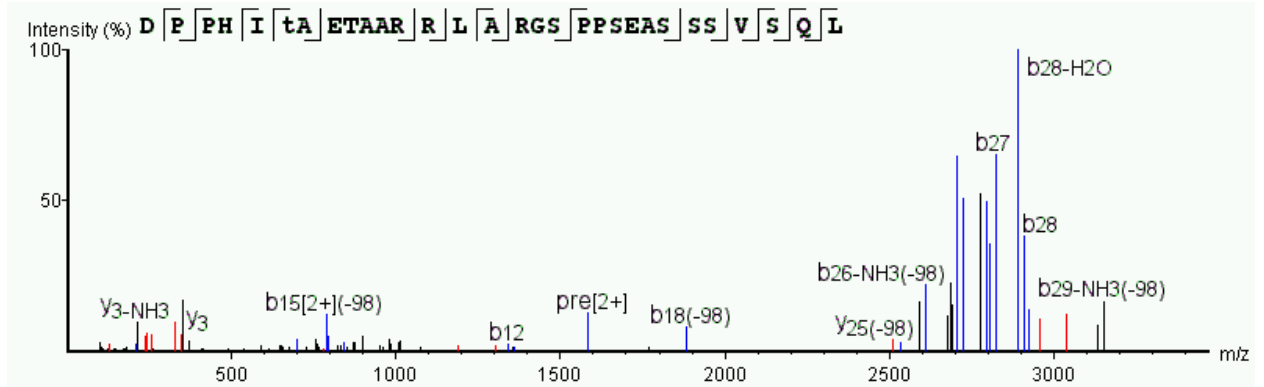
T204 (GluC Digestion, HCD, digestion, A Score = 28.22)



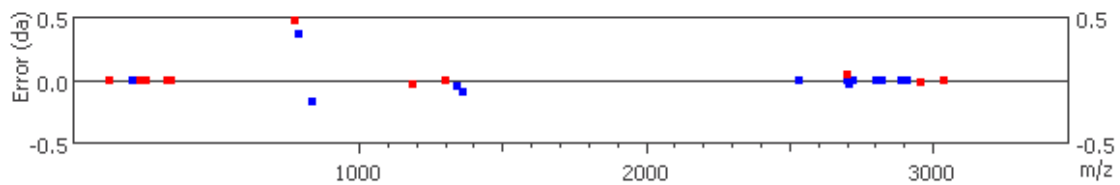
#	b	b-H2O	b-NH3	b (2+)	Seq	y	y+H2O	y-NH3	y (2+)	#
1	116.03	98.02	99.01	58.52	D					15
2	215.20	197.18	198.25	108.05	V	1630.80	1612.79	1613.78	815.56	14
3	328.34	310.22	311.16	164.59	L	1531.82	1513.72	1514.71	766.37	13
4	484.43	466.45	467.26	242.29	R	1418.65	1400.64	1401.62	709.73	12
5	571.32	552.99	554.19	286.25	S	1262.55	1244.54	1245.52	632.11	11
6	702.44	684.01	685.50	352.16	M	1175.52	1157.51	1158.49	588.38	10
7	815.56	797.23	798.42	408.43	L	1044.40	1026.47	1027.45	522.54	9
8	996.46	978.52	979.43	498.73	T(+79.97)	931.49	913.16	914.37	466.45	8
9	1111.52	1093.50	1094.56	556.16	D	750.49	732.37	733.35	375.96	7
10	1208.65	1190.53	1191.51	604.83	P	635.35	617.57	618.32	318.36	6
11	1305.59	1287.58	1288.56	653.52	P	538.23	520.27	521.27	269.23	5
12	1442.65	1424.64	1425.62	722.18	H	441.62	423.36	424.30	221.15	4
13	1555.73	1537.72	1538.71	778.71	I	304.50	286.25	287.21	152.59	3
14	1656.78	1638.77	1639.76	829.15	T	191.08	173.09	174.08	96.05	2
15					A	90.05	72.04	73.03	45.53	1



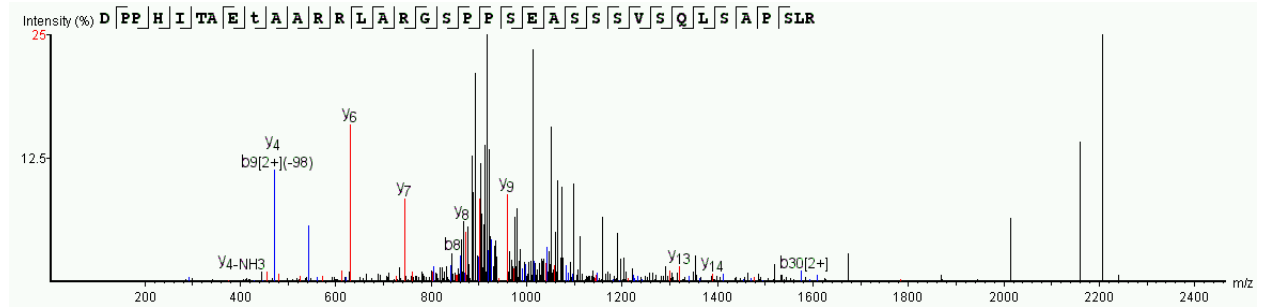
T210 (AspN, CID, A-Score =13.22)



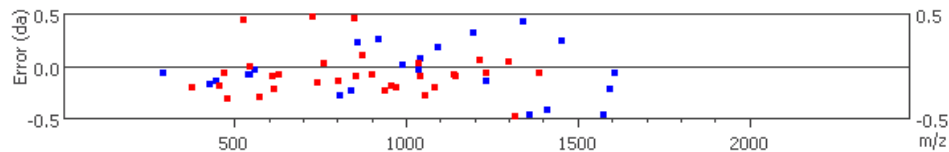
#	b	b-H2O	b-NH3	b (2+)	Seq	y	y-H2O	y-NH3	y (2+)	#
1	116.03	98.02	99.01	58.52	D					30
2	213.09	195.08	196.06	107.04	P	3053.52	3035.51	3036.49	1527.26	29
3	310.14	292.13	293.11	155.57	P	2956.48	2938.45	2939.44	1478.73	28
4	447.20	429.19	430.17	224.10	H	2859.41	2841.40	2842.38	1430.21	27
5	560.28	542.27	543.26	280.64	I	2722.35	2704.34	2705.28	1361.68	26
6	741.30	723.29	724.27	371.15	T(+79.97)	2609.27	2591.26	2592.24	1305.14	25
7	812.33	793.94	795.31	406.67	A	2428.25	2410.24	2411.23	1214.63	24
8	941.38	923.37	924.35	471.19	E	2357.22	2339.21	2340.19	1179.11	23
9	1042.42	1024.41	1025.40	521.71	T	2228.17	2210.16	2211.15	1114.59	22
10	1113.46	1095.45	1096.43	557.23	A	2127.13	2109.12	2110.10	1064.06	21
11	1184.50	1166.49	1167.47	592.75	A	2056.09	2038.08	2039.06	1028.54	20
12	1340.65	1322.59	1323.57	670.80	R	1985.05	1967.04	1968.03	993.03	19
13	1496.70	1478.69	1479.67	748.85	R	1828.95	1810.94	1811.92	914.98	18
14	1609.79	1591.77	1592.76	805.39	L	1672.85	1654.84	1655.82	836.92	17
15	1680.82	1662.81	1663.80	841.09	A	1559.77	1541.76	1542.74	779.90	16
16	1836.92	1818.91	1819.90	918.96	R	1488.73	1470.72	1471.70	744.86	15
17	1893.94	1875.93	1876.92	947.47	G	1332.63	1314.62	1315.60	666.81	14
18	1980.98	1962.97	1963.95	990.99	S	1275.61	1257.60	1258.58	638.30	13
19	2078.03	2060.02	2061.00	1039.51	P	1188.61	1170.56	1171.55	594.79	12
20	2175.08	2157.07	2158.06	1088.04	P	1091.52	1073.51	1074.49	546.26	11
21	2262.11	2244.10	2245.09	1131.56	S	994.47	976.46	977.44	497.73	10
22	2391.16	2373.15	2374.13	1196.08	E	907.44	889.43	890.41	454.22	9
23	2462.19	2444.18	2445.17	1231.60	A	778.39	760.38	761.37	389.70	8
24	2549.23	2531.22	2532.21	1275.11	S	707.36	689.35	690.33	354.18	7
25	2636.26	2618.25	2619.23	1318.63	S	620.32	602.31	603.30	310.66	6
26	2723.30	2705.28	2706.31	1362.25	S	533.29	515.28	516.27	267.15	5
27	2822.36	2804.34	2805.33	1411.68	V	446.26	428.25	429.23	223.63	4
28	2909.38	2891.38	2892.36	1455.20	S	347.19	329.18	330.17	174.10	3
29	3037.45	3019.44	3020.42	1519.22	Q	260.16	242.15	243.14	130.58	2
30					L	132.10	114.09	115.07	66.55	1



S213 (Trypsin Digestion, HCD, A-Score =0)

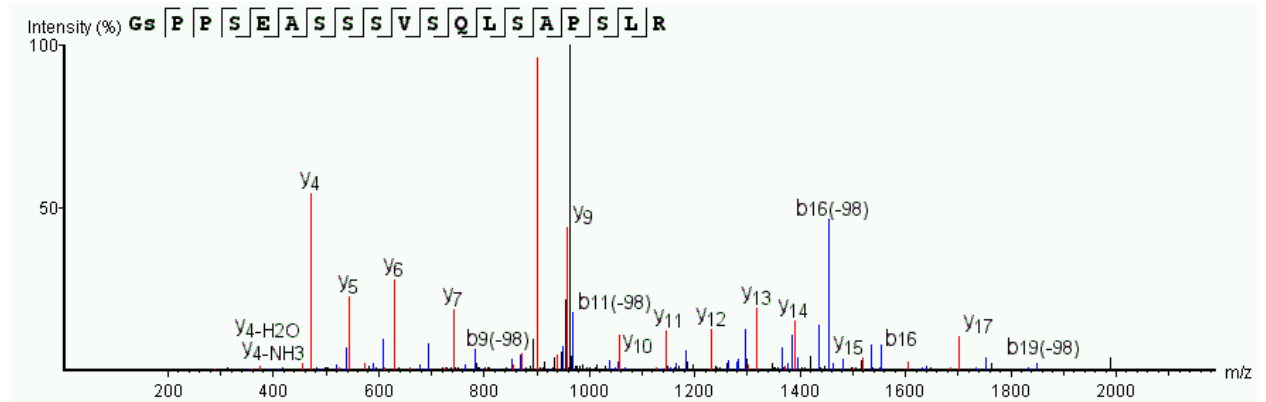


#	b	b-H2O	b-NH3	b (2+)	Seq	y	y-H2O	y-NH3	y (2+)	#
1	116.03	98.02	99.01	58.52	D					36
2	213.09	195.08	196.06	107.04	P	3664.86	3646.84	3647.83	1832.93	35
3	310.14	292.20	293.11	155.57	P	3567.80	3549.79	3550.78	1784.40	34
4	447.35	429.37	430.17	224.10	H	3470.75	3452.74	3453.72	1735.87	33
5	560.32	542.36	543.33	280.64	I	3333.69	3315.68	3316.66	1667.35	32
6	661.33	643.32	644.30	331.17	T	3220.61	3202.60	3203.58	1610.80	31
7	732.37	714.36	715.34	366.68	A	3119.56	3101.55	3102.53	1560.28	30
8	861.17	843.40	844.38	431.21	E	3048.52	3030.51	3031.50	1524.76	29
9	1042.34	1024.41	1025.40	521.71	T(+79.97)	2919.48	2901.47	2902.45	1460.24	28
10	1113.46	1095.26	1096.43	557.23	A	2738.47	2720.46	2721.44	1369.73	27
11	1184.50	1166.49	1167.47	592.75	A	2667.43	2649.42	2650.40	1334.21	26
12	1340.16	1322.59	1323.57	670.80	R	2596.39	2578.38	2579.36	1298.70	25
13	1496.70	1478.69	1479.67	748.85	R	2440.29	2422.28	2423.26	1220.65	24
14	1609.85	1591.77	1592.97	805.67	L	2284.19	2266.18	2267.16	1142.68	23
15	1680.82	1662.81	1663.80	841.15	A	2171.10	2153.09	2154.08	1086.26	22
16	1836.92	1818.91	1819.90	918.70	R	2100.07	2082.06	2083.04	1050.53	21
17	1893.94	1875.93	1876.92	947.47	G	1943.97	1925.96	1926.94	972.69	20
18	1980.98	1962.97	1963.95	990.97	S	1886.95	1868.93	1869.92	943.97	19
19	2078.03	2060.02	2061.00	1039.55	P	1799.91	1781.90	1782.89	900.55	18
20	2175.08	2157.07	2158.06	1088.04	P	1702.86	1684.85	1685.83	851.47	17
21	2262.11	2244.10	2245.09	1131.56	S	1605.81	1587.80	1588.78	803.55	16
22	2391.16	2373.15	2374.13	1195.75	E	1518.78	1500.77	1501.75	759.84	15
23	2462.19	2444.18	2445.17	1231.74	A	1389.80	1371.72	1372.71	695.37	14
24	2549.23	2531.22	2532.20	1275.11	S	1319.18	1300.64	1301.67	659.85	13
25	2636.26	2618.25	2619.23	1318.63	S	1231.74	1213.59	1214.64	616.33	12
26	2723.29	2705.28	2706.26	1362.61	S	1144.73	1126.62	1127.61	573.11	11
27	2822.36	2804.35	2805.33	1412.10	V	1057.88	1039.55	1040.67	529.30	10
28	2909.39	2891.38	2892.36	1454.95	S	958.72	940.76	941.50	480.08	9
29	3037.45	3019.44	3020.42	1519.22	Q	871.38	853.60	854.47	436.25	8
30	3150.53	3132.52	3133.51	1576.24	L	743.60	725.43	725.93	372.22	7
31	3237.57	3219.55	3220.54	1619.28	S	630.44	612.45	613.55	315.68	6
32	3308.60	3290.59	3291.58	1654.80	A	543.33	525.31	525.84	272.16	5
33	3405.66	3387.64	3388.63	1703.33	P	472.36	454.28	455.46	236.64	4
34	3492.69	3474.68	3475.66	1746.84	S	375.45	357.22	358.21	188.12	3
35	3605.77	3587.76	3588.74	1803.39	L	288.20	270.19	271.18	144.60	2
36					R	175.12	157.11	158.09	88.06	1

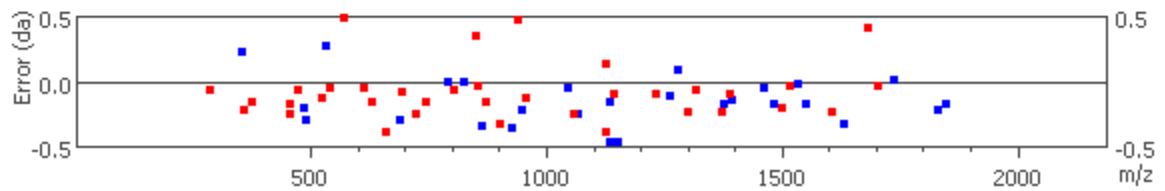


The presence of the b-ions at b8, b9 and b12 supports phosphorylation at S13 (Serine 9 in this peptide).

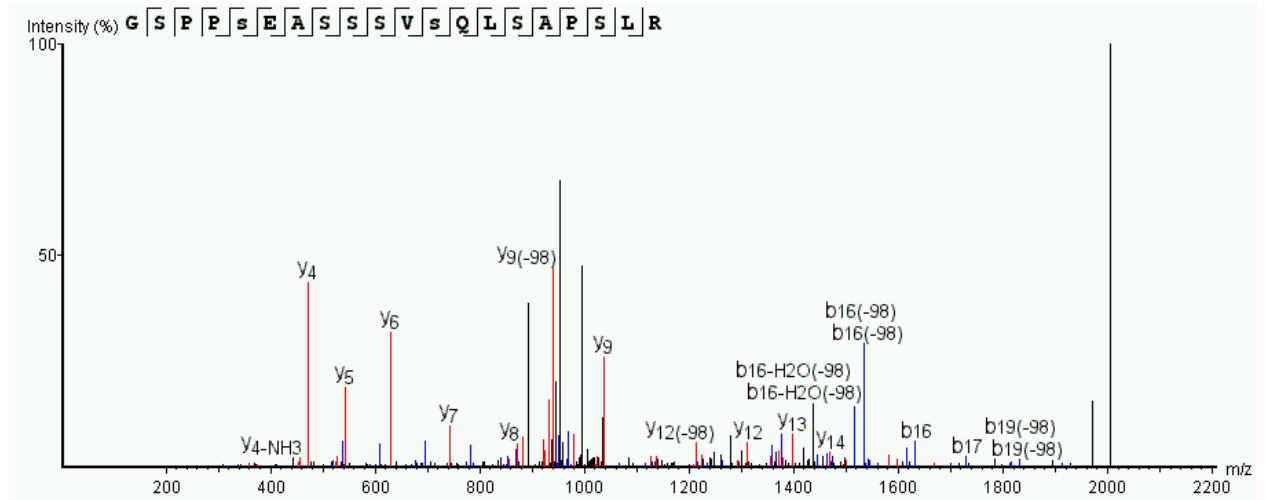
S222 (Trypsin Digestion, HCD, A-Score =28.36)



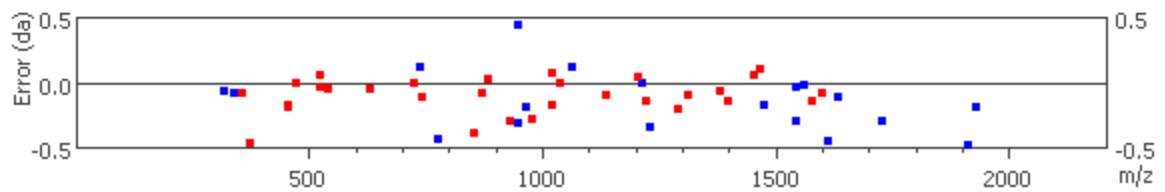
#	b	b-H2O	b-NH3	b (2+)	Seq	y	y-H2O	y-NH3	y (2+)	#
1	58.03	40.02	41.00	29.51	G					20
2	225.03	207.02	208.00	113.01	S(+79.97)	1966.91	1948.90	1949.88	983.96	19
3	322.08	304.07	305.05	161.54	P	1799.91	1781.90	1782.89	900.78	18
4	419.13	401.12	402.11	210.07	P	1702.90	1684.85	1685.41	851.57	17
5	506.17	488.15	489.43	253.58	S	1606.05	1587.80	1588.78	803.47	16
6	635.21	617.20	618.18	318.10	E	1518.81	1500.97	1501.75	759.89	15
7	706.24	688.23	689.51	353.39	A	1389.84	1371.97	1372.71	695.46	14
8	793.26	775.27	776.25	397.14	S	1318.76	1300.93	1301.67	660.24	13
9	880.31	862.30	863.63	440.65	S	1231.76	1213.65	1214.64	616.33	12
10	967.34	949.33	950.54	484.38	S	1144.73	1126.48	1128.00	572.32	11
11	1066.66	1048.46	1049.38	533.42	V	1057.86	1039.59	1040.57	529.30	10
12	1153.90	1135.60	1136.89	577.22	S	958.66	940.03	941.50	479.77	9
13	1281.40	1263.61	1264.47	641.25	Q	871.67	853.49	854.51	436.25	8
14	1394.73	1376.75	1377.56	697.79	L	743.60	725.68	726.41	372.22	7
15	1481.79	1463.66	1464.59	741.31	S	630.52	612.40	613.33	315.68	6
16	1552.83	1534.67	1535.63	776.83	A	543.39	525.45	526.30	272.16	5
17	1649.71	1632.02	1632.68	825.35	P	472.36	454.53	455.43	236.64	4
18	1736.71	1718.73	1719.71	868.87	S	375.40	357.22	358.43	188.12	3
19	1850.00	1832.04	1832.80	925.78	L	288.28	270.19	271.18	144.60	2
20					R	175.12	157.11	158.09	88.06	1



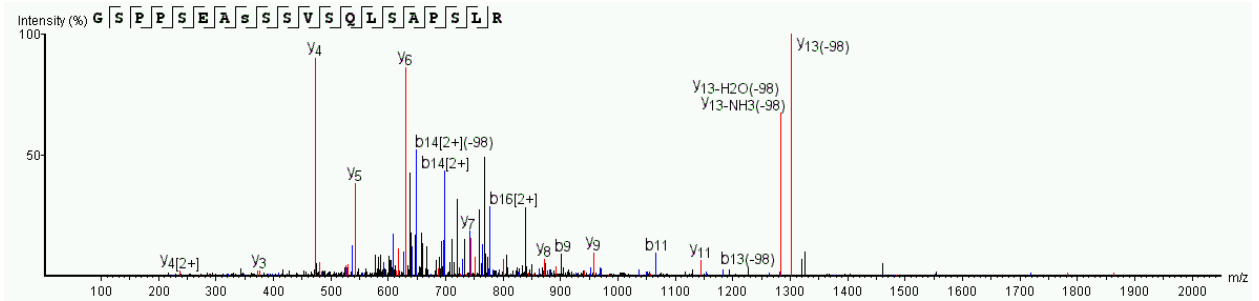
S225 (Trypsin Digestion, CID, A-Score =32.28)



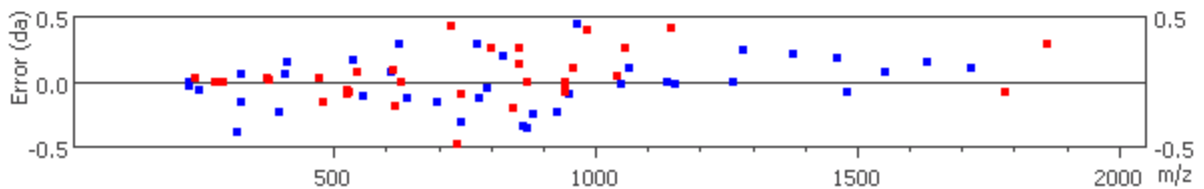
#	b	b-H2O	b-NH3	b (2+)	Seq	y	y-H2O	y-NH3	y (2+)	#
1	58.03	40.02	41.00	29.51	G					20
2	145.06	127.05	128.03	73.03	S	2046.88	2028.87	2029.85	1023.85	19
3	242.11	224.10	225.09	121.56	P	1959.85	1941.84	1942.82	980.71	18
4	339.26	321.16	322.14	170.08	P	1862.79	1844.78	1845.77	932.20	17
5	506.17	488.15	489.14	253.58	S(+79.97)	1765.74	1747.73	1748.71	883.33	16
6	635.21	617.20	618.18	318.17	E	1598.83	1580.87	1581.72	799.87	15
7	706.24	688.23	689.22	353.62	A	1469.58	1451.69	1452.61	735.35	14
8	793.28	775.70	776.25	397.14	S	1398.81	1380.72	1381.64	699.83	13
9	880.31	862.30	863.28	440.65	S	1311.72	1293.83	1294.60	656.32	12
10	967.53	948.88	950.62	484.17	S	1224.75	1206.59	1207.51	612.80	11
11	1066.29	1048.40	1049.38	533.70	V	1137.67	1119.56	1120.54	569.28	10
12	1233.75	1215.40	1216.38	617.20	S(+79.97)	1038.51	1020.66	1021.47	519.75	9
13	1361.47	1343.46	1344.44	681.23	Q	871.58	853.49	854.87	436.25	8
14	1474.73	1456.54	1457.52	737.64	L	743.55	725.44	726.41	372.22	7
15	1561.61	1543.61	1544.86	781.29	S	630.41	612.35	613.33	315.68	6
16	1632.73	1615.06	1615.59	816.81	A	543.38	525.25	526.34	272.16	5
17	1729.97	1711.66	1712.65	865.34	P	472.29	454.47	455.44	236.64	4
18	1816.70	1798.69	1799.68	908.85	S	375.70	357.22	358.30	188.12	3
19	1929.98	1911.78	1913.25	965.39	L	288.20	270.19	271.18	144.60	2
20					R	175.12	157.11	158.09	88.06	1



S228 (Trypsin Digestion, CID, A-Score = 0)

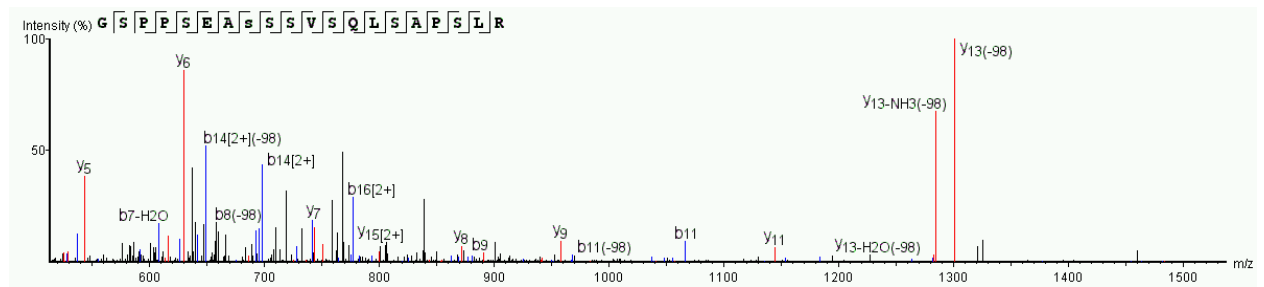


#	b	b-H2O	b-NH3	b (2+)	Seq	y	y-H2O	y-NH3	y (2+)	#
1	58.03	40.02	41.00	29.51	G					20
2	145.06	127.05	128.03	73.03	S	1966.91	1948.90	1949.88	983.55	19
3	242.18	224.14	225.07	121.56	P	1879.88	1861.87	1862.55	940.52	18
4	339.17	321.31	322.07	170.08	P	1782.91	1764.82	1765.80	891.91	17
5	426.20	408.12	409.00	213.60	S	1685.77	1667.76	1668.75	843.59	16
6	555.35	537.05	538.21	278.12	E	1598.74	1580.73	1581.72	799.60	15
7	625.98	608.19	609.25	314.04	A	1469.70	1451.69	1452.67	735.83	14
8	793.33	774.96	776.25	397.38	S(+79.97)	1398.66	1380.65	1381.64	699.83	13
9	880.56	862.64	863.28	440.65	S	1231.66	1213.65	1214.64	616.52	12
10	966.89	949.43	950.31	484.17	S	1144.21	1126.62	1127.61	572.82	11
11	1066.29	1048.42	1049.38	533.70	V	1057.32	1039.59	1040.52	529.39	10
12	1153.46	1135.44	1136.41	577.22	S	958.41	940.52	941.54	479.93	9
13	1281.24	1263.48	1264.47	641.38	Q	871.50	853.35	854.20	436.25	8
14	1394.58	1376.57	1377.34	697.95	L	743.54	724.99	726.41	372.19	7
15	1481.70	1463.41	1464.59	741.62	S	630.36	612.35	613.24	315.68	6
16	1552.56	1534.64	1535.63	776.96	A	543.24	525.41	526.37	272.16	5
17	1649.71	1631.70	1632.52	825.15	P	472.24	454.28	455.26	236.61	4
18	1736.74	1718.60	1719.71	869.24	S	375.22	357.22	358.21	188.12	3
19	1849.82	1831.81	1832.80	925.66	L	288.21	270.19	271.18	144.60	2
20					R	175.12	157.11	158.09	88.06	1

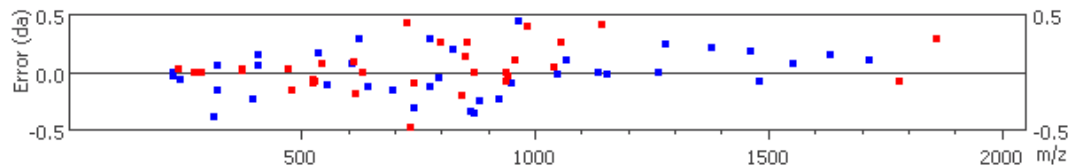


The presence of the b-ion run from b6 to b13 strongly suggests phosphorylation at S228 (Serine 8 in this peptide). Note that y11 is present limiting the phosphorylation event to the first nine amino acids in the peptide.

S229 (Trypsin Digestion, CID, A-Score = 0)

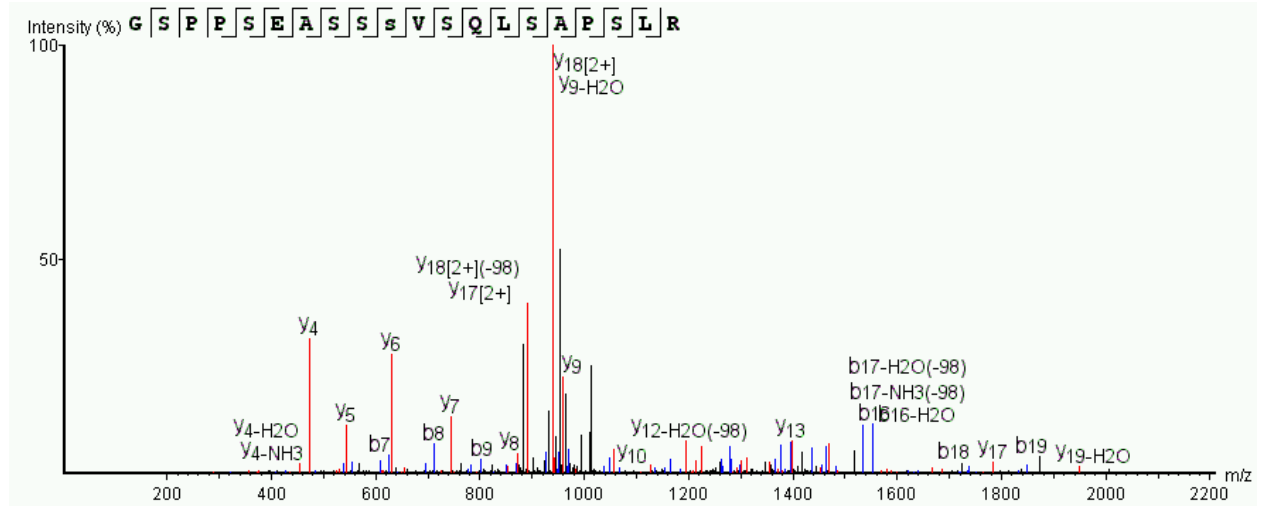


#	b	b-H2O	b-NH3	b (2+)	Seq	y	y-H2O	y-NH3	y (2+)	#
1	58.03	40.02	41.00	29.51	G					20
2	145.06	127.05	128.03	73.03	S	1966.91	1948.90	1949.88	983.55	19
3	242.18	224.14	225.07	121.56	P	1879.88	1861.87	1862.55	940.52	18
4	339.17	321.31	322.07	170.08	P	1782.91	1764.82	1765.80	891.91	17
5	426.20	408.12	409.00	213.60	S	1685.77	1667.76	1668.75	843.59	16
6	555.35	537.05	538.21	278.12	E	1598.74	1580.73	1581.72	799.60	15
7	625.98	608.19	609.25	314.04	A	1469.70	1451.69	1452.67	735.83	14
8	793.33	774.96	776.25	397.38	S(+79.97)	1398.66	1380.65	1381.64	699.83	13
9	880.56	862.64	863.28	440.65	S	1231.66	1213.65	1214.64	616.52	12
10	966.89	949.43	950.31	484.17	S	1144.21	1126.62	1127.61	572.82	11
11	1066.29	1048.42	1049.38	533.70	V	1057.32	1039.59	1040.52	529.39	10
12	1153.46	1135.44	1136.41	577.22	S	958.41	940.52	941.54	479.93	9
13	1281.24	1263.48	1264.47	641.38	Q	871.50	853.35	854.20	436.25	8
14	1394.58	1376.57	1377.34	697.95	L	743.54	724.99	726.41	372.19	7
15	1481.70	1463.41	1464.59	741.62	S	630.36	612.35	613.24	315.68	6
16	1552.56	1534.64	1535.63	776.96	A	543.24	525.41	526.37	272.16	5
17	1649.71	1631.70	1632.52	825.15	P	472.24	454.28	455.26	236.61	4
18	1736.74	1718.60	1719.71	869.24	S	375.22	357.22	358.21	188.12	3
19	1849.82	1831.81	1832.80	925.66	L	288.21	270.19	271.18	144.60	2
20					R	175.12	157.11	158.09	88.06	1

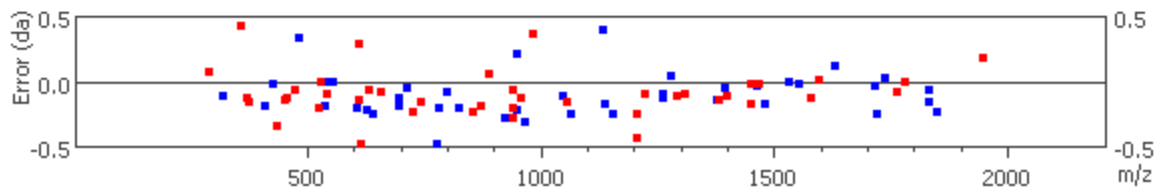


The presence of the b-ion run from b6 to b10 strongly suggests phosphorylation at S229 (Serine 8 in this peptide). Note that y11 is present limiting the phosphorylation event to the first nine amino acids in the peptide.

S230 (Trypsin Digestion, CID, A-Score = 20.41)

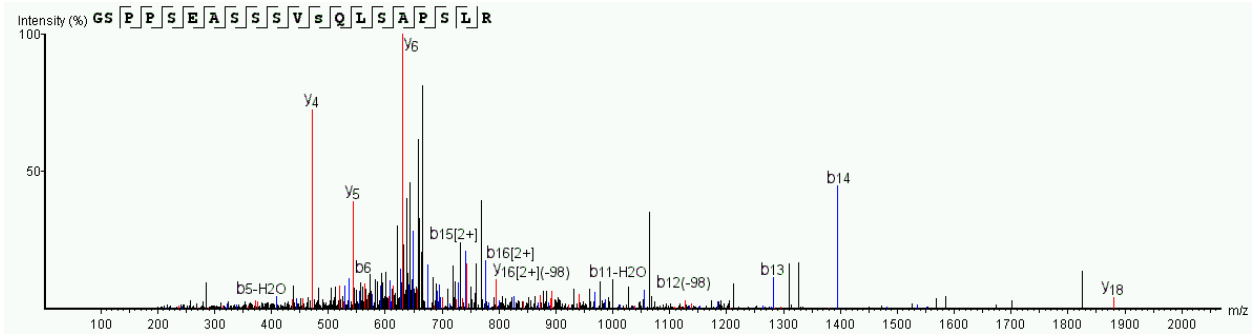


#	b	b-H2O	b-NH3	b (2+)	Seq	y	y-H2O	y-NH3	y (2+)	#
1	58.03	40.02	41.00	29.51	G					20
2	145.06	127.05	128.03	73.03	S	1966.91	1948.71	1949.88	983.58	19
3	242.11	224.10	225.09	121.56	P	1879.88	1861.87	1862.85	940.73	18
4	339.17	321.28	322.14	170.08	P	1782.84	1764.82	1765.88	891.85	17
5	426.22	408.39	409.17	213.60	S	1685.77	1667.76	1668.75	843.39	16
6	555.26	537.24	538.40	278.12	E	1598.71	1580.86	1581.72	799.87	15
7	626.51	608.47	609.25	313.64	A	1469.72	1451.71	1452.85	735.35	14
8	713.37	695.48	696.41	357.16	S	1398.78	1380.80	1381.64	699.83	13
9	800.43	782.54	783.32	400.67	S	1311.73	1293.73	1294.60	656.40	12
10	967.66	949.10	950.54	483.82	S(+79.97)	1224.69	1206.84	1208.01	612.50	11
11	1066.66	1048.52	1049.38	533.70	V	1057.76	1039.59	1040.57	529.29	10
12	1153.70	1135.02	1136.59	577.22	S	958.66	940.73	941.57	479.77	9
13	1281.45	1263.58	1264.61	641.50	Q	871.69	853.72	854.47	436.60	8
14	1394.64	1376.72	1377.56	697.79	L	743.60	725.68	726.41	372.36	7
15	1481.80	1463.64	1464.59	741.31	S	630.42	612.50	613.81	315.68	6
16	1552.67	1534.64	1535.63	777.31	A	543.43	525.52	526.30	272.16	5
17	1649.71	1631.57	1632.68	825.56	P	472.36	454.43	455.39	236.64	4
18	1736.69	1718.77	1719.97	868.87	S	375.39	357.22	357.77	188.12	3
19	1850.06	1831.97	1832.86	925.69	L	288.12	270.19	271.18	144.60	2
20					R	175.12	157.11	158.09	88.06	1

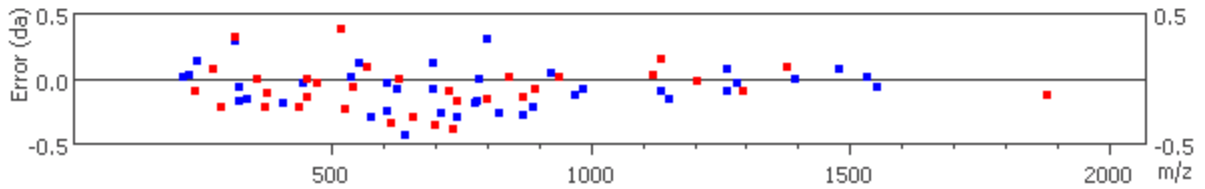


The presence of the b-ion run from b6 to b16 and y ion runs from y2 to y15 strongly suggests phosphorylation at S230 (Serine 10 in this peptide).

S232 (Trypsin Digestion, HCD, A-Score =42.61)

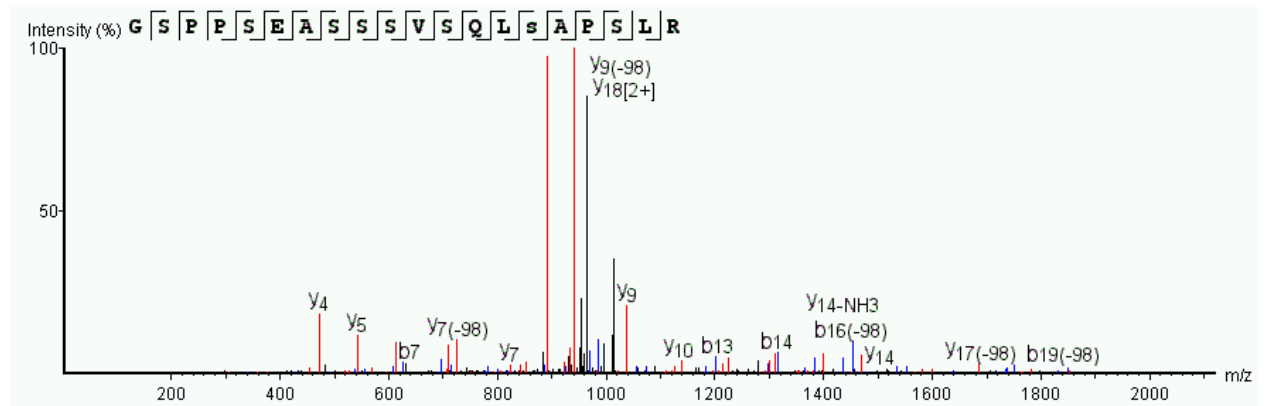


#	b	b-H2O	b-NH3	b (2+)	Seq	y	y-H2O	y-NH3	y (2+)	#
1	58.03	40.02	41.00	29.51	G					20
2	145.06	127.05	128.03	73.03	S	1966.91	1948.90	1949.88	983.96	19
3	241.97	224.10	225.04	121.56	P	1880.02	1861.87	1862.85	940.41	18
4	339.33	321.23	322.32	170.08	P	1782.83	1764.82	1765.80	891.99	17
5	426.20	408.38	409.17	213.58	S	1685.77	1667.76	1668.75	843.36	16
6	555.12	537.20	538.21	278.12	E	1598.74	1580.73	1581.72	800.03	15
7	626.37	608.30	609.51	313.34	A	1469.70	1451.69	1452.67	735.74	14
8	713.58	695.38	696.16	357.16	S	1398.66	1380.56	1381.64	700.20	13
9	800.03	782.52	783.33	400.67	S	1311.63	1293.62	1294.70	656.61	12
10	887.59	869.65	870.35	444.22	S	1224.60	1206.61	1207.57	612.80	11
11	986.53	968.57	969.42	493.72	V	1137.41	1119.56	1120.51	569.18	10
12	1153.61	1135.53	1136.41	577.52	S(+79.97)	1038.50	1020.49	1021.47	519.36	9
13	1281.55	1263.58	1264.38	641.69	Q	871.65	853.49	854.47	436.47	8
14	1394.59	1376.57	1377.56	697.79	L	743.61	725.53	726.41	372.44	7
15	1481.53	1463.61	1464.59	741.60	S	630.34	612.35	613.67	315.35	6
16	1552.72	1534.62	1535.63	777.02	A	543.40	525.31	526.54	272.16	5
17	1649.71	1631.70	1632.68	825.62	P	472.33	454.43	455.26	236.75	4
18	1736.74	1718.73	1719.71	868.87	S	375.35	357.22	358.22	188.12	3
19	1849.82	1831.81	1832.80	925.35	L	288.43	270.19	271.09	144.60	2
20					R	175.12	157.11	158.09	88.06	1

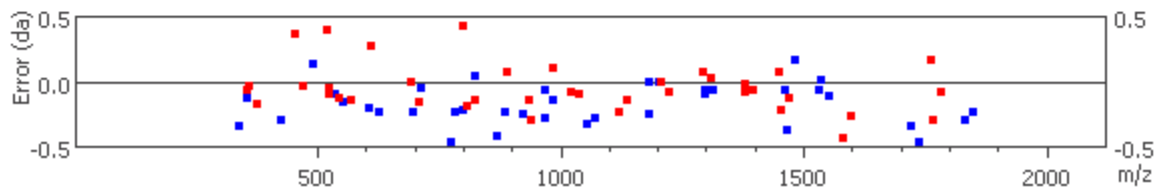


The presence of the b-ion run from b6 to b16 strongly suggests phosphorylation at S232 (Serine 12 in this peptide). Note that y8 and y10 ions constrain the phosphorylation event to S212 (Serine 12 in this peptide).

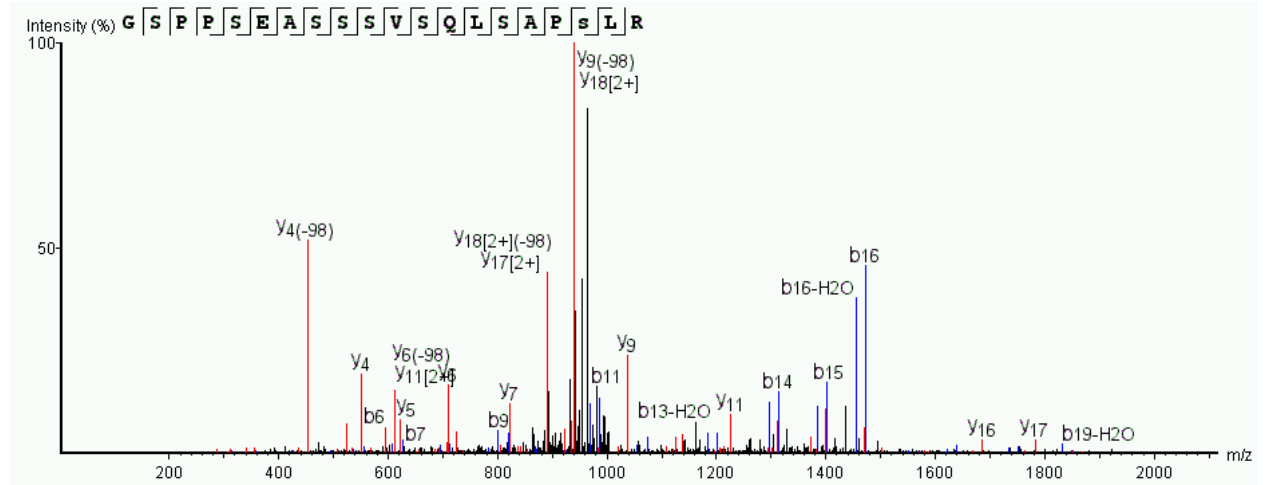
S235 (Trypsin Digestion, HCD, A-Score =42.61)



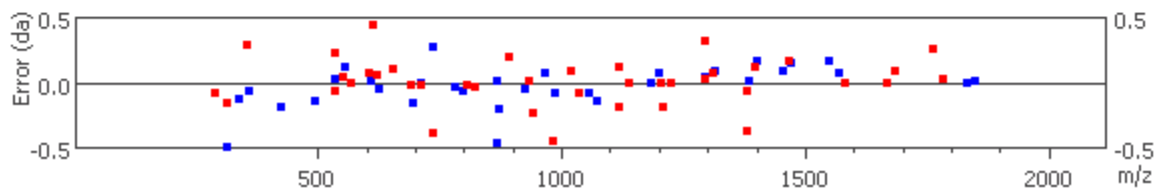
#	b	b-H2O	b-NH3	b (2+)	Seq	y	y-H2O	y-NH3	y (2+)	#
1	58.03	40.02	41.00	29.51	G					20
2	145.06	127.05	128.03	73.03	S	1966.91	1948.90	1949.88	983.84	19
3	242.11	224.10	225.09	121.56	P	1879.88	1861.87	1862.85	940.73	18
4	339.51	321.16	322.14	170.08	P	1782.91	1764.64	1766.10	891.83	17
5	426.51	408.19	409.17	213.60	S	1685.77	1667.76	1668.75	843.39	16
6	555.41	537.34	538.21	278.12	E	1599.01	1581.17	1581.72	799.43	15
7	626.51	608.48	609.25	313.64	A	1469.83	1451.61	1452.90	735.35	14
8	713.37	695.54	696.28	357.29	S	1398.74	1380.68	1381.72	699.83	13
9	800.56	782.57	783.32	400.67	S	1311.59	1293.54	1294.60	656.32	12
10	887.61	869.36	870.77	444.19	S	1224.68	1206.59	1207.57	612.52	11
11	986.59	968.51	969.70	493.58	V	1137.71	1119.79	1120.54	569.43	10
12	1073.75	1055.79	1056.45	537.34	S	1038.60	1020.58	1021.47	519.33	9
13	1201.55	1183.52	1184.77	601.27	Q	951.47	933.46	934.59	476.23	8
14	1314.69	1296.71	1297.66	657.81	L	823.55	805.40	806.57	412.20	7
15	1481.44	1463.68	1464.97	741.31	S(+79.97)	710.48	692.32	693.30	355.66	6
16	1552.77	1534.71	1535.60	777.30	A	543.45	525.42	526.36	272.16	5
17	1649.71	1631.70	1632.68	825.30	P	472.33	454.28	454.89	236.64	4
18	1737.21	1718.73	1720.05	868.87	S	375.41	357.29	358.25	188.12	3
19	1850.06	1832.12	1832.80	925.67	L	288.20	270.19	271.18	144.60	2
20					R	175.12	157.11	158.09	88.06	1



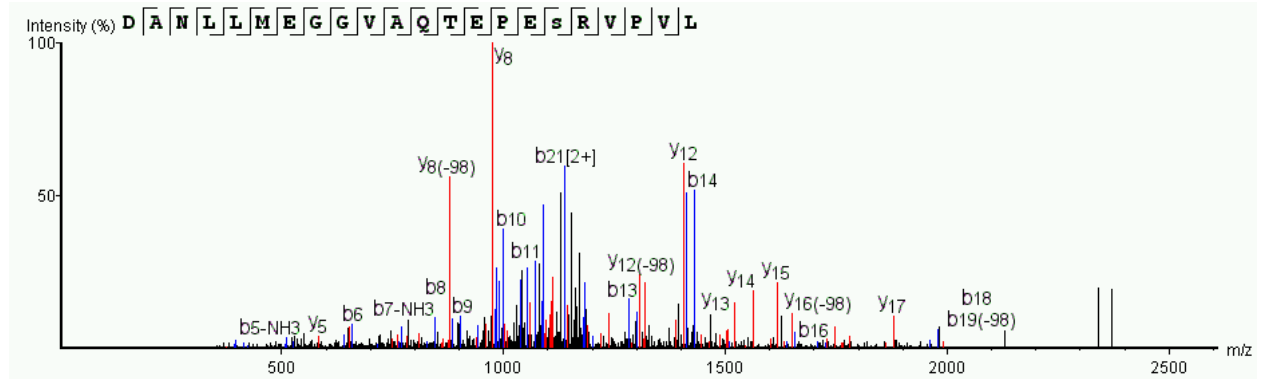
S238 (Trypsin Digestion, CID, A-Score =48.45)



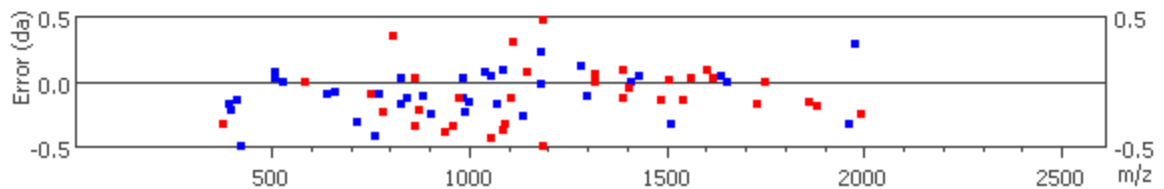
#	b	b-H2O	b-NH3	b (2+)	Seq	y	y-H2O	y-NH3	y (2+)	#
1	58.03	40.02	41.00	29.51	G					20
2	145.06	127.05	128.03	73.03	S	1966.91	1948.90	1949.88	984.41	19
3	242.11	224.10	225.09	121.56	P	1879.88	1861.87	1862.85	940.67	18
4	339.30	321.16	322.14	170.08	P	1782.80	1764.55	1765.80	891.71	17
5	426.39	408.19	409.17	213.60	S	1685.67	1667.76	1668.75	843.39	16
6	555.11	537.19	538.21	278.12	E	1598.74	1580.72	1581.72	799.87	15
7	626.34	608.24	609.25	314.14	A	1469.53	1451.69	1452.67	735.74	14
8	713.30	695.47	696.28	357.22	S	1398.53	1381.03	1381.70	699.83	13
9	800.42	782.37	783.32	400.67	S	1311.55	1293.28	1294.57	656.20	12
10	887.37	869.34	870.56	444.19	S	1224.60	1206.58	1207.77	612.34	11
11	986.53	968.34	969.42	493.87	V	1137.56	1119.75	1120.41	569.28	10
12	1073.62	1055.56	1056.45	537.19	S	1038.59	1020.38	1021.47	519.75	9
13	1201.44	1183.51	1184.51	601.27	Q	951.47	933.46	934.41	476.23	8
14	1314.51	1296.56	1297.59	657.81	L	823.45	805.41	806.38	412.20	7
15	1401.47	1383.61	1384.62	701.32	S	710.34	692.33	693.30	355.37	6
16	1472.53	1454.57	1455.66	736.55	A	623.22	605.28	606.18	312.31	5
17	1569.65	1551.55	1552.71	785.37	P	552.19	534.31	534.98	276.63	4
18	1736.74	1718.73	1719.71	869.34	S(+79.97)	455.20	437.19	438.17	228.10	3
19	1849.81	1831.82	1832.80	925.46	L	288.29	270.19	271.18	144.60	2
20					R	175.12	157.11	158.09	88.06	1



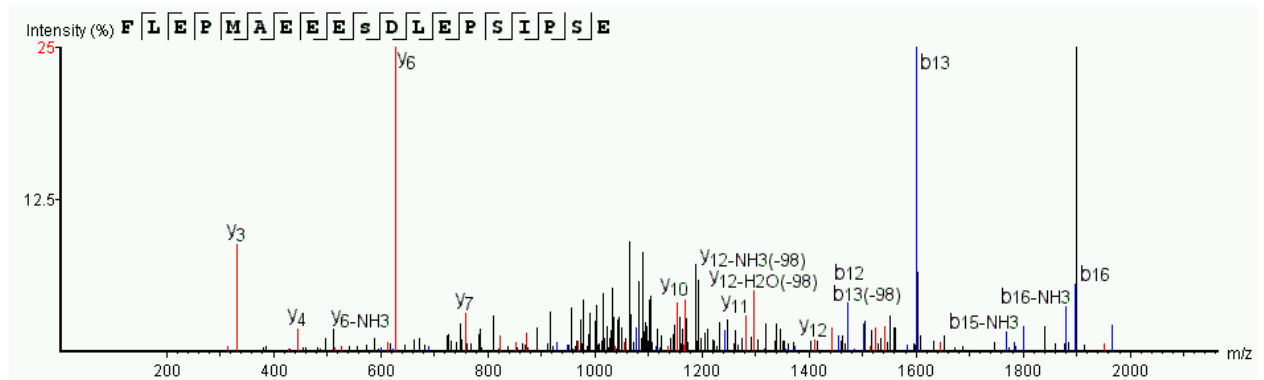
T272 (AspN Digestion, CID, A-Score =32.48)



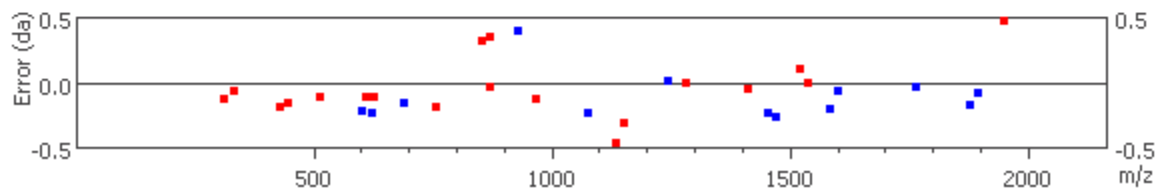
#	b	b-H2O	b-NH3	b (2+)	Seq	y	y-H2O	y-NH3	y (2+)	#
1	116.03	98.02	99.01	58.52	D					22
2	187.07	169.06	170.04	94.04	A	2290.11	2272.10	2273.09	1145.47	21
3	301.11	283.10	284.09	151.06	N	2219.08	2201.07	2202.05	1109.72	20
4	414.34	396.42	397.17	207.60	L	2105.03	2087.02	2088.01	1053.45	19
5	527.29	509.18	510.23	264.14	L	1992.20	1973.94	1974.92	996.48	18
6	658.41	640.31	641.40	329.66	M	1879.05	1861.01	1861.84	940.32	17
7	787.37	769.36	770.43	394.36	E	1747.81	1730.00	1730.80	874.63	16
8	844.52	826.55	827.53	423.19	G	1618.74	1600.77	1601.66	809.53	15
9	901.66	883.40	884.51	451.20	G	1561.72	1543.89	1544.74	781.62	14
10	1000.64	982.60	983.42	500.74	V	1504.72	1486.87	1487.71	752.87	13
11	1071.70	1053.45	1054.49	536.26	A	1405.72	1387.80	1388.54	703.34	12
12	1199.57	1181.32	1182.57	600.29	Q	1334.64	1316.55	1317.60	667.82	11
13	1300.73	1282.48	1283.59	650.81	T	1206.58	1189.06	1189.06	603.79	10
14	1429.61	1411.66	1412.64	715.65	E	1105.66	1087.89	1088.83	553.26	9
15	1526.72	1508.71	1510.02	764.29	P	976.61	958.82	959.46	488.74	8
16	1655.77	1637.69	1638.73	828.34	E	879.43	861.77	862.38	440.22	7
17	1822.76	1804.75	1805.73	911.88	S(+79.97)	750.49	732.38	733.36	376.03	6
18	1978.56	1960.85	1962.16	990.16	R	583.41	565.38	566.37	292.20	5
19	2077.93	2059.92	2060.90	1039.39	V	427.29	409.28	410.26	214.15	4
20	2174.98	2156.97	2157.95	1087.89	P	328.22	310.21	311.20	164.61	3
21	2274.05	2256.04	2257.02	1137.79	V	231.17	213.16	214.14	116.09	2
22					L	132.10	114.09	115.07	66.55	1



S288 (GluC Digestion, HCD, A-Score = 34.44)

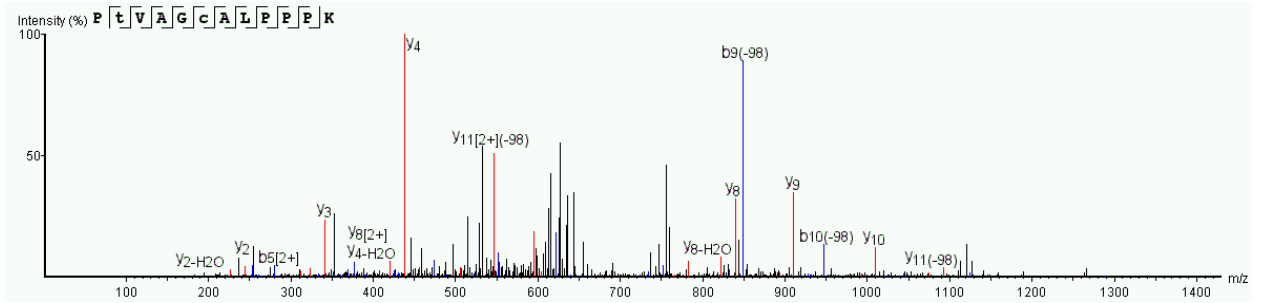


#	b	b-H2O	b-NH3	b (2+)	Seq	y	y-H2O	y-NH3	y (2+)	#
1	148.08	130.07	131.05	74.54	F					19
2	261.16	243.15	244.13	131.08	L	2081.85	2063.84	2064.82	1041.43	18
3	390.20	372.19	373.18	195.60	E	1968.77	1950.27	1951.74	984.88	17
4	487.26	469.25	470.23	244.13	P	1839.72	1821.71	1822.70	920.36	16
5	618.30	600.51	601.27	309.65	M	1742.67	1724.66	1725.64	871.47	15
6	689.50	671.32	672.31	345.17	A	1611.63	1593.62	1594.60	806.32	14
7	818.38	800.37	801.35	409.69	E	1540.61	1522.58	1523.45	770.80	13
8	947.42	929.00	930.39	474.21	E	1411.60	1393.54	1394.52	706.28	12
9	1076.70	1058.45	1059.43	538.73	E	1282.50	1264.50	1265.48	641.75	11
10	1243.44	1225.45	1226.43	622.47	S(+79.97)	1153.78	1135.93	1136.44	577.23	10
11	1358.49	1340.48	1341.46	679.74	D	986.47	968.59	969.44	493.73	9
12	1471.84	1453.56	1454.78	736.29	L	871.47	853.43	854.09	436.22	8
13	1600.68	1582.60	1583.79	800.81	E	758.55	740.35	741.33	379.68	7
14	1697.67	1679.66	1680.64	849.33	P	629.43	611.30	612.41	315.16	6
15	1784.70	1766.69	1767.71	892.85	S	532.26	514.37	515.23	266.63	5
16	1897.86	1879.77	1880.93	949.39	I	445.40	427.22	428.39	223.11	4
17	1994.83	1976.82	1977.81	997.92	P	332.22	314.27	315.12	166.57	3
18	2081.87	2063.86	2064.84	1041.43	S	235.09	217.08	218.07	118.05	2
19					E	148.06	130.05	131.03	74.53	1

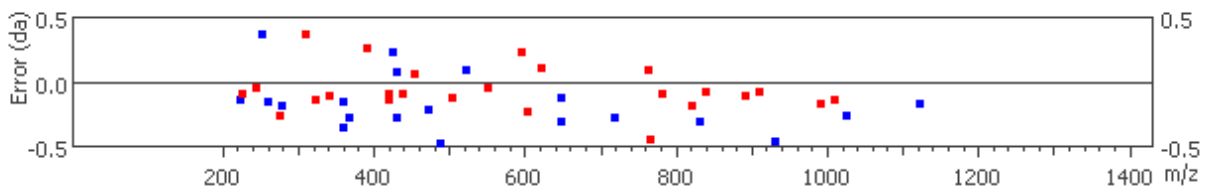


The presence of the b-ions at position b8 and b10 limit the phosphorylation event to E9 and E14 in this peptide. There is only one serine residue in this region therefore S288 (Serine 11 in this peptide) is phosphorylated.

T334 (Trypsin Digestion, CID, A-Score = 1000)

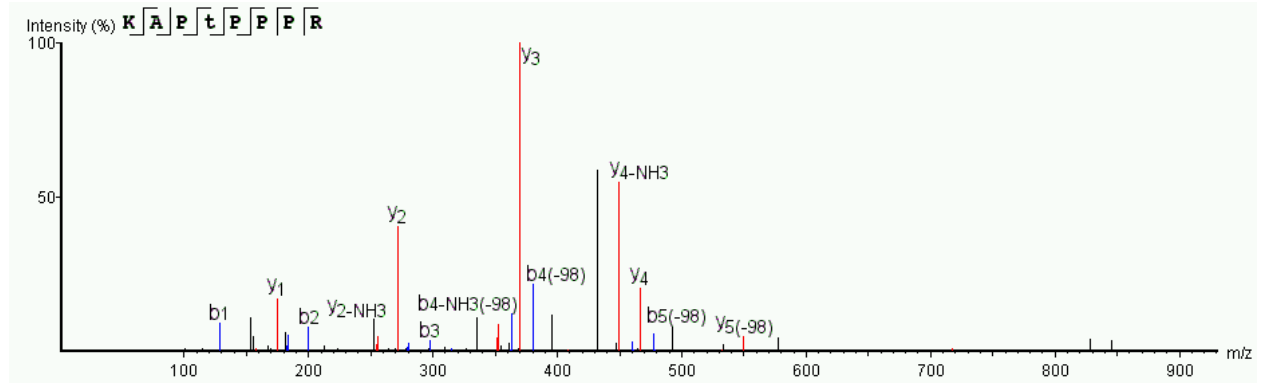


#	b	b-H2O	b-NH3	b (2+)	Seq	y	y-H2O	y-NH3	y (2+)	#
1	98.06	80.05	81.03	49.53	P					12
2	279.27	261.23	262.05	140.04	T(+79.97)	1190.56	1172.55	1173.54	595.54	11
3	378.14	360.49	361.28	189.57	V	1009.69	991.54	992.70	505.40	10
4	449.18	431.09	432.44	225.23	A	910.56	892.47	893.57	455.66	9
5	506.20	488.19	489.66	253.23	G	839.53	821.63	822.42	420.37	8
6	666.23	648.54	649.33	333.62	C(+57.02)	782.53	764.31	765.85	391.45	7
7	737.27	719.26	720.53	369.43	A	622.28	604.62	605.37	311.31	6
8	850.35	832.65	833.33	425.44	L	551.41	533.34	534.33	276.45	5
9	947.41	929.40	930.85	474.42	P	438.37	420.37	421.24	219.64	4
10	1044.46	1026.72	1027.43	522.63	P	341.34	323.35	324.19	171.11	3
11	1141.51	1123.68	1124.66	571.26	P	244.22	226.25	227.14	122.58	2
12					K	147.11	129.10	130.09	74.06	1

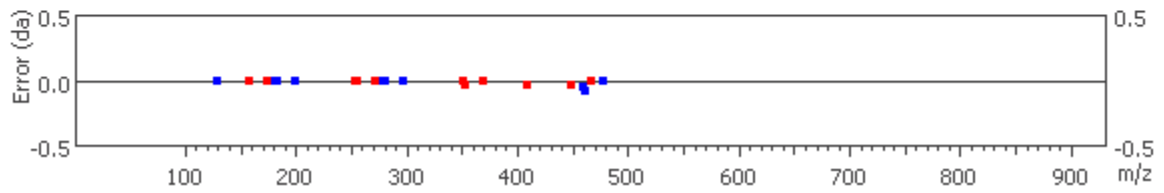


Note this is a ragged N-terminus (breakage occurred after a glutamine residue).

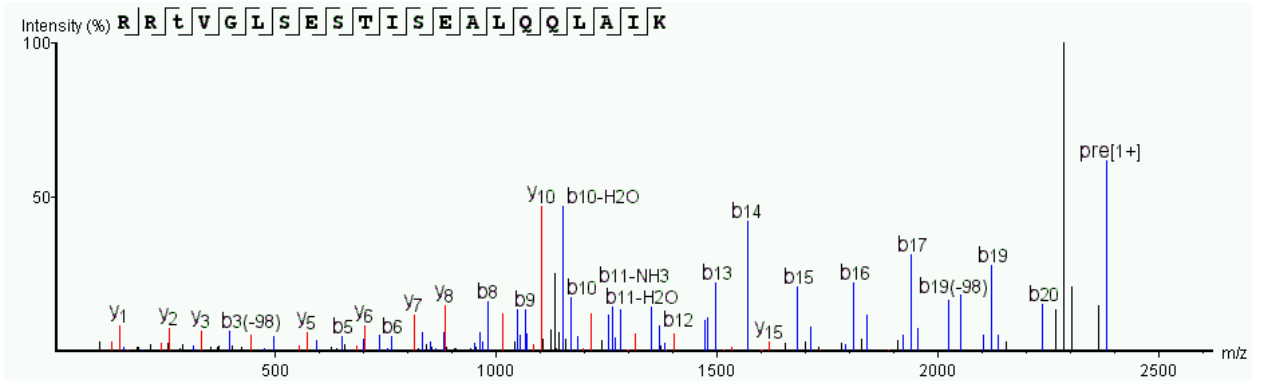
T348 (Trypsin Digestion, HCD, A-Score =1000)



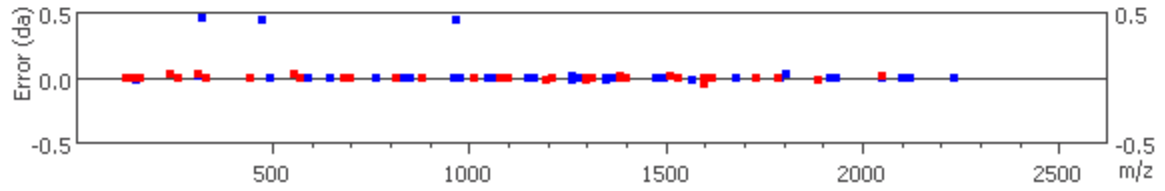
#	b	b-H2O	b-NH3	b (2+)	Seq	y	y-H2O	y-NH3	y (2+)	#
1	129.10	111.09	112.08	65.05	K					8
2	200.14	182.13	183.11	100.57	A	815.38	797.37	798.35	408.22	7
3	297.19	279.18	280.17	149.10	P	744.34	726.33	727.32	372.67	6
4	478.20	460.26	461.26	239.60	T(+79.97)	647.29	629.28	630.26	324.15	5
5	575.26	557.25	558.23	288.13	P	466.28	448.27	449.29	233.64	4
6	672.31	654.30	655.29	336.66	P	369.23	351.21	352.23	185.11	3
7	769.36	751.35	752.34	385.18	P	272.17	254.16	255.15	136.59	2
8					R	175.12	157.11	158.09	88.06	1



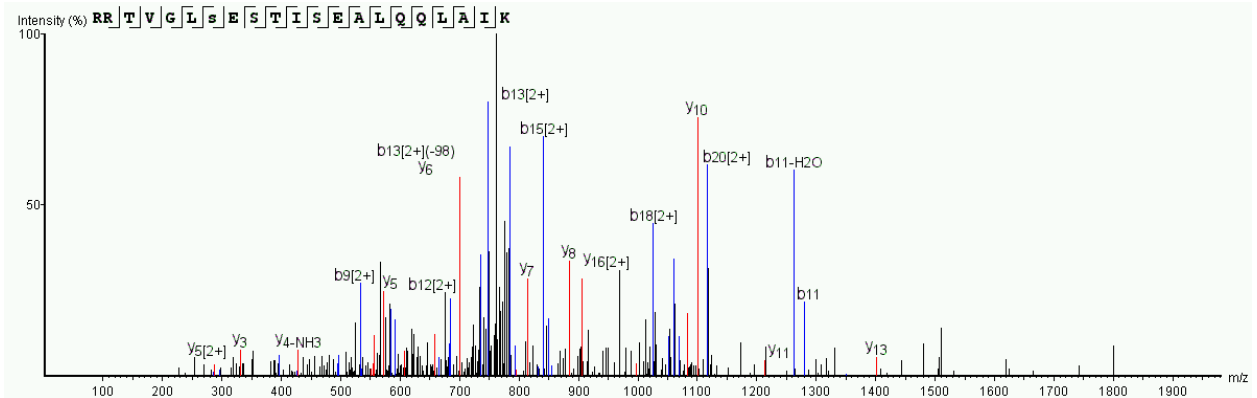
T356 (Trypsin Digestion, CID, A-Score =72.72)



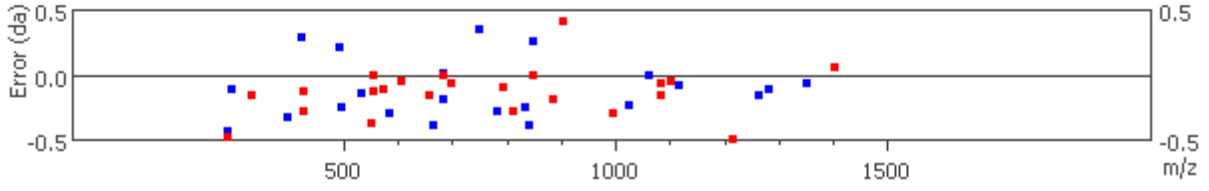
#	b	b-H2O	b-NH3	b (2+)	Seq	y	y-H2O	y-NH3	y (2+)	#
1	157.13	139.10	140.08	79.05	R					21
2	313.19	295.20	296.18	157.13	R	2224.16	2206.15	2207.13	1112.58	20
3	494.22	475.76	477.20	247.61	T(+79.97)	2068.06	2050.03	2051.03	1034.53	19
4	593.29	575.28	576.27	297.15	V	1887.06	1869.03	1870.02	944.02	18
5	650.31	632.30	633.29	325.19	G	1787.98	1769.96	1770.95	894.49	17
6	763.40	745.39	746.37	382.20	L	1730.97	1712.94	1713.93	865.98	16
7	850.43	832.42	833.40	425.71	S	1617.87	1599.85	1600.89	809.43	15
8	979.47	961.46	962.45	490.24	E	1530.84	1512.83	1513.78	765.92	14
9	1066.50	1048.49	1049.48	533.75	S	1401.80	1383.77	1384.77	701.40	13
10	1167.55	1149.54	1150.53	584.28	T	1314.77	1296.75	1297.76	657.88	12
11	1280.64	1262.61	1263.64	640.82	I	1213.72	1195.73	1196.71	607.36	11
12	1367.67	1349.66	1350.66	684.33	S	1100.63	1082.61	1083.61	550.82	10
13	1496.71	1478.70	1479.68	748.86	E	1013.60	995.59	996.57	507.30	9
14	1567.77	1549.74	1550.72	784.37	A	884.56	866.55	867.53	442.78	8
15	1680.83	1662.82	1663.81	840.92	L	813.52	795.51	796.49	407.26	7
16	1808.85	1790.88	1791.86	904.95	Q	700.44	682.42	683.41	350.72	6
17	1936.95	1918.93	1919.92	968.53	Q	572.38	554.32	555.35	286.69	5
18	2050.03	2032.02	2033.01	1025.52	L	444.32	426.31	427.29	222.66	4
19	2121.07	2103.06	2104.04	1061.04	A	331.23	313.19	314.21	166.11	3
20	2234.15	2216.14	2217.13	1117.58	I	260.20	242.15	243.17	130.60	2
21					K	147.11	129.10	130.09	74.06	1



S360 (Trypsn Digestion, CID, A-Score =3.13)

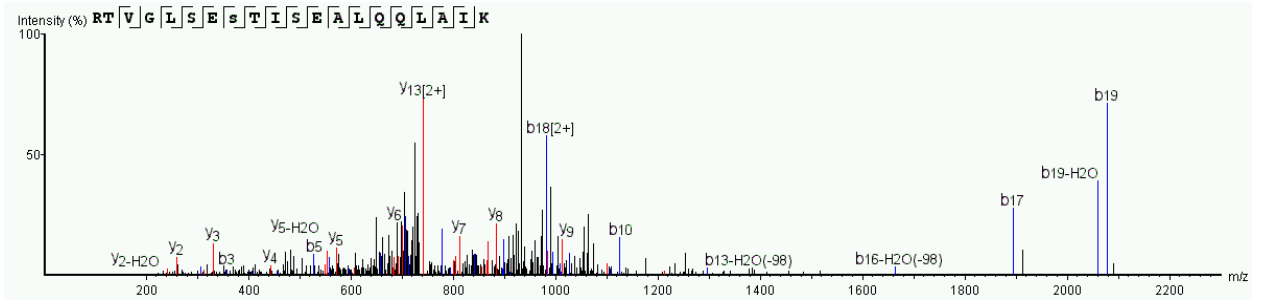


#	b	b-H2O	b-NH3	b (2+)	Seq	y	y-H2O	y-NH3	y (2+)	#
1	157.11	139.10	140.08	79.05	R					21
2	313.21	295.20	296.29	157.11	R	2224.16	2206.15	2207.13	1112.58	20
3	414.26	396.58	397.23	207.63	T	2068.06	2050.05	2051.03	1034.53	19
4	513.33	495.10	496.55	257.16	V	1967.01	1949.00	1949.98	984.00	18
5	570.35	552.34	553.32	286.11	G	1867.94	1849.93	1850.91	934.47	17
6	683.41	665.81	666.40	342.22	L	1810.92	1792.91	1793.89	905.53	16
7	850.16	832.67	833.40	425.41	S(+79.97)	1697.84	1679.83	1680.81	849.41	15
8	979.47	961.46	962.45	490.24	E	1530.84	1512.83	1513.81	765.92	14
9	1066.50	1048.49	1049.48	533.90	S	1401.73	1383.78	1384.77	701.40	13
10	1167.55	1149.54	1150.53	584.58	T	1314.76	1296.75	1297.74	658.05	12
11	1280.76	1262.79	1263.61	640.82	I	1214.21	1195.70	1196.69	607.40	11
12	1367.67	1349.66	1350.71	684.53	S	1100.69	1082.78	1083.68	551.20	10
13	1496.71	1478.70	1479.68	748.49	E	1013.60	995.59	996.87	507.30	9
14	1567.75	1549.74	1550.72	784.66	A	884.76	866.55	867.53	442.78	8
15	1680.83	1662.82	1663.81	841.30	L	813.80	795.60	796.49	407.26	7
16	1808.89	1790.88	1791.86	904.95	Q	700.51	682.42	683.41	350.72	6
17	1936.95	1918.94	1919.92	968.97	Q	572.49	554.38	555.49	287.17	5
18	2050.03	2032.02	2033.01	1025.75	L	444.32	426.44	427.57	222.66	4
19	2121.07	2103.06	2104.04	1061.05	A	331.39	313.22	314.21	166.12	3
20	2234.15	2216.14	2217.13	1117.66	I	260.20	242.19	243.17	130.60	2
21					K	147.11	129.10	130.09	74.06	1

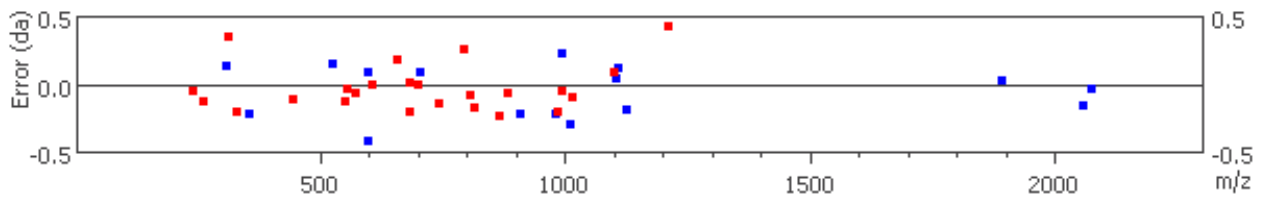


The presence of b6 and b7 ions strongly suggests phosphorylation at S360 (Serine 7 in this peptide). Note that y13 is present limiting the phosphorylation event to the first eight amino acids in the peptide.

S362 (Trypsn Digestion, CID, A-Score =0)

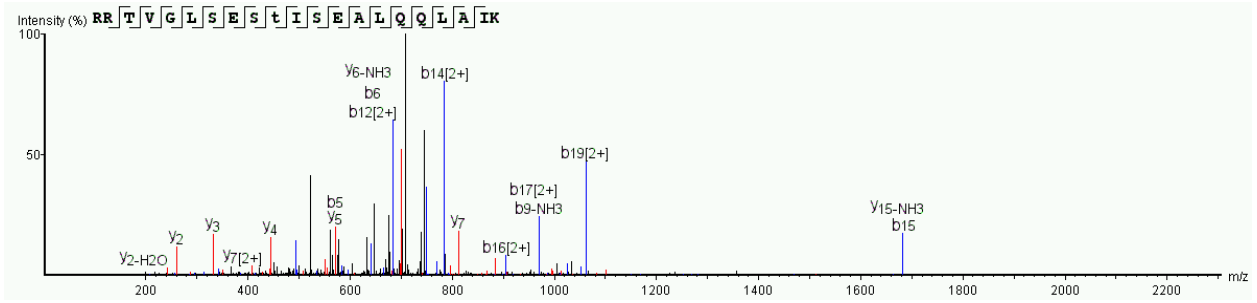


#	b	b-H2O	b-NH3	b (2+)	Seq	y	y-H2O	y-NH3	y (2+)	#
1	157.11	139.10	140.08	79.05	R					20
2	258.16	240.15	241.13	129.58	T	2068.06	2050.05	2051.03	1034.53	19
3	357.45	339.21	340.20	179.11	V	1967.01	1949.00	1949.98	984.22	18
4	414.25	396.24	397.22	207.62	G	1867.94	1849.93	1850.91	934.47	17
5	527.17	509.32	510.30	264.17	L	1810.92	1792.91	1793.89	905.96	16
6	614.36	596.26	597.76	307.54	S	1697.84	1679.83	1680.81	849.42	15
7	743.41	725.39	726.38	372.20	E	1610.80	1592.79	1593.78	805.99	14
8	910.62	892.39	893.38	455.70	S(+79.97)	1481.76	1463.75	1464.73	741.52	13
9	1011.76	993.44	994.19	506.23	T	1314.76	1296.75	1297.74	657.70	12
10	1124.73	1106.48	1107.38	562.77	I	1213.27	1195.70	1196.69	607.36	11
11	1211.57	1193.56	1194.54	606.28	S	1100.53	1082.62	1083.60	550.95	10
12	1340.61	1322.60	1323.58	670.80	E	1013.70	995.65	996.57	507.30	9
13	1411.65	1393.64	1394.62	706.22	A	884.63	866.78	867.76	442.78	8
14	1524.73	1506.72	1507.70	762.87	L	813.69	795.24	796.49	407.26	7
15	1652.79	1634.78	1635.76	826.89	Q	700.44	682.41	683.62	350.72	6
16	1780.85	1762.84	1763.82	890.92	Q	572.44	554.41	555.35	286.69	5
17	1893.89	1875.92	1876.91	947.47	L	444.43	426.31	427.29	222.66	4
18	1964.97	1946.96	1947.94	983.21	A	331.43	313.22	313.85	166.12	3
19	2078.10	2060.20	2061.03	1039.53	I	260.33	242.24	243.17	130.60	2
20					K	147.11	129.10	130.09	74.06	1

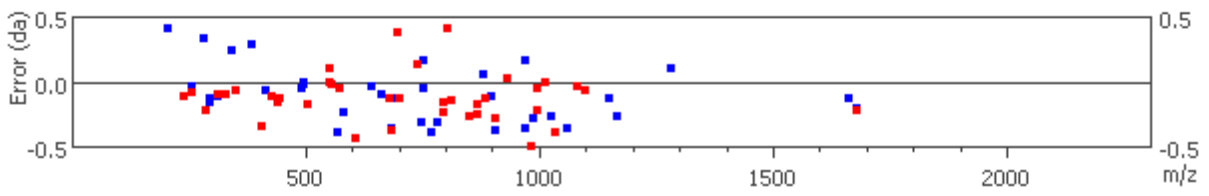


The presence of the b8 to b10 ion run supports phosphorylation at S362 (Serine 8 in this peptide). Note that y11 is present limiting the phosphorylation event to the first eight amino acids in the peptide.

T363 (Trypsn Digestion, CID, A-Score =0)

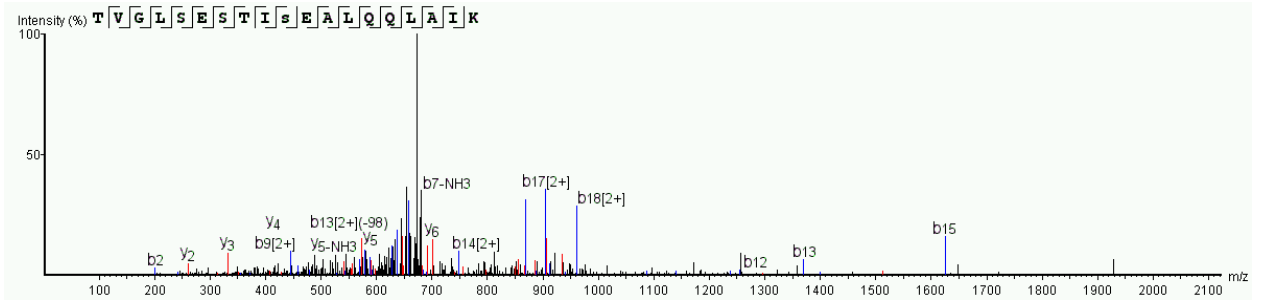


#	b	b-H2O	b-NH3	b (2+)	Seq	y	y-H2O	y-NH3	y (2+)	#
1	157.11	139.10	140.08	79.05	R					21
2	313.33	295.33	296.35	157.11	R	2224.16	2206.15	2207.13	1112.58	20
3	414.32	396.25	397.23	207.20	T	2068.06	2050.05	2051.03	1034.91	19
4	513.33	495.30	496.32	257.20	V	1967.01	1949.00	1949.98	984.50	18
5	570.73	552.34	553.32	285.33	G	1867.94	1849.93	1850.91	934.44	17
6	683.79	665.52	666.40	341.96	L	1810.92	1792.91	1793.89	906.24	16
7	770.86	752.51	753.26	385.44	S	1697.84	1679.83	1681.04	849.68	15
8	899.62	881.50	882.41	450.25	E	1610.80	1592.79	1593.78	805.48	14
9	986.82	968.53	969.34	493.82	S	1481.76	1463.75	1464.73	741.23	13
10	1167.82	1149.67	1150.53	584.52	T(+79.97)	1394.73	1376.72	1377.70	697.47	12
11	1280.52	1262.63	1263.61	640.86	I	1213.71	1195.70	1196.69	607.79	11
12	1367.67	1349.66	1350.64	684.46	S	1100.70	1082.65	1083.60	550.71	10
13	1496.71	1478.70	1479.68	749.17	E	1013.60	995.81	996.62	507.48	9
14	1567.75	1549.74	1550.72	784.69	A	884.69	866.81	867.71	442.94	8
15	1681.04	1662.96	1663.81	840.92	L	813.66	795.75	796.65	407.60	7
16	1808.89	1790.88	1791.86	905.32	Q	700.56	682.55	683.79	350.78	6
17	1936.95	1918.94	1919.92	969.34	Q	572.43	554.35	555.37	286.91	5
18	2050.03	2032.02	2033.01	1025.78	L	444.45	426.31	427.41	222.66	4
19	2121.07	2103.06	2104.04	1061.40	A	331.33	313.33	314.21	166.12	3
20	2234.15	2216.14	2217.13	1117.58	I	260.27	242.29	243.17	130.60	2
21					K	147.11	129.10	130.09	74.06	1

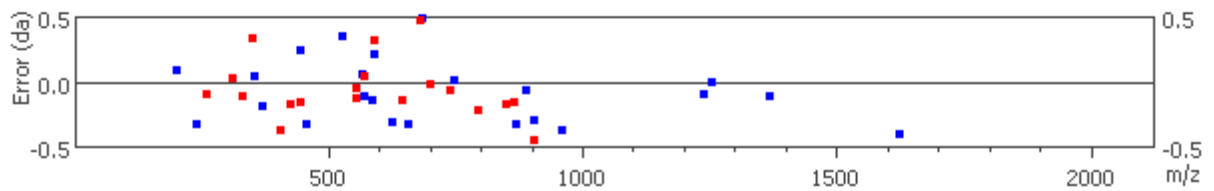


The presence of the b-ion run from b5 to b11 strongly suggests phosphorylation at T363 (Threonine 10 in this peptide). Note that y10 is present limiting the phosphorylation event to the first twelve amino acids in the peptide.

S365 (Trypsn Digestion, CID, A-Score =0)

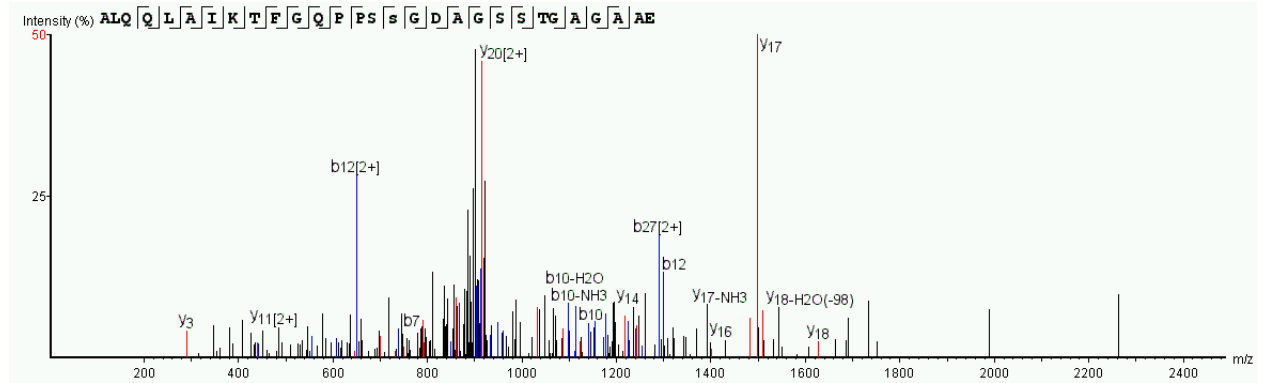


#	b	b-H2O	b-NH3	b (2+)	Seq	y	y-H2O	y-NH3	y (2+)	#
1	102.06	84.04	85.03	51.53	T					19
2	201.03	183.11	184.10	101.06	V	1967.01	1949.00	1949.98	984.00	18
3	258.15	240.13	241.45	129.57	G	1867.94	1849.93	1850.91	934.47	17
4	371.42	353.22	354.14	186.11	L	1810.92	1792.91	1793.89	906.42	16
5	458.59	440.25	441.23	229.63	S	1697.84	1679.83	1680.81	849.60	15
6	587.45	569.22	570.40	294.15	E	1610.80	1592.79	1593.78	805.90	14
7	674.34	656.33	657.65	337.67	S	1481.76	1463.75	1464.73	741.45	13
8	775.38	757.37	758.36	388.19	T	1394.73	1376.72	1377.70	697.86	12
9	888.54	870.46	871.44	444.48	I	1293.68	1275.67	1276.65	647.48	11
10	1055.47	1037.46	1038.44	527.86	S(+79.97)	1180.60	1162.59	1163.57	590.47	10
11	1184.51	1166.50	1167.48	592.53	E	1013.60	995.59	996.57	507.30	9
12	1255.54	1237.54	1238.62	628.58	A	884.56	866.55	867.70	442.78	8
13	1368.75	1350.62	1351.60	684.32	L	813.52	795.51	796.72	407.64	7
14	1496.69	1478.68	1479.66	748.83	Q	700.46	681.95	683.41	350.37	6
15	1625.15	1606.74	1607.72	812.87	Q	572.32	554.50	555.40	286.69	5
16	1737.83	1719.82	1720.80	869.74	L	444.48	426.31	427.47	222.66	4
17	1808.87	1790.86	1791.84	905.24	A	331.35	313.18	314.21	166.12	3
18	1921.95	1903.94	1904.93	961.86	I	260.30	242.19	243.17	130.60	2
19					K	147.11	129.10	130.09	74.06	1

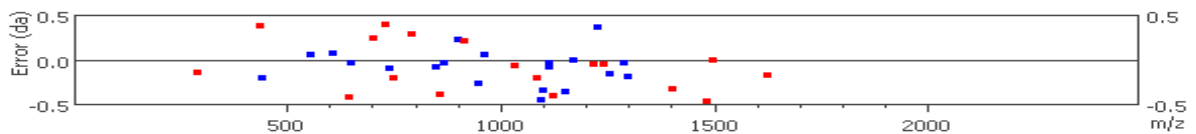


The presence of the b9 and b12 ions limit the region of phosphorylation to a single serine residue at position 365.

S381/S382 (GluC Digestion, CID, A-Score =0)

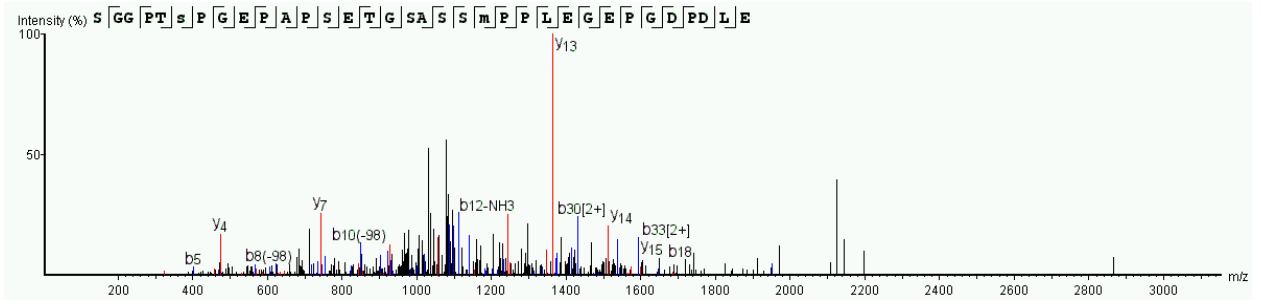


#	b	b-H2O	b-NH3	b (2+)	Seq	y	y-H2O	y-NH3	y (2+)	#
1	72.04	54.03	55.02	36.52	A					29
2	185.13	167.12	168.10	93.06	L	2726.27	2708.26	2709.24	1363.63	28
3	313.19	295.18	296.16	157.09	Q	2613.18	2595.17	2596.16	1307.09	27
4	441.45	423.24	424.22	221.12	Q	2485.12	2467.11	2468.10	1243.12	26
5	554.26	536.32	537.30	277.67	L	2357.07	2339.06	2340.04	1179.03	25
6	625.37	607.36	608.25	313.18	A	2243.98	2225.97	2226.95	1122.90	24
7	738.55	720.44	721.42	369.73	I	2172.94	2154.93	2155.92	1087.18	23
8	866.59	848.62	849.52	433.77	K	2059.86	2041.85	2042.83	1030.43	22
9	967.59	949.85	950.57	484.30	T	1931.77	1913.75	1914.74	966.38	21
10	1114.75	1097.10	1097.98	557.83	F	1830.72	1812.71	1813.69	915.64	20
11	1171.69	1154.03	1154.66	586.34	G	1683.65	1665.64	1666.62	842.32	19
12	1299.93	1281.73	1282.72	650.42	Q	1626.80	1608.62	1609.60	813.81	18
13	1396.80	1378.78	1379.77	698.90	P	1498.58	1480.56	1482.02	749.78	17
14	1493.85	1475.84	1476.82	747.42	P	1401.85	1383.51	1384.49	701.01	16
15	1580.88	1562.87	1563.85	790.94	S	1304.46	1286.45	1287.44	652.73	15
16	1747.88	1729.87	1730.85	874.44	S(+79.97)	1217.48	1199.42	1200.40	609.22	14
17	1804.90	1786.89	1787.87	902.72	G	1050.43	1032.42	1033.48	525.72	13
18	1919.93	1901.92	1902.90	960.39	D	993.41	975.40	976.38	497.21	12
19	1990.96	1972.95	1973.94	995.98	A	878.38	860.77	861.36	439.29	11
20	2047.99	2029.97	2030.96	1024.49	G	807.35	789.34	790.02	404.17	10
21	2135.02	2117.01	2117.99	1068.01	S	750.53	731.90	733.30	375.66	9
22	2222.05	2204.04	2205.02	1111.56	S	663.29	645.71	646.27	332.15	8
23	2323.10	2305.09	2306.07	1162.05	T	576.26	558.25	559.24	288.63	7
24	2380.12	2362.11	2363.09	1190.56	G	475.21	457.20	458.19	238.11	6
25	2451.16	2433.15	2434.13	1225.70	A	418.19	400.18	401.17	209.60	5
26	2508.18	2490.17	2491.15	1254.75	G	347.16	329.15	330.13	174.08	4
27	2579.21	2561.20	2562.19	1290.15	A	290.28	272.12	273.11	145.57	3
28	2650.25	2632.24	2633.22	1325.63	A	219.10	201.09	202.07	110.05	2
29					E	148.06	130.05	131.03	74.53	1

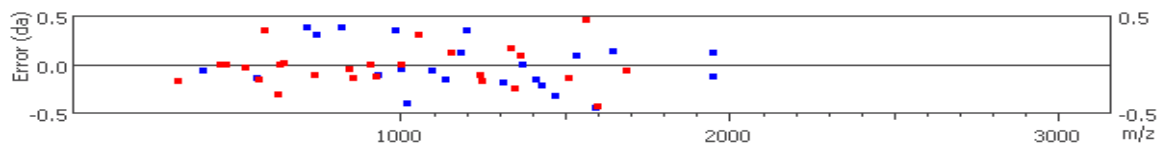


The presence of the y-ions at y14 and y16 limit the phosphorylation site to likely position S382 (S 16 in peptide). The absence of supporting b ions and the limited run of y ions upstream of y14 also raise the possibility of the phosphorylation occurring on S381 (S15 on this peptide).

S401 (GluC Digestion, CID, A-Score =0)

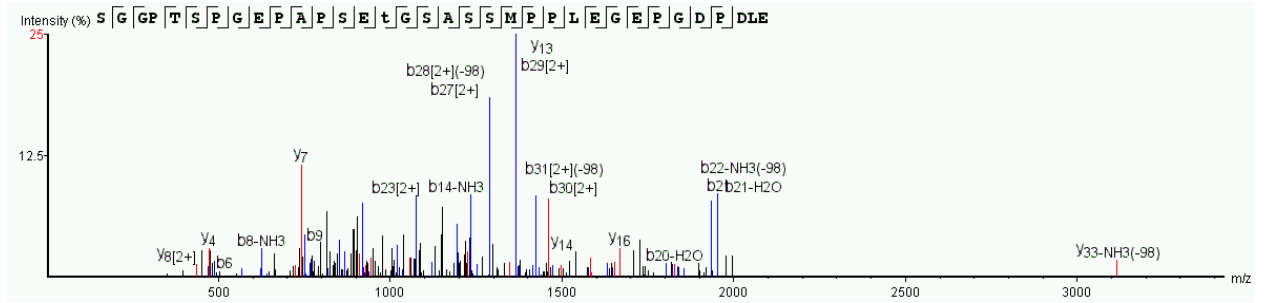


#	b	b-H2O	b-NH3	b (2+)	Seq	y	y-H2O	y-NH3	y (2+)	#
1	88.04	70.03	71.01	44.52	S					34
2	145.06	127.05	128.03	73.03	G	3245.33	3227.32	3228.31	1623.17	33
3	202.08	184.07	185.06	101.54	G	3188.31	3170.30	3171.29	1594.66	32
4	299.14	281.12	282.11	150.07	P	3131.29	3113.28	3114.27	1565.67	31
5	400.26	382.17	383.16	200.59	T	3034.24	3016.23	3017.21	1517.62	30
6	567.33	549.17	550.15	284.09	S(+79.97)	2933.19	2915.18	2916.16	1467.10	29
7	664.23	646.22	647.21	332.62	P	2766.19	2748.18	2749.17	1383.60	28
8	721.26	703.25	704.23	361.13	G	2669.14	2651.13	2652.11	1334.89	27
9	850.30	832.29	833.27	425.65	E	2612.12	2594.11	2595.09	1306.56	26
10	947.35	929.34	930.43	474.18	P	2483.08	2465.07	2466.05	1242.16	25
11	1018.80	1000.38	1001.42	509.69	A	2386.02	2368.01	2369.00	1193.51	24
12	1115.44	1097.43	1098.49	558.22	P	2314.99	2296.98	2297.96	1157.99	23
13	1202.11	1184.46	1185.31	601.74	S	2217.93	2199.92	2200.91	1109.47	22
14	1331.52	1313.51	1314.68	666.26	E	2130.90	2112.89	2113.87	1065.95	21
15	1432.56	1414.72	1415.54	716.39	T	2001.86	1983.85	1984.83	1001.42	20
16	1489.58	1471.91	1472.56	744.97	G	1900.81	1882.80	1883.78	950.91	19
17	1576.62	1558.61	1559.59	788.81	S	1843.79	1825.78	1826.76	922.40	18
18	1647.50	1629.64	1630.63	823.93	A	1756.76	1738.75	1739.73	878.88	17
19	1734.69	1716.68	1717.66	867.84	S	1685.79	1667.71	1668.69	843.41	16
20	1821.72	1803.71	1804.69	911.36	S	1599.13	1580.68	1581.66	799.84	15
21	1968.75	1950.62	1951.86	984.52	M(+15.99)	1511.80	1493.65	1494.63	756.33	14
22	2065.81	2047.80	2048.78	1033.40	P	1364.53	1346.87	1347.59	682.81	13
23	2162.86	2144.85	2145.83	1081.93	P	1267.57	1249.73	1250.54	634.27	12
24	2275.94	2257.93	2258.92	1138.63	L	1170.52	1152.51	1153.36	585.40	11
25	2404.99	2386.98	2387.96	1202.99	E	1057.12	1039.42	1040.41	529.25	10
26	2462.01	2444.00	2444.98	1231.50	G	928.51	910.37	911.36	464.69	9
27	2591.05	2573.04	2574.02	1296.02	E	871.37	853.36	854.48	436.18	8
28	2688.10	2670.09	2671.08	1344.55	P	742.44	724.31	725.30	371.66	7
29	2745.12	2727.11	2728.10	1373.07	G	645.25	627.26	628.56	323.32	6
30	2860.15	2842.14	2843.12	1430.80	D	588.25	570.40	571.22	294.63	5
31	2957.20	2939.19	2940.18	1479.10	P	473.22	455.21	456.21	237.11	4
32	3072.23	3054.22	3055.20	1536.51	D	376.17	358.16	359.14	188.59	3
33	3185.31	3167.30	3168.29	1593.61	L	261.14	243.13	244.12	131.07	2
34					E	148.06	130.05	131.03	74.53	1

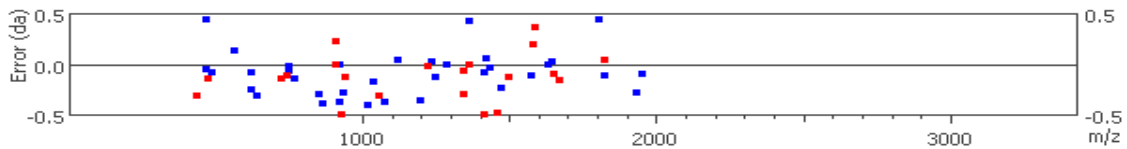


The presence of the b ion at b5, b6 and b11 supports phosphorylation at position S401 (Serine 6 in this peptide). The b ions at b10 and b13 exclude a number of potential residues.

T410 (GluC Digestion, CID, A-Score =0)



#	b	b-H2O	b-NH3	b (2+)	Seq	y	y-H2O	y-NH3	y (2+)	#
1	88.04	70.03	71.01	44.52	S					34
2	145.06	127.05	128.03	73.03	G	3229.34	3211.33	3212.31	1615.17	33
3	202.08	184.07	185.06	101.54	G	3172.32	3154.31	3155.29	1586.28	32
4	299.14	281.12	282.11	150.07	P	3115.30	3097.29	3098.27	1558.15	31
5	400.18	382.17	383.16	200.59	T	3018.24	3000.23	3001.22	1509.62	30
6	487.30	469.25	470.19	244.11	S	2917.20	2899.19	2900.17	1459.58	29
7	584.27	566.26	567.10	292.63	P	2830.16	2812.15	2813.14	1416.08	28
8	641.61	623.54	624.34	321.14	G	2733.11	2715.10	2716.08	1367.06	27
9	770.48	752.39	753.32	385.67	E	2676.09	2658.08	2659.06	1338.55	26
10	867.38	849.37	850.66	434.19	P	2547.05	2529.04	2530.02	1274.02	25
11	938.70	920.43	921.78	469.25	A	2450.00	2431.98	2432.97	1225.52	24
12	1035.65	1017.46	1018.86	518.24	P	2378.96	2360.95	2361.93	1189.98	23
13	1122.46	1104.50	1105.48	561.75	S	2281.91	2263.89	2264.88	1141.45	22
14	1251.68	1233.54	1234.48	626.27	E	2194.87	2176.86	2177.85	1097.94	21
15	1432.60	1414.64	1415.54	716.78	T(+79.97)	2065.83	2047.82	2048.80	1033.42	20
16	1489.58	1471.82	1472.56	745.29	G	1884.82	1866.81	1867.79	943.04	19
17	1576.73	1558.61	1559.59	788.81	S	1827.74	1809.78	1810.77	914.40	18
18	1647.62	1629.64	1630.64	824.33	A	1740.76	1722.75	1723.74	870.88	17
19	1734.69	1716.68	1717.66	868.23	S	1669.89	1651.81	1652.70	835.36	16
20	1821.84	1803.25	1804.69	911.36	S	1582.48	1564.68	1565.67	791.85	15
21	1952.86	1935.03	1935.73	976.88	M	1495.80	1477.65	1478.64	748.33	14
22	2049.81	2031.80	2032.78	1025.41	P	1364.63	1346.91	1347.67	682.81	13
23	2146.86	2128.85	2129.84	1074.31	P	1267.57	1249.56	1250.54	634.28	12
24	2259.95	2241.94	2242.92	1130.47	L	1170.52	1152.51	1153.49	585.76	11
25	2388.99	2370.98	2371.96	1195.36	E	1057.75	1039.42	1040.41	529.22	10
26	2446.01	2428.00	2428.98	1223.51	G	928.88	910.14	911.36	464.69	9
27	2575.05	2557.04	2558.03	1288.02	E	871.37	853.36	854.34	436.50	8
28	2672.11	2654.10	2655.08	1336.55	P	742.44	724.46	725.30	371.66	7
29	2729.13	2711.12	2712.10	1364.63	G	645.27	627.26	628.25	323.14	6
30	2844.16	2826.15	2827.13	1422.51	D	588.25	570.24	571.22	294.63	5
31	2941.21	2923.20	2924.18	1471.10	P	473.36	455.21	456.20	237.11	4
32	3056.24	3038.23	3039.21	1528.62	D	376.17	358.16	359.14	188.59	3
33	3169.32	3151.31	3152.29	1585.16	L	261.14	243.13	244.12	131.07	2
34					E	148.06	130.05	131.03	74.53	1



The presence of the b-ion run from b11 to b15 strongly suggests phosphorylation at T410 (Threonine 15 in this peptide). Note that y18 is present limiting the phosphorylation event to the first seventeen amino acids in the peptide.